A Characterisation of Combustion and Gasification Residues from Biomass and other Fuels

by

Samantha Cooke

A thesis submitted for the degree of Doctor of Philosophy of the University of London and for the Diploma of Membership of Imperial College

Department of Materials,
Imperial College of Science, Technology and Medicine,
Prince Consort Rd,
London. SW7 2BP

July 1998

Contents

Glossary of terms and acronyms

acicular	needle-like (crysals)
ash	inorganic residue of combustion and gasification processes
AFT	ash fusion temperatures (IDT, HDT and FT) at which a cone of ash shows signs of deformation on heating
BR	cis-1, 4-polybutadiene rubber
BSI	back-scattered electron image
CAP	Common Agricultural Policy
CCSEM	computer controlled scanning electron microscopy
char	solid carbon residue of pyrolysis or of partially burnt biomass
CHP	combined heat and power
CV	calorific value
dab	dry ash basis
DNC	declared net capacity; the maximum capacity of a facility, reduced by a specific factor to account for the intermittent nature of the output, for example the DNC for wind power is 43% of the installed capacity
DTI	Department of Trade and Industry
EC	European Community
ECU	European Currency Unit
EDAX	energy dispersive analysis of X-rays
EDS	energy dispersive spectroscopy
ETSU	Energy Technology Support Unit of the DTI, Harwell, Oxfordshire
euhedral	showing perfect or near perfect crystal form
FB(G)	fluidised bed (gasifier)
FT	flow temperature
HDT	hemispherical deformation temperature
HTA	high temperature ash, as produced in a muffle furnace at 850°C
ICPS	induction coupled plasma spectroscopy
IDT	initial deformation temperature
IR	cis-1, 4-polyisopropene rubber
LTA	low temperature ash, produced by oxidising carbonaceous material in a low temperature oxygen plasma
MSW	municipal solid waste
MW_e	boiler generating capacity, megawatt electrical
MW_{th}	megawatt thermal

NEI	Northern Engineering Industries
NFFO	Non Fossil Fuel Obligation
NO_x	oxides of nitrogen
NR	natural rubber
Parenchyma	elongate cells of the vascular system
PAH	polynuclear aromatic hydrocarbons
PCDD	polychlorinated dibenzodioxins
PCDF	polychlorinated dibenzofurans
pf	pulverised fuel
PGIL	Power Gasifiers International Ltd.
phloem	soft vascular tissue in bark
PVC	polyvinylchloride
REC	regional electricity company
RDF	refuse derived fuel
c-RDF	coarse RDF
d-RDF	densified RDF, highly processed into refined pellets
SBR	styrene-butadiene rubber
SEI	secondary electron image
SEM	scanning electron microscopy
SO_x	oxides of sulphur
SRC	short rotation coppice
SRI	Silsoe Research Institute, Bedfordshire
SRO	Scottish Renewable Order
TEQ	tonnes equivalent
TPS	Termiska Processer Sweden
XAFS	X-ray absorption fine structure
XRD	X-ray diffraction
xylem	principal water-conducting and supporting tissue of vascular plants

Chemical composition of minerals and inorganic phases encountered in this study

Akermanite	$2CaO.MgO.2SiO_2$
Anatase	TiO_2 (tetragonal -)
Anhydrite	$CaSO_4$
Anorthite	$CaO.Al_2O_3.2SiO_2$
Aragonite	$CaCO_3$ (orthorhombic -)
Arcanite	K_2SO_4
Biotite	$K_2(Mg,Fe^{2+})_{6-4}(Fe^{3+},Al,Ti)_{0-2}[Si_{6-5}Al_{2-3}O_{20}](OH,F)_4$
Calcite	$CaCO_3$ (trigonal -)
Calcium orthophosphate	$CaHPO_4$
Calcium oxalate	CaC_2O_4
Calcium phosphate	$Ca_3(PO_4)_2$
Chalcopyrite	$CuFeS_2$
Cristobalite	SiO_2 (tetragonal -)
Dickite	$Al_2O_3.2SiO_2.2H_2O$
Diopside	$CaO.MgO.2SiO_2$
Dolomite	$CaMg(CO_3)_2$
Feldspars	*alkali feldspars*: $(K,Na)[AlSi_3O_8]$
	plagiclase felspars: $Na[AlSi_3O_8]$-$Ca[Al_2Si_2O_8]$
Forsterite	$2MgO.SiO_2$
Gypsum	$CaSO_4.2H_2O$
Gehlenite	$2CaO.Al_2O_3.SiO_2$
Halite	$NaCl$
Halloysite	$Al_2O_3.2SiO_2.4H_2O$
Hematite	Fe_2O_3
Hydroxyapatite	$Ca_5(PO_4)_3(OH)$
Illite (muscovite)	$K_2Al_4[Si_6Al_2O_{20}](OH)_4$
Kalsilite	$KAlSiO_4$
Kaolinite	$Al_2O_3.2SiO_2.2H_2O$
Lime	CaO
Maghemite	γ-Fe_2O_3
Magnetite	Fe_3O_4
Montmorillonite	$(Na)_{0.7}(Al_{3.3}Mg_{0.7})Si_8O_{20}(OH)_4.nH_2O$
Monmorillonite group	$(½Ca, Na)_{0.7}(Al,Mg,Fe)_4[(SiAl)_8O_{20}](OH)_4.nH_2O$
Nacrite	$Al_2O_3.2SiO_2.2H_2O$
Nepheline	$(Na,K)AlSiO_4$

Portlandite	$Ca(OH)_2$
Potassium amidophosphate	$K_2PO_3NH_2$
Potassium calcium phosphate	$KCaPO_4$
Potassium calcium phosphate	$K_3CaH(PO_4)_2$
Potassium chloride	KCl
Potassium orthophosphate	KH_2PO_4
Pseudowollastonite	β-$CaO.SiO_2$
Pyrite	FeS_2
Pyroxenes	*orthorhombic pyroxenes*: Enstatite-Orthoferrosilite, $MgSiO_3$-$FeSiO_3$ *monoclinic pyroxenes*: Diopside-Hedenbergite-Johannsenite, $Ca(Mg,Fe^{2+},Mn)Si_2O_6$
Pyroxyferroite	$(Fe,Ca)SiO_3$
Quartz	SiO_2 (trigonal +)
Rutile	TiO_2 (tetragonal +)
Sphalerite	ZnS
Spinel	$MgAl_2O_4$
Syngenite	$K_2Ca(SO_4)_2.H_2O$
Talc	$Mg_6[Si_8O_{20}](OH)_4$
Tridymite	SiO_2 (orthorhombic +)
Troilite	FeS
Ulvöspinel	Fe_2TiO_4
Whitlockite	$(Ca,Mg)_3(PO_4)_2$
Wollastonite	$CaO.SiO_2$
Zinc oxysulphate	$Zn_3O(SO_4)_2$
Zincite	ZnO
Zinkosite	$ZnSO_4$

List of Tables

List of Figures

Axes on phase equilibrium diagrams

Compositions are in wt% oxide and temperatures in degrees centigrade, unless otherwise stated.

Acknowledgements

I would like to express my gratitude to Professor Williamson, my academic supervisor, for the guidance, encouragement and confidence he maintained throughout the course of my doctorate. My thanks also to Dr W. Livingston (Mitsui Babcock Energy Ltd.) for contributing literature, materials and industrial knowledge to this study.

The technical aid and expertise of Mr F. Wigley, Mr K. Sweeney, Mr J. Wright and Mr N. Salpadoru have been invaluable. Many thanks to Mr D. Waters and Mrs P. Potter for the loan of a PC.

I would also like to acknowledge with thanks Mr N. Barker (ETSU), Mr T. Rampling (ex-Warren Springs), and Mr B. McGhee (Strathclyde University, now Mitsui Babcock Energy Ltd.) for the provision of samples and data.

In addition, the studentship provided by the Engineering and Physical Sciences Research Council, and bursaries from Mitsui Babcock Energy Ltd. and the Department of Trade and Industry are gratefully acknowledged.

I am most grateful to the following people whom, through their love, friendship and moral support, have always been prepared to help: Scott Robertson, Fiona Lowrie, Angela Salami, Griselda Daesslé, Mary Wiles, Norma, Gill Hopkins, Mrs Kim, Fiona McQuillan, Lucy Mason, Andrew Bushel, and Mary Ward.

To my family, I thank them for their unconditional love and patience.

Finally to my son, Michael, for bringing me such joy at the most difficult of times.

Abstract

The use of biomass, domestic refuse and industrial wastes as alternative energy sources to fossil fuels for electrical power generation is actively encouraged by EU and government energy policies.

A variety of raw materials were obtained for this study, including poplar and willow short rotation coppice, poultry litter, cereal straw, scrap tyres, sewage sludges and refuse derived fuels. In addition, deposits and residues were acquired from pilot plant and commercial operations currently using biomass for combustion and gasification processes. The nature and variability of the raw materials have been investigated in terms of their moisture and ash contents, ash chemistry and ash fusion behaviour, with the objective of identifying potential problems associated with ash deposition on heat transfer surfaces. The deposits and residues have been characterised with respect to the chemical composition and microstructure, in order to elucidate the bonding mechanisms and hence the possible reasons for deposition. The high temperature behaviour of biomass and waste ashes has been predicted using phase equilibria, vapour pressure data and calculated ash viscosities.

The results of such a characterisation revealed the biomass and waste materials to be grossly inhomogeneous in nature with the deposits and residues reflecting the heterogeneity of the fuels.

Willow and poplar short rotation coppice produce an ash which is rich in CaO, K_2O, P_2O_5 and SO_3 with variations in ash composition throughout the plant anatomy. The fuel is generally low in ash, although the ash content of the bark is 4-5 times that of the sapwood. Considerable variations in ash chemistry were noted for the same species cultivated in different regions. Ash fusion data reflected changes in ash composition.

Several power plants in the UK use poultry litter as a fuel. The litter has a high moisture content and ~14wt% ash. The ash contains appreciable K_2O, P_2O_5, CaO and SO_3. The high volatility of K^+ species and P_2O_5 vapours gave rise to K_2SO_4 bonded

fouling deposits, and predominantly crystalline slags containing phosphate phases which were predicted from relevant phase equilibria data.

Sewage sludges have relatively high ash contents (~30wt%) with ash compositions rich in Al_2O_3 and SiO_2. CaO and P_2O_5 lower the ash fusion temperatures, and this has given rise to deposits in a pilot plant gasifier.

While scrap tyres offer a potentially high calorific fuel, fillers ($CaCO_3$ and kaolin) and vulcanising agents (ZnO) readily react at combustion temperatures. The condensation of ZnO on the surfaces of aluminosilicate particles provides a bonding phase for deposit formation.

Attempts to provide electrical power from the incineration of refuse (RDF) have so far experienced only limited success. The processes have suffered from high corrosion rates and alkali deposition. Attempts to reduce these problems have been made by co-firing RDF with chestnut. Deposits from a pilot plant gasifier have been characterised in terms of ash chemistry and fusion properties of the mixed fuel, the results being consistent with predictions based upon thermodynamic data.

The project also examined the reactivity of carbon chars produced by the pyrolysis of pine, straw and RDF. The reactivity of chars was found to decrease with increasing pyrolysis temperature, with evidence to support the catalytic activity of alkali and alkaline earth metal ions (Ca^{2+}, K^+, Na^+) for carbon oxidation.

The successful development of power plant using biomass, domestic refuse, and industrial wastes will depend on a knowledge of the variability and inhomogeneity of the residual ash. Ash chemistry, ash fusion, viscosity and vaporisation of alkali species, all play a significant role in maintaining clean heat transfer surfaces.

Given the unfavourable ash chemistry of many potential fuels, gasification presents a more potentially viable option than combustion or incineration.

Chapter One

Introduction

The use of biomass and waste materials as alternative sources to fossil fuels for power generation is now actively encouraged by all industrialised countries. In the UK, a market for wastes and energy crops has been established via the Non Fossil Fuel Obligation, implemented by the Government to enable these sources to compete equitably with conventional fuels. The need for such diverse resources has strong environmental, economic, political and social implications. The disposal of wastes produced by households, industry and agriculture present ever increasing problems as environmental constraints become progressively more stringent. The effective use of the calorific value of these materials is to be encouraged as local authorities are compelled to seek alternative methods of disposal. The food surplus throughout the EC has resulted in the Common Agricultural Policy Reform and the search for productive use of set-aside land to preserve and maintain rural communities. The substitution of energy crops for cereals is a viable alternative, and reduces the dependency of many countries on imported fossil fuels. With mounting concerns for the environment regarding CO_2 emissions from the combustion of fossil fuels, energy crops which effectively recycle carbon resulting in zero net CO_2 emissions, are an attractive proposal.

While residues from the combustion of fossil fuels are not without their own problems, the power generation industry, with many years experience, has come to terms with the problems of variable fuel quality and developed plant to tolerate such issues. However, the high alkali, alkaline earth metal ion and P_2O_5 content of the non-combustible fraction of biomass and wastes present many new technical challenges, with slagging, fouling and corrosion of heat exchange surfaces in conventional steam raising processes. Gasification may prove a more satisfactory means of recovering the chemical energy of these fuels, since the temperatures of operation preclude ash fusion and reduce the

these fuels, since the temperatures of operation preclude ash fusion and reduce the vapour pressure of volatile species, thereby avoiding the formation of sintered deposits and the fouling of convective passes. However, large scale gasification processes have yet to be developed and detailed information concerning the high temperature chemistry of biomass and waste ashes is essential for the design and efficient operation of gasification systems.

The objective of this study has been to characterise the residues from the combustion and gasification of biomass and wastes, and to predict the high temperature behaviour of the inherent inorganic matter under combustion/gasification conditions. A variety of raw materials were obtained, including poplar and willow short rotation coppice, cereal straw, poultry litter, sewage sludges, and refuse derived fuels. The nature and variability of these materials have been investigated in terms of their moisture and ash content, ash chemistry and ash fusion behaviour. In addition to the raw materials, the residues from small scale and pilot plant operations have been characterised with respect to the chemical composition and microstructure, in order to elucidate the bonding mechanisms and hence the possible reasons for deposition. The technical data obtained in this study should be of value to potential designers and operators of both plant and processes which use biomass as an energy resource.

The high temperature behaviour of biomass and waste ashes has been predicted using phase equilibria and vapour pressure data, highlighting the problems to be anticipated for fuels of a high alkali metal content. In essence, deposits are initiated when a bond forms by the collision and adhesion of particles, facilitated by the presence of a molten or partially molten surface. Consolidation of the deposit subsequently occurs via a viscous flow sintering mechanism. The effect of composition and temperature on the viscosity of liquids formed during ash fusion has been predicted using an Urbain model, emphasising the consequences for ash sintering and the development of deposit strength.

This project is one of two, supported by Mitsui Babcock Energy and the Department of Trade and Industry, which aims to provide data on the basic characteristics of a range of biomass and waste materials relevant to combustion and gasification processes.

Chapter Two

Literature

2.1 Biomass defined

Biomass is an ecological term for photosynthetic matter, from which fuels may be derived in solid, liquid or gaseous form. The term broadly encompasses terrestrial and aquatic plant life, and is also synonymous with animal and human carbonaceous waste products, which are essentially undigested plant residues. Photosynthesis, the source of all conventional fossil fuels, is essentially the conversion of radiant electromagnetic energy into chemical energy which eventually permits the fixation of CO_2 into carbohydrates. Energy may be recovered from carbohydrate molecules (sugars, starches, lignocellulose) by the direct or indirect reaction with oxygen. For the United Kingdom, indigenous biomass resources include traditional fuels such as agricultural, livestock and forestry residues, and those more contemporary such as short rotation energy crops, specialised industrial and hospital wastes, refuse derived fuels (RDFs), sewage sludges and various types of aquaculture.

The accessible resources of a nation play a major role in determining energy policy. Most of the global energy supply comes from finite resources, 77% from conventional fossil fuels (coal, oil and natural gas). Proven world reserves of all coals are estimated to be sufficient for 200-400 years, whereas oil and gas reserves are ~50-55 and ~60 years respectively; these figures are however under constant review as technologies of exploration and recovery are modified and improved, in addition to the fluctuations in the world commodity prices.[1] The geographic distribution of fossil fuel resources is extremely disproportionate throughout the world, causing some countries to rely on substantial imports of coal, oil and natural gas. With the exception of the Netherlands and Denmark, all other EU countries are net importers of energy.[2] The security of a long term energy supply is thus a major concern, and research for biomass-to-energy processes is actively encouraged by the European R&D programme.[3]

The fuels used in electricity generation in Britain are illustrated in Figure 2.1.[4] Coal fired power stations produce ~42% of UK electricity requirements. Due to privatisation and deregulation, new power stations burn natural gas from the North Sea. Ever tightening environmental constraints have led to improved efficiency and lower emissions of NO_x and SO_x using fluidised bed combustion and gasification, flue gas desulphurisation and advanced gas clean-up technologies.

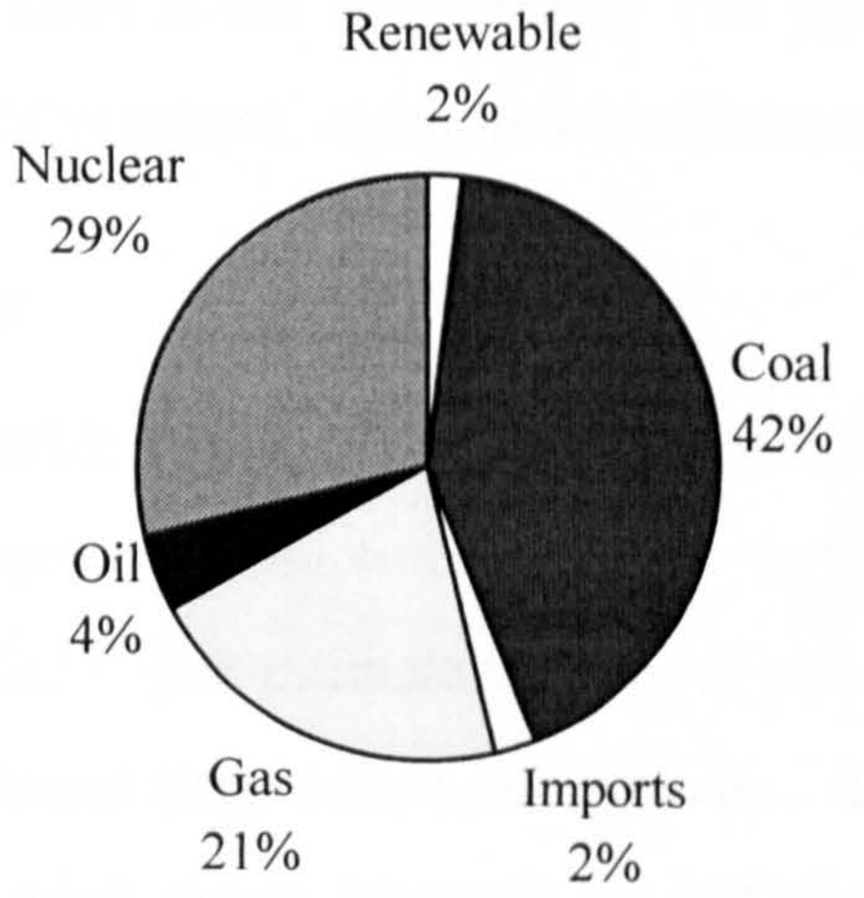

Figure 2.1 Fuels used in UK electricity generation 1996 (energy supplied basis)[4]

2.1.1 Environmental concerns

The environmental problem of most concern at global proportions is that of the 'enhanced greenhouse effect'. Despite particular uncertainties regarding the scientific foundations to the problem, the available evidence suggests that greenhouse gas emissions (CO_2, H_2O, CH_4, N_2O, O_3 and chlorofluorocarbons) have increased over the past 200 years resulting in discernable climate change, and thus warrants the taking of precautionary measures to avert irreversible damage to the atmosphere.

The temperature of the Earth's atmosphere is governed by many factors, but is essentially a product of the interaction of adjacent solar radiation with a variety of compounds in the atmosphere. The absorption of infrared by certain gaseous components of the atmosphere, such as water vapour and carbon dioxide, warms the trophosphere, and subsequently heat is radiated back to the Earth's surface; the phenomenon is known as the greenhouse effect. Research has shown a close correlation between atmospheric CO_2 levels and global temperature. CO_2 is in rapid circulation with the biosphere being removed by photosynthetic processes and solution in the seas, and evolved during plant and animal respiration and the decomposition of organic matter. CO_2 is also produced by the activities of man, notably the combustion of fossil fuels, forest conversion, and the calcination of limestone for cement, and has resulted in a measurable perturbation of the carbon cycle over the last 2-3 decades. Combustion of fossil fuels releases CO_2 fixed by plants over a period of millions of years, and thus increases the CO_2 concentration in the atmosphere. The prudent course is to conserve resources, minimise wasteful practices, and improve efficiency.[5,6]

2.1.2 Renewable energy

Biomass represents a renewable source of energy. Renewable energy is the term used to describe energy which occurs naturally and repeatedly in the environment and can be harnessed for human benefit.[7] The ultimate sources of renewable energy are the Sun, the Earth's rotation and internal temperature, and gravity. The renewable sources thus manifest themselves as the wind, ocean, biomass, the fall of water from lakes and rivers, and animal and human wastes. The extent to which renewable energy technologies are already deployed varies widely throughout the world depending on geographic and climatic features, the comparative economics of other energy systems and the level of

development of the respective technology. In general, the development of renewable energy technologies has yet to attain maturity.

The penetration of renewable sources to the world energy market is significant, providing approximately 20% of mankind's electricity requirements.[8] The supply is dominated by traditional biomass (stem and branch wood, bark, roots, leaves, shrubs, cereal straws, corn stover, cane bagasse, cotton and jute stalks, tuber and legume vines, and animal manures) and conventional large-scale hydro power, with a combined contribution of ~18% to the energy supply of the world.

Renewable energy sources provide approximately 6% of the primary energy production (4% consumption) of the European Community, of which biomass, large-scale hydro power and geothermal energy contribute ~60%, 30% and 6% respectively. The use of renewable sources for electricity generation in Europe is governed by large-scale hydro power, although in recent years there have been increasing contributions from biomass and wind.

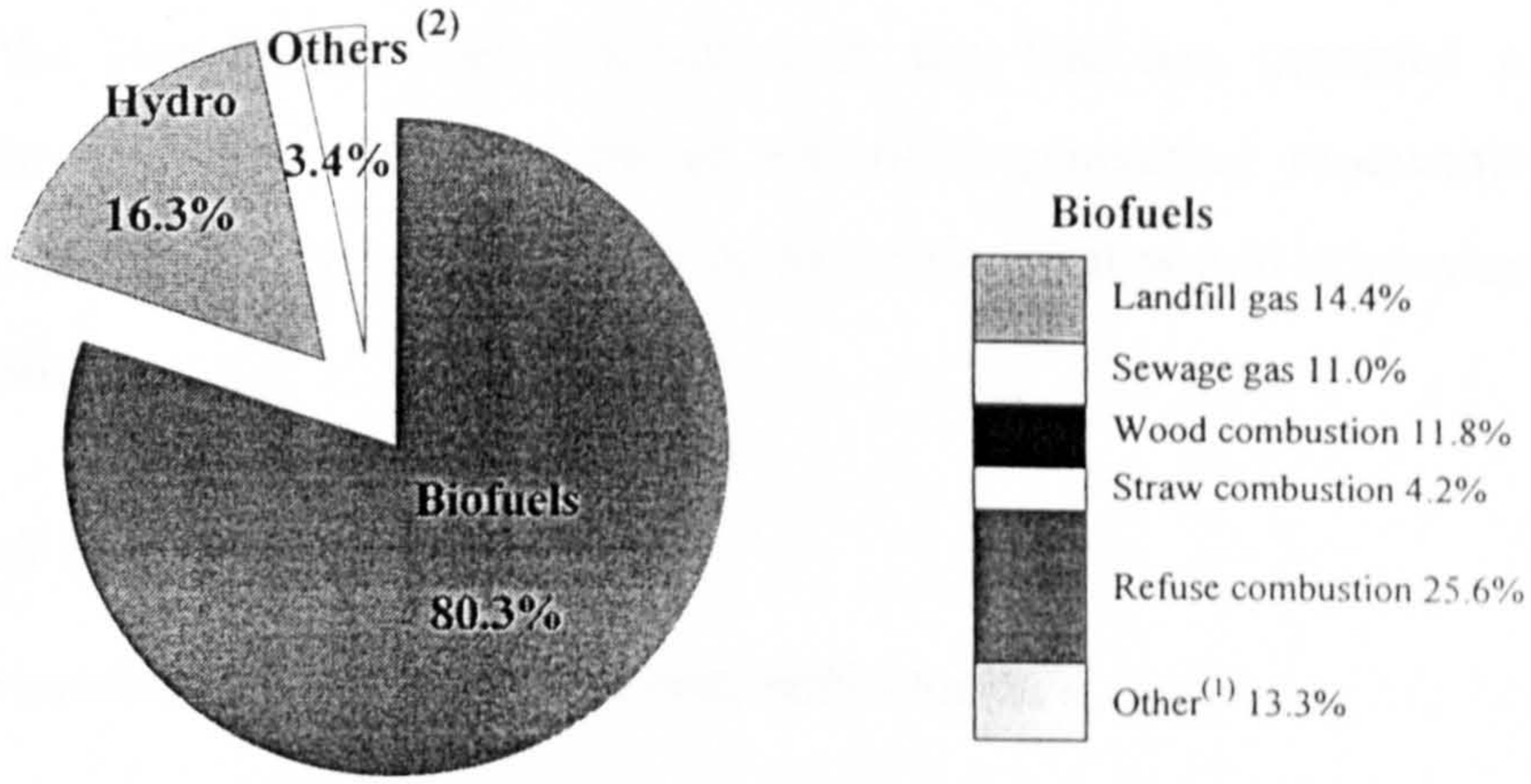

(1) 'Other' includes farm waste digestion and chicken litter, waste tyres, industrial and hospital waste combustion

(2) 'Others' : active solar heating 0.5% excludes all passive use of solar energy, wind 2.4% and small scale hydro 0.4%

Figure 2.2 UK renewable energy statistics, 1996[4]

Within the UK, renewables provided ~2% of the 1996 electricity supply. Figure 2.2 illustrates the renewable energy statistics for 1996 with the largest contribution (80%) from biomass derived fuels, particularly using combustion technologies.[4] The histogram of Figure 2.3 shows renewable energy sources which were used to generate

electricity and/or heat in 1996. Most renewable energy is in the form of electricity, with municipal solid waste (MSW) combustion dominant in terms of measured fuel input.

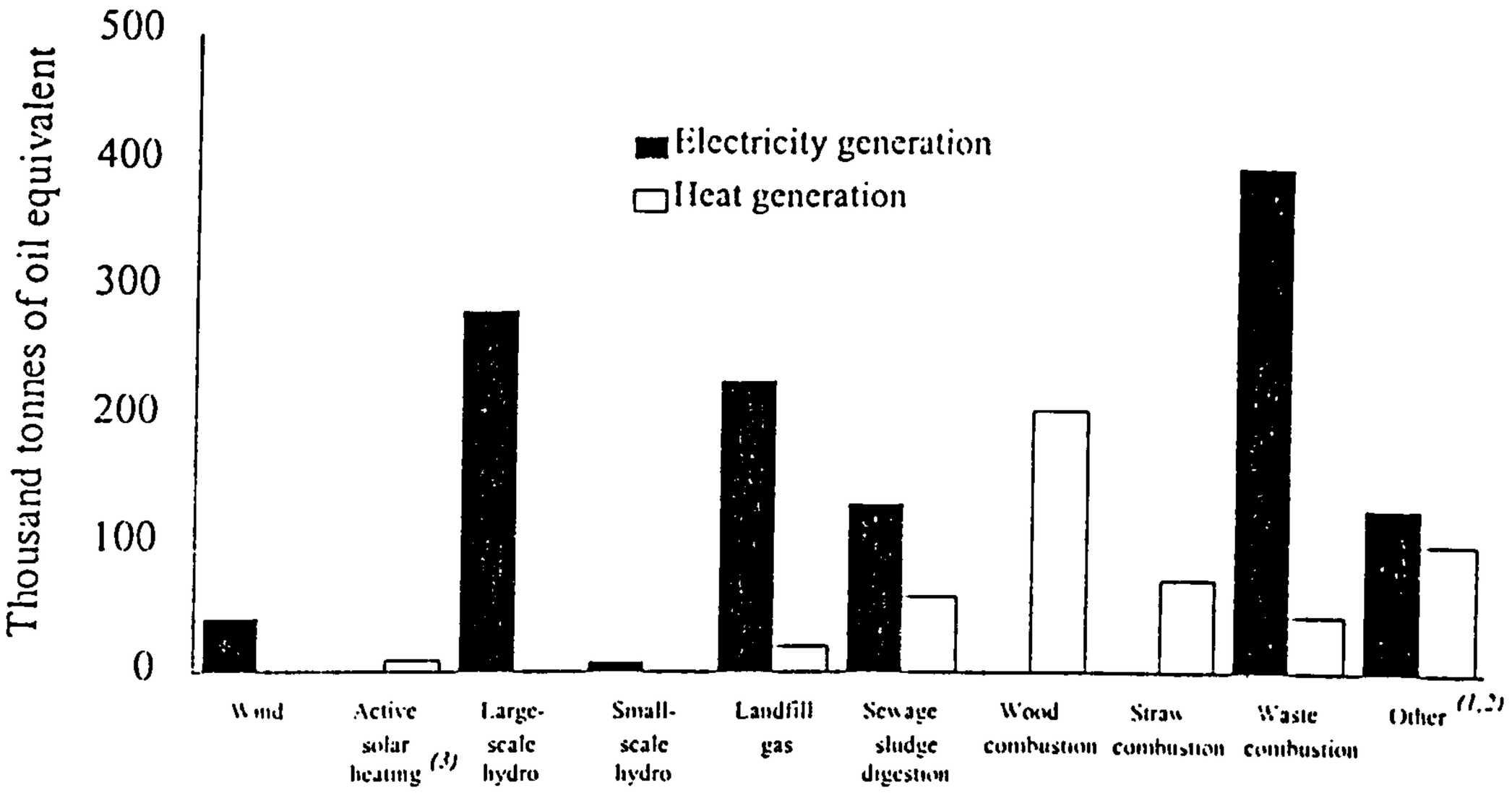

(1) Includes farm waste digestion and poultry litter combustion and waste tyre combustion
(2) Includes industrial and hospital waste combustion and farm waste combustion
(3) Excludes all passive use of solar energy.

Figure 2.3 Renewable energy sources used to generate electricity and heat 1996[4]

The introduction of the Non-Fossil Fuel Obligation in the UK has provided a tremendous impetus for the active development of electricity-generating renewable energy technologies, with a number of projects coming to fruition that would otherwise not have been self-sustaining.

2.1.3 The Non Fossil Fuel Obligation (NFFO)

A guaranteed premium market for electricity from renewable sources

The Government policy regarding renewable energy aims to stimulate the development of new and renewable energy technologies with economically viable and environmentally acceptable prospects, in order to contribute towards

- a diverse, secure and sustainable supply of energy;
- a reduction in the emission of pollutants;
- the encouragement of internationally competitive renewables industries.[8]

The Non Fossil Fuel Obligation (NFFO), introduced with the privatisation of the Electricity Supply industry in 1989, is the major Government strategy employed to implement this policy, prompting the development of an industrial market infrastructure

so that renewable sources of energy are given the opportunity to compete equitably with other energy technologies in a self-sustaining market. The intention to pursue a figure of 1500MW DNC (declared net capacity) of electrical power from UK renewable sources by the year 2000 was documented in The Coal Review White Paper of 1993.

The Electricity Act (1989) and broadly similar legislation in Northern Ireland empowers the relevant UK Secretary of State to make Orders obliging the Regional Electricity Companies (RECs) to contract for a defined quota of non-fossil fuel sourced electricity generating capacity. To secure the necessary capacity, a premium price is awarded to generators of renewable energy with the cost compensated by means of a Fossil Fuel levy on electricity sales. The Obligations arising from such Orders are known as Non-Fossil Fuel Obligations in England and Wales, and as the Scottish Renewable Obligation (SRO) and the Northern Ireland Non Fossil Fuel Obligation (NINFFO).

The strategy focuses primarily upon the technologies with the most potential to contribute economically to the UK electricity supply by the year 2005. The technologies that have been awarded market support via the NFFO include wind power (on-shore), hydro power (small-scale), and energy from municipal and industrial wastes, landfill gas, agricultural and forestry wastes and energy crops. Photovoltaics, fuel cells, active solar and photoconversion are at an early stage of assessment, and technologies such as wave, geothermal and tidal, which are unlikely to contribute significantly by the year 2005, are subject only to a watching brief.[8]

Research, development and field trials in collaboration with suppliers and developers are imperative to assess the technical feasibility and commercial prospects of the technology. Once a degree of commercial maturity is demonstrated, facilitated by the established NFFO market, it is anticipated that the projects will become viable without further financial support.

To date, four renewable NFFO Orders have been made. A summary of the renewable orders is given in Table 2.1.[4] The fourth Order was announced in February 1997. Contracts have been let to 195 projects with a total DNC of 842.7MW, at an average price of 3.46p/kWh.

Table 2.1 Renewable orders and operational capacity[4]

	Technology Band	Contracted Projects Number	Contracted Projects Capacity MW	Live Projects - Operational at 31 December 1996 Number	Live Projects - Operational at 31 December 1996 Capacity MW
England and Wales					
NFFO - 1 (1990)	Hydro	26	11.85	21	10.00
	Landfill gas	25	35.50	20	31.68
	Municipal and industrial waste	4	40.63	4	40.63
	Other	4	45.48	4	45.48
	Sewage gas	7	6.45	7	6.45
	Wind	9	12.21	7	11.66
	Total	**75**	**152.11**	**63**	**145.90**
NFFO - 2 (late 1991)	Hydro	12	10.86	8	10.25
	Landfill gas	28	48.45	26	46.39
	Municipal and industrial waste	10	271.48	2	31.50
	Other	4	30.15	1	12.50
	Sewage gas	19	26.86	19	26.86
	Wind	49	84.43	26	53.91
	Total	**122**	**472.23**	**82**	**181.42**
NFFO - 3 (1995)	Energy crops and agricultural and forestry waste - gasification	3	19.06		
	Energy crops and agricultural and forestry waste - other	6	103.81		
	Hydro	15	14.48	2	0.26
	Landfill gas	42	82.07	25	46.18
	Municipal and industrial waste	20	241.87	1	28.20
	Wind - large	31	145.92	3	6.45
	Wind - small	24	19.71	1	0.21
	Total	**141**	**626.90**	**32**	**81.30**
NFFO - 4 (1997)	Hydro	31	13.22		
	Landfill gas	70	173.68		
	Municipal and industrial waste - CHP	10	115.29		
	Municipal and industrial waste - fluidised bed combustion	6	125.93		
	Wind - large	48	330.36		
	Wind - small	17	10.33		
	Anaerobic digestion of agricultural waste	6	6.58		
	Energy crops and forestry waste gasification	7	67.34		
	Total	**195**	**842.72**		
NFFO Total		**338**	**1,251.24**	**177**	**408.62**
Scotland					
SRO - 1 (1994)	Biomass	1	9.80		
	Hydro	15	17.25	1	0.66
	Waste to Energy	2	3.78	2	3.78
	Wind	12	45.6	4	14.60
	Total	**30**	**76.43**	**7**	**19.04**
SRO - 2 (1997)	Biomass	1	2.00		
	Wind	7	44.00		
	Waste to Energy	9	55.00		
	Hydro	9	11.00		
	Total	**26**	**112.00**		
SRO Total		**56**	**118.43**	**7**	**19.04**
Northern Ireland					
NI NFFO - 1 (1994)	Hydro	9	2.37	5	1.01
	Sewage gas	5	0.56		
	Wind	6	12 66	5	10 61
	Total	**20**	**15.60**	**10**	**11.62**
NI NFFO - 2 (1996)	Biogas	1	0.25		
	Biomass	2	0.30		
	Hydro	2	0.25		
	Landfill gas	2	6.25		
	Municipal and industrial waste	1	6.65		
	Wind	2	2.57		
	Total	**10**	**16.27**		
NI NFFO Total		**30**	**31.87**	**10**	**11.62**
All Renewables Obligations		**619**	**2,314.26**	**194**	**439.28**

The Non-Fossil Fuel Obligation has an international reputation as a policy of success in stimulating the market and manufacturing industry. The continuation of such a policy will enable renewable energy sources to contribute to electricity generation, at market prices, in the medium to long term.

2.2 Short Rotation Coppice (SRC)

The potential of wood, the most traditional of fuels, as a renewable energy source is under increasing scrutiny in Britain. Of particular interest is the development of arable crops farmed by short rotation coppicing techniques. There are several advantageous reasons for such interest in the use of arable coppice as a fuel.[7,10,11]

Agriculture and trade

Perhaps the most powerful impetus towards expanding the use of energy crops in industrial countries will be the opportunity to make productive use of cultivated land no longer required for food overproduction, thus sustaining rural employment.

The potential contribution of biomass fuels to energy independence and security

For the European Community, the prospect of using indigenous biomass as fuel for electricity generation could be a welcome alternative to the substantial imports of fossil fuel resources (some 50%).

Reduced CO_2 emissions by the displacement of fossil fuels

The use of coppice wood as a fuel is environmentally beneficial with no net CO_2 emissions from combustion since the carbon involved is effectively recycled. The combustion of wood also produces emissions low in NO_x and SO_x pollutants.

Local heat and power for rural communities

The technical and commercial viability in using biomass to generate heat and power on a local scale for rural communities is recognised. Apart from generating profit for the promoters, the local farming community would benefit from an increased return over and above that which would be gained under existing set aside rules.

A fertile habitat for wildlife

A positive impact of arable coppice will be the greater diversity of flora and fauna produced within and at the margins of the crop. The diversity will be partly brought about by the less frequent disturbance of the crop and land, since cropping will occur once in every 3-5 years. Furthermore since cropping will be in rotation, the whole field will not be cleared as in the case of food crops: this will create a greater opportunity for wildlife to take advantage of the substantial ground cover.

A further advantage is the possible use of the crop and its fibrous root structure to absorb nutrients from sewage, farmyard slurries and other sludges by acting as a

biofilter. This is potentially beneficial and could markedly improve the prospects for energy crops in areas particularly vulnerable to the effects of agricultural nitrification, for example in East Anglia, where the cultivation of energy crops could prevent leachate run-off and associated eutrophication. Short rotation coppice has found an application in 'buffer zones' to prevent the agricultural pollution (nitrate and phosphate) of rivers in several of the major valleys in Britain. Thus, SRC may be an attractive crop for water companies to cultivate on their own land, or in co-operation with farmers and land-owners.[11]

A potential also exists for the production of energy crops in areas of derelict land in metalliferous mining districts where the soil is often contaminated with heavy metals. Cornwall contains approximately 3200 hectares of land made derelict by mining activity; a legacy of the intensive tin and copper mining history of the area. An assessment of the potential of Cornish soils and mine waste for the growing media of energy crops is in progress, with particular emphasis on the metal tolerance of Miscanthus sinens Giganteous and Alnus glutinosa (Alder).[12] If the crops were to be grown for energy production, it would not be satisfactory to recycle the toxic metals as emissions from a combustion system. In addition, if the ash remaining after the combustion of the crop were to be returned to the plantation as a fertiliser, the heavy metal contamination would be exacerbated. The initial harvest material from the Miscanthus trials indicated that polluted growth media would be unlikely to have a major deleterious effect on the suitability of the feedstock for combustion processes.
The production of energy crops in areas with substrates contaminated by metals is an option which, on agricultural land, may be eligible for set-aside within the EU, while on derelict land, may be established using derelict land grants in the UK.

2.2.1 The Common Agricultural Policy (CAP) Reform

The European Commission introduced a Common Agricultural Policy (CAP) Reform programme during the autumn of 1992 because of the mounting food surplus and the consequent financial burden. An element of the CAP Reform entails the setting aside of a designated fraction of productive arable land for non-food crops per annum, including energy crops. The initial amount set aside was 15% of the eligible arable area which was rotated around the farm to avoid only poorer land falling into the scheme.[7] The

surplus land figure is subject to continuous review in the light of rapid changes in agricultural policy and practice. To compensate for reduced support prices, farmers receive an area payment for eligible arable crops. The benefit of such an approach is that the land will remain productive and not fall derelict, thereby maintaining farm incomes and rural economies.

2.2.2 Short Rotation Coppicing

In essence, biomass of rapid growth is planted in the spring as a high density of unrooted stems (~10,000 trees per hectare). At the end of the season the growth is cut back to within a few centimetres of the ground to initiate coppicing (sprouting a series of stems from the root to the stool), and after two to five years the coppice is harvested in the winter.[13] UK trials have indicated that willow and poplar are decidedly the most suitable species for this method of cultivation, providing high yields and a favourable overall energy balance.

Willow is best suited to a 2-3 year harvesting cycle, and poplar to a 2-5 year cycle. The latter, on a five year rotation, requires less dense planting (~6,700 trees per hectare) and will be adopted where existing forestry equipment and expertise is available. In each case, the average yield is in the range 10-15 dry tonnes per hectare per year.[7]

Other energy crops under research elsewhere in Europe include the C4 grasses such as Miscanthus (non-native species to the UK) which bear resemblance to coppice in that they are perennial in nature and are harvested annually each winter using similar machinery. The potential advantages offered by the C4 grasses are that at harvest the fuel is relatively dry (most of the stem moisture being translocated into the rhizome) and that the yield potential is significantly greater (15-30 dry tonnes per hectare).

Combustible biomass fuels such as wood and Miscanthus have a calorific value of around 19MJkg^{-1}. The calorific value of these fuels falls linearly with increasing moisture content such that at 55% moisture by weight (the typical moisture content at which wood is harvested) the CV is around 10MJkg^{-1}.[7,14]

Drying and Storage

Storage of the harvested material collected during the winter months, December to February, would be essential in order to provide a continuous supply of fuel throughout

the year. During storage (which can be of cut sticks or chipped material) some drying will occur either naturally by the ambient air and via respiration, or by way of forced draught ventilation as in a grain store.

Freshly harvested, the moisture contained within the crops presents a breeding medium for degenerative pathogens like fungus, which not only diminish the value of the fuel by loss of material, but also constitute a health hazard during the drying and handling of the material due to the liberation of spores. Furthermore, in a large stockpile of material, there is a significant risk of over-heating and self-ignition.

The arable coppice may be harvested as whole stems ('sticks') or by cutting and chipping in a single operation. Provided there is land available for the storage of whole sticks, drying would occur naturally with negligible associated dry matter loss. However the handling of the whole sticks would be more cumbersome and a larger storage area would be required; furthermore the dry stems are more difficult to comminute than the freshly harvested material. Cutting and chipping in one operation presents fewer handling problems, yet the increased surface area of the comminuted wood is more amenable to microbial degradation and thus creates drying and storage problems.[7,11,14]

Siting of the energy crop production projects will occur in rural areas. The arable coppice will be extensive but not over-intrusive since it will be grown like other agricultural crops in traditional field settings. The height of arable coppice, particularly in the third and final growing season before cropping, will be several metres. Due to the long production cycle of coppice and the use of rotational planting, the general visual appearance will be stable but there will be continual variations within the crop.[7]

Arable coppice and the perennial C4 grass plantations have a life expectancy of 30 years and premature change of use will require tree stump and root removal before other uses can be made of the land. However, this is a relatively easy operation (unlike conventional forestry) and the land can return to food cropping in one season. The ease with which land previously under SRC can be converted back to normal agricultural use is an incentive to comply with the Sludge (Use in Agriculture) Regulations concerning the maximum permissible levels for heavy metal accumulation on agricultural land.[7,11]

Since the crop, of deciduous nature, is harvested in the winter many of the nutrients in the soil are replenished by leaf fall and decomposition. The recovery of nutrients from senescing leaves can contribute 60-80% of the nutrients required for new growth the following season.[14] Nonetheless, in order to obtain the greatest crop yields and hence maximum profit, a fertiliser is necessary. Inorganic soil additives such as phosphate rock, potash and sulphur are earth's resources mined principally to provide nutrients for soils. Worldwide, in excess of 90% of phosphate rock and potash, and approximately half of the sulphur produced are used for agricultural purposes. Potash cannot be reclaimed or recycled and there is no known substitute.[15] Due to the high energy input required during manufacture, the use of inorganic fertilisers would appear to defeat the purpose of cultivating an energy efficient crop. The DTI and Anglian and Severn Trent Water Service companies are supporting research into the nutritional management of SRC and in particular the application of sewage sludge on the plantation.[10]

Sewage sludge has several advantages over inorganic fertilisers. The sludge may be applied to the growing crop in liquid form, when access for conventional granular fertiliser spreaders is severely restricted. Consequently, it may be applied more frequently than the inorganic fertiliser which may practically only be applied after harvest. Sufficient inorganic fertiliser must then be applied to sustain growth for several years, depending on the rotation period, during which time substantial nutrient losses through leaching and denitrification may occur. Regular applications of sludge may better satisfy the crops' nutrient demand. Sludge will be supplied and applied free of charge, hence greater crop yields may be obtained with no increase in cost to the farmer.[15]

Many potentially toxic metals are also essential plant nutrients, hence mechanisms exist for their absorbtion and translocation through the plant structure. The accumulation of heavy metals in the tree stems could potentially be a source of metal diffusion into the atmosphere when the wood is combusted. Metal uptake and partitioning by different clones is being monitored during trials to investigate the extent to which this may limit the application of sludge to coppice. It is not anticipated that metal uptake in trees will limit sludge use in SRC since the woody species are generally low accumulators of heavy metals. The concentration of heavy metal elements in plant tissues is found to be

of highest concentration in the roots, less so in the leaves and at the lowest level in the stems. Consequently, metal export from the plantation is likely to be minimal.[12,15,17]

2.2.3 The inorganic matter in woody stems

The ash contents of wood and Miscanthus are only 1 or 2wt% (dab).[7] The fundamental elements that constitute carbohydrates, fats and proteins (carbon, hydrogen, oxygen, nitrogen, phosphorus and sulphur) are accompanied by other indispensable elements that have no obvious link with organic substances but nonetheless appear essential to plant life. These essential nutrients include potassium, calcium, magnesium and iron. The elements boron, copper, manganese, molybdenum, zinc and chlorine are also requisite micro-nutrient constituents of particular enzyme systems.

Elucidation of the function of mineral elements in plant nutrition remains far from complete. The typical range of macro and micro-nutrient elemental concentrations in the foliage of a variety of plants is shown in Tables 2.2 and 2.3.[18] The distribution of inorganic material within plant tissues is largely heterogeneous. Furthermore, some species are more selective of particular elements than others.

Table 2.2 Range of macro-nutrients in leaves of normal plants (ppm in dry matter)[18]

ELEMENT	N	P	S	Ca	Mg	K	Na	Fe
Concentration (ppm, dab)	15000 - 35000	1500 - 3000	1000 - 3000	10000 - 50000	10000 - 25000	15000 - 50000	200 - 2000	50 - 300

Table 2.3 Range of micro-nutrients in leaves of normal plants (ppm in dry matter)[18]

ELEMENT	Mn	B	Zn	Cu	Mo	Co	Cl
Concentration	25 - 250	15 - 100	15 - 75	5 - 15	0.5 - 5	0.2 - 29	100 - 1000

All the elements fulfil an important physiological function in maintaining an acid-base equilibrium. Potassium, which is generally the most abundant cation in the sap of plant cells, is an osmotic regulator, but must be balanced by its antagonists, principally magnesium and calcium. Magnesium is a constituent of chlorophyll, the essential photocatalyst of photosynthesis, and is also associated with many plant proteins.[19]

The function of calcium in plant metabolism is less well understood. It appears that calcium is implicated in some way with membrane stability, with the maintenance of

chromosone structures and with the activation of many enzymes. Calcium may be found in significant concentrations in cell walls as the insoluble salt of pectic acid. It appears that calcium pectate acts as a cementing agent in the cell wall thereby increasing the rigidity of the structure. Other acid radicals include carbonates, phosphates, silicates, sulphates, and oxalates. The inorganic matter is found to be distributed throughout the cell wall or as accumulations in the form of crystals or amorphous deposits.[18,20,21]

The lumina of living and dead wood cells may contain a variety of substances described as cell inclusions or extraneous materials. The main inorganic inclusions found in a wide variety of plants and woods are crystals of calcium salts and silica grains. The most common consist of calcium oxalate deposits, although other crystals in the cells include the calcium salts of phytic acid, and in certain seaweeds calcium carbonate provides a hard articulated external casing. More rarely, calcium phosphate cell inclusions have been reported. Calcium salts do not occur widely in plants as supporting structures in contrast to their widespread use as skeletal and protective structures in the animal kingdom. Calcium oxalate crystals are usually formed close to the surface of the plant. It is believed that the morphology, hardness and relative insolubility of calcium oxalate crystals serve to deter chewing insects and moluscs. It appears that water in the xylem evaporates from mature photosynthetic tissue to precipitate calcium oxalate.[18,20,22,23]

Calcium oxalate crystals have been found in a variety of shapes and sizes, and occur mainly in wood species. The calcium salts tend to develop as either 'rhomboidal' structures occupying almost an entire cell, or as bundles of needle-like parallel crystals termed 'raphides'. Silica is deposited as grains, 'crystal sand', or amorphous granulated lumps and are a feature of the axial and ray parenchyma cells of certain woods, particularly tropical woods.[22,23]

The micro-elements also have specific functions in plant metabolism. For example, iron is an element of the organic molecule that ensures cellular respiration. Zinc appears to be involved in the biosynthesis of enzymes and hormones, boron in the transport of carbohydrates, and chlorine in an essential stage of photosynthesis. As for manganese, of which plants may abstract excessive quantities from the soil, trace amounts can

activate a whole sequence of enzyme catalysed reactions. Molybdenum is the essential trace constituent for the enzymatic mechanism for the reduction of nitrates.

2.2.4 Nutrients of the soil

Unlike the major cell wall components such as cellulose and lignin, the nature and amount of the inorganic material has been reported to vary to a great extent with the environmental conditions under which the wood is cultivated, in particular the nutrient status of the soil. Calcium, potassium and magnesium occur in the soil mainly in inorganic compounds but significant amounts are associated with organic materials in humus. The larger part is present in minerals such as feldspar, biotite, montmorillonite and anorthite in combined forms which are not directly available to plants but from which the elements are released as exchangeable and soluble cations by weathering. Most of the exchangeable K, Ca and Mg are associated with clay particles. Both the chemical and physical properties of the clay component of a soil have a direct bearing on the plant life which the soil supports. The bulk of the sulphur in fertile soils is present as insoluble minerals such as pyrite (FeS_2), sphalerite (ZnS), chalcopyrite ($CuFeS_2$) which are slowly oxidised to sulphates, and gypsum ($CaSO_4.2H_2O$). Most of the inorganic phosphorus occurs as iron and aluminium phosphates and also in association with clay minerals. These nutrients are absorbed from the soil in the oxidised forms (SO_4^{2-} and $H_2PO_4^-$).[24]

Fuels may be derived from crops in solid, liquid and gaseous form. The methods of converting crops to biofuels are varied and reflect the diversity of the biomass resource. The drier, lignin-rich materials (wood for example) are best converted by thermal processing (combustion, gasification and pyrolysis). Biomass of a higher moisture content can be converted to either a liquid or a gaseous fuel through biological processing (fermentation under anaerobic conditions). In the latter case, anaerobic digestion will yield a methane-rich biogas of medium calorific value. Other fermentation techniques can yield liquid fuels, the most important of which is ethanol. More recently the conversion of rapeseed oil via esterification to a diesel substitute has received much attention.[7]

2.2.5 The Enniskillen CHP Unit

The first combined heat and power installation in the UK fuelled by short rotation willow is operational at Enniskillen Agricultural College, County Armagh, Northern Ireland. The CHP unit consists of a Belgian designed Louvain-Martin downdraft gasifier, a gas clean-up train, and an Iveco 100kW$_e$ dual fuel generator set. Exhaust heat is used to dry the fuel on an under-floor ventilated system, and the jacket heat preheats the central heating water returning to the boilers from the college. The annual consumption of SRC wood chips is 489 tonnes at an average moisture content of 25%.[11,25]

2.2.6 The THERMIE programme

In 1990, the Directorate-General for Energy (DGXVII) of the European Commision launched a programme called THERMIE, with a budget of 700 million ECU, to foster innovative non-nuclear energy technologies under four categories: rational use of energy, hydrocarbons, solid fuels and renewable energy. In principle, the THERMIE programme was prepared to offer financial support to projects involving major investment, up to the scale of demonstration plant.[10]

The THERMIE programme is promoting a biomass gasification project, entitled Project ARBRE (Arable Biomass Renewable Energy). The project is a joint venture conducted by AEP (Associated Energy Project), TPS (Termiska Processer) and Yorkshire Environmental, a subsidy of Yorkshire Water and leader of the consortium. TPS Termiska Processer is an independent Swedish company, formerly part of the Swedish energy engineering group Studsvik and now owned by a group of Swedish municipal energy suppliers and the Federation of Swedish Farmers. For more than ten years the group, known as TPS, has been involved in advanced combustion and gasification technology of biomass fuels, including wood, and more prominently refuse derived fuels (RDF). TPS developed a design for a circulating fluidised bed gasifier operating at atmospheric pressure, suitable for gasifying biomass including RDF; two 15MW$_{th}$ units based on the design have been operating in Greve-in-Chianti in Italy since 1991, gasifying RDF.[10] TPS has placed particular emphasis on gas clean-up technology,

including a proprietory tar cracking technology, essential if the fuel gas from the atmospheric pressure gasifier is to be compressed to feed a gas turbine.

AEP, a subsidy of a French Water Company, are the part owners of the SELCHP (South East London Combined Heat and Power) municipal solid waste incinerator.

The prospect of applying sewage sludge as a fertiliser for the SRC is an attractive means of sewage sludge disposal in light of the international agreements to prohibit the disposal of sludge at sea. Thus Yorkshire Water have a vested interest in Project ARBRE.

Project Arbre has also received NFFO support, the premium price of electricity secured at 8.75p/kWh.

A $10MW_{th}$ circulating fluidised bed gasifier designed to accommodate biomass in the form of SRC is proposed. Willow of a three year cropping cycle, is to be cultivated on 2000ha of land, some of which is registered as set-aside, specifically as fuel dedicated to the project, with the plant in commercial operation by 1999. The yield of SRC is expected to be of the order 12 dry tonnes per hectare per annum. Initially, whilst the SRC is reaching harvesting maturity, wood chips derived from local woodland and forestry management practices will be required.

The plant will incorporate a tar cracker with a dolomite catalyst, a conventional gas cleaning facility (a hot cyclone, bagfilter and wet scrubber), and a gas turbine configuration linked to a steam turbine via a heat exchanger (boiler). Gases leaving the tar cracker at a temperature of ~900°C contain entrained particles of ash and dolomite. The adjacent boiler is designed to cool the exit gases to the region of 200°C for the Teflon based bagfilter. On the pilot plant, the Shell cooling boiler experienced fouling problems, even on runs of short duration. A comprehensive analysis of the fuel ash characteristics is a prerequisite to the successful design and operation of the plant.

2.3 Poultry litter

Poultry litter is composed of droppings, feathers and bedding material (up to 10% straw or wood shavings) and is removed from broiler houses where birds are intensively reared for meat production. Approximately 1.8 million tonnes of poultry waste is

produced in the UK per annum and disposal presents an escalating problem.[26] The traditional method of disposal has been by direct use as a fertiliser, yet in some instances the local production outweighs demand and the material is landfilled. These disposal routes have the potential to cause contamination of ground water by nitrate leaching from the litter, with fines for the adulteration of watercourses as much as £20,000 per offence.[7] The Government has announced plans for a restriction on the application of organic manures on land vulnerable to nitrate saturation, to comply with the EC directive which aims to protect water from nitrate pollution. The compulsory measures, enforced in 1996, include a limit of 210kg per hectare of nitrogen for organic manure, a closed period for slurry spreading on grassland between September and November, and on other land between August and November. Records of all fertiliser application will be obligatory. With ample quantities of litter available, and with the tendency to use it close to where it is produced due to high transport costs, certain parts of the country are becoming saturated with the phosphates and potash contained in the fertiliser. Alternative, environmentally acceptable disposal routes lie in its use as a potential fuel to provide energy for the space heating of broiler houses or for larger schemes involving power generation or combined heat and power. Poultry litter has a calorific value of 13.5MJkg^{-1}, about half that of coal.[13] The ash remaining after combustion retains much of the original phosphate and potash but none of the nitrates, making the ash a useful fertiliser which is sterile, creates no odour, and is easier to handle and cheaper to transport than the poultry litter itself. The ash can be sold as a fertiliser for about £40 per tonne.

2.3.1 The Eye power station

A 12.5MW$_e$ poultry litter fired power station is now operational at Eye in Suffolk. The Fibropower plant, commissioned in July 1992, is the world's first commercial power station fuelled by poultry litter. The fuel is gathered from around 200 local intensive chicken and turkey farms within a 40km radius of the site; 30 lorries, each bearing 25 tonnes of litter, arrive every day. Once transported to the power station, the litter is stored in a specially designed fuel hall at a sub-atmospheric pressure, to ensure that odours and dust are contained within the plant.[27] The combustion system is a 56MW$_{th}$ water-tube boiler fitted with a hearth comprising of four reciprocating grates. The boiler

consumes approximately 16 tonnes of fuel per hour providing steam at 65 bar and 450°C to a condensing turbo-alternator.[26] The boiler is a three pass, natural convection system, with an economiser and two banks of superheaters.

Ash from the bottom of the furnace and fly ash from the electrostatic precipitator are retained for sale as a nitrate-free fertiliser, 'Fibrophos'. The fertiliser is rich in phosphate (at least 24wt%), potash (12wt%) and lime (14wt%), and contains additional plant nutrients (3wt% magnesia and 5wt% sulphate) and essential trace elements which include manganese, copper, cobalt, zinc, molybdenum, chlorine, iron, sodium and boron.[28]

As designed, the boiler suffered from severe slagging and fouling when first operated. Slags formed readily on the water walls and excessive formation of deposits occurred in the convective passes on both the superheater and economiser heat transfer surfaces. This problem has now largely been overcome with the addition of sootblowers to both the boiler and the convective pass regions.

A second power station, commissioned in 1993, is also in function at Glanford, Humberside. The boiler, rated at 13.5MW_e, involves a combustion system more complex than at Eye, and comprises a plate-chain grate fitted with a spreader stoker. The fuel handling system is designed to break up large agglomerations of litter and remove stones and other contraries. Initially, a NFFO contract was secured for each power station, under the first and second Renewables Orders. Thus a guaranteed market for electricity at a premium price has been established making poultry litter a renewable source which is economically competitive with traditional methods of power generation.

Following the commercial success of the Eye and Glanford plants, a larger electricity generating power station of 38MW_e is proposed for Thetford, Suffolk.

Legislation to control the current disposal practices of poultry litter and other animal slurries is becoming ever more stringent. Interest into biomass-to-energy schemes is expected to grow since they provide an environmentally acceptable disposal route and generate revenue from heat, electricity and fertiliser sales.

2.4 Forestry residues

Forestry wastes arise as the result of forestry management practices designed to yield a timber crop. Production cycles for timber vary from 40-80 years for conifers, and 80-120 years for hardwoods.[8] The greatest commercial value of the tree lies in the stem; straight, knot-free stems in particular. This is achieved by planting the trees in close proximity to stimulate rapid, straight growth. Subsequent thinning operations continue throughout the year to maintain the maximum rate of growth and improve the quality of the stand by removing defective or misshapen trees. At the final harvest (clearfell) only the stem is removed. The residues (branches, thinnings and tree-tops) which are not desired remain on the forest floor as brash. Brash comprises some 30-40% by weight of a tree for conifer crops and over 50% for deciduous crops. Each year around 4 million tonnes of residue material is produced post-harvest.

Most forest owners do not harvest their own trees but employ a contractor. The trees are often sold standing, after negotiation with the harvesting contractor, yet the residues usually remain the property of the woodland owner and a second contractor may be hired to clear the site.[7] Removing the brash from forest sites aids replanting and minimises the risk of pathogen infection for the new crop, but can deplete the soil of nutrients. In recent years, particularly in Southern Europe, a number of serious forest fires have resulted from the presence of decaying residue on the forest floor.

The markets for the products of forestry thinning operations (small roundwood) are varied. The main use is in paper and particle boards, but traditionally other markets such as pit-props and fencing have been significant, though these are now in decline. However, all these markets tend to be volatile and subject to interference from cheap imports from Europe and Canada. Clearfell residues have a less well defined outlet. Given the nature of the resource, it is common for the wood to be left on the forest floor to rot. Where the material is recovered, it is comminuted (usually by chipping) to decrease the handling costs. Wood chips can be marketed for horticultural mulch or equestrian flooring.[7]

The brash may be used as a fuel. Wood has a net calorific value of around 19MJ per dry kg, irrespective of tree species. The wood of a felled tree contains varying amounts of moisture, depending upon the species, type of tissue and position within the tree. For

example, the moisture content (expressed as a percentage of the dry weight) can range from as low as 35% in the heartwood of Douglas-fir to as high as 300% for old growth redwood. On average, freshly harvested wood has a moisture content of the order 55% by weight. The calorific value at this moisture content falls to 10MJkg^{-1} or so. Hence the removal of moisture by drying prior to combustion will improve the net calorific value; it is also a prerequisite operation for some designs and types of combustor or gasifier. Drying may be assisted by enhanced ventilation or forced moisture extraction in a grain dryer. Using such techniques, a water loss of 25-40 % may be achieved over a 48 hour time period.

In the UK, electricity generation from wood is restricted to locations where sawmill or paper making residues are co-fired with fossil fuels in existing CHP plants. The extent to which this practice is currently employed is unknown, but it is unlikely to yield more than a few megawatts of power. By comparison, electricity generation from wood is commonplace in North America with 6000MW$_e$ of installed capacity. In Scandinavia wood fuel is routinely used in district heating plants.[7]

The ash produced from combustion of the wood fuel presents few disposal problems as it is not contaminated and has value as a fertiliser. Indeed, in Scandinavia the ash is routinely returned to the forest as a means of nutrient recycling.

2.4.1 Wood ash composition

Wood has a complex structure which is composed of three major organic substances, cellulose, hemicellulose and lignin, all polymeric in nature.[29] Wood wastes such as pine sawdust average about 50% moisture, 40% volatile matter and 10% fixed carbon, and have an ash content of less than 1wt% of the dry wood. It is apparent from the literature that the physical and chemical properties of wood vary widely not only with species but also with the available mineral nutrients of the growth media. The range in composition of wood ashes from various species of tree is given in Table 2.4.[30]

Table 2.4 Range of ash composition in wood ash[30]

OXIDE	SiO_2	Fe_2O_3	CaO	MgO	K_2O	Na_2O	P_2O_5	SO_3
wt% (dab)	2 - 7	1 - 2	30 - 60	5 - 10	10 - 30	2 - 15	5 - 15	1 - 5

Calcium, potassium, sodium and phosphorus are the dominant elements in a wood ash, in comparison with silicon, aluminium and iron in a coal ash. Wood combustion therefore produces a highly alkaline ash (pH 9-13.5).[31] The ash may be used in a variety of agricultural applications since it is an excellent source of potash (K_2O), lime (CaO) and other plant nutrients. Alternative markets exist, including the application of wood ash as a binding agent, a glazing base for ceramics, a road base, an additive in cement production, and an alkaline material for the neutralisation of wastes.

Table 2.5 Composition of wood ash (in ppm) as a function of combustion temperature[31]

ELEMENT (ppm)	TEMPERATURE (°C)					
	538	649	760	871	982	1093
Silicon	33867	39777	42647	31997	46477	35267
Aluminium	10415	12825	13115	10115	13415	11015
Iron	8796	11951	9981	8219	22411	16781
Calcium	187480	217480	241180	216080	238980	264580
Magnesium	59730	68060	76970	69170	80470	89100
Potassium	110500	86590	47720	79860	51970	4026
Sodium	2961	4947	4365	1643	1479	<100
Phosphorus	16950	19060	21720	19370	21030	25460
Manganese	10549	11789	13489	11859	16609	21680
Titanium	780	1060	1012	777	957	796

The physical and chemical characteristics of Lodgepole pine sawdust ash have been reported by Etegni and Campbell.[31] The results, shown in Table 2.5, constitute a more detailed wood ash composition, and show a temperature dependence of the wood ash yield and composition. The ash content was found to decrease by 45% as the combustion temperature was raised from 500 to 1200°C. The reduction in ash content with temperature was caused by the progressive volatilisation of alkali metal (K, Na)

compounds. Using X-ray diffraction the major components of the wood ash were found to be lime, calcite, portlandite [$Ca(OH)_2$] and calcium silicates.

The inherent ash content of bark from various trees lies between 0.5 and 5wt% and is five to ten times greater than that of the whole wood. Typical ash analyses of various kinds of wood bark are shown in Table 2.6.[30] However, the bark residue from timber production processes is often severely contaminated by soil, gravel and sand. Subsequently, the ash content is considerably increased and the ash chemistry altered. A detailed analysis of all parts of various trees indicates that the nitrogen concentrations in bark are 3-9 times higher than those in wood (~0.1%), which is important in evaluating the amount of prompt NO_x produced and the consequential impacts on the environment.

Table 2.6 Typical ash compositions of various wood bark[30]

OXIDE (wt%)	Douglas fir	Cedar	Lodgepole pine	Spruce
SiO_2	13.9	44.0	12.2	32.0
Al_2O_3	8.7	13.8	8.7	11.0
Fe_2O_3	4.4	7.2	5.6	6.4
CaO	51.4	13.9	48.0	25.3
MgO	3.2	3.1	1.8	4.1
Na_2O	5.3	6.6	8.4	10.4
MnO	0.3	0.1	0.2	1.5
TiO_2	0.4	0.8	0.3	0.8
SO_3	2.9	3.1	3.3	2.1
Cl	0.4	0.7	0.4	Trace

2.5 Straw

Agricultural wastes include stems, leaves, roots, seeds and chaff. In Britain the major crop residues are the cereal straws such as wheat, barley, oats and rye. Straw is also available from other crops such as oil seeds. The production of straw is seasonal and localised, with the greatest straw density in East Anglia. An estimated 13.7 million tonnes of straw are produced at cereal harvest in the UK each year, of which half is baled for animal bedding and roughage, and to fuel small on-site boilers for heating farmhouses.[8] The remaining residues are waste. Former tradition was to burn the

residues in the fields along with the stubble, however since the harvest of 1992, EC legislation condemns such practices. At present the straw is ploughed back into the soil. This practice does have some value as direct nutrient replacement on some soils, but deep cultivation is often required and this is a highly energy-intensive process. In addition there is some doubt as to the long-term viability of this disposal option for particular soils. This provides a strong incentive to develop alternative uses for crop wastes. Arguments have been made that the removal of straw will rapidly deplete the soil of valuable nutrients and accelerate soil erosion. However current harvesting machinery does not pull out the plant roots which contain many more nutrients than the stems and leaves.[32] The attraction of agricultural wastes for potential fuels is that the cost of producing the fuel is included in the cost of producing the primary crop, and the additional expenses are for harvesting, storage and transportation of the residue itself. These costs may, however, be considerable given the low bulk density of the residues and the large areas over which they are distributed.

The level of straw production will ultimately be reduced by reform of the Common Agriculture Policy (CAP) by the EU. A main element of this policy is Set-Aside, which is a measure to reduce the overproduction of food by effectively subsidising farmers to leave parts of their land fallow. In 1993, 15% of arable land was eligible for set-aside.[7] There is some evidence that introducing a fallow year into the cropping cycle actually leads to increased yields in the following years.

The use of straw as a fuel is commonplace at the small scale (up to 100kW$_{th}$), using whole bale burners mainly for on-farm domestic space heating[4]. The only country exploiting straw for electrical power generation is Denmark, where taxes on imported fossil fuels make the conversion of agricultural wastes such as straw economically attractive. Originally the taxation was introduced as the result of the energy crisis in the 1970's increasing the price of fossil fuels. At that time, prior to the development of the Danish gas fields, almost all Denmark's fossil fuels were imported. The tax is now retained for environmental reasons. In Denmark, the energy produced is mainly used in district heating plants, although power generation via CHP schemes at around 30MW$_{th}$ is also in commercial operation.

2.5.1 Straw ash characteristics

Straw is a material of low bulk density averaging 15% moisture at the time of harvesting, 70% volatile matter, 15% fixed carbon, and less than 8% ash on a dry basis.[33,34] At this moisture content the calorific value of straw is approximately 15MJkg^{-1}, about half that of coal, and this value is independent of straw type. A considerable variation in the ash contents and ash compositions of several cereal crops is reported.

The range of ash contents and compositions of several cereal crops, are given in Table 2.7, which has been compiled from the results obtained by Livingston[33] and Ghaly[34]. The diversity of data from one location to another may be attributed to the difference in soil quality and pH, climate, irrigation practices and fertiliser applications. As with wood fuel, the ash left after straw combustion has value as a fertiliser and can be returned to the soil.

Table 2.7 Ash content and composition of cereal straws[33,34]

Wt%	Cereal				
	Wheat	Barley	Oats	Rye	Rape
Ash content	3 - 4	3 - 6	4 - 8	2 - 6	2 - 3
SiO_2	27 - 70	26 - 54	15 - 66	40 - 47	8 - 12
Al_2O_3	<1 - 1	<1 - 6	<1 - 5	1 - 6	<1 - 3
Fe_2O_3	<1 - 1	<1 - 3	<1 - 3	1 - 3	<1 - 4
CaO	8 - 15	6 - 12	3 - 9	8 - 16	40 - 47
MgO	1 - 5	2 - 4	2 - 7	4 - 6	4 - 5
K_2O	12 - 51	9 - 41	10 - 41	14 - 18	8 - 17
Na_2O	<1 - 2	<1 - 1	<1 - 2	1 - 2	1 - 3
P_2O_5	3 - 10	4 - 7	3 - 9	6 - 9	3 - 6
SO_3	1 - 3	1 - 3	<1 - 2	<1 - 1	2 - 3

The major problem associated with the use of cereal straw as a fuel is the low temperature at which ash fusion occurs, and the high volatility of alkali species. This can lead to boiler slagging and fouling, and necessitates careful design and good combustion control. This is less of a problem with oilseed straws, which produce ashes with a higher melting point.

The oil seed rape straws have significantly higher levels of CaO and lower levels of SiO_2 than the cereal straws. Lime is a refractory compound with a melting point of ~2580°C in isolation. Potassium compounds act as fluxes for the more refractory materials, yet with a high CaO content, the Ash Fusion Temperatures (initial deformation, softening, hemispherical and fluid temperatures) are relatively high with an IDT of 1300°C and complete fusion occurring at 1400°C. The rape straw ash is hardly an aluminosilicate or silicate system but behaves as a complex mixture of salts.[33] The initial deformation temperature corresponds to the temperature in an operating furnace at which the particles of ash, in transit through the furnace, have been cooled to a point where they still retain the slight tendency to sick together and slowly form a deposit on heat exchange surfaces.[35] The IDT varied from 900°C for wheat straw ash to 1000°C for oat straw ash under reducing conditions; the ash fusibility temperatures are generally of a higher value in an oxidising atmosphere. This indicates that to avoid slagging problems during the gasification of the majority of straws under review, the temperatures should be kept below 900°C.[34] The inorganic residues in these straw samples were found to consist of a mixture of SiO_2, either in amorphous form or as quartz, and inorganic salts, principally phosphates, carbonates and hydroxides of the alkali and alkaline earth metals.[33]

As with other biomass fuels, co-firing with coal is a feasible option to give benefits of higher conversion efficiencies in a larger plant, shared costs for infrastructure, capital, and labour, and reduced emissions from the fossil fuel. However, co-firing with coal is likely to increase maintenance costs of the fossil fuel plant and the risks of boiler slagging and fouling. Furthermore, by co-firing with a fossil fuel the ash creates a disposal problem.

2.6 Municipal Solid Waste

Wastes produced by households, industry and commerce (municipal solid waste, MSW) pose a difficult, costly and potentially hazardous disposal problem. It is estimated that 30 million tonnes of household refuse and 25 million tonnes of combustible general commercial and industrial wastes are generated in the UK each year.[7] Table 2.8[36] is a digest of the annual occurrence of a variety of wastes in Great Britain, including household, commercial and industrial wastes.

Municipal solid waste (MSW) is a most heterogeneous material, with the quantity of any particular constituent subject to variation depending upon the location and season. The average content of MSW is shown in Table 2.9.[37,38] Cellulosic materials, including paper, newsprint, packaging materials and food wastes constitute over 50wt% of MSW. The remainder is a mixture of mineral fines (from domestic vacuum cleaners), metals, glass, textiles and plastics. The moisture content of MSW may range from 15 to 30%, although it may occasionally be higher depending on the climate.

Also summarised in Table 2.9 are the typical heating values (on a dry basis) of various MSW components.[38] These values indicate that MSW is a potential source of energy, with the bulk calorific value averaging 9 $MJkg^{-1}$ for household refuse, and 16.5 $MJkg^{-1}$ for commercial wastes.

Table 2.8 Annual arisings of waste in the UK, 1990-1992[36]

Type of waste	Annual arisings (million tonnes)	Percentage of total arisings
Household [1]	30	8
Commercial [2]	15	4
Industrial:		
blast furnace and steel slag	6	2
power station ash	13	3
Agriculture [3]	80	20
Sewage sludge [4]	35	9
Dredged spoils	29	7
Mining and quarrying:		
colliery and slate	51	13
china clay	27	7
quarrying	30	8
Demolition and construction	32	8
Other	50	13

1 Includes up to 5 million tonnes from Civic Amenity Sites

2 Includes ~5 million tonnes of waste collected from retail and small commercial premises by Local Authorities

3 Refers to wastes from housed livestock only (wet weight)

4 Wet weight

The energy content can be recovered by a number of technologies which include

(i) combustion of the raw waste (mass burn incineration)

(ii) combustion after processing to reclaim recyclable components, such as metals and glass, and reject undesirable components (Refuse Derived Fuel)

(iii) landfill gas collection and utilisation

At present, over 85% of all household and commercial refuse is consigned to landfill, which in general presents the lowest cost waste disposal option in the UK.[8] The responsibilities for dealing with MSW in England are divided amongst the collection authorities (District Councils) and disposal authorities (County Councils). General industrial waste is mostly collected by private contractors. Current landfill practice is to deposit the refuse in layers, usually in clay pits or quarries, subsequently compacting and covering the waste with soil or an inert fill material. Constituents of the buried waste decompose biologically and chemically to produce solid, liquid and gaseous products. Initially, decomposition is aerobic until the oxygen supply is exhausted. Once anaerobic conditions are established, generally within 2 to 4 years, the bacterial activity on the organic material leads to the formation of landfill gas. Landfill gas is primarily a mixture of carbon dioxide and methane (approximately 1:1), with a large number of trace components such as halogenated hydrocarbons and organosulphur

Table 2.9 Constituents of MSW and typical heating values (dry basis)[38]

MATERIAL	Fraction of total waste (wt%)	Potential recoverable material (% of total waste)	Typical heating value ($MJkg^{-1}$)
Paper	33	10 - 20	20
Fine material (<20mm)	19		--
Vegetable matter	18		21
Glass and ceramics	10	5 - 7	--
Metals	10 *(non-ferrous 0.7 wt %)*	5 - 7 *(ferrous)*	--
Textiles	3		20
Plastic	3		37
Others	3		--
Bulk calorific value	9 - 10 MJ/kg		
Ash content	15 - 20 wt%		

compounds.[7] The mixture of gases percolates through the fill and escapes to the atmosphere. Emissions of landfill gas, if not controlled, can have serious environmental consequences. Methane, a colourless, odourless gas, is generally very stable; however, when mixed with air at a concentration of 5-15% by volume, the mixture is explosive. Furthermore, methane in the atmosphere is estimated to have a global warming potential per unit release many times that of CO_2. To meet more stringent regulations on the control of landfill gas, site operators must consider subsurface gas migration, gas collection, control and recovery systems.[39] The calorific value of landfill gas, attributable to methane in particular, is around half that of natural gas.

The leachate formed by the infiltration of rain through the waste mass, contains organic and inorganic pollutants and must also be contained and treated to prevent the contamination of the soil, groundwater and the surface water.

A landfill tax, introduced in October 1996, adds about £5 per tonne to current landfill prices of between £5 and £50 a tonne.[40] Furthermore regulatory pressures are set to tighten landfill standards, forcing waste management costs to greater limits. Tightening landfill standards will increase the cost of landfill, thus improving the competitiveness of alternative disposal routes.

2.6.1 Incineration of MSW

Incineration is an established means of processing wastes. The principal aim is to reduce the waste to a small volume (~10%) of sterile ash and thereby provide savings in transport costs and landfill requirements. Approximately 9% of UK MSW is incinerated. In many European countries the disposal of wastes by landfill is not favoured and mass burn incineration has been adopted to a significantly greater extent than in the UK, for example Sweden 50%, Denmark 60%, France 40%, Italy 20% and Germany 45%.[8] The incineration systems are well developed and fully commercial; the energy is recovered and used for power production or CHP, with the heat often used in district heating schemes. Such plants typically handle between 35 and 80 tonnes of waste per hour (250,000 to 600,000 tonnes per year) and produce between 15 and $40MW_e$.[7]

In the UK there are 34 large scale MSW incineration plants, mostly built in the 1960's and early 1970's. Of these, only five installations employ energy recovery systems. All 34 plants will require extensive refurbishment in the next few years in order to comply with the Commision of the European Communities' Directives on Emissions. The stricter EC environmental legislation limits the quantities of HCl, cadmium, mercury and dioxins and other heavy metal vapours and compounds and acidic gases. As a result the majority are expected to close or to be replaced by new plant incorporating advanced flue gas cleaning equipment. In all circumstances this will require the use of filtration and gas scrubbing equipment and the installation of monitoring systems for process control. Indeed, incineration and flue gas cleaning technologies have advanced considerably in response to stringent air pollution standards. The present NFFO arrangements have provided an immediate boost to incineration technologies in particular. Nonetheless, incineration projects often still face opposition at the planning stage because of concerns over the environmental effects of these emissions. It is worth noting that the requirements on emissions control are more stringent than those imposed for fossil fuel combustion; the range of species regulated is broader and the permissible levels of emissions required significantly lower.

Only one mass burn incinerator has been constructed in the UK during the last 20 years, the South East London Combined Heat and Power plant (SELCHP). The refuse incinerator in North Deptford, Lewisham generates approximately 30MW of electrical power, consuming over 420,000 tonnes of MSW per annum.[41] After many years of development and sensitive planning, the incinerator was constructed in the heart of a residential area. The premium electricity price, secured by NFFO, enables SELCHP to offer refuse disposal contracts at prices that are competitive with landfill costs.

The strict emission regulations now embodied in the EU and UK legislation on incineration have stimulated interest in gasification and other advanced thermal processing technologies that may achieve lower overall emissions and greater conversion efficiencies.

2.6.2 Refuse derived fuel

MSW may be processed to remove putrescibles, glass, metals and other inert materials, leaving behind a waste fraction rich in paper and plastics. Hence a fuel of higher calorific value (17-19MJkg^{-1}) may be produced, termed refuse derived fuel, RDF. The constituents of RDF are shown in Table 2.10[42]. The removal of non-combustible components would reduce the associated ash handling and disposal problems. The combustible RDF thus obtained can be treated as a composite of cellulosic (more correctly, polysaccharides) and plastic (synthetic polymers) fractions.

Table 2.10 Constituents of RDF[42]

MATERIAL	Paper	Plastic	Glass	Wood	Textile	Al foil	Others
Wt%	79-90	9-16	1.5	3.4	1.0	0.5	1.0

Various components of the cellulosic fraction (paper, food and garden waste etc.) have a heating value of ~20MJkg^{-1} (dry basis) and decompose over the temperature interval of 300-400°C.[38] The plastic fraction (polyethylene, polystyrene, polypropylene) depolymerise at higher temperatures (400-500°C) and their energy content is about twice that of cellulosic materials. The plastics previously mentioned exclude chlorinated plastics such as polyvinylchloride (PVC), which decompose at lower temperatures, within the range 250-400°C. The average distribution of plastic material in MSW and RDF is presented in Table 2.11.[43] Newsprint and polyethylene constitute the major portion of paper and plastic wastes in RDF.

Table 2.11 Average distribution of plastic material in domestic refuse[43]

PLASTIC	Wt%
Polyethylene (PE)	58
Polystyrene (PS)	20
Polyvinylchloride (PVC)	8
Polypropylene (PP)	8
Thermosetting resins *(e.g. phenol formaldehyde resins & miscellaneous plastics)*	6

Minimal processing of MSW results in coarse RDF (c-RDF) which is normally burned in a dedicated combustion plant using either fluidised bed or conventional grate technology. It is most likely that future plants employing c-RDF will be established as large scale, integrated waste processing power generation facilities. Secondary products will be recovered from the gas stream (ferrous and non-ferrous metals have reliable markets) and the fuel fraction will be combusted on site in high efficiency, probably fluidised bed boilers to generate electricity at over 500kWh per tonne of waste.[7] Fluidised bed combustors firing pre-sorted waste are common in Japan. Elsewhere in Europe and the USA the fluidised bed technology for RDF combustion is being reviewed with increasing popularity.

MSW may be further treated to recycle certain materials. In essence the waste is pulverised and then divided into three size fractions, <15mm, 15-150mm, and >160mm. Fines and oversize material are transported to landfill, whereas the bulk section passes through an air classifier, a scalping magnet to remove the ferrous metals, a drier to reduce the moisture content to ~10%w/w and finally a pelletiser.[44] The refined, dried and compressed product, termed densified RDF (d-RDF), is amenable to storage and transportation, however the net energy per tonne of waste is significantly lower than that available from c-RDF.

Developments in the UK have largely focused on the production of d-RDF aimed at the industrial boiler market. Several full scale fuel production plants have been built and operated, with a total annual production capacity of ~130,000 tonnes.[45] The manufactured d-RDF pellets consist principally of paper and plastics and to a lesser extent textiles and miscellaneous combustible matter (wood, garden waste etc.). The non-combustible matter (ash) consists primarily of silica and alumina, with substantial amounts of Na, K, Mg and Ca oxides.

2.6.3 RDF ash characteristics

The average ash content of RDF lies within the range 12-15% on a dry basis. The contents of both volatile organic and inorganic material are much higher in RDF than in bituminous coals, averaging 60-70%. The ash composition data shown in Table 2.12 originate from RDF samples from three different areas in the UK.[42]

Table 2.12 Ash composition of RDF[42]

OXIDE	SiO_2	Al_2O_3	Fe_2O_3	CaO	MgO	Na_2O	K_2O	TiO_2	P_2O_5	SO_3
Wt%	46-48	15-19	4-6	14-16	2-3	4-6	1-2	2-4	0.5-1	1-2

The RDF ashes have similar levels of SiO_2 and K_2O to those of coal ashes, but possess relatively high CaO and Na_2O contents. The ashes also have relatively short fusion ranges; initial deformation to complete fusion occurs between about 1100 and 1250°C. This is fairly typical of ashes with relatively high levels of alkali and alkaline earth metals.

RDF is usually incinerated on chain grate stokers. Fouling rather than slagging is predominant during RDF incineration, although some sintering of ash is possible as the deposits build up and the outer surfaces approach the high temperature of the flue gas stream. Species which lead to fouling are generated either from the non-combustible material, for example fillers in paper, or from entrained particulate matter and volatile molecular species.[43] In fixed and moving grate boilers it has been found that the ash deposits formed during the combustion of RDF differ considerably from the slag formed during coal combustion. The deposits from low alkali coals are similar in composition to the fuel ash, whereas the deposits formed on RDF combustion contain more than 90%w/w alkali sulphates (that is Na_2SO_4 and K_2SO_4).[44] The sulphate content of a RDF ash deposit has been found to decrease by ~10% from the inner layer adjacent to the boiler tube, to the outer layer. The change has been attributed to the increase in surface temperature as the deposit thickened, causing the higher melting material to soften and become sticky. Alkali silicates were formed in preference to alkali sulphates, resulting in a strong fused bond in the outer layer.

The principal step in the process of deposit formation during RDF combustion involves the volatilisation of the alkali metal species, which condense on the cooler heat transfer surfaces to form the bulk of the deposit. The alkali metals in RDF can be present as simple inorganic salts or as constituents of clay minerals, glass or other silicate based materials. The alkali metals in the inorganic salts are more likely to volatilise during the combustion process than those present in silicate form. Tests performed on RDF ashes, involving a solution to leach out the inorganic salts from the ash, indicated that around

45% of the total Na_2O and 70% of the total K_2O in RDF can be considered available for volatilisation during combustion.[42] Furthermore the volatilisation of alkali metal salts is enhanced at increased heating rates. The implication of these results is that a significant release of sodium and potassium compounds is to be expected under combustion conditions.

2.6.4 Dioxins and Furans

The formation of small amounts of the highly toxic species 2,3,7,8-TCDD (tetrachlor-dibenzo-dioxin) has repeatedly been confirmed during the operation of certain industrial processes, in particular processes used for the incineration of waste.[46] According to a recent review of dioxin emissions in the UK, municipal solid waste combustion is a principal source of dioxin production, as indicated in Table 2.13.[47] Since December 1996, a limit of 1 nanogram per cubic metre has been enforced, following increased public concern over the toxicity of dioxin emissions, which are considered powerful carcinogenic compounds.

Table 2.13 Dioxin emissions from combustion in the UK[47]

SOURCE	grams TEQ
MSW combustion	460 - 580
Coal combustion	5 - 67
Sewage sludge combustion	0.7 - 6
Clinical waste combustion	18 - 88
Landfill gas combustion	1.6 - 5.5

Of the plastic constituents of RDF (Table 2.11), a significant proportion can be attributed to PVC (polyvinyl chloride). Incomplete combustion of chlorinated organic compounds can lead to the formation and subsequent emission of dioxins (polychlorinated di-benzo-p-dioxins, PCDDs) and furans (polychlorinated dibenzo-furans, PCDFs), although the mechanisms involved in the formation of the compounds can only be hypothesised at present. Dioxin and furan compounds are also emitted during the combustion of clinical waste and coal, and to a lesser extent from sewage sludge and landfill gas.

In order to minimise emissions of dioxins, restrictions are placed on waste fired combustion systems relating to minimum temperatures and residence times, including

the specification of a secondary combustion chamber for certain wastes. More recently attention has focused on the downstream conditions, and restrictions have been placed on boiler exit gas temperatures and gas cooling, to avoid long periods in the temperature regime 450°C and 200°C which favours the synthesis of dioxin compounds.[48]

2.6.5 Inorganic fillers

Refuse derived fuel is predominantly comprised of paper (79-90wt%) and plastics (9-16wt%), as shown in Table 2.10. Thus, RDF ashes will contain the residues of inorganic material derived from the fillers, of which kaolin, calcite, silica and titania are most widely employed in paper, plastics, rubbers, and textiles.

Fillers, described as inert or reinforcing materials, are particulate additives which differ from the material of the matrix with respect to their composition and structure for the purpose of reinforcement or dilution. Fillers are generally inorganic by nature, and less frequently organic. Inert fillers, or extenders, serve to increase the bulk density and reduce the cost of a product, there being generally no alteration in mechanical properties. Reinforcing fillers produce specific improvements in mechanical and physical properties. Effective reinforcement depends on:

(i) the net surface area of filler per unit volume in contact with the matrix
(ii) the specific activity of the filler-matrix interface,
resulting in chemical and/or physical bonding
(iii) a geometrical factor:
the structure, morphology and porosity of the filler particle.

2.6.6 Kaolin

One of the most widely used minerals for fillers and coatings is kaolinite, a hydrated aluminium silicate ($Al_2O_3.2SiO_2.2H_2O$). Kaolinite is a major clay mineral constituent of the rock kaolin. The term kaolin, also known as porcelain earth and china clay, is a name for the group of minerals kaolinite, nacrite, dikite and halloysite. Kaolinite is by far the most common mineral of the group. The structure of kaolinite is based upon composite layers which comprise extended sheets of SiO_4 tetrahedra in a hexagonal array, bonded to a layer of composition $(OH)_6$-Al_4-$(OH)_2O_4$.[51]

Kaolin is primarily employed as a filler in the paper industry, which accounts for 50% of the total consumption of the mineral world-wide. The structural backbone of all

paper grades consists of an interlocking hydrogen-bonded network of cellulose fibres. Kaolin is incorporated into the cellulose matrix to enhance the texture, print quality, opacity and brightness of bleached paper. The fine-grained nature and plate-like morphology of kaolinite crystals improve the opacity and surface uniformity by occupying voids in the fibre network. To increase the fidelity of ink on paper, kaolin is also employed as a coating, further improving texture and reducing paper porosity. Other specific fillers used in paper manufacture include $CaCO_3$ (natural and precipitated) and TiO_2 (anatase and rutile). Fillers may comprise up to 25-50% of the total product weight.[52]

In Britain, kaolin is generally of a lower cost than most filler materials with which it competes due to the extensive china clay deposits in Cornwall. Kaolin is also used as a filler or extender in the rubber industry, in which kaolin imparts increased tensile strength and dimensional stability, increased resistance to tear and abrasion, smoother surfaces, and improved aesthetics. Kaolin is widely used in plastics to produce products of increased durability and dimensional stability, to increase resistance to chemical attack, reduce costs, and improve surface properties. Kaolin has many other significant filler applications, which include detergents, pastes, textiles, linoleum, inks, adhesives, insecticides, medicines, catalyst preparations, fertilisers, and cosmetics.

2.6.7 Calcite

Calcite is one of the most abundant and widespread minerals in the Earth's crust and is found in a great variety of sedimentary, metamorphic and igneous rocks. It is an important rock-forming mineral and is the major constituent of limestones, marbles, and many carbonatites. $CaCO_3$ has three polymorphs, calcite, aragonite and valerite (metastable), of which calcite is the most stable under atmospheric pressure-temperature conditions and the most common polymorph to form as a result of CO_2 in the atmosphere, hydrosphere, lithosphere, and in the upper mantle reacting with CaO in magmas, crustal rocks and the oceans. Calcite crystals exhibit a variety of crystal morphology of which rhombohedra are the most common. When pure, calcite is either colourless or white and is the most important filler, in terms of weight, used in plastics to provide opacity, and reduce costs. Ground chalks are frequently employed in thermoplastics, particularly in PVC. Synthetic, precipitated carbonates (CCP) are

custom-made for individual fields of application in which an aragonite structure, a high degree of purity, and particle sizes in the range 0.004-0.07μm are preferred. Improvements in impact and tensile strengths, and elastic moduli are to be gained in using CCPs.

2.6.8 Titania (TiO_2)

Of all white pigments, TiO_2 is now the most widely employed in the manufacture of paint (>50%), paper (25%), rubbers and plastics(15%). Titania has three naturally occurring polymorphs, rutile (tetragonal), anatase (tetragonal), and brookite (orthorhombic), of which rutile is the most prominent. Rutile is widely distributed as an accessory mineral in many rock types, ranging from plutonic to metamorphic rocks, and even as detrital material in sediments and placers because of the resistance to weathering. Rutile and anatase, when pure, are used as white pigments and are of particular value because of the exceptionally high refractive indices of both polymorphs in the visible region of the spectrum. Rutile has a higher refractive index than anatase, and a somewhat greater opacity, thus most of the TiO_2 currently produced is of this form. Only rutile is of significance to the manufacture of thermoplastics and quality paper, whereas as anatase finds application in automotive tyres.

2.6.9 Silica

Naturally occurring silicas include quartz, quartzite, novaculite, tripoli, and diatomaceous earth, which differ relative to the degree of crystallinity and particle size. Quartz is commonly used as a filler, as are ground silica glasses.

2.7 Tyre Waste

36 million tyres (470,000 tonnes) are scrapped annually in the UK, and disposal presents a mounting environmental and economic problem.[13] It is estimated that around 380,000 tonnes per year are surplus to current recycling activities, which include reclaimation of the rubber, remoulding and processing to rubber crumb. Outside the rubber industry, scrap tyres are used to some extent as fillers for asphalt in the surface treatment of playgrounds and racing tracks. Disposal is primarily by landfill or surface stockpile and costs on average £40 per tonne, but can in some instances be as much as £60. The calorific value of scrap tyres is on average 32MJkg^{-1} which is in fact greater

than that of a typical UK coal. Waste tyres are thus an attractive feed stock for energy recovery processes which provide a constructive solution to the waste disposal problem.

Scrap tyres are an inhomogeneous form of waste, and the composition varies depending on the tyre grade, age and manufacturer. The tyre is a composite structure, designed to meet several contradictory demands. The conventional passenger car tyre, the radial tyre, has three distinct components:

(i) steel wire beads to anchor the tyre to the wheel rim;

(ii) high tensile cords (polyester, rayon, nylon, finely drawn steel) secured to each bead to provide strength, rigidity and support

(iii) a matrix of rubber compounds to provide road contact and traction, contain air and insulate the cords from self-abrasion and fatigue.

2.7.1 The rubber compound

Rubber compounds are a complex mixture of polymers, carbon black, mineral fillers, curatives, plasticisers and other components. The composition of a typical car tyre rubber compound is shown in Table 2.14.[53] The greatest volume of rubber used in tyre manufacture is a synthetic co-polymer, styrene-butadiene rubber (SBR). Other rubbers consumed by the tyre industry include natural rubber (NR), the synthetic counterpart cis-1,4-polyisoprene (IR), and cis-1,4-polybutadiene rubber (BR).

Table 2.14 Composition of a typical car tyre rubber compound[53]

COMPOSITION	Wt%
SBR	62.1
Carbon black	31.0
Extender oil *	1.9
Zinc oxide	1.9
Stearic acid	1.2
Sulphur	1.1
Accelerator	0.7

* The extender oil, a mixture of aromatic hydrocarbons, serves to improve the workability of the rubber.

In every part of the tyre, a compromise is made between conflicting materials properties. Rubber blends are used to obtain the most favourable balance of properties which include the desired performance characteristics, the material costs and processability. Solution polybutadienes, used almost exclusively in tyre manufacture, are blended with

SBR and natural rubber to impart outstanding abrasion resistance to the tread compounds of both passenger (SBR) and heavy-duty (NR) tyres respectively. For applications in which good hysteresis properties are required, such as in heavy-duty tread and carcass formulations for lorries, aeroplanes and tractors, polyisoprene rubbers are used in combination with natural rubber and BR.[54,55]

Raw uncompounded and unvulcanised rubber is itself of negligible use. Rubber is ultimately composed of long flexible coiled molecules, randomly agglomerated and entangled. The molecules are formed by the repetition of one or two, occasionally several, alternating monomers repeated in varying ratios and sequences. The secondary forces acting between the molecular chains are of a physical nature and decrease rapidly with increasing distance between molecules and with increase in temperature. Unsatisfactory mechanical properties, weak form stability, predominant plasticity, considerable sensitivity to temperature change, solubility in organic liquids and further technicalogical factors prevent the direct use of unmodified rubber. The introduction of primary chemical bonds between neighbouring molecules by vulcanisation, converts the structure into a three dimensional cross-linked network and produces a material of a more durable character. The elastic properties are markedly enhanced and extended over a greater temperature range, the tensile strength and abrasion resistance are increased, and the hysteresis loss is reduced.[55,56]

There are four vulcanising agents and systems in widespread use within the rubber industry: sulphur systems, peroxides, urethane crosslinkers and polyvalent metallic oxides (Zn, Ca, Mg, Pb). By far the most common vulcanising methods for natural and synthetic rubbers are those dependent on sulphur. A substantial increase in the efficiency of sulphur vulcanisation can be achieved by the addition of a catalyst (accelerator, typically an organosulphur compound) which significantly reduces the curing time, promoting successful continuous vulcanisation. The vast majority of rubber compounds employ vulcanisation activators, of which the most popular activator system is zinc oxide and stearic acid. The mechanism by which these compounds facilitate the chemical cross-linking process has not been exhaustively studied and results to date indicate the complexity of the cross-linking reaction.[54,57]

2.7.2 Fillers

The mechanical properties of even vulcanised rubbers are not satisfactory in terms of tensile strength, abrasion, tear resistance, and stiffness. These characteristics, including the viscoelastic properties, may be further improved by the addition of fillers. Some fillers mainly affect the processability of rubber mixes prior to vulcanisation and serve to reduce the cost of the vulcanisate. By convention, such fillers are called inert, inactive or extenders (clay may serve as an example). Other fillers, reinforcing or active fillers, considerably improve the physical properties of the vulcanisate, in particular the tensile strength, wear and abrasion resistance. The addition of a reinforcing filler also increases the energy necessary for the rupture of the rubber and this value may be considered a simple criterion of the reinforcement.

Carbon black is the outstanding reinforcing filler for both natural and synthetic rubbers. Inorganic fillers are also employed in car tyre manufacture, of which kaolin, $CaCO_3$ and TiO_2 (anatase) are of most significance. Vulcanisation restrains the long-range movements of the polymer molecules but leaves the local segmental mobility high; reinforcement restricts the local freedom of movement.

2.7.3 The ash chemistry of waste car tyres

Scrap tyres have a very high volatile matter content of 60wt%, and a low moisture content of 3wt% as received, 30% fixed carbon and an ash content of 3wt% on a dry basis. The composition of rubber tyre ash is given in Table 2.15, adapted from the data given by Rampling.[58]

Table 2.15 Typical composition of a scrap tyre ash[58]

OXIDE	SiO_2	Al_2O_3	Fe_2O_3	CaO	MgO	K_2O	Na_2O	ZnO	SO_3
Wt %	36.7	5.3	16.5	15.4	1.2	2.5	0.9	12.4	9.1

Thermogravimetric analysis (TGA) has been used to study the thermal decomposition of waste tyre samples, by pyrolysis in a nitrogen atmosphere. The thermal degradation of a tyre produces a wide variety of liquid and gas phase products in addition to the residual char. The char yield from tyres was found to range from 32-42wt%, depending on the composition, in particular the carbon black content. The major products of the initial stages of pyrolysis at ~330°C are isoprene and dipentene and other smaller compounds.

Further reaction results in the formation of a wide variety of compounds, by polymer chain scission or via degradation of the isoprene and dipentene, or (particularly at higher temperatures or longer residence times) via secondary reactions to form aromatic compounds. The main gases produced during the pyrolysis of tyres are CO_2, CO, H_2, CH_4, C_2H_6, C_3H_6, C_3H_8 and C_4H_6 with lower concentrations of hydrocarbon gases.[53]

Results of research on the combustion of tyres show that they readily ignite and combust rapidly producing large amounts of heavy volatile hydrocarbons, which must then undergo further combustion above the bed to achieve a 'clean burn'. [58] After each trial in a combustion pot furnace, powdery deposits of carbon and ZnO were found on the inside of the pot and ducting. The deposition of carbon was the result of incomplete combustion. It has been suggested that gasification may be a more suitable process for recovery of the full thermal energy of this type of material.

A 25MW, power station dedicated to the combustion of whole car tyres has operated in Wolverhampton with limited success. The incinerator generated electricity, under a NFFO contract, by the combustion of more than 8 million tyres a year, supplied by tyre distributors such as Michelin, Pirelli, and Goodyear.[59] An advanced flue gas cleaning technology system was employed to comply with strict emission regulations. However, the plant failed to operate to specification, exasperated by the incomplete combustion of the fuel and severe ash deposition on convector heat transfer surfaces.

Some of the residues from the combustion process have a market value, for example a fly ash rich in zinc oxide is produced. The tyre industry reclaims the ZnO which is effectively recycled, steel particles are sold for scrap, and calcium sulphate is used for building materials.

2.8 Sewage sludge

2.8.1 Methods of disposal

Currently in Britain, 1.5 million dry tonnes of sewage sludge is produced per annum.[7] In England and Wales around 8% is incinerated with 50% used as a fertiliser in agriculture, 14% consigned to landfill and approximately 22% discharged at sea. Table 2.16 shows the methods adopted for sewage sludge disposal in England and Wales,

Scotland and Northern Ireland.[36] The data was collected during a survey of the sewage authorities in the UK and is tabulated as a percentage of the dry weight.

Table 2.16 Sewage sludge disposal in the United Kingdom, 1992/93[36]

% dry weight	England & Wales	Scotland	Northern Ireland
Farmland	50	13	52
Landfill	14	5	6
Sea disposal	22	75	42
Incineration	8	1	0
Other *	6	6	0

* Other includes beneficial uses of land reclaimation and forestry, and soil and compost products

Since 1989, a little over 25% of sewage sludge has been disposed of at sea. The main dumping grounds are the Thames Estuary, Liverpool Bay and the Clyde Estuary. Following international agreements to eliminate disposal of sludge at sea by 1998, there has been renewed interest in sewage sludge incineration in the UK. However at present the level of incineration adopted is of the same order as the average within the EU (~9%), but is substantially lower than that in France, USA and Japan, where sewage sludge incineration accounts for 25-50%.[60] The use of digested sewage sludge on farmland is objectionable due to the enrichment of toxic constituents, particularly heavy metals, in the soil and consequently in the crops and the ground and surface waters. However, from 1998 agriculture is most likely to remain the principal outlet for sludge in the UK. Sewage sludge is a source of the essential plant nutrients nitrogen and phosphorus, as shown in Table 2.17.[11]

Table 2.17 Typical nitrogen and phosphorus content of sewage sludges (kgm^{-3} for liquids, kgt^{-1} for cakes)[11]

Sludge type	Dry matter (%)	Nitrogen	Phosphorus
Liquid raw	5	1.8	0.6
Liquid digested	4	2.0	0.7
Raw cake	25	7.5	2.8
Digested cake	25	7.5	3.9

The application of sewage sludge to agricultural land is regulated by the principal legislative statues, The Sludge (Use in Agriculture) Regulations and the Code of Good Agricultural Practice for the Protection of Water. The Sludge Regulations dictate the

maximum permissible levels to which heavy metals may accumulate in sludge treated soils. They may also require that raw sludge be incorporated into the soil or injected to prevent odour nuisance. Treated sludge may be surface applied without the need for incorporation.

In 1992, approximately 465,000 dry tonnes of sludge solids were applied as fertiliser to some 5600 hectares of arable land in the UK. By 2006 it is proposed to dispose of nearly 1 million dry tonnes of sewage on the land. The majority of the sludge will be applied free of charge, although some water companies, for example Wessex Water, have begun processing the sewage into pasteurised granules of 92% dry matter at a predicted cost of £10 per tonne. The granules (containing ~3.5% nitrogen) provide a form of slow-release nitrogen into the soil, with only half emerging in the first year.

The Agricultural Development and Advisory Service (ADAS) will lead a £1.7m research programme into the beneficial use of sewage sludge on farmland. The work will be based at Rothamsted Research Station and the Water Research Centre, with six sites across the country chosen to study the effects of the sludge on soils and the implications for productivity and long-term soil fertility.[11]

2.8.2 Incineration of sewage sludge

The conventional approach to the incineration of sewage sludge involves the partial dewatering of the sludge, using centrifuges and belt presses, before combustion in either a multiple hearth furnace or a fluidised bed combustor. Traditionally, the multiple hearth furnace (MHF) has been used to incinerate sewage sludge and a large number of these units are in operation world-wide. However, the great majority of MHF incinerators were originally intended for sludge disposal only and are not suitable for heat recovery. In recent years, the fluidised bed incinerator has been preferred for sewage sludges and such a plant was commissioned at Esholt, Yorkshire in 1989. It was designed to handle 240,000 tonnes (18,000 dry tonnes) per annum of primary and secondary sludges with an average solids content of around 7-8 wt%.[60]

2.8.3 Constitution of sewage sludge

Domestic sewage sludge contains ~95% water, the remaining dry solids are predominantly organic. When dry, sewage sludge has a relatively high calorific value of 15-20MJkg^{-1}. The calorific value of the dry matter varies according to the type and pre-treatment of the sludge. For example digested sludge, that which has undergone anaerobic biological conversion, contains dry solids with the lowest calorific value (9-10MJkg^{-1}), since during the digestion process a proportion of the organic matter is converted to gaseous products.[61] Consequently the ash content is increased.

The ash contents of sewage sludges tend to be relatively high, compared to those of more conventional fuels, lying in the range 25-40wt% on a dry basis. The chemical properties of sewage sludge ashes are largely unexplored. The composition of a sewage sludge ash from the Sewage Treatment works at Paisley is shown in Table 2.18.[60] It is not known, however, whether the data is representative of the full range of British sludges, particularly those from sewage treatment works which handle large volumes of industrial effluents.

Table 2.18 Composition of sewage sludge ash from Paisley Sewage Treatment works[60]

OXIDE	SiO_2	Al_2O_3	Fe_2O_3	CaO	MgO	K_2O	Na_2O	P_2O_5	TiO_2	SO_3
wt %	48.2	15.6	11.3	9.0	3.4	1.7	2.0	2.1	4.2	1.8

Apart from the substantial phosphate level, the ash composition is similar to that of many coal ashes. The sewage sludge appears to be essentially an aluminosilicate system. The ash fusion temperatures are also similar to those of many coal ashes. Under reducing conditions, the IDT was found to be 1100°C with complete fusion around 1250°C. It is thought that the relatively high phosphate content may contribute significantly to the formation of a slag or fouling deposit, as found in some combustion plants.

It is possible that sewage sludge may contain debris from the wear of roads and pavements that are washed into the drains to join the biological material. For example, gravel and sand are used for road surfacing, road base, fill and as aggregates in both bituminous and cement mixes. The predominant materials in gravel/fill are silica, mica, feldspar, calcite and dolomite, ferromagnesium minerals, iron oxides and clay minerals, many of which are essentially aluminosilicates. It has been reported that dried sewage

sludges possess a high hardness and are more difficult to grind to pf size than a typical coal. The presence of materials such as gravel and sand in sewage sludge may contribute to a high hardness value.

It is suspected that the relatively high levels of phosphorus may arise from the phosphates used as water softeners in washing detergents. Therefore the composition of sewage sludge ash may be expected to differ with respect to phosphorus levels in countries where the use of phosphates in detergents is prohibited. Sodium salts of condensed phosphates are widely used as water softeners as they form soluble complexes with calcium, magnesium and other metal ions. The use of such salts has lead to some ecological problems, since phosphates also act as fertilisers and can lead to abnormally high growth rates of algae and other biological organisms. Thus, there is presently much interest in controlling the amount of phosphorus compounds that enter rivers and other surface waters from domestic and industrial discharges.

Nutrients such as phosphorus and nitrogen are removed from wastewater and thus become enriched in the sludge. Phosphorus appears in wastewater in the form of an orthophosphate (for example PO_4^{3-}, HPO_4^{2-}, H_2PO^{4-}, or H_3PO_4), polyphosphate (P_2O_7), and organically bound phosphorus. Chemicals such as alum, sodium aluminate, ferric chloride/sulphate and lime are added to wastewater to produce insoluble or low-solubility salts when combined with phosphate. Phosphorus can also be removed during a biological treatment by means of incorporating orthophosphate, polyphosphate, and organically bound phosphorus into the cell tissue of a biological organism.[62] A flow diagram of a tertiary sewage treatment process is shown in Figure 2.4.[5]

Lime is added to untreated sewage to 'stabilise' the organic material in the sludge. Sewage sludge needs to be stabilised in order to destroy pathogens, eliminate offensive odours, and inhibit the potential for putrefaction. The survival of pathogens, putrefaction, and the release of odours occur when micro-organisms are allowed to flourish in the organic fraction of the sludge. Lime is added to untreated sewage to raise the pH to 12 or higher, thereby creating an environment that is not conducive to the survival of micro-organisms. As long as the pH is maintained at this level, the sewage sludge does not pose a health hazard. Lime is also used to reduce the moisture content of the sludge; chemical conditioning, as it is known, can reduce the moisture content of

the sludge from 90-99% to 65-85%. Conditioning is used in advance of mechanical dewatering systems such as vacuum filtration, centrifugation and filter presses.

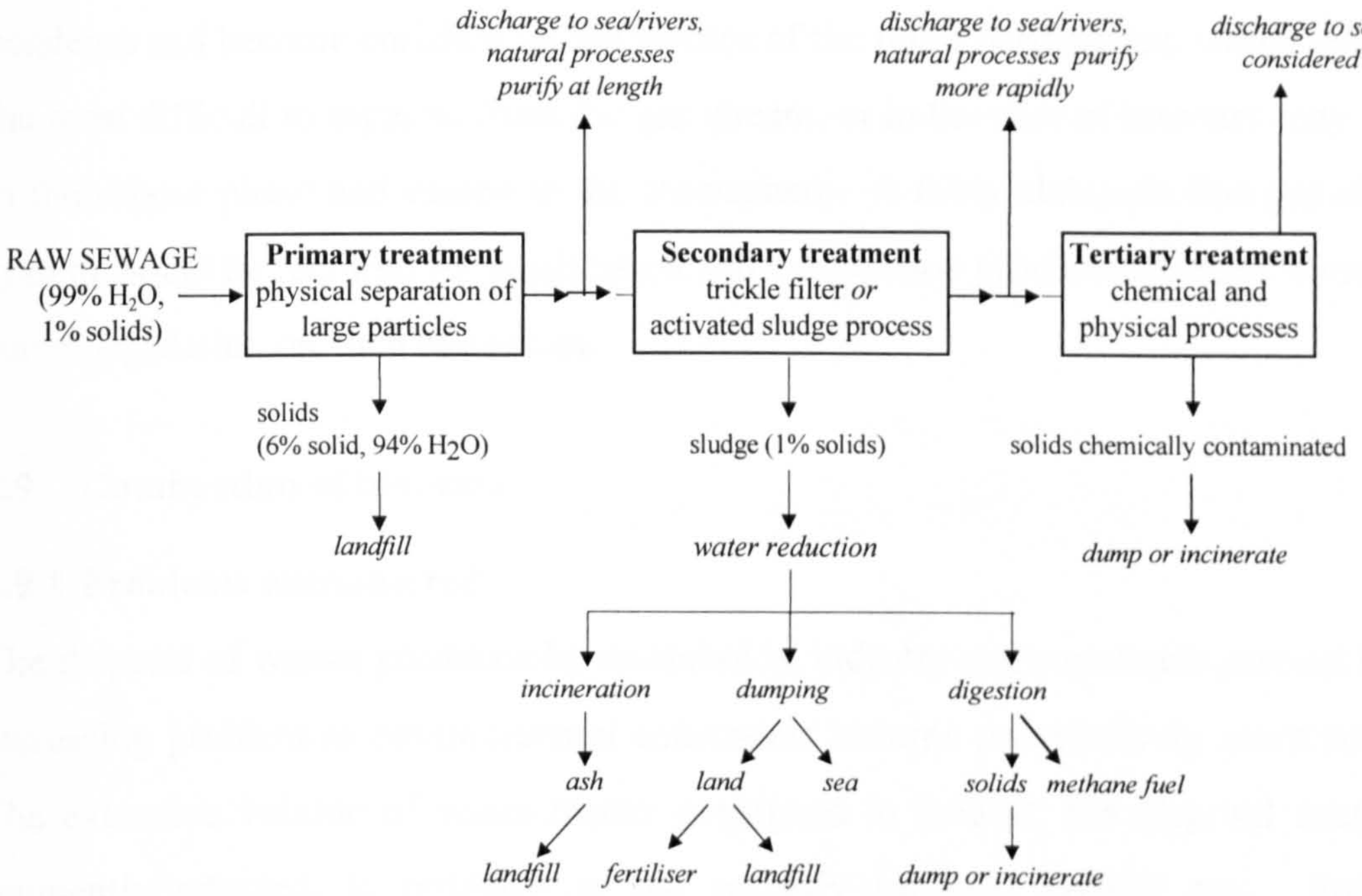

Figure 2.4 A tertiary sewage treatment process[5]

Some sewage sludges have been found to contain quite a high degree of environmentally sensitive heavy metals. The Water Research Centre in Stevenage have listed the following typical ranges of values for some of the heavy metal contaminants in sewage sludge, Table 2.19.[60]

Table 2.19 Typical concentration ranges of heavy metal contaminants in sewage sludge ashes[60]

METAL	CONCENTRATION (mg/kg in ash)
Cadmium	21 - 150
Copper	1800 - 2400
Lead	600 - 2100
Molybdenum	~15
Nickel	150 - 240
Zinc	4500 - 9000

During combustion, metals of low volatility such as copper, nickel and chromium would be retained in the residues and the fly ash, and a reasonable degree of particulate

processing should be sufficient to control their release into the atmosphere. The more volatile elements such as lead, cadmium, arsenic and especially mercury are more problematic, since on cooling of the flue gases downstream of the furnace they may condense and become enriched on the surface of the finest particulates, which tend to be the most difficult to separate from the gas stream, or in the case of mercury may remain in the vapour phase and escape to the atmosphere. A fairly elaborate flue gas clean up system would be required for gasification and combustion processes to meet current and future legislation on such emissions.

2.9 Combustion of biomass

2.9.1 Problems encountered

The disposal of wastes produced by households, industry and commerce present an ever increasing problem as environmental constraints become progressively more stringent. The extensive volume of waste matter consigned to landfill, the disposal route most frequently adopted, is reflected in the recently imposed landfill tax. Following international agreements to prohibit the discharge of wastes at sea by 1998, local authorities have been compelled to seek alternative methods of disposal.

At one time incineration was considered a simple solution. An established means of waste processing, the principal aim of incineration is to reduce the volume of material destined for landfill. Indeed the incineration of waste before disposal in landfill sites is already policy in France, Germany, Austria and Holland. To a greater advantage, the inherent calorific value of the waste could be recovered and used as a low heat source for steam generation and heating purposes. However, the inorganic constituents of the refuse may pose serious and perpetuating problems at high temperatures (~1500°C). Fouling, slagging, attack of refractory furnace linings, and corrosion of heat exchangers have all presented innumerable problems for the operation of these systems. The phenomena of ash deposition may be largely attributed to the presence of relatively volatile alkali (Na, K) and alkaline earth (Ca, Mg) species which assume the vapour phase in combustion gases.[35,63] Other inorganic species which can volatilise during combustion can contribute to deposit formation or condense as a submicron fume and be emitted to the atmosphere presenting potential environmental and health hazards. A

significant consequence of deposit formation is the effect on the heat transfer potential of the boiler design by the thermal insulation of furnace linings and convective tube banks. Reducing the efficiency of radiant absorption and convective transfer leads to a subsequent increase in gas temperatures throughout the reactor, which exacerbates the release of volatile species, enhancing the rate of ash deposition. The reduction in heat transfer that results from deposition has a number of significant effects on the overall performance of power plants. In particular, for a given output and level of availability, these effects include

- increased maintenance cost
- a reduction in boiler efficiency, and hence an increase in the amount of required fuel, and in the quantity of CO_2 formed
- increased capital cost (for new plant).[64]

The abrasive nature of certain inorganic species, such as quartz, can contribute towards erosion and wear, depending on the size and shape of the impacting particle.[35] Erosion is most apparent in the convective regions of a boiler, and is further aggravated by the partial blockage between tube banks, caused by deposit accumulation, leading to an increase in local gas velocity. The presence of certain inorganic species in the layers of a deposit adjacent to tube metal and furnace wall surfaces may present an environment conducive to the corrosion of protective metal oxide coatings and refractory linings. Furthermore, dense deposits that become dislodged may cause physical damage to neighbouring tubes and internal structural components.

The deposits can be difficult and expensive to remove. On-load removal of deposits is most successfully achieved by the incorporation of soot blowers which direct a jet of high pressure air, steam or water, through retractable lances, at the surface of the deposit. A combination of thermal and mechanical shock is used to initiate crack formation within the deposit which is subsequently dislodged by the scouring action of the jet.[65] The material which is removed may fall into the bottom ash hopper, or it may be transferred downstream with the combustion gases to re-deposit elsewhere, for example in the cooler section of the boiler where the heat transfer tubes are closely spaced. The smaller particles that arise from the cleaning operation may pass through the boiler and leave with the flue gases. Deposits of a tenacious nature may require manual removal, during boiler shut-down.

The process of gasification presents a solution to many of these problems, since the gasification temperature (some 500-600°C lower than for incineration) is below the temperature at which the volatilisation of alkalis and the corrosion of refractories is of significant detriment to heat transfer, refractory and tube metal surfaces and gas turbomachinary.

2.10 Gasification

The essence of gasification, as the name implies, is the conversion of a carbonaceous feedstock such as biomass or coal into a gaseous energy carrier by means of sub-stoichiometric oxidation at elevated temperatures. This is contrary to the process of combustion which takes place with excess oxygen or at least with the theoretical, stoichiometric, oxygen requirement. The partial oxidation can be accomplished using air, oxygen, steam, or mixtures thereof. The product gas of low to medium calorific value (~4-18MJm^{-3}), contains carbon monoxide, carbon dioxide, hydrogen, steam and nitrogen (if air is used as the oxidising agent) in varying amounts. [66,67] Additional gaseous products may include methane, trace amounts of higher hydrocarbons such as ethane and ethene, and various contaminants such as char particles, ash, tars and oils. The combustible product gases can be fired into a relatively conventional boiler plant to generate steam, or with suitable cleaning can be used as a fuel for a gas turbine or diesel engine. The gases produced during the thermochemical conversion of biomass can also be used as synthesis gas (a mixture predominantly of hydrogen and carbon monoxide) in the process industry to produce methanol, gasoline and ammonia.[67,68]

The gasification of biomass using air produces a poor-quality gas in terms of heating value (4-7MJm^{-3}) which is satisfactory for boiler, engine and turbine operation. Oxygen gasification produces a gas of medium calorific value (10-18MJm^{-3} higher heating value) which is suitable for industrial process heating and limited pipeline distribution, or for use as synthesis gas.[66,69] Gasification with air is the more widely employed technology since the cost and hazards associated with oxygen production and application are avoided.

The chemistry of the gasification of a carbonaceous material has been the subject of intensive scientific investigations throughout the years, although a comprehensive

understanding of the chemical and physical processes is yet to be attained.[70] Despite the complexity of the chemistry, gasification can be defined by a series of consecutive, or parallel steps:

- drying to evaporate moisture,
- pyrolysis to yield gaseous species, vaporised tars and oils, and a solid char residue,
- gasification or partial oxidation of the solid char, pyrolysis tars and volatile matter to produce combustible gases.

Depending on the gasifier design and the heat and mass transfer processes involved, the steps may be completed in a matter of seconds, or may take up to an hour. [6]

2.10.1 Pyrolysis

The pyrolysis or decomposition of the solid fuel proceeds over the temperature range 100°C to 500°C in the absence of an oxidising agent. The products of pyrolysis comprise a carbon rich solid char, condensable hydrocarbons or tar vapours, and gases (for example H_2, CH_4, H_2O and CO).[71] Conditions prevailing in the reactor system will determine the yield of devolatilisation products. The non-reactive volatiles escape. The reactive volatiles are further converted to char via polymerisation or are hydrogenated to methane.

Generally, pyrolysis proceeds more rapidly than gasification, and the latter is the rate-controlling step. The gaseous, liquid and solid products of pyrolysis then react with the oxidising agent to give permanent gases (CO, CO_2, H_2). [4]

Char gasification is the interactive combination of several gas-solid and gas-gas reactions in which solid carbon is oxidised to CO and CO_2. Hydrogen is generated in the water-gas shift reaction. Reactions occurring in the gas phase are listed in the summary of gasification reactions in Table 2.20.[72]

The gas-solid reactions of the char oxidation are the slowest and limit the overall rate of the gasification process. Many of the reactions are catalysed by the alkali metals present in the biomass ash, but still do not attain equilibrium. The gas composition is influenced by many factors such as the feed composition, moisture content, reaction temperatures, and the extent of oxidation of the pyrolysis products. [66]

2.10.2 Fundamental equations of gasification

The gasification process can be described by the following basic chemical reactions between solid carbon and the oxygen carriers or the gases from them. Gasification reactions are heterogeneous in nature, and take place at the gas-solid phase boundary, i.e. the surface of the solid. The gas formed in the boundary layer is mixed by diffusion and convection with the gas of combustion leaving the oxidation zone.

Gasification of the char remaining after devolatilisation occurs by the reaction of carbon with carbon dioxide, and of carbon with steam. Both reactions are highly endothermic, and enhanced by elevated temperatures and limited by chemical equilibria. The principal reactions are as follows:

The Boudouard reaction:	$C + CO_2 = 2CO$	ΔH +ve	(1)
The steam - carbon reaction:	$C + H_2O = H_2 + CO$	ΔH +ve	(2)

Equations (1) and (2) are related by the water-gas shift equation as follows:

The water-gas shift reaction:	$CO_2 + H_2 = CO + H_2O$	ΔH +ve	(3)

A further heterogeneous equilibrium gasification reaction between char and hydrogen to form methane must be considered on the basis of the simple overall equation:

Methane formation	$C + 2H_2 = CH_4$	ΔH -ve	(4)

This exothermic reaction has an associated volume decrease and is consequently favoured by low temperatures and high pressures.

Carbon conversion is completed, in the region where the oxidant is introduced, by the reaction with oxygen resulting in the formation of CO (partial combustion) and CO_2 (total combustion), the relative quantities depending on the temperature of the reactor system. The total combustion of part of the carbon is an intensely exothermic reaction and provides the energy to sustain the endothermic gasification reactions that produce H_2 and CO for the sensible heat in the products and the heat losses.[71]

Partial oxidation	$C + ½\ O_2 = CO$	ΔH -ve	(5)
Total oxidation	$C + O_2 = CO_2$	ΔH -ve	(6)

During gasification reaction (6) is minimised in order to increase the calorific value of the product gas, however the reaction is dominant in combustion processes.

The basic gasification reactions are summarised in Table 2.20.[72]

Table 2.20 Basic reactions in the gasification of carbonaceous materials[72]

Combustion		**ΔH (kJmol^{-1})**
$C + ½O_2 = CO$	Partial combustion	-123.1
$C + O2 = CO_2$	Total combustion	-405.9
Gasification		
$C + CO_2 = 2CO$	Boudouard reaction	+159.7
$C + H_2O = H_2 + CO$	Steam-carbon reaction	+118.7
$C + 2H_2 = CH_4$	Hydrogasification	-87.4
Pyrolysis		
$4C_nH_m = mCH_4 + (4n\text{-}m)C$	Pyrolysis	Exothermic
Gas Phase reactions		
$CO + H_2O = H_2 + CO_2$	Water gas-shift reaction	-40.9
$CO + 3H_2 = CH_4 + H_2O$	Methanation	-206.3

The previously described equations, although major, do not represent the whole gasification process. For instance, the inorganic matter in biomass is also subject to thermochemical phase changes and interactions, and a description of such reactions is reserved for section 2.14. Different gasifiers produce ashes with differing physical and chemical properties. The nature of the residual ash depends both on process features and the type of biomass used.

The complete conversion of the pyrolysis products into CO, CO_2 and H_2 may be hindered by the physical and geometrical constraints of the reactor and the chemical limitations of the reactions involved. Tars and other contaminants may arise in the final product gas. Table 2.21 lists several contaminants of the fuel gas, and the precautionary clean-up methods employed.[66]

The vast majority of biomass plants operate on a steam-Rankine cycle, a steam-turbine technology which was initially commercialised about 100 years ago. Combustion of the biomass takes place in a conventional boiler producing pressurised steam. The steam is expanded through a turbine to produce electricity. For the production of power only, a fully condensing turbine is used. The co-generation of heat and electricity (combined

Table 2.21 Contaminants of the fuel gas, subsequent problems and clean-up processes[66]

Contaminant	Example	Problems	Clean-up method
Particulates	Ash, char, fluid bed material	Erosion, fouling	Filtration, scrubbing, soot-blowing of deposits
Alkali metals	Sodium and potassium compounds	Hot corrosion, fouling	Cooling, condensation, filtration, adsorption
Fuel nitrogen	NH_3 and HCN	NOx formation	Scrubbing, selective catalytic reduction
Tars	Refractory aromatic compounds	Clog filters, difficult to burn, deposit internally	Tar cracking and removal
Chlorine, sulphur	HCl, H_2S	Corrosion, emissions	Lime or dolomite scrubbing or absorption

turbine. Biomass plants are usually of modest scale (less than 100MW_e) due to the dispersed nature of biomass supplies. To minimise the dependence of unit cost on scale, vendors use lower grade steels in the boiler tubes of small-scale steam-electric plants and make other modifications that reduce capital costs, but also require more modest steam temperatures and pressures, thereby leading to reduced efficiency. Biomass facilities operating world-wide have efficiencies of 14-18%, compared with 35% for a modern coal plant.[73]

A promising alternative to the steam-turbine cycle for biomass power generation is a set of biomass-integrated gasifier/gas turbine technologies that offer the potential for low unit capital cost and high thermodynamic efficiency at modest scales. This set of technologies involves marrying advanced Brayton cycle (gas turbine) power generating or cogenerating cycles, which have already been developed for natural gas and clean liquid fuel applications, to closely coupled biomass gasifiers, which can be based to a large extent on gasifiers already developed for using coal in gas-turbine power cycles. In contrast to steam-cycle technologies, the unit capital cost of gas turbine systems are relatively low and insensitive to scale. Thus from a capital cost perspective, the gas turbine is an interesting candidate for biomass-based power generation.

2.10.3 Gasification Technology

Three generic types of gasifier reactor have been developed, primarily for the gasification of coal. The reactor designs differ in the characteristics of the zone where the gasification reactions take place.[74]

The main types of gasifier configuration are briefly discussed below, with significant features and limitations highlighted.

2.10.4 Fixed bed reactors - downdraft (concurrent)

The downdraft gasifier features a concurrent flow of gases and solids through a descending packed bed which is supported across a constriction known as a throat, where the reactant gases are injected via tuyeres and most of the gasification reactions occur. The reduced cross-sectional area of the reactor vessel forces the pyrolysis gases to filtrate an incandescent hot carbon bed. The reaction products are intimately mixed in the turbulent high temperature (~ 1200°C) partial combustion region around the throat, which facilitates the cracking of heavy hydrocarbons reducing tars, oils and phenols to non-condensible gaseous products. The configuration thus results in a high conversion of pyrolysis intermediates and hence a relatively clean gas and is generally favoured for small-scale electricity generation with an internal combustion engine. The product gas composition and tar yield are dependent upon the geometry of the partial combustion zone and the method of oxidant injection.[66,71,75]

Downdraft gasification is a simple, reliable and proven technology for certain fuels of relatively low moisture (< 25%) and low ash (< 5wt%) contents, and with a particle size distribution of 0.01-0.3m; fine material is not tolerated.[66,71] The practical upper limit to the capacity of the downdraft gasifier is 500kW$_e$ and is a consequence of the physical limitations of the design, in particular the relationship between the throat geometry and particle size.

Most of the inorganic material and unburnt carbon fall into the ash collection chamber, through the lower grate of the gasifier. The high temperatures in the oxidation zone can exceed the fusion temperature of some constituents of the ash and slag formation may be consequential. To ensure efficient ash removal riddling grates are fitted, often of the semi-rotary type, with automatic operation.[71]

A relatively new concept of stratified or open-core downdraft gasifier has been developed, in which the bed is supported on a grate in the absence of a throat. This was first devised by the Chinese for rice husk gasification and further developed by Syngas Inc.

2.10.5 The updraft (countercurrent) fixed bed gasifier

An updraft gasifier exhibits clearly defined zones for partial combustion, gasification and devolatilisation. The flow of the reactant gases is countercurrent to the fuel motion. The downward feed of biomass is initially dried by the rising stream of hot product gases and is subsequently pyrolysed. The resulting char continues to descend and experience gasification, yet the pyrolysis vapours are swept upwards by the product gases. The pyrolysis tars condense on the descending fuel at temperatures between 125°C and 400°C or are carried out of the reactor uncracked.[75] In the gasification zone the solid char, from pyrolysis and tar cracking, is partially oxidised and combustion is completed at the bottom of the bed where the oxidant is introduced. The product gas from an updraft gasifier thus contains a significant proportion of tars and hydrocarbons which contribute to a high heating value. The gases are suitable for direct firing, however extensive gas clean-up is required for engine and turbine operation.

The principal advantages of the updraft gasifier include a high thermal efficiency, basic design and robust construction. The sensible heat of the gas produced is recovered by the direct heat exchange with the entering feed, which is dried, preheated and pyrolysed before entering the gasification zone. In principle there is little scaling limitation, although few large updraft biomass gasifiers in excess of a 10MW$_e$ capacity have been constructed.[66]

The system is illustrated in Figure 2.5 and is employed in the commercial Lurgi and British Gas Lurgi Slagging Gasifiers for the conversion of coal to electrical power. The Lurgi Gasifier operates under pressure (2.5MPa) and employs a gasifying medium of steam and oxygen. The feedstock is lump coal which is admitted to the reactor via a pressurised hopper and kept in motion during reaction by means of a rotating grate through which the ash is discharged and periodically removed. The Lurgi Gasifier

operates under non-slagging conditions with prevailing gas temperatures in the oxidation zone of ~1000°C.[76]

Conversely, the high temperature (~1900°C) operation of the British Gas Lurgi Slagging Gasifier, an advanced derivative of the Lurgi dry-ash gasifier, causes the inorganic material to fuse. The burden must produce a well-fused slag of relatively low viscosity. In order to moderate fusion temperatures and control the viscosity of the molten ash, a flux such as limestone or iron furnace slag, may be added to the fuel. The ash and flux combine in the high temperature hearth region of the gasifier to form an eutectic mixture.[76] The molten slag is drained from the gasifier base and water quenched to be discharged as a granular, vitreous frit.

2.10.6 Fluidised bed gasification

Theory of fluidisation

A bed of particles offers resistance to fluid flow through it. As the velocity of flow increases, the drag force exerted on the particles will be sufficient to support the weight of the particles in the bed. The fluid/particle system then begins to exhibit fluid-like properties and will flow under the influence of a hydrostatic head. This is the point of incipient fluidisation and the gas velocity needed to achieve this is referred to as the minimum fluidising velocity, U_{mf}. Beyond this velocity, the pressure drop across the bed will be approximately equal to the weight of the bed per unit area. Thus:

$$\Delta P_b A_b = \frac{m}{\rho_p} (\rho_p - \rho_f) g \qquad (2.1)$$

where ΔP_b = pressure drop across the bed
A_b = cross sectional area of bed
m = mass of particles in bed
ρ_p = effective density of particle
ρ_f = density of fluid
g = acceleration due to gravity

With the gas-fluidised system instabilities form. These resemble bubbles of vapour in a boiling liquid and, as they rise through the bed, they are responsible for mixing the solids which is such an important feature of gas-fluidised behaviour.[77]

2.10.7 The fluidised bed gasifier (FBG)

In the fluidised bed gasifier a high velocity stream of reactant gases are used to fluidise a bed of particulate material containing the fuel. The degree of disturbance is determined by the velocity of the gas. Bubbles, similar in nature to those in a briskly boiling liquid, pass through the bed. Solid particles are violently agitated resulting in rapid mixing, high reaction rates, and ensuring near uniformity of temperature as in a stirred liquid. A variable temperature distribution is encountered in the immediate vicinity of a reaction. The fresh fuel feed is rapidly distributed throughout the bed which is maintained in turbulent motion by the gasifying agent. Thus the operating temperatures for biomass gasification (~800-850°C) are subsequently lower than for the fixed bed reactor configurations. The fluidising medium is usually a silica sand, although alumina and other refractory oxides have been employed for fuels of a high sintering propensity.[66,78]

Bubbles bursting on the surface generate pressure fluctuations and throw a spray of particles into the freeboard space above the bed. As the material is gasified, the smaller and lighter particles of unconverted carbon and ash are elutriated by the gases. Entrainment will occur until an equilibrium depth of the fluid bed is established, depending on the particle size distribution and the fluidising velocity. Gasifier designs in which the fluidising material retains a well defined surface level are referred to as 'bubbling beds'. The whole bed is a seething mass of particles and bubbles. The velocity of the primary gasifying agent is limited to 1-2m/s to prevent excessive turbulence. Bubbling bed FBGs can be applied to both new and retrofit situations. In some instances the entrained particles are continuously recycled to the gasifier and the fine particulates fill the entire vessel, with a relatively low concentration. This type of bed is known as a 'fast fluidised bed' or a 'fast recycling bed'. In other applications the mixing of solids in the fluidised bed is enhanced by using a non-uniform distribution of the oxidant to the bed, often coupled with an inclined distributor plate. The velocity of the reactant gases is approximately 8m/s. This type of system is referred to as a 'circulating bed'.[78] Conversion of the feedstock to product gas takes place predominantly within the bed, however the gasification of entrained char particles and thermal cracking of pyrolysis products continues in the freeboard section.

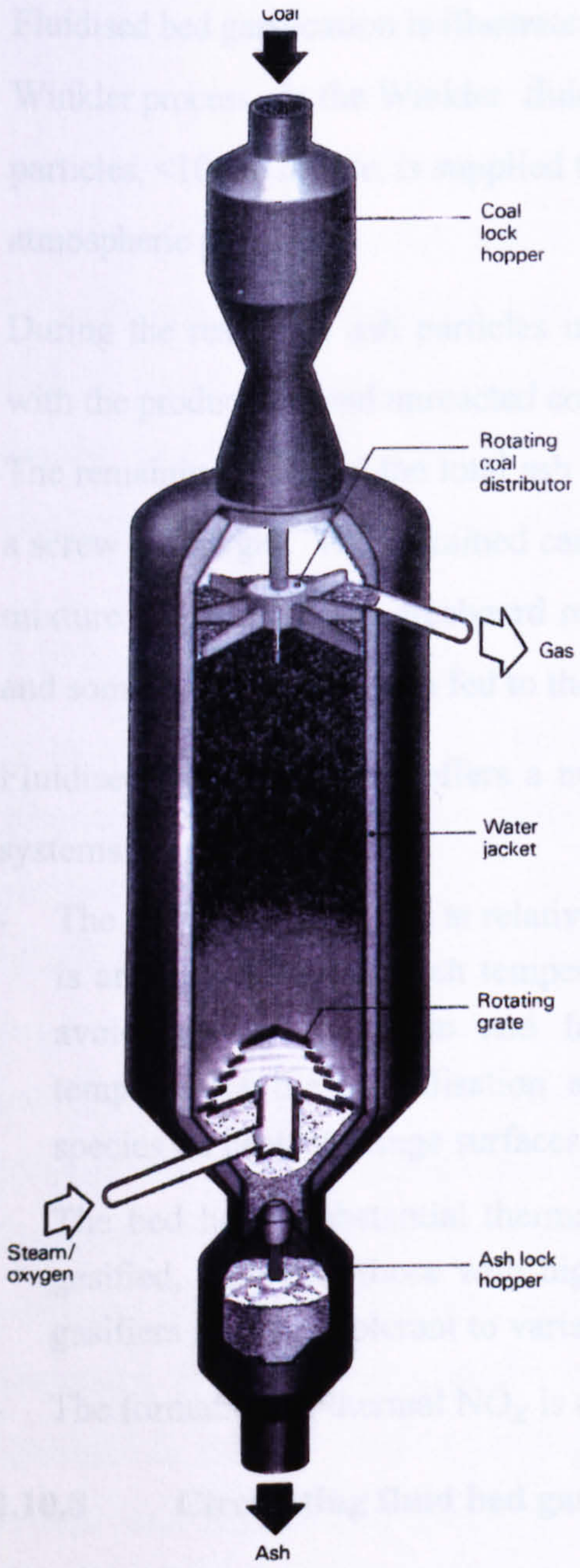

Figure 2.5 Lurgi gasifier

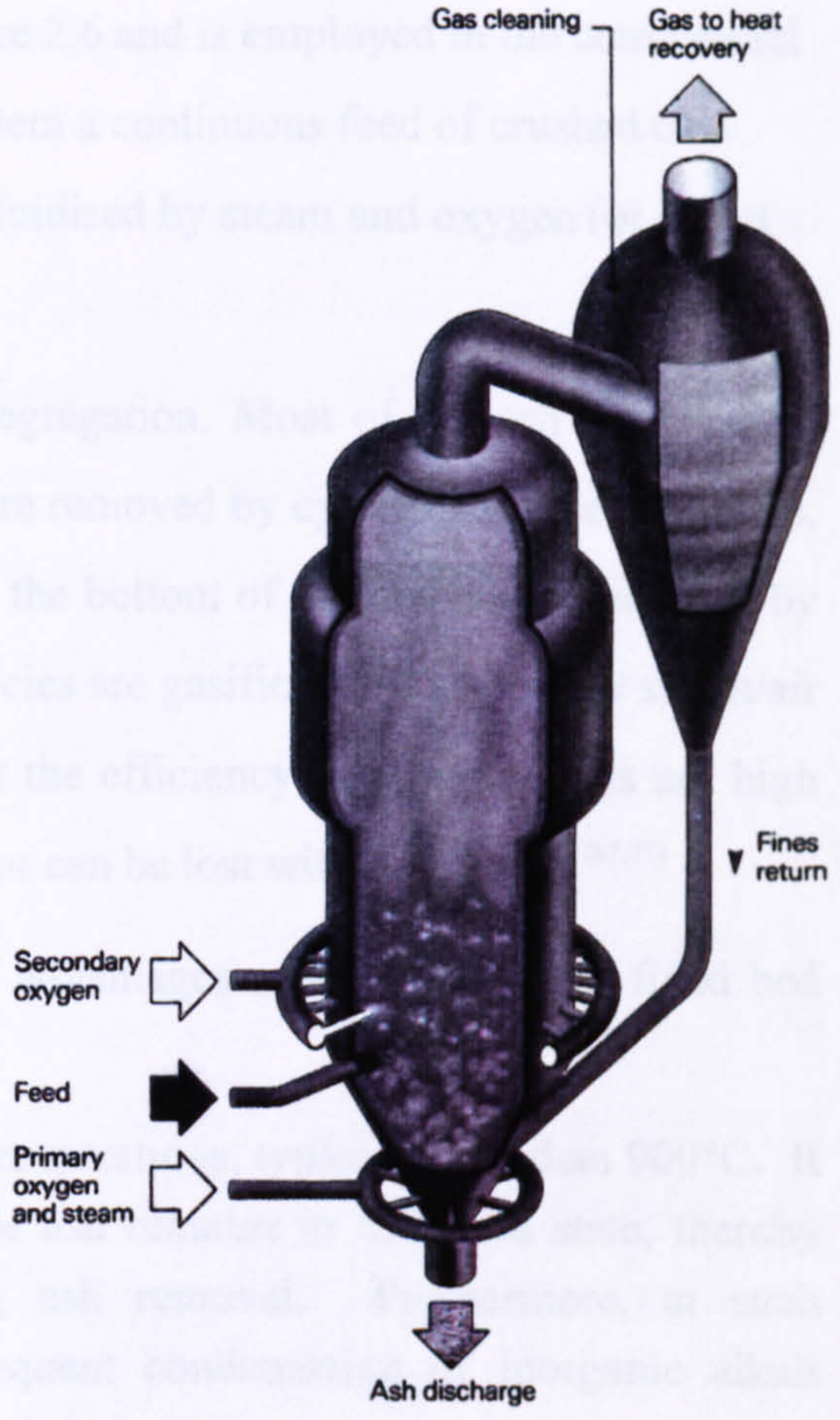

Figure 2.6 Winkler gasifier

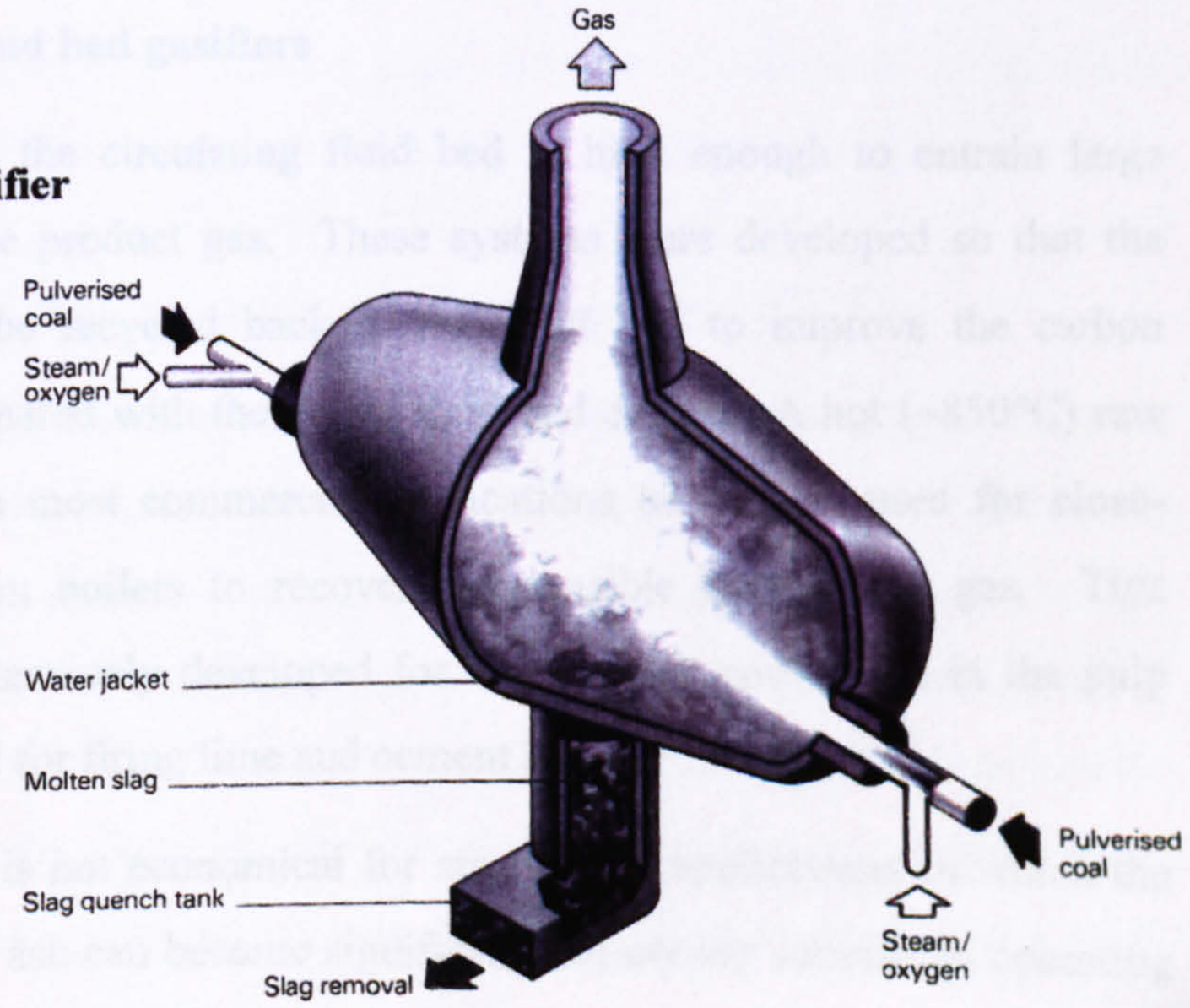

Figure 2.7 Koppers-Totzek gasifier

Fluidised bed gasification is illustrated in Figure 2.6 and is employed in the commercial Winkler process. In the Winkler fluidised system a continuous feed of crushed coal particles, <10mm in size, is supplied to a bed fluidised by steam and oxygen (or air) at atmospheric pressure.

During the reactions, ash particles undergo segregation. Most of the ash is elutriated with the product gas and unreacted coal fines are removed by cyclones and precipitators. The remaining ~30% of the total ash settles to the bottom of the bed and is removed by a screw discharger. The entrained carbon particles are gasified by a secondary steam/air mixture injected into the freeboard region, but the efficiency of conversion is not high and some 20% of the carbon fed to the generator can be lost with the fly ash.[67,77]

Fluidised bed gasification offers a number of advantages over conventional fixed bed systems.

- The bed can be operated at relatively low temperatures, typically less than 900°C. It is anticipated that at such temperatures the ash remains in the solid state, thereby avoiding slag formation and facilitating ash removal. Furthermore, at such temperatures the volatilisation and subsequent condensation of inorganic alkali species on heat exchange surfaces may be minimised.
- The bed has a substantial thermal capacity. This allows a variety of fuels to be gasified, including those with high moisture and ash contents. Thus fluidised bed gasifiers are more tolerant to variations in fuel particle size and quality
- The formation of thermal NO_x is curbed since operating temperatures are reduced.

2.10.8 Circulating fluid bed gasifiers

The fluidising velocity in the circulating fluid bed is high enough to entrain large amounts of solids with the product gas. These systems were developed so that the entrained material could be recycled back to the fluid bed to improve the carbon conversion efficiency compared with the single fluid bed design. A hot (~850°C) raw gas is produced which, in most commercial applications to date, is used for close-coupled process heat or in boilers to recover the sensible heat in the gas. This configuration has been extensively developed for wood waste conversion in the pulp and paper mill industry and for firing lime and cement kilns.[66]

The fluidised bed gasifier is not economical for small scale applications in which the loss of carbon in entrained ash can become significant. Moreover substantial operating

costs are incurred. The potential to increase the generating capacity of FBGs is most favourable, and the design can be readily scaled up with considerable confidence. Alternative configurations such as twin-bed systems and circulating FBs are also available to accommodate almost every type of feedstock or thermochemical process. In catalytic thermochemical processes, the bed material can be replaced by the catalyst, thereby avoiding costly impregnation techniques. Alternatively a second catalytic reactor can be added as in the TPS (Thermal Processing Systems, Sweden) or a thermal cracking reactor can be added as in the Steine Industrie gasifier.[66]

2.10.9 Entrained phase

In an entrained phase gasifier, a finely reduced feedstock is injected into the gasifier in suspension with the reactant gases. An inert fluidising medium is absent. The gasification reactions take place virtually simultaneously in the temperature regime of ~1200-1500°C, depending upon the oxidant employed. Consequently the product gas has a low concentration of tars and condensable gases. This approach is used in the commercial Koppers-Totzek process, shown in Figure 2.7, for the gasification of dried pulverised coal with oxygen and steam. A high reaction rate and hence carbon conversion is achieved by operation under ash slagging conditions despite the short residence time of the entrained solids.[77] About 60% of the ash falls into a water quenching bath forming granules of slag. The resultant fine ash particulates are entrained in the raw product gas leaving the gasifier. The entrained flow gasification system was designed primarily to produce gases for the manufacture of synthetic organic chemicals. There is little experience with biomass fuels in such systems.

2.10.10 The integrated gasification combined cycle system (IGCC)

Gas turbine/steam turbine combined cycle systems have been developed in recent years in an effort to increase the overall conversion efficiency, and is the generating technology of choice in many utility and independent power markets with natural gas firing. Gasification produces a hot product gas which leaves the reactor vessel under pressure. After passing through a clean-up system, the gas is supplied to a combustion turbine/generator coupled with a steam turbo-alternator. Waste heat recovered from the gas turbine exhaust is used to generate high pressure steam which is directed to a turbo-

alternator which produces 30-40% of the total plant electrical output. The integrated gasification combined cycle plant achieves a net efficiency of approximately 43%, higher than the efficiency achieved with most gasification plants (~35% average). An example of an IGCC developed for coal and coal/biomass mixtures is shown in Figure 2.8, a schematic of the British Coal Topping Cycle.[78]

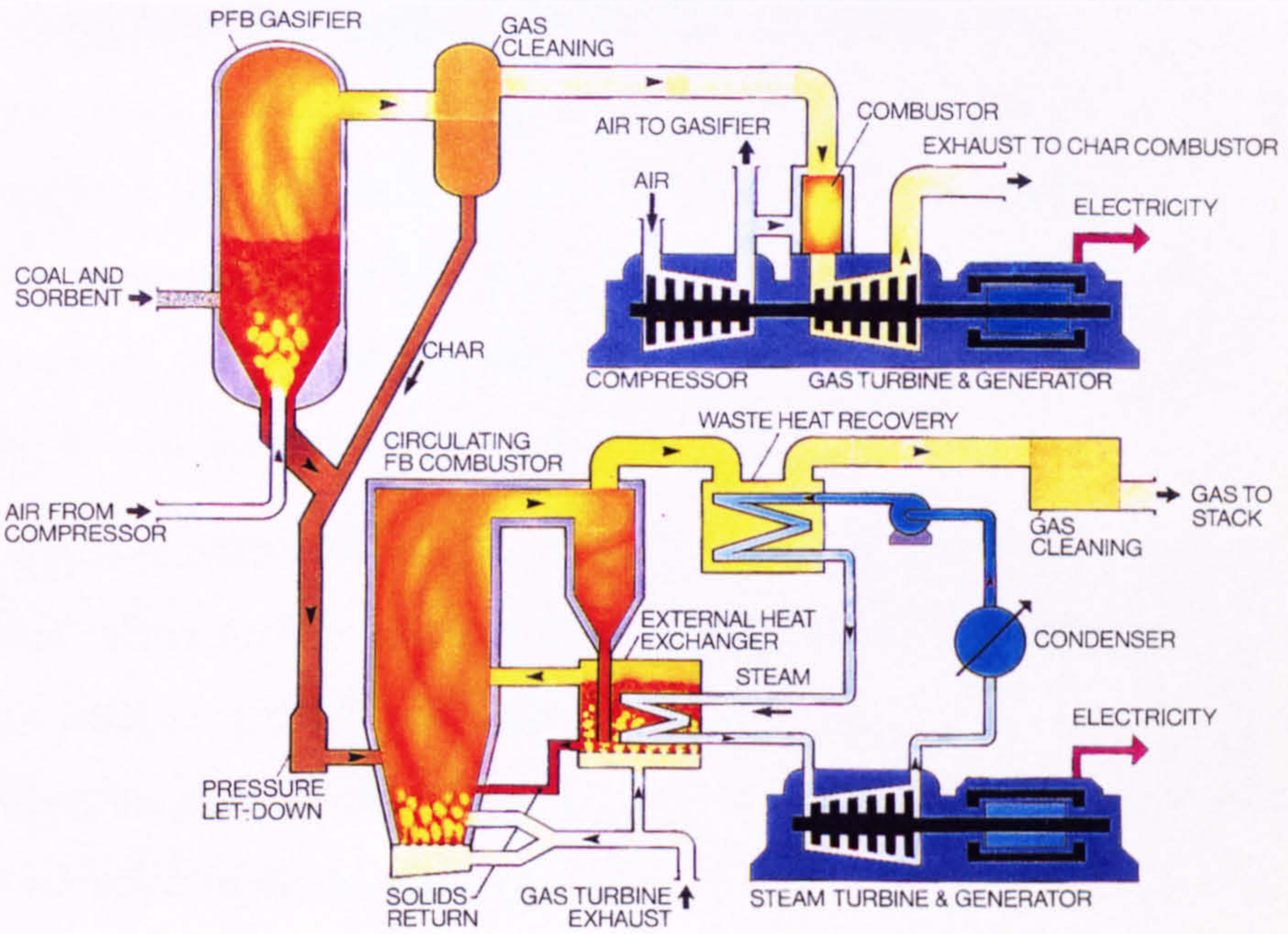

Figure 2.8 Integrated gasification combined cycle system- British Gas Topping Cycle[78]

2.11 Deposit formation

Definitions

Ash deposits are described, somewhat arbitrarily, as slagging, fouling or agglomerate. 'Slagging' is a term which is reserved for the formation of ash deposits in the radiant zone of a boiler. The deposits accumulate when molten or partially fused particles of ash impinge and adhere to a surface. The term 'fouling' is used to describe an accumulation of bonded and sintered deposits in the convective passes of a boiler.[35] The gas temperatures in this region are appreciably lower and any molten material will have solidified. However, the condensation of alkali vapours on the surfaces of gas borne ash particles produces a viscid surface which causes the particles to adhere to surfaces and to one another.

The agglomeration of ash particles can occur when a bond forms by the collision and adhesion of two or more particles of fluidised bed material. A molten or partially

molten surface must be present to facilitate the binding mechanism.[35] A molten surface can be formed by fusion of the inorganic particles or as a result of the chemical interaction of two particles in which a liquid phase forms as part of an eutectic reaction; such a process is commonly termed a fluxing reaction. Once an initial bond has formed, diffusion and viscous flow may increase the contact area between the particles and this leads to a strengthening of the bond. Subsequent interaction with other particles in the bed can increase the size of the ash agglomerate, and this can eventually lead to a loss in fluidisation of the bed. Solid state reactions may occur if the local temperature is two thirds of the melting point of the solid, with transport via the vapour phase from one particle to another at the point of contact producing a bond called a sinter bridge.[80] For this to occur, the particles must be in contact for quite some time.

The literature is replete with studies concerned with the slagging and fouling of coal-fired systems. Since no two coals are the same in terms of the degree of metamorphism or mineral constituents, the range of problems encountered is legion. The deposits have a complex and variable morphology, microstructure and composition which depend on the ash composition of the feed material, boiler design and mode of operation. It would appear that the formation of fouling deposits in particular, may be enhanced when considering the gasification of biomass and refuse, which contain greater quantities of alkalis and alkali metals than the majority of coals. Indeed in Denmark where substantial operational experience in biomass combustion, in particular straw firing for combined heat and power, has been established, extensive boiler slagging and fouling have been reported.[81] However, there remains a distinct paucity of fundamental information pertaining to the nature of such deposits and their mode of formation.

2.11.1 Fouling deposits

The fouling of heat exchanger surfaces during the combustion of coal has been the subject of many studies. Compounds of sodium and potassium, including chlorides, sulphates, carbonates and hydroxides, are major contributors to fouling problems in industrial boilers as a result of the ease with which the alkalis are volatilised at combustion temperatures. Potassium compounds have greater vapour pressures than their sodium counterparts, however the release of a particular alkali compound during combustion is dependent upon the chemical state and distribution of the alkali in the

feed material. Once volatilised, the alkalis condense on cool boiler surfaces and on gas borne ash particles. There is a general consensus that these condensed alkali-rich surface films on wall tubes and superheater elements facilitate the encapsulation of particles transported by the flue gas. The high concentration of alkalis condensed on ash particles leads to a mutual reaction producing a thin sticky surface which increases the probability of particle-to-particle adherence following collision. This surface layer also encourages viscous flow sintering, resulting in stronger deposits that adhere to heat receiving surfaces and are exposed to furnace temperatures. The deposits accumulate in a direction counter to the gas flow, and may also form downstream of a tube under the influence of eddy currents.[64,65,66]

For the range of UK coals, fouling is generally initiated by the deposition of alkali metal (Na^+, K^+) sulphates in the cooler boiler reaches, which constitute a low melting and hence tacky surface layer to bond other types of impinging gas borne particle. The subsequent sintering of the ash particles is assisted by the continued condensation of sulphates to form an adhesive matrix. As the deposit accumulates the temperature gradient between the tube metal and outer surface becomes significant and the outer region of the deposit approaches gas temperatures. If the temperature becomes sufficiently high, bulk sintering will occur.

2.11.2 Slag deposits

The initiation and adhesion of coal-derived slag deposits has been studied in some detail. The initial layer of deposit material is formed by the impaction of molten ash droplets on the oxide layer of the boiler steel substrate. The adhesion of the ash deposit constituents to boiler tubes begins with ash particle retention as a result of van der Waals, electrostatic and liquid film surface tension forces. For molten or partially molten ash species, favourable wetting of the steel surface by the particle results in a large contact area for chemical bonding to the oxide layer. Slagging deposits on coal-fired boiler tubes consist largely of flame vitrified silicate ash, ferrous oxide, and calcium and alkali sulphates.[35] The fused silicates and molten sulphates form immiscible phases at high temperature, first on individual particles and then as separate layers in the deposit. The slags consist of a complex mixture of glassy and crystalline phases and the tenacity of the deposit is dependent on the degree of fusion and

crystallinity. Some systems use fluxes, such as limestone, to maintain and control slag viscosity, and this is reflected in the slag composition.

A preliminary investigation of the nature and extent of deposits in biomass fired plants by Baxter et al[82], indicated that high alkali fuels such as energy crops, agricultural and forestry residues were not suitable feedstocks for conventional boiler systems due to the extensive formation of slagging deposits on boiler grates, fouling deposits in convective passes, and agglomerates in fluidised bed processes. The fouling deposits were found to comprise of alkali chlorides, sulphates and carbonates intimately mixed with silica, alumina and complex silicates from elutriated ash or fluidised bed media. The evidence is consistent with the fouling mechanism previously described. Potassium sulphates and chlorides were found condensed on upper furnace refractory walls. In the majority of deposits, compounds containing potassium, sulphur and chlorine were found to be the principal bonding agents, and the presence of these constituents in the biomass ash were assumed to be the most appropriate indication of the tendency of the fuels to form deposits.

The processes which result in deposition depend directly on the nature of the inherent inorganic material in the feedstock. Other influencing factors include the boiler conditions such as temperature, residence time, fluid dynamics, and local oxidising or reducing environments.

2.12 Nucleation and crystal growth

The nature of the residues from combustion and gasification processes using biomass, domestic refuse and industrial wastes as fuels are both complex and subject to great variability. If rapid cooling of molten ash occurs, such as in a water quenching bath, a state of equilibrium is not attained and the material is unable to crystallise before solidification resulting in the formation of a vitreous slag. Slower cooling rates may allow equilibrium conditions to be reached and crystallisation to occur. The inter-relationships between the liquid, crystalline and vitreous states of a material are best explained in terms of the volume-temperature diagram for a glass forming substance shown in Figure 2.9.[83]

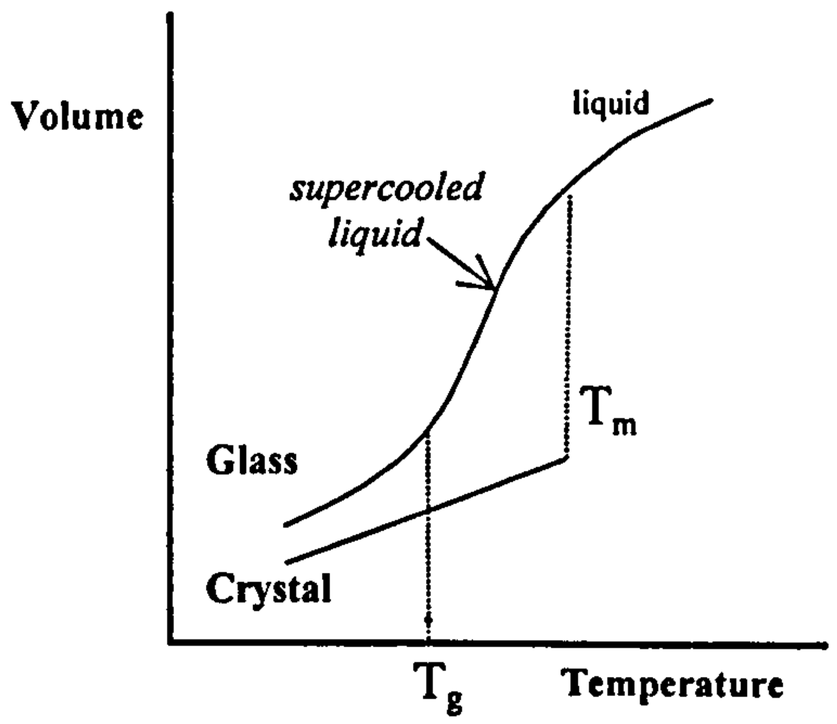

Figure 2.9 Volume-temperature relations for liquid, glass and crystal

The crystalline form of a material has a lower free energy than a supercooled liquid and crystallisation will occur at T_m, accompanied by a decrease in volume, if nuclei are present in the melt. However, at rapid cooling rates, crystallisation is inhibited, and the volume of the now supercooled liquid decreases at about the same rate as above the melting point. The volume-temperature curve of the supercooled liquid undergoes a change in direction which corresponds to a marked decrease in the expansion coefficient at a range of temperatures characterised by the glass transformation range. Abrupt changes in other physicochemical properties are also observed at the glass transformation, T_g, and include a reduction in the specific heat and thermal expansivity and an increase in the activation energies for diffusion and viscous flow. Such changes are a consequence of the lattice relaxation effect. In this region, the viscosity of the

material has increased to a sufficiently high value, typically 10^{11} to 10^{12} Pa s, so that the material exhibits solid-like behaviour. Below T_g the material is described as a glass. The value of T_g is not absolute, but is influenced by the thermal history of the sample, rate of cooling and the method of determination.[84]

In relation to the crystalline state, a glass is in a state of metastable equilibrium. The permanence of a glass at a particular temperature is due to the relative immoblity of the ions of the structure, which precludes simultaneous movement of groups large enough to form the minimum energy configuration of a crystalline structure.[85]

2.12.1 Crystallisation

The nucleation and growth of crystals in a multicomponent oxide system, such as in a biomass ash melt, is an extremely complicated process which has not been studied in any great depth. However the basic physical principles established for the crystallisation of liquids consisting of a single component or a simple mixture of two components, serve as a useful general background.

The crystallisation of a liquid, or the condensation of a vapour, is generally regarded as a process which involves two distinct steps, nucleation and subsequent crystal growth. The first step involves the formation of a stable nucleus and the second the growth of the nucleus to form a crystal. If nucleation occurs spontaneously within a pure phase, and the probability of nucleus formation is the same throughout the system, the process is described as homogeneous. Thus the parent phase must be chemically, structurally and energetically homogeneous.[86]

The transformation from a supercooled liquid to the crystalline state involves a decrease in free energy, which provides the driving force for solidification. The free energy change per unit volume, ΔG_V, on transforming a liquid to a crystalline solid can be estimated as follows. From the definition of the Gibbs free energy,

$$\Delta G_V = \Delta H_V - T\Delta S_V \qquad (2.2)$$

where ΔH_V and ΔS_V are the latent heat and entropy of fusion per unit volume, respectively.[83] At the melting point, T_m, $\Delta G_V = 0$; hence the entropy of fusion (ΔS_V) is given by,

$$\Delta S_V = \frac{\Delta H_V}{T_m} \tag{2.3}$$

At temperatures not far from T_m the difference in the specific heats of the liquid and solid can be ignored, therefore ΔH_V and ΔS_V are approximately independent of temperature. Combining Equations (2.2) and (2.3) gives

$$\Delta G_V = \frac{\Delta H_V(T_m - T)}{T_m} = \frac{\Delta H_V \Delta T}{T_m} \tag{2.4}$$

where ΔT denotes the undercooling.

The decrease in free energy in forming a spherical crystalline region of radius r is $4/3\pi r^3 \Delta G_V$. However the formation of a crystal nucleus in a liquid involves the creation of a liquid-nucleus interface with an associated surface energy (γ_{LN} per unit area), and is thus accompanied by a free energy increase. The net change in free energy on forming the crystal nucleus (ΔG_{hom}) is[87]

$$\Delta G_{hom} = -\frac{4}{3}\pi r^3 \Delta G_V + 4\pi r^2 \gamma_{LN} \tag{2.5}$$

Where r = radius of particle
γ_{LN} = liquid-nucleus interfacial energy (assumed to be independent of orientation)
ΔG_V = free energy change per unit volume accompanying the liquid-solid phase transformation

The Gibbs free energy of the system as a function of the radius of a nucleus is illustrated in Figure 2.10. It is envisaged that the formation of a crystalline region, initially termed an 'embryo', is provoked by random atomistic fluctuations in the structure of the liquid. An embryo will be a stable nucleus if several atoms in close proximity, and with an ordered arrangement corresponding to a crystalline structure occupy a volume of radius greater than r^*, the critical nucleus size. If $r < r^*$, the positive contribution of the surface energy of the interface between the crystal and the adjacent liquid to the net free energy change, is of significant magnitude to prevail over the decrease in free energy associated with crystallisation. A state of lower free energy is obtained by dissolution of the solid. When $r > r^*$, the free energy of the system is reduced by growth of the established nucleus. When $r = r^*$ the critical nucleus is effectively in (unstable) equilibrium with the surrounding liquid.[88]

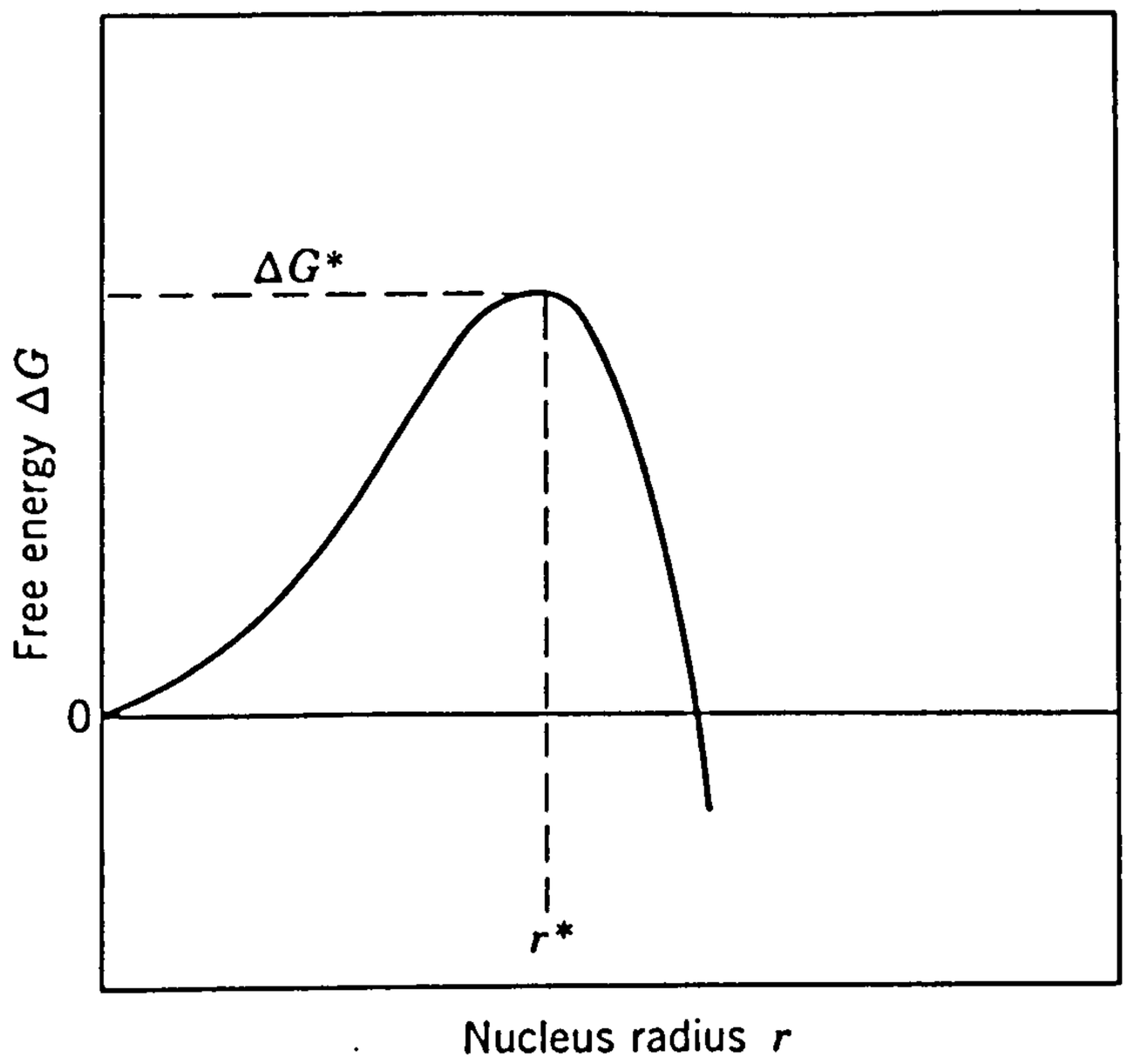

Fig 2.10 Free energy change associated with homogeneous nucleation of a spherical nucleus of radius r[83]

The size of the embryo which has the maximum free energy, and which on further growth leads to a continuous decrease in free energy, is determined from the relation $\delta(\Delta G_{hom})/\delta r = 0$ and is given by[83]

$$r^{*} = \frac{2\gamma_{LN}}{\Delta Gv} \qquad (2.6)$$

Thus the energy barrier to homogeneous nucleation (ΔG^{*}_{hom}) is given by,

$$\Delta G^{*}_{hom} = \frac{4}{3}\pi(r^{*})^{2}\gamma_{LN} = \frac{16\pi\gamma^{3}_{LN}}{3(\Delta G_{v})^{2}} \qquad (2.7)$$

Substituting Equation (2.4) for ΔG_v in Equation (2.7) gives,

$$\Delta G^{*}_{hom} = \frac{16\pi\gamma^{3}_{LN}T_{m}^{2}}{3\Delta H_{v}^{2}}\frac{1}{(\Delta T)^{2}} \qquad (2.8)$$

Thus the growth of a crystal nucleus is not necessarily spontaneous but depends on

(*i*) the formation of nuclei exceeding a critical size, and

(*ii*) the extent to which a liquid is supercooled.

2.12.2 Rate of homogeneous nucleation

The rate of crystallisation of a supercooled liquid is specified by the rate of crystal nucleation and the speed with which the crystal grows at the expense of the liquid. Considerations based on statistical thermodynamics show that the probability of thermal

fluctuations leading to an increase in free energy equal to or greater than ΔG^* is given by the Boltzmann equation:

$$\rho(\Delta G^*_{hom}) = \exp\left(\frac{-\Delta G^*_{hom}}{RT}\right) \quad (2.9)$$

where R is the gas constant.[84] Thus the rate at which nuclei form will be proportional to $\rho(\Delta G^*_{hom})$. The term ΔG^*_{hom} may be referred to as the 'thermodynamic barrier to nucleation' and is given by Equation 2.7.

However, the formation of a crystalline nucleus involves some structural rearrangement in the melt, requiring that atoms overcome the energy barriers which impede these rearrangements. This may involve a diffusion process (over small distances) or a reorientation of molecules into a configuration of greater stability. The rate at which the material can be transformed from a structure characteristic of a liquid to that of a crystal is proportional to an Arrhenius-type rate factor, $[\exp(-\Delta G_D/RT)]$ where ΔG_D is the activation energy associated with the structural rearrangement process. The rate factor decreases as the temperature is reduced. ΔG_D may also be referred to as the 'kinetic barrier to nucleation'.

The rate of homogeneous nucleation is[84]

$$I = n\nu \exp\left(\frac{-N\Delta G^*_{hom}}{RT}\right)\exp\left(\frac{-\Delta G_D}{RT}\right) \text{ nuclei } m^{-3}\ s^{-1} \quad (2.10)$$

where, I = number of stable nuclei formed per unit volume of liquid per second
n = number of atoms per unit volume
ν = vibrational frequency of atoms at the nucleus-liquid interface
N = Avogadros number
ΔG^*_{hom} = 'thermodynamic barrier to nucleation'
ΔG_D = 'kinetic barrier to homogeneous nucleation'
R = gas constant
T = temperature

Assuming an activated process, the rate of nucleation increases to a maximum value as the undercooling is increased, with further undercooling the kinetics of the transformation begin to exert a controlling influence and the rate decreases exponentially as the proportion of atoms with sufficient thermal energy to traverse the melt-crystal interface is decreased. Thus the relationship between the rate of homogeneous nucleation (I) and temperature (T) has the form shown in Figure 2.11.

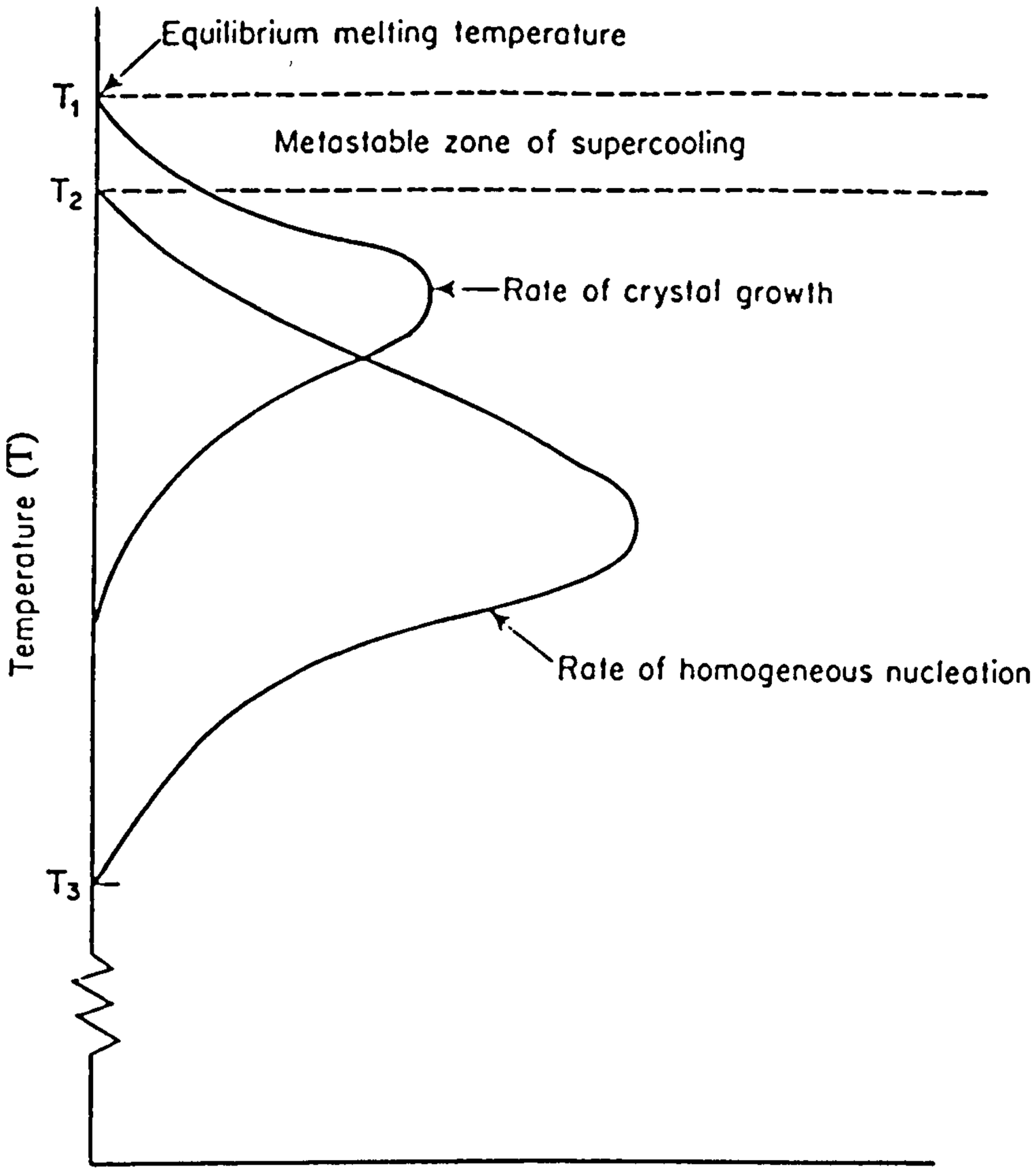

Figure 2.11 Effect of temperature on the rates of homogeneous nucleation and crystal growth in a viscous liquid

In practice, homogeneous nucleation is rarely encountered in solidification. Nucleation in inorganic melts is usually heterogeneous in nature, occurring externally or at surfaces within the melt.

2.12.3 Heterogeneous nucleation

The nucleation of stable crystalline particles may be aided by inhomogeneities present in the liquid. Minute fragments of incompletely melted material, particles of a second phase, dust on the melt surface or the wall of the containing vessel may provide energetically favourable sites for nucleus formation. These inhomogeneities provide an interface upon which atoms of the liquid can crystallise. This process is known as heterogeneous nucleation.

The undercooling required for heterogeneous nucleation depends on the rate of cooling, composition of the liquid and the crystal structure of the seed material on which the crystallisation occurs. In most practical situations, crystallisation in undercooled liquids is controlled primarily by the rate of crystal growth.

Consider the formation of a crystal nucleus on a planar solid substrate in contact with a supercooled liquid phase as depicted in Figure 2.12.[86] The total interfacial energy of the system is minimised if the nucleus adopts the configuration of a spherical cap with a contact, or 'wetting', angle θ given by the condition that the interfacial energies of the liquid-substrate (γ_{LS}), nucleus-substrate (γ_{NS}) and the liquid-nucleus (γ_{LN}) balance in the plane of the substrate. Thus

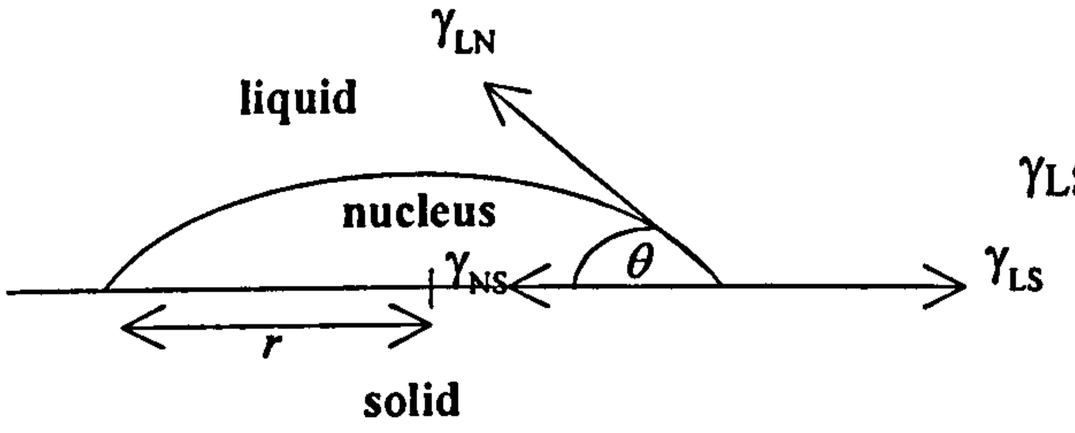

$$\gamma_{LS} = \gamma_{NS} + \gamma_{LN}\cos\theta \qquad (2.11)$$

Figure 2.12 Spherical cap model of heterogeneous nucleation

The free energy change associated with the formation of the nucleus (ΔG_{het}) is given by the relationship

$$\Delta G_{het} = -V_s\Delta G_V + A_{LN}\gamma_{LN} + A_{NS}\gamma_{NS} - A_{NS}\gamma_{LS} \qquad (2.12)$$

where, the volume of the spherical cap, $V_s = \pi r^3(2+\cos\theta)(1-\cos\theta)^{2/3}$

the liquid-nucleus interfacial area, $A_{LN} = 2\pi r^2(1-\cos\theta)$

the nucleus-substrate interfacial area, $A_{NS} = \pi r^2\sin^2\theta$

Equation (2.12) can be written in terms of the contact angle θ and the cap radius r as

$$\Delta G_{het} = [-\frac{4}{3}\pi r^3\Delta G_V + 4\pi r^2\gamma_{LN}]f(\theta) \qquad (2.13)$$

where, $f(\theta) = (2+\cos\theta)(1-\cos\theta)^{2/4}$

With the exception of the factor $f(\theta)$, the expression for heterogeneous nucleation is identical to that for homogeneous nucleation defined by Equation (2.5). $f(\theta)$ has a numerical value ≤ 1 dependent only on the shape of the nucleus defined by θ, and is therefore referred to as a shape factor. By differentiation of Equation (2.12) it can be shown that $\Delta G_{het} = \Delta G^*_{hom} f(\theta)$.[88] Therefore, the activation energy barrier to

heterogeneous nucleation (ΔG_{het}) is less than that for homogeneous nucleation (ΔG^{*}_{hom}) by the shape factor $f(\theta)$. Thus the general action of a nucleating substrate is to reduce the barrier to nucleation represented by the surface energy. The ability to produce large densities of internal nuclei in glass-forming liquids by the addition of selected nucleation agents to the melt has important applications in producing glass-ceramic materials, as well as in producing glazes and enamels having desired degrees of crystallinity. In boiler systems, crystallisation is undoubtedly initiated by heterogeneous nucleation due to the presence of undissolved material dispersed in the melt.

2.12.4 Rate of heterogeneous nucleation

The steady state heterogeneous nucleation rate (I_{het}) per unit area of substrate in condensed phases may be written as[83]

$$I_{het} = n_1 \nu \exp\left(\frac{-\Delta G_{het}}{RT}\right)\exp\left(\frac{-\Delta G_D}{RT}\right) \qquad (2.14)$$

where, n_1 = number of molecules in contact with the substrate
ν = molecular jump frequency
ΔG_{het} = free energy of formation of a heterogeneous nucleus of critical size
ΔG_D = activation energy for transport across the liquid-nucleus interface

The expression is similar to its counterpart for homogeneous nucleation.

2.12.5 Crystal growth

Once a stable nucleus has been established, the rate at which a crystal will grow is fixed by conditions of temperature and the degree of supersaturation. An atom or molecule must aquire an activation energy in order to detach itself from the attractions of neighbouring atoms of the liquid phase and diffuse to the crystal-liquid interface and form new bonds determined by the structure of the growing crystal. Figure 2.13 represents the energy-position relationship which exists for atoms at the solid-liquid interface. It is assumed that atoms in the liquid possess a free energy per unit gram higher than that possessed by atoms in the crystal by an amount equal to the bulk free energy of crystallisation, ΔG.[87] To cross the interface from liquid to solid, an atom requires a free energy of activation ΔG_a, and to cross from solid to liquid a free energy

of activation $\Delta G_a + \Delta G$. The growth rate is limited by the rate at which atoms can diffuse across the interface.

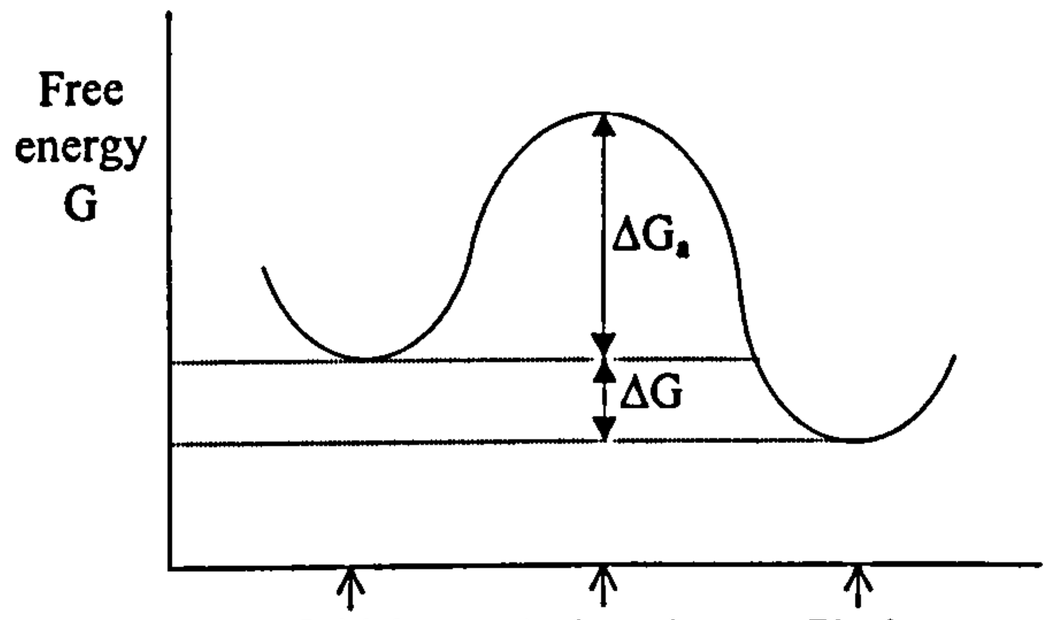

Figure 2.13 Transformations from initial to final state through an activated state of higher free energy

The net rate of crystal growth will be proportional to the difference between the frequency of liquid-solid transitions, ν_{LS} and the frequency of solid-liquid transitions ν_{SL}

where, $\nu_{LS} = \nu \exp\left(\frac{-\Delta G_a}{RT}\right)$

$$\nu_{SL} = \nu \exp\left[\frac{-(\Delta G + \Delta G_a)}{RT}\right]$$

Therefore, the rate of crystal growth, $u = f\delta\,(\nu_{LS} - \nu_{SL})$

$$u = f\delta\nu \exp\left(\frac{-\Delta G_a}{RT}\right)\left[1 - \exp\left(\frac{\Delta G}{RT}\right)\right] \quad (2.15)$$

Where, δ = interatomic jump distance
ν = frequency of molecular vibration
f = fraction of sites at the interface to which molecules can be attached

All sites on the crystal surface may not be available for molecular attachment, thus a factor, f, defined as the fraction of sites to which molecules can be attached, is introduced. For undercoolings where the thermodynamic driving force is appreciable, growth can occur almost anywhere on the crystal surface, and the factor f approaches unity. However, at small undercoolings, f would be expected to exhibit a temperature dependency which would vary with the growth mechanism.[83,86,87]

Liquid silicates have high viscosities, compared to metals, and consequently mass diffusion in polymeric melts is much slower than thermal diffusion. Thus, thermal

diffusion has less of a controlling effect on crystal growth, particularly in multicomponent systems in which marked compositional changes occur at the crystal-melt interface. The activation energy for viscous flow is frequently used to approximate the activation energy for diffusion.[87] In some systems, but not all, this assumption provides reasonable agreement between theory and experiment. The theoretical equation for the velocity of crystal growth in a homogeneous melt may also be expressed as follows[89]

$$u = \frac{f\mathrm{RT}}{3\pi\delta^2\mathrm{N}\eta}\left[1-\exp\left(\frac{-\Delta\mathrm{S}\Delta\mathrm{T}}{\mathrm{RT}}\right)\right] \qquad (2.16)$$

where, N is the Avogadro's number, η the melt viscosity, ΔS the entropy of fusion (assumed to be independent of the crystallisation temperature T), and ΔT the undercooling. One cannot expect Equation 2.16 to be applicable to more complex materials such as multicomponent oxide glasses. Indeed, it is well known that for these materials the rate of crystal growth varies with temperature much less rapidly than might be expected from the viscosity data.[87]

The temperature dependency of the growth rate of crystals in a supercooled melt follows a curve which is similar in shape to that of nucleation, as illustrated in Figure 2.11. The rate of growth of a crystal nucleus will be zero at the melting point, where $\Delta G = 0$, and will increase rapidly as the supercooling is increased but will eventually pass through a maximum. At large undercoolings, the growth rate is limited by the rate at which atoms can diffuse across the melt-crystal interface.

There are basically two different types of solid-liquid interface. One is essentially an atomically flat close-packed interface, where the transition from liquid to solid occurs over a rather narrow zone approximately one atom thick. Such interfaces can also be described as smooth, faceted, or sharp and are often associated with non-metals. The other type is an atomically diffuse, rough or non-faceted interface, characteristic of metallic systems, in which the transition from liquid to solid occurs over several atom layers. On account of the differences in atomic structure these two types of interface migrate in quite different ways. Diffuse interfaces migrate by a continuous growth process, while flat interfaces advance by a lateral growth mechanism.[88] The type of

structure adopted by a particular system will be that which minimises the interfacial free energy.

Two types of mechanism have been postulated for lateral growth: (i) a screw dislocation mechanism and (ii) a surface nucleation mechanism; for both cases, the morphology of growth is faceted. It is recognised that in practical applications the continuous growth of a crystal is sustained by the presence of a particular type of lattice defect, a screw dislocation. The emergence of a screw dislocation at a crystal surface causes a tapering step. The addition of atoms to this step creates a self-perpetuating spiral. Thus each new atomic layer does not need to be initiated in the same way as a critical nucleus as in the latter case of surface nucleation. Experimental observations are in general accord with those predicted from theoretical considerations, however it is plausible that one type of growth mechanism may not apply for all values of undercooling.[89]

A liquid which is a homogeneous mutual solution of two or more different substances does not have a single melting point above which the equilibrium form is liquid and below which it is crystalline. For any given pressure and composition of the mixture, there are two different temperatures which characterise the crystallisation. The *liquidus* temperature is that above which no solid exists in equilibrium, and the *solidus* temperature is that below which no liquid exists in equilibrium. The difference between the liquidus and solidus temperatures may not be trivial and has direct consequences in the formation of ash deposits in a gasification or combustion system. For a mixture of 90wt% SiO_2 and 10wt% Na_2O the liquidus is ~1520°C and the solidus ~800°C.[83] At temperatures intermediate between the solidus and liquidus the equilibrium form is a mixture of liquid and one or more crystalline solids.

2.13 Phase equilibrium diagrams

At equilibrium a system occupies a state of minimal free energy for a given composition, temperature, pressure and other imposed conditions. When a given set of system parameters is fixed, there is only one mixture of phases that can be present, and the composition of each of these phases is determined. Phase equilibrium diagrams provide a clear and concise method of graphically representing the equilibrium situation and are an invaluable tool for characterising such a system.

Phase diagrams are defined by the number of components in a system. Biomass and waste ashes are multicomponent systems. However, to graphically represent the systems containing four or more components is extremely complex. Perhaps the simplest phase diagrams that can be used to describe the melting and crystallisation behaviour of ash at high temperatures, are three component (ternary) systems. In some cases the ash may contain only three major oxides, that together comprise over 90 wt% of the total ash. We may assume that the minor components have only a small effect on the major oxides, and normalise the composition to that of a three component mixture. However some oxides, for example CaO and MgO, have similar fluxing properties and we may assume that they behave similarly; thus the chemical composition of the bulk ash can be converted to the ternary mixture by combining the 'equivalent' oxides.

In many actual systems more than three components are important, but the extension of our treatment to this more complicated case uses the same principals which are to be described and discussed. The primary difficulty with including a greater number of components is not so much conceptual, as in the representation of a large body of data in concise diagrammatic form.[83]

When a system is in equilibrium, it is necessary that the temperature and pressure be uniform throughout and that the chemical potential or vapour pressure of each constituent be the same in every phase. Otherwise there would be a tendency for heat or material to be transferred from one part of the system to another. These conditions can only occur if the relationship

$$P + F = C + 2 \qquad (2.17)$$

is satisfied. A phase is defined as any part of the system which is physically homogeneous and bounded by a surface so that it is mechanically seperable from other parts of the system. The number of degrees of freedom, or the variance, is the number of intensive variables (pressure, temperature, composition) that can be altered independently and arbitrarily without bringing about the disappearance of a phase or the appearance of a new phase. The number of components is the smallest number of independently variable chemical constituents necessary and sufficient to express the composition of each phase present.[83,90]

To represent completely the phase equilibria in a condensed system, a three dimensional model, commonly termed a space model, is required; the representation of composition necessitates two dimensions, and that of temperature, a third. The model used is a triangular prism with the temperature on a vertical ordinate, and the composition plotted on the prism base, as shown in Figure 2.14.[91] For two dimensional representation the temperature can be projected onto the base, with the liquidus temperatures represented by isotherms.

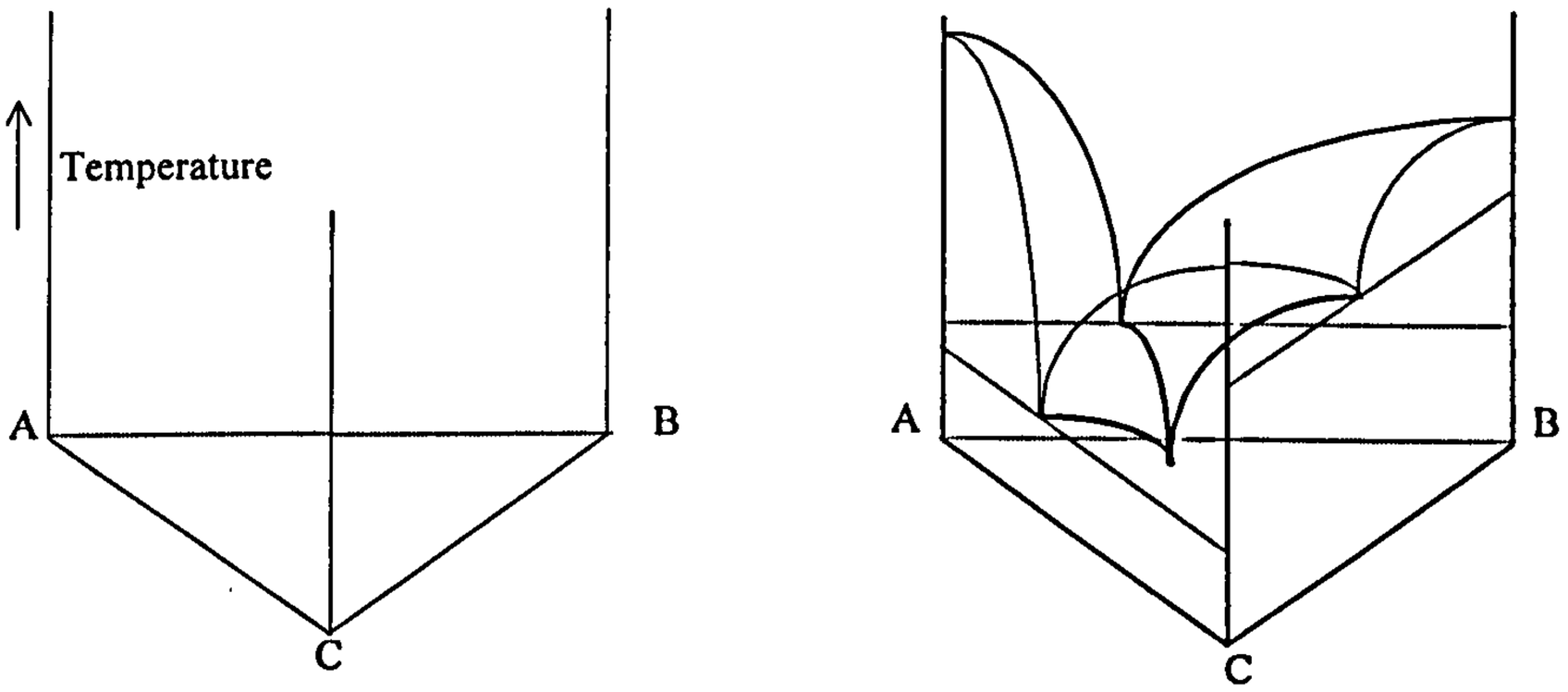

Figure 2.14 Space model used to represent the ternary system ABC

A, B and C represent the three components, the vertical faces the binary systems, and all the ternary points of the system are located within the prism. For qualitative plots, isothermal sections are used; these two dimensional diagrams can be viewed as 'slices' through the space model parallel to the composition plane ABC, at a constant temperature. Changes in temperature cannot be shown directly on a 2D surface; however, the temperatures of the liquidus surface may be indicated for uniform temperature intervals by isotherms in much the same way as elevation contours are shown on topographic maps.[90] This is the most common method of representing ternary condensed systems since each isothermal section is a complete equilibrium diagram in which all compositions can be located. Each apex of the equilateral triangle represents 100 % (wt or mole) of one of the components. Regions of univariance (F=1) are represented as boundaries between crystalline phases, and regions of invariance (F=0) by points at which three crystalline phases meet. The liquidus surface is curved, and a decrease in temperature is indicated by arrows along the boundaries. Points of invariance, at which all the arrows converge to a point, are eutectic compositions, and those where only two arrows converge are peritectic points.

Qualitative predictions of the relative amounts of the phases present at a given temperature under equilibrium conditions may be obtained by constructing compatibility or tie triangles. For example, let us consider a composition *w* lies in a compatibility triangle *x*, *y*, *z*, as shown in Figure 2.15. Using the 'centre of gravity' principle, the triangle may be considered as being supported on a point fulcrum at *w* and having masses at its corners proportional to the amounts of the phases *x*, *y*, and *z*. The proportions of the three phases in the mixture *w* are given by

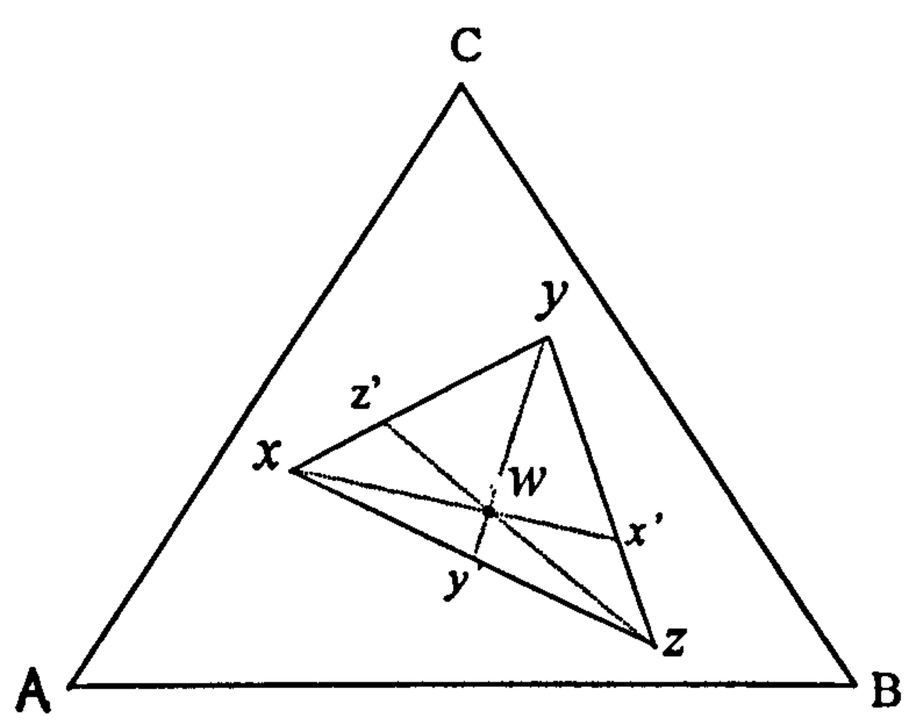

$$\%x = \frac{x'w}{xx'} \times 100 \qquad \%y = \frac{y'w}{yy'} \times 100 \qquad \%z = \frac{z'w}{zz'} \times 100$$

Figure 2.15 A diagram showing a compatibility triangle *xyz* in a ternary system ABC.

Phase diagrams can be used to study the interactions between the oxide components of an ash and deduce the most likely path of crystallisation of the liquids formed at high temperature. Phase equilibria studies have proved extremely valuable in predicting the nature of ash deposits. Three and four component phase diagrams have been used by Sanyal and Williamson[92] and by Kalmanovich[93] to predict coal ash crystallisation behaviour. Normalisation of the ash to three and four component systems enables one to:

(i) predict the temperature at which a liquid phase would first appear

(ii) predict the primary and secondary crystalline phases as the melt is cooled

(iii) estimate the change in composition of the residual liquid phase, which becomes enriched or depleted in various oxide constituents, as crystallisation proceeds, and the effect which this in turn will have on the viscosity of the ash.

To illustrate such principals, the average composition of RDF ash from Table 2.12 has been normalised to three components and the resultant composition plotted on the ternary system CaO-Al_2O_3-SiO_2 shown in Figure 2.16a.[94]

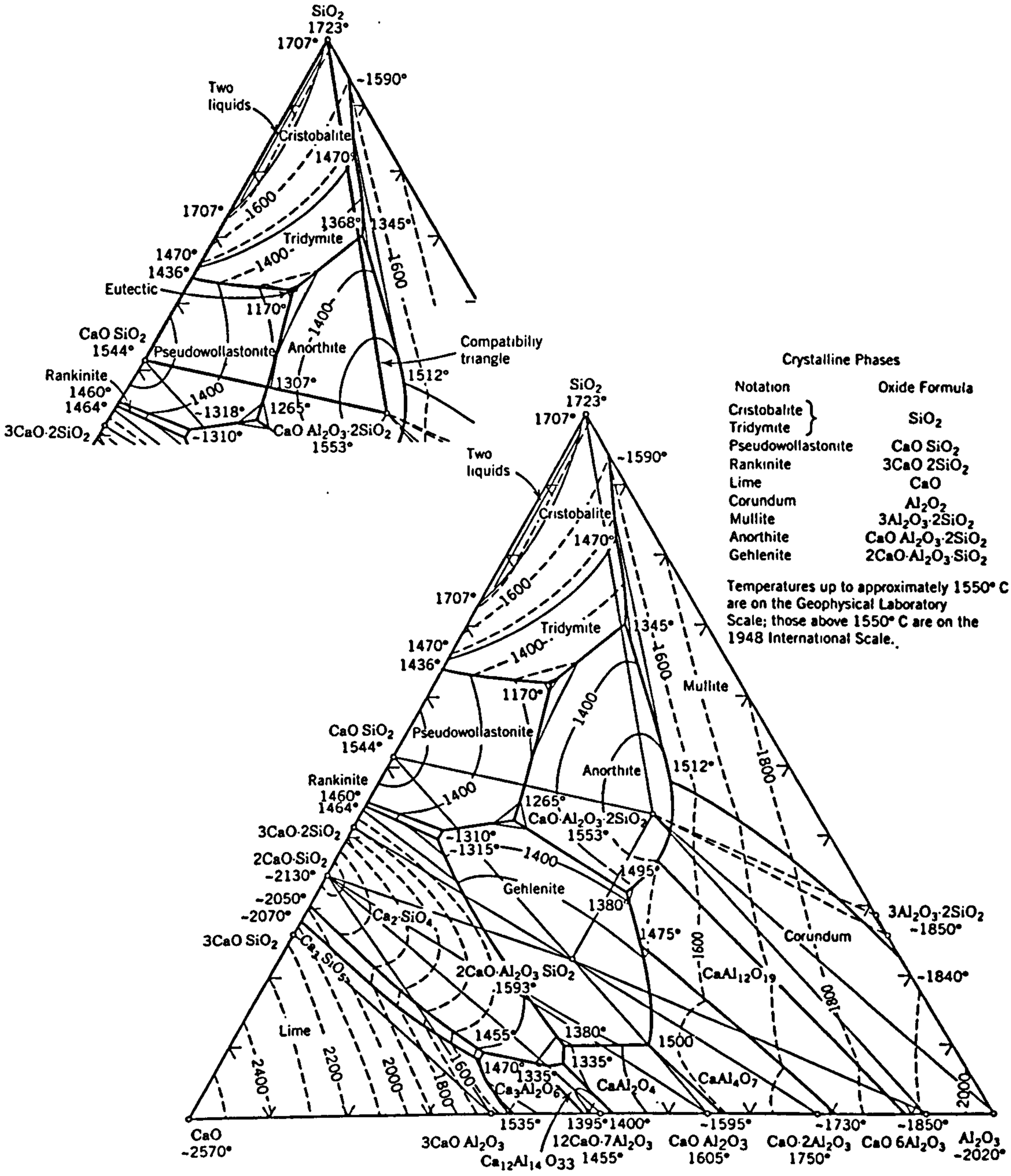

Figure 2.16a Ternary equilibrium phase diagram for the system CaO-Al_2O_3-SiO_2[94]

The RDF composition lies within the compatabiliy triangle bounded by silica, pseudowollastonite ($CaO.SiO_2$), and anorthite ($CaO.Al_2O_3.2SiO_2$) and has a liquidus temperature (T_l) of ~1420°C. On cooling from the melt under equilibrium conditions, anorthite is the first solid to crystallise since the RDF ash composition lies in the anorthite primary phase field. The initial crystallisation path, defined by the projection of the line between the composition of the primary crystalline phase and the composition of the melt, is shown on Figure 2.16b. The path represents the change in

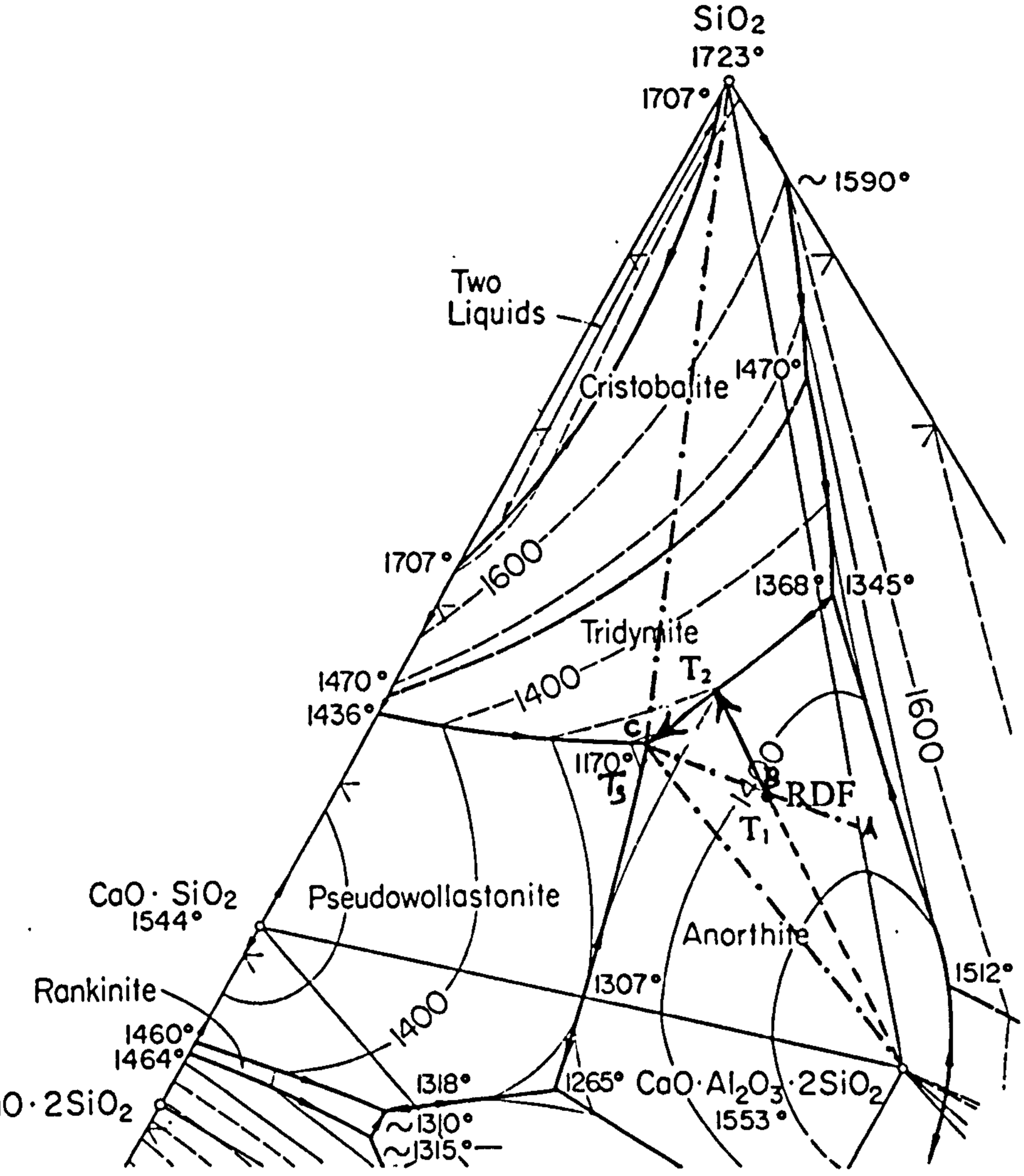

Figure 2.16b Compatability triangle silica-pseudowollastonite-anorthite, illustrating the crystallisation of a liquid of RDF ash composition

composition of the residual liquid phase with decreasing temperature. The composition of the residual liquid becomes increasingly rich in silica as anorthite is depleted from the melt. Along this trajectory the binary lever principle can be used to calculate the percentage of anorthite/liquid at any point, using the plotted RDF ash composition as a fulcrum. At T_2, the crystallisation path reaches the binary eutectic boundary and the primary solidification of anorthite would cease. At this point the binary eutectic reaction

$$\text{Liquid} \rightarrow \text{anorthite} + \text{tridymite}$$

would begin. With a continuing decrease in temperature, the eutectic mixture of anorthite + tridymite would continue to precipitate, and the residual liquid composition would change as indicated by the arrow on the boundary curve between the anorthite

and tridymite phase fields. Solidification would be complete when the liquid composition reaches the ternary eutectic point at 1170°C (T_3), where three adjacent crystalline phases would be in equilibrium with the liquid phase. The ternary eutectic reaction may be written as follows,

$$\text{Liquid} \rightarrow \text{anorthite} + \text{tridymite} + \text{pseudowollastonite}$$

Ternary eutectics indicate the composition of, and temperature at which the very last liquid phase would be present during solidification. Conversely, the ternary eutectic denotes the point at which the *first* liquid phase would appear on fusion.

The percentage of liquid that would be first to appear during the fusion of RDF ash can be calculated from the tie-triangle SiO_2-anorthite-ternary eutectic, as shown in Figure 2.16b, and is given by 100(BA/CA). Thus ~44% of a liquid phase of composition 62wt% SiO_2, 15wt% Al_2O_3 and 23wt% CaO would be present at the ternary eutectic at 1170°C.

Thus, phase equilibrium considerations yield the lowest temperature at which the ash will be completely molten (the liquidus), the maximum temperature at which the ash will be completely solid (the solidus), and the composition and relative quantities of solid and residual liquid at intermediate temperatures. However, one cannot neglect the effect the fluxing properties which relatively minor constituents of the ash, in particular K_2O and Na_2O, may have in lowering the estimated liquidus temperature. Typically, measured liquidus and solidus temperatures are 100-200°C lower due to the fluxing action of a few percent of minor oxides, in particular K_2O and Na_2O.

In a boiler system, equilibrium is seldom attained due to the heterogeneous nature of the ash and to the relative short residence time at high temperatures. However, the possibility of liquid formation at relatively low temperatures, as indicated by the phase diagrams, is of major significance in the formation of deposits.

2.13.1 The ash fusion test

The behaviour of coal ashes at high temperature has traditionally been characterised by ash fusion temperatures, as illustrated in Figure 2.17. In the British Standard ash fusion test, a high temperature ash is prepared by heating the coal in air to 800°C.[95] The ash is

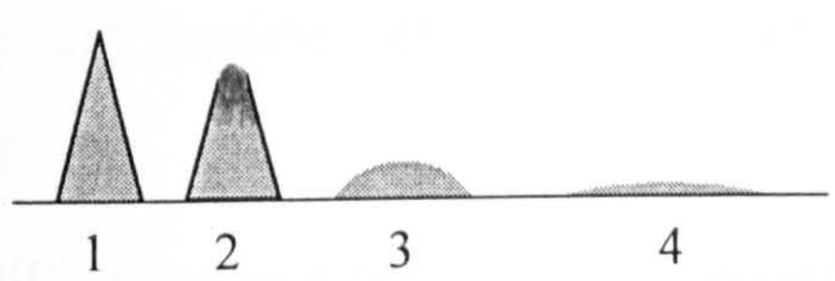

1. ash cone
2. initial deformation temperature (IDT)
3. hemispherical temperature (HT)
4. fluid temperature (FT)

Figure 2.17 Standard sample profiles for the BS ash fusion test

ground to pass a 63μm BS test sieve and is then formed into a pyramid by means of a mould with rigidly defined dimensions. The pyramid or 'cone', is placed on a refractory tile in a furnace at 900°C for ten minutes, after which time the temperature is increased at a rate of 10°Cmin^{-1}. The furnace atmosphere may be oxidising (air) or reducing (H_2:CO_2, 1:1). The deformation of the cone with increasing temperature is determined optically by the use of a graticule-fitted telescope. The initial deformation temperature (IDT) is taken at the first sign of fusion at the specimen tip, and corresponds to the temperature at which the ash particles passing through a boiler have cooled to the extent that they have only a slight tendency to stick together. On further heating a temperature is reached where there is sufficient liquid phase for the sample to assume a hemispherical shape (HT) where the height = 1/2 base width. At this temperature there is an accelerated tendency for the ash particles to agglomerate and stick to heat transfer surfaces. The difference in the fluid temperature (FT) and initial deformation temperature is generally regarded as the range over which the ash will be sticky or viscous. An ash with low fusion temperatures will have a higher slagging propensity than an ash with higher ash fusion temperatures.

Studies by Huffman et al[96] on the behaviour of coal ash at high temperature in both oxidising and reducing conditions have shown that the IDT did not correspond to the temperature at which a liquid phase first appears (the solidus). The analysis of ash samples quenched from their respective IDTs confirmed the presence of significant amounts of a liquid phase (≥25%). Huffman et al[97] also attempted to correlate ash deformation temperatures with ternary phase equilibrium diagrams. Three coal ashes with the same silica:alumina ratio were mixed with oxides of iron, calcium and potassium. The ash fusion temperatures of the resulting mixtures were determined and compared with the liquidus temperatures derived from the relevant ternary phase diagram (Al_2O_3-SiO_2-XO, where X = Fe, Ca, K_2). It was found that the variation in ash

fusion and liquidus temperatures with increasing percentage of XO followed similar trends.

The difference in ash fusion temperatures between oxidising and reducing conditions is of significance to systems in which there is an appreciable quantity of iron-bearing phases. In the Fe^{3+} oxidation state, as in Fe_2O_3, the oxide is considered a network former, but in the Fe^{2+} reduced state, as in FeO, the oxide is more fluxing and has the characteristics of a network modifer.

2.14 Phase transformations in inorganic material

During combustion and gasification, the inorganic constituents of biomass and waste materials participate in a variety of reactions and phase transformations that yield a complex mixture of solid, molten and volatile species. The nature of the inherent inorganic matter is both complex and subject to considerable variability. Furthermore, there remains a distinct paucity of documented information on the original composition of biomass in terms of mineral and other inorganic groups of material. It is therefore almost beyond the bound of possibility to predict the reaction products of combustion and gasification. However it is plausible to consider, in isolation, the apparent major constituents of biomass and refuse, and produce a comprehensive account of the decomposition process. In so doing it may be possible to predict the reaction products in biomass and waste systems.

The behaviour of inorganic materials at elevated temperatures has been most frequently studied in inert atmospheres using thermal analysis techniques such as differential thermal analysis (DTA). Most reactions commence with the release of surface adsorbed H_2O at ~100-120°C.

2.14.1 Thermal behaviour of quartz

Quartz is generally inert up to the melting point of 1723°C. Under equilibrium conditions, several polymorphs of SiO_2 exist, each with a well-defined field of stability and with quite distinct crystal structures, as shown in Figure 2.18.[51] At 573°C, α-quartz (trigonal) transforms to the β phase (hexagonal). The α-β displacive transformation is one of relatively minor atomic rearrangement involving no beakage of Si-O bonds or interchange of atoms. β-Tridymite (hexagonal) is the stable form of SiO_2

in the range 870-1470°C, and β-cristobalite (cubic) is stable from 1470°C to the melting point. The phase transformations between quartz, tridymite and cristobalite are reconstructive and somewhat sluggish, involving the breaking if Si-O bonds and the migration of Si and O atoms in several directions. If conditions do not approach equilibrium the reconstructive transformations may not take place.

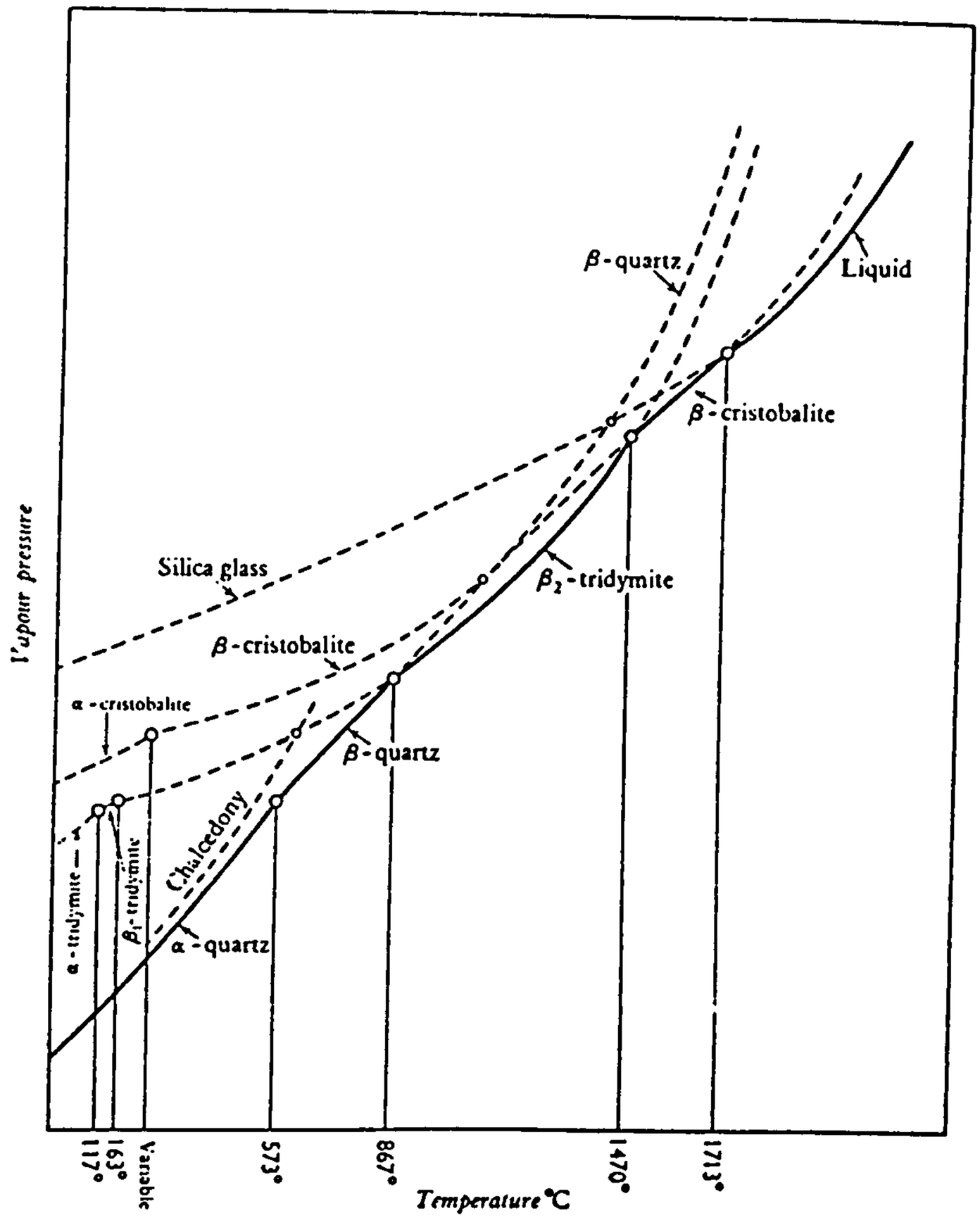

Figure 2.18 Stability regions of polymorphs of SiO_2[51]

The presence of fluxing cations, such as Na^+, K^+, Ca^{2+}, and Mg^{2+}, greatly reduce the melting point of SiO_2.

2.14.2 Decomposition of calcite and other carbonates

Each carbonate has a characteristic threshold temperature at which thermal decomposition will commence. Carbonates dissociate at temperatures between 530 and 930°C, to form a solid oxide and CO_2 gas. The thermal dissociation of calcite takes place at temperatures in excess of 850°C according to the following reaction:

$$CaCO_3 \xrightarrow{>800^oC} CaO + CO_2$$

Aragonite, a metastable polymorph of $CaCO_3$, transforms to calcite at temperatures in the range 400-500°C. The polymorphic phase transformation reaches completion in a matter of minutes.

Mixed carbonates, for example dolomite [$CaMg(CO_3)_2$], undergo a multistage reaction. The decomposition of dolomite takes place in two characteristic steps: firstly the transformation consists of a resolution of $MgCO_3$ which decomposes over the range 600-800°C[98]

$$CaMg(CO_3)_2 \xrightarrow{\sim 800^\circ C} CaCO_3 + MgO + CO_2$$

The second transformation consists of the subsequent decomposition of the calcite component.

2.14.3 Decomposition of Calcium oxalate

The decomposition of calcium oxalate ($CaC_2O_4.H_2O$) proceeds with the release of adsorbed water at ~200°C, then decomposing to $CaO+CO_2$ via the formation of calcium carbonate at 800°C.

2.14.4 Decomposition of kaolinite

The thermal decomposition of kaolinite and other clay minerals involves a series of structural changes, of lattice destruction, and phase transformations. The decomposition of kaolinite ($Al_2O_3.2SiO_2.2H_2O$) proceeds with the dehydration of surface and interlayer adsorbed water at 110°C. Dehydration of OH lattice water takes place between 400°C and 525°C, the intensity and temperature of the endothermic reaction depends upon the particle size and degree of crystallinity.[99] The nature of the material immediately following dehydration is debatable. In poorly crystallised kaolinite, the loss of constitutional OH is accompanied by a near-complete loss of structure, but in kaolinites with a high degree of crystallinity some structural remnants persist. The resultant product of dehydration, which is reached by 800°C in all specimens, is known as metakaolinite. An exothermic reaction which occurs between 900-1000°C may be attributed to the formation of an intermediate spinel phase, identified by some investigators as γ-Al_2O_3. The final products of decomposition in all kaolinite specimens

are mullite ($3Al_2O_32SiO_2$), cristobalite and/or amorphous SiO_2, which form at temperatures of ~1200°C.

2.14.5 Decomposition of talc

Several studies of the thermal decomposition of talc have been made and all have shown that the end products are clino-enstatite and cristobalite. An intermediate phase is formed at 950°C, with composition $MgSiO_3$ which has a crystal structure different to that of enstatite. X-ray investigation of the thermal decomposition of talc shows intermediate phases with features of amphibole chains and, at higher temperatures, of pyroxene chains.[100]

2.15 Structural aspects of melts and glasses

Structural aspects of glasses and polymeric melts have been studied extensively using a variety of experimental techniques, of which X-ray and neutron diffraction are most common. Also included in a number of analytical studies are various types of spectoscopy such as infrared, ultraviolet, nuclear magnetic resonance, Raman and Mossbauer.[89]

2.15.1 The random network model

The random network model adopted the hypothesis that a glass should have an energy content similar to that of the corresponding crystal. According to this model, glasses are viewed as three-dimensional networks or arrays, lacking symmetry and periodicity, in which no unit of the structure is repeated at regular intervals. In the case of oxide glasses, these networks are composed of oxygen polyhedra. It is now believed that kinetic considerations preventing crystallisation during cooling are of major importance in glass formation. However, the model remains the best general picture of many silicate glasses, and may also be used to describe a variety of liquid and glass structures, both oxide and nonoxide, in which crystalline three-dimensional networks are not possible.[83]

The silicates

The principal features of the atomic arrangement in silica and silicate glasses were first conceived by Zachariasen and Warren from X-ray diffraction measurements.[85,101] Vitreous silica consists of a random arrangement of linked SiO_4^{4-} tetrahedra. Each silicon atom is tetrahedrally surrounded by four oxygen atoms and each oxygen atom is bonded to two silicon atoms. It has become traditional to use a two-dimensional random network analogue, proposed by Zachariasen, to illustrate the structure of an oxide glass in comparison with the regularly repeating structure of the crystalline state, as shown in Figure 2.19. It is the general consensus, from subsequent studies, that in the vitreous state silica possesses a closed structure in which the 'quartz-like' arrangement predominates; in the molten state, an open structure with a 'cristobalite-like' arrangement prevails.

According to the early concepts of the 'random network' structure of silicate glasses, the addition of monovalent ions, in the form of an oxide such as Na_2O, to vitreous or molten silica disrupts the continuity of the network by the rupture of Si-O-Si linkages.[89,101]

To preserve the local charge neutrality, the modifying cations are located in the vicinity of the so-called 'non-bridging' oxygens. One such consequence of the breaking of the Si-O bridging bonds is a reduction in the viscosity of a glass melt. With divalent cations, two non-bridging oxygen ions are required for each cation; for univalent alkali ions, only one such oxygen is required. A two-dimensional analogue of a modified glass, such as Na_2O-SiO_2 is illustrated in Figure 2.20.[102]

At the disilicate composition, the structure would consist of infinite two-dimensional sheets of composition $(Si_2O_5)_n^{2n-}$ with one non-bridging oxygen per silicon atom. With further addition of the metal oxide, the silicate sheets break down to smaller units such that at the metasilicate composition the system would consist of infinite chains of SiO_4 tetrahedra and/or a metasilicate ring structure with two non-bridging oxygen ions to one silicon. As the M_2O/SiO_2 ratio further increases, the chain breakdown continues until the system consists entirely of discrete SiO_4^{4-} anions at the orthosilicate composition.

According to the random network theory, the one essential ingredient for an oxide glass is a network forming oxide; SiO_2, B_2O_3 and P_2O_5 (small ions with 3, 4 and 5 positive

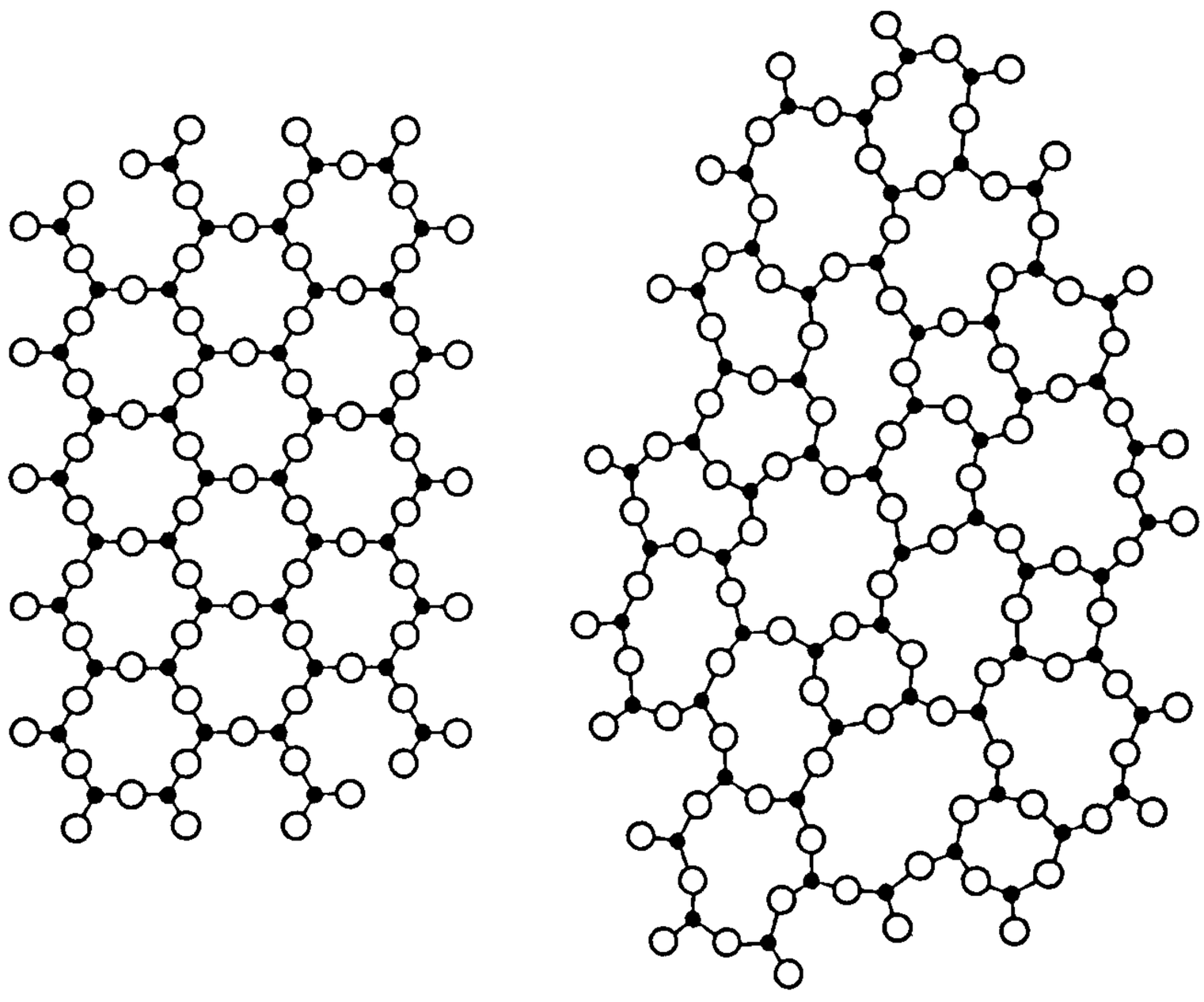

(i) *(ii)*

Figure 2.19 Structure of an oxide A_2O_3 in *(i)* the ordered crystalline form and *(ii)* the continuous random network model of a glass[83]

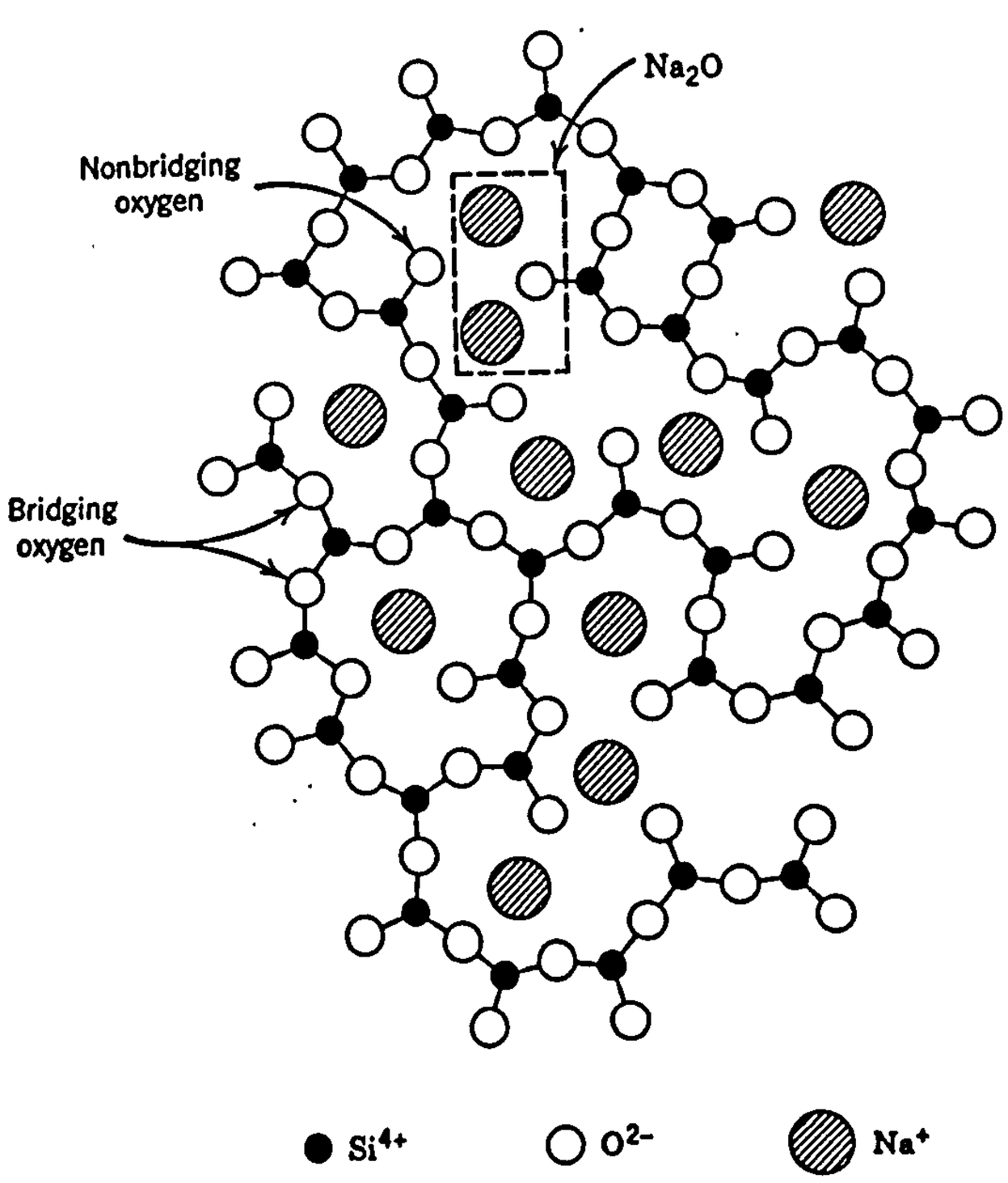

Figure 2.20 Schematic representation of a sodium silicate glass. Each Na_2O addition results in the formation of two non-bridging oxygen terminating silica tetrahedra[102]

charges) are such examples. Oxides which disrupt the continuity of the network are designated 'network modifiers' since their major function is viewed as providing additional oxygen ions which modify the network structure. Network modifiers, usually mono or divalent ions of large ionic radii, include the alkali and alkaline earth metal oxides Na_2O, K_2O, CaO and MgO. ZnO, MnO and FeO have a similar effect.

The fluxing behaviour of each modifying oxide is dependent on the ionic radius of the cation in question and on the relative concentration of the modifier to network former. The effect on the viscosity, liquidus and solidus temperatures of a coal ash doped with increasing quantities of lime, was investigated by West.[103] It was found that at relatively low concentrations, CaO acted as a flux and minimum liquidus temperatures were reached with additions of 15-25 wt% CaO. Thereafter, further additions of CaO increased the liquidus temperature, as CaO itself is a refractory oxide.

Oxides such as Al_2O_3 and TiO_2 are characterised as amphoteric or intermediate oxides, on account of their dual behaviour as basic or acidic oxides in slags and glasses. For example, the addition of alumina to molten silica lowers the viscosity much like other metal oxides. In such melts, the Al^{3+} cation is mostly in sixfold co-ordination with oxygen. With the addition of alumina and a network modifying oxide to molten silica, the aluminium enters the tetrahedral structure isomorphous with silicon. The modifying cation is located in the vicinity of Al-O bonding to preserve the local charge balance. In general, the role of cations depends on valence and coordination number and the related value of the single bond strength.[83,89]

2.15.2 Other structural models

Several other models have been suggested to represent the structure of a glass. There is experimental evidence to suggest that the alkali cations may not be randomly distributed throughout the structure, as postulated by the random network theory. The exploration of silicon and sodium ion environments in silicate glasses, using a X-ray absorption fine structure (XAFS) technique, indicates that mobile cations are restricted to percolation channels that extend in three dimensions throughout the network. This is the concept of the modified random network theory proposed by Greaves.[104] Atomistic computer simulation methods demonstrate that modifying oxides form clusters within the

simulated network; when two or more cations are present in the same glass structure, they are intimately mixed within these segregated regions.[105]

2.15.3 Phosphate glasses

The cross-linking and branching ability of the phosphate ion is limited by the presence of a double bond (P=O), hence phosphate anionic groups form primarily chains of the formula $(PO_4)_n^{3n-}$. These are analogous to the $(SiO_3)_n^{2n-}$ in silicates. Relative concentrations of PO_4^{3-} ions in phosphate melts determined chromatographically are much lower than those of SiO_4^{4-} ions calculated from structural considerations, suggesting that the free energies of formation of phosphate melts are lower than those of the silicate melts.[106] Such a prediction from structural considerations is substantiated by thermodynamic data.

The role of P_2O_5 in silicate melts has been investigated by considering the phase equilibrium relationships in binary and ternary phosphate and silicophosphate systems in conjuction with chromatographic and spectral data. It is now believed that P_2O_5 plays a dual role in influencing the structure of molten silica and metal silicates. It has been shown using differential infrared techniques that both P=O and P-O - Si linkages are present throughout the compositional range in the P_2O_5-SiO_2 system. On the basis of these observations it has been argued that the dramatic decrease in activity of SiO_2 by the addition of P_2O_5 is due to co-polymerisation of P^{5+}, as well as to the distortion of the silica network produced by the double bond P=O, rather than to the action as a network modifier. However, when P_2O_5 is added to molten metal silicates, the metal cations coordinated by non-bridging oxygens associated with silicon now become associated with the phosphate anions, resulting in polymerisation of the melt.

Phosphate glasses containing alkali metal cations exist as entirely random three-dimensional ultraphosphate networks with the cations occupying interstitial sites. Phosphate glasses have relatively specialised applications in comparison with other commercial glass products. Simple two-component Na_2O-P_2O_5 glasses are frequently used as water softening and sequestering agents in detergents. Multicomponent glasses have also been patented for similar purposes, for example MgO-Na_2O-K_2O-P_2O_5. The

soluble nature of some phosphate glass systems has also found an application as micronutrient carriers in agriculture. [106]

2.16 Solid state sintering

The free energy change that gives rise to the sintering, or densification, of particulate matter, is the decrease in surface area and lowering of the surface energy by the elimination of solid-vapour interfaces. This usually takes place with the coincidental formation of new but lower-energy solid-solid interfaces.[83] The transfer of material is influenced by the difference in local vapour pressure and changes in free energy across a curved surface. This is a consequence of the surface energy.

The driving force is the same in all systems, and thus considerable differences in behaviour in various types of system must be related to different mechanisms of material transfer; evaporation-condensation, viscous flow, surface diffusion, grain-boundary or lattice diffusion, and plastic deformation.

2.16.1 Vaporisation-condensation

During the solid state sintering process, material transfer occurs because of the differences in surface curvature and consequently the differences in vapour pressure within various parts of the system. Material transfer brought about in this way is of importance in ceramic systems and is the simplest sintering process to treat quantitatively.

For the sake of simplicity let us concentrate on the interaction of two adjacent spherical particles, as shown in Figure 2.21. At the surface of each particle there is a positive radius of curvature so that the vapour pressure is somewhat larger than would be observed for a flat surface of the same composition. However, just at the junction between particles there is a neck with a small negative radius of curvature and a vapour pressure an order of magnitude lower than that for the particle itself. The vapour pressure difference between the neck area and the particle surface allows transfer of material by vaporisation from surfaces of positive curvature and deposition at the neck area. The relationship for the rate of growth of the bond area between particles

according to the vaporisation-condensation mechanism for solid-state sintering is given by Equation 2.17:[83]

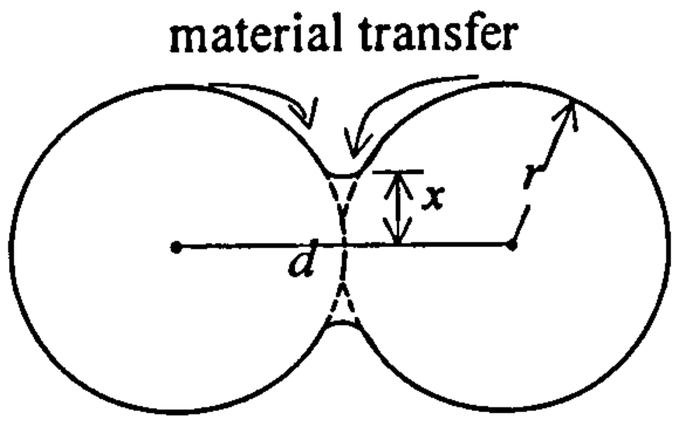

$$\frac{x}{r} = \left[\frac{3\sqrt{\pi}\gamma M^{3/2} P_o}{\sqrt{2} R^{3/2} T^{3/2} d^2}\right]^{1/3} r^{-2/3} t^{1/3} \qquad (2.17)$$

Figure 2.21 Sintering by vaporisation-condensation

where, x = radius of neck
r = particle radius
γ = surface energy
M = molecular mass
P_o = partial pressure of vapour species over a flat surface
R = gas constant
T = temperature
d = distance between particle centres
t = time

Since the vapour pressure increases exponentially with temperature, the process of vapour phase sintering is strongly temperature dependent. Vapour-phase-material transfer requires that the materials possess a fine particle size (a few microns or less) and are heated to a temperature sufficiently high for vapour pressures to be appreciable. Vapour phase transfer plays an important role in the reactions of the halides, for example NaCl. Although the vaporisation process produces changes in pore shape and bonds particles together, the centre-centre distance between particles remains constant, and thus there is no change in bulk density with this process.

2.16.2 Diffusion processes

The difference in free energy or chemical potential between the neck area and the surface of the particle provides a driving force which causes the transfer of material by the fastest means available. If the vapour pressure is low, material transfer may occur more readily by solid state processes. As shown in Figure 2.22[83], in addition to vapour

transport (process 3), matter can move from the particle surface, from the particle bulk, or from the grain boundary between particles by surface, lattice, or grain boundary diffusion. Which of these processes actually contributes significantly to the sintering process in a particular system depends on their relative rates, since each is a parallel method of lowering the free energy of the system.

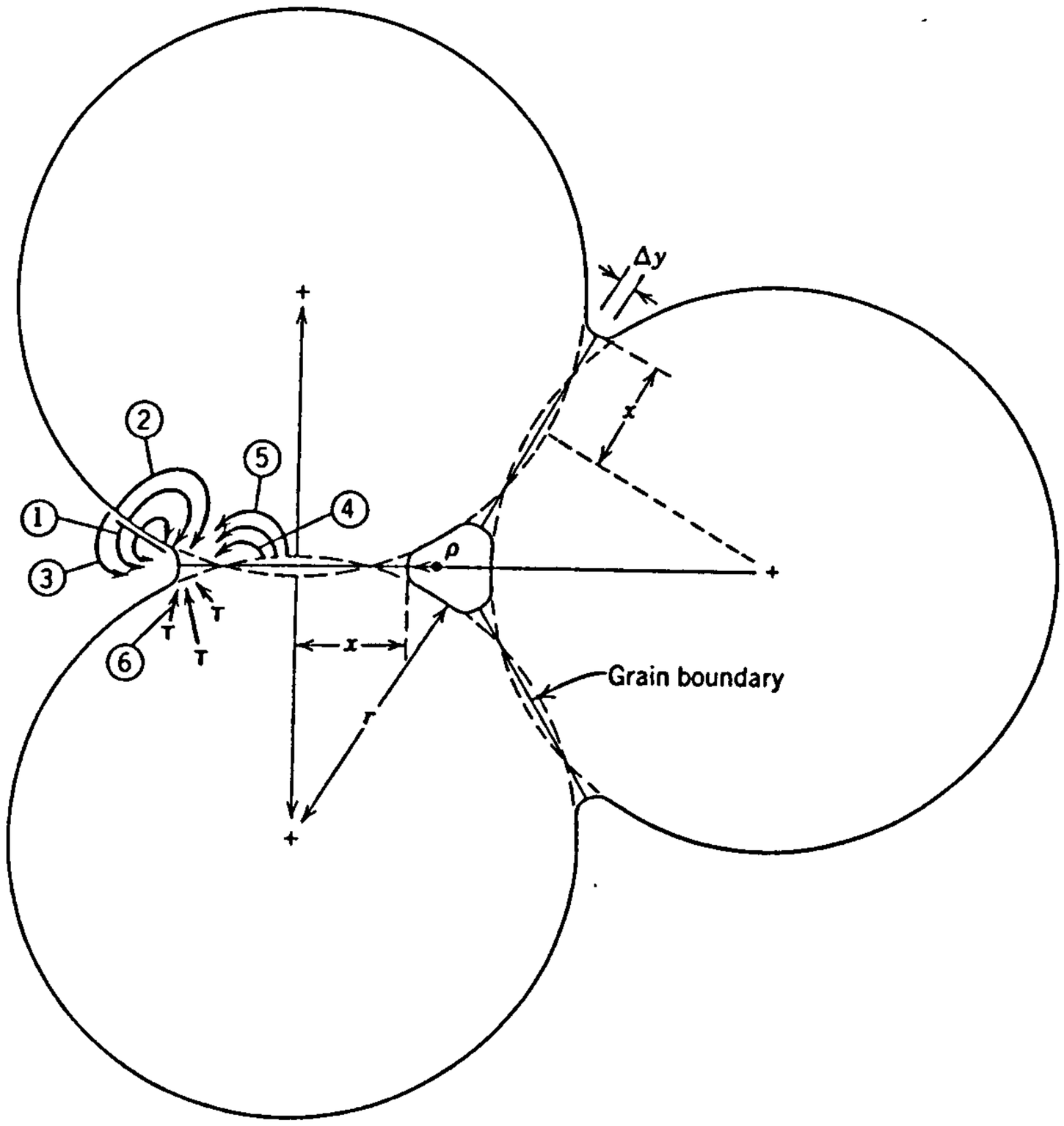

Mechanism	Transport path	Source of matter	Sink of matter
1	Surface diffusion	Surface	Neck
2	Lattice diffusion	Surface	Neck
3	Vapour transport	Surface	Neck
4	Boundary transport	Grain boundary	Neck
5	Lattice diffusion	Grain boundary	Neck
6	Lattice diffusion	Dislocations	Neck

Figure 2.22 Alternative paths for matter transport during the initial stages of sintering[83]

The mechanism of surface and lattice diffusion is similar in nature to that of vaporisation-condensation in that material is transferred to the neck region, and does not lead to a decrease in the distance between particle centres. Calculation of the kinetics for this process is analogous to the determination of the rate of sintering by a vapour phase mechanism. Only transfer of matter from the particle volume or from the grain boundary between particles causes shrinkage and pore elimination. The mechanism can

be visualised most easily by considering the rate of migration of vacancies, diffusing away from the neck area. The rates of grain boundary and volume diffusion increase exponentially with temperature, thus the rate of sintering is strongly dependent on temperature.

2.16.3 Liquid phase sintering

Liquid phase sintering is a process more rapid than that of the solid state. The prerequisite for densification is the presence of a liquid phase on the particle surface. On cooling, the liquid may crystallise or form a glass to serve as a strong bond for the body. The process kinetics are similar in nature to those of solid state reactions.

The temperatures experienced in a gasifier are probably too low for solid state mechanisms to operate. Mass transfer via a viscous liquid phase is the predominant sintering mechanism at the temperatures of interest. Viscous flow is influenced by surface tension which varies with the curvature of a surface. If we consider two spherical particles initially in contact under the influence of surface tension forces, viscous flow of material will occur from regions of high pressure (convex surfaces) to the lower potential energy concave surface at the point of contact, to form a neck. The difference in free energy between the neck area and the surface of the particles provides a driving force for mass transfer. The rate of initial neck growth, or the degree of sintering, can be described by equation 2.19 derived by Frenkel for viscous flow sintering[83]

$$\text{degree of sintering } \left(\frac{x}{r}\right)^2 = \frac{3\gamma t}{2\eta r} \qquad (2.19)$$

where, x = radius of neck formed between spheres in contact
r = radius of spheres
γ = surface tension
η = viscosity
t = time

The factors of most importance in determining the rate of the liquid phase sintering process are the viscosity, particle size and surface tension. For silicate materials the surface tension is relatively insensitive to variations in composition and temperature. The particle size has a pronounced effect on the sintering rate, and is one of the reasons

why successful compositions in silicate systems are composed of substantial amounts of talc and clays that are naturally fine-grained and provide a sufficient driving force for the sintering process. The sintering rate of particles 10μm in size is increased tenfold for 1μm particles. The most critical variable in the Frenkel Equation is the viscosity, in particular the marked dependence of viscosity on temperature and composition.

2.16.4 Sintering with a reactive liquid

Another quite different process which leads to densification is sintering with the participation of a reactive liquid. If an appreciable amount of a liquid phase is present, in which the solid phase exhibits partial solubility, the liquid may wet and penetrate between the particles, exerting a capillary pressure to pull the particles together. The driving force for the reaction is thus derived from the capillary pressure of the liquid phase located between the solid particles, as illustrated in Figure 2.23.[83] The solubility of the solid particle in the liquid is enhanced by the high pressure at the point of contact. Consequently, material is dissolved at the point of contact and reprecipitated elsewhere in the system.

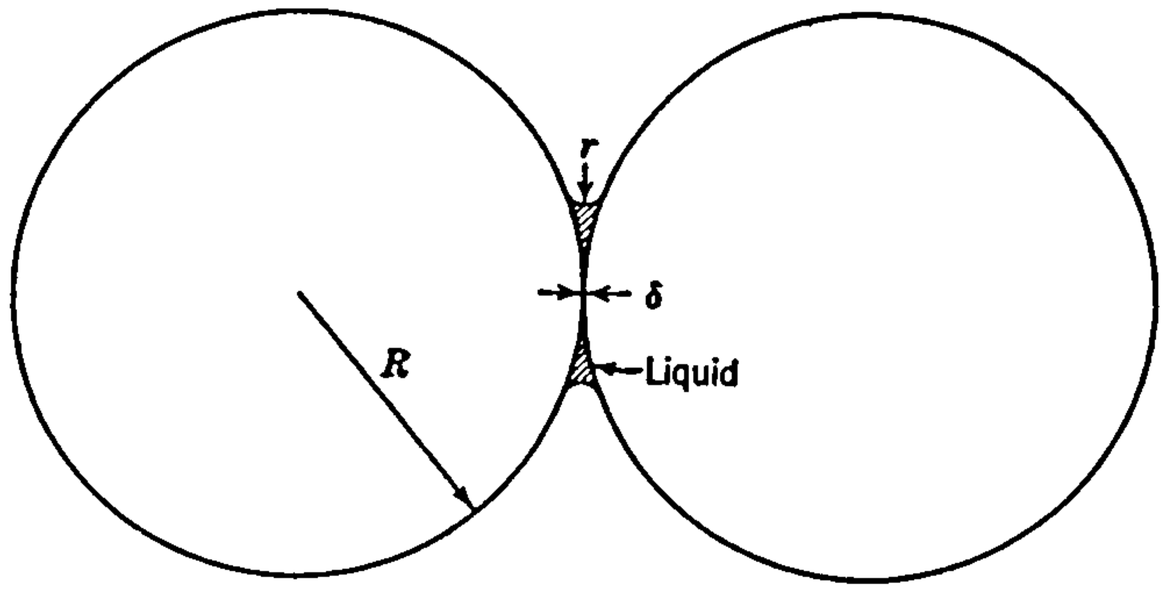

Figure 2.23 An illustration of the sintering of two spherical solid particles in the presence of a reactive liquid which brings the particles together by capillary action[83]

On formation of the liquid phase, particle re-arrangement occurs resulting in a more effective packing. If the liquid is present in sufficient volume to fill the interstices, sintering will proceed to completion. During the sintering process, smaller particles dissolve at the expense of larger particles, which grow by material transfer through the liquid phase.

Sintering in the presence of a liquid phase is a complex process in which a number of phenomena occur coincidentally. In accord with other sintering processes, the reaction requires a fine-particulate solid phase. In this case, small particles are needed to

develop substantial capillary pressures, which are proportional to the inverse of the capillary diameter. It is essential that the liquid wets the solid. Furthermore, the liquid composition must be conducive to solution and re-precipitation.

Nowok et al[107] used a sintering parameter, expressed as the surface tension/viscosity ratio (γ/η), of coal ash slags to determine their sintering propensity. The surface tension/viscosity ratios were calculated above the temperature of the critical viscosity, T_{cv}. The temperature of critical viscosity being defined as the temperature at which the flow behaviour of a melt changes from Newtonian to non-Newtonian behaviour. Calculations of γ/η from the Frenkel equation indicated that the γ/η ratios are comparable with similar parameters determined for bulk melts in the initial stages of sintering. However, during subsequent sintering, a decrease in γ/η was observed. This implied that the Frenkel model was no longer applicable and that other mechanisms prevailed. The Frenkel equation was modified to include a Poisson's ratio correction, to account for the possibility of the melt forming closed pores, or pore filling and shrinking. Equation 2.20[107] describes three basic stages of sintering:

1. formation of necks;
2. shrinkage of pores;
3. filling of pores by slag owing to a fluxing effect with particle rearrangement.

$$\frac{\Delta L}{L_o} = \frac{3}{8}\left(\frac{\gamma}{\eta}\right)\frac{t}{r} + \frac{2}{3}\left(\frac{\gamma}{\eta}\right)(1-2\upsilon)\frac{t}{r} + k\left(\frac{\gamma}{\eta}\right) \qquad (2.20)$$

where, υ = Poisson's ratio
ΔL = initial length
L_O = change in length on sintering

2.17 Viscosity

Viscosity plays an important role in the process of liquid phase sintering, as described by the Frenkel equation (Equation 2.19). The ash particles deposited on boiler tubes are initially held in place by surface forces, such as van der Waals, electrostatic, and surface tension forces[35] If the particles have experienced high enough temperatures they may still be molten or partially molten. The viscosity of the liquid phase at a given temperature is a major factor influencing the rate at which sintering will occur and the strength of the sintered deposit.

The growth of a wall deposit in the radiant zone of a boiler furnace assumes that fused or partially fused ash particles adhere to each other by a process of viscous flow sintering. The greater the degree of sintering the more consolidated the deposit becomes with a consequent increase in strength.

2.17.1 Temperature dependence

The temperature dependence of viscosity varies widely for different groups of materials, and a number of models have been proposed to describe such a dependence. According to the absolute rate theory, viscous flow can be considered a rate process dominated by a transition state of high energy. The movement of atoms, molecules or chains of a liquid is inhibited by surrounding structural components. Thermal energy is required to surmount the energy barrier for mass transport. Considerations of this kind yield an Arrhenius expression for the viscosity, η, of the form[108]

$$\eta = A \exp\left(\frac{\Delta E}{RT}\right) \tag{2.21}$$

where A is a constant, T the absolute temperature, and R the gas constant. ΔE is the activation energy for viscous flow, and is a measure of the magnitude of the energy barrier for mass transport. The relationship is satisfied by simple ionic melts and molten metals.[89] Pure silica glass exhibits Arrhenian behaviour over the full range of temperatures for which data is available and thus a plot of $\ln\eta$ versus reciprocal temperature yields a straight line. However, other materials such as the alkali silicates show a change in ΔE with temperature.

The temperature dependence of viscosity for several multicomponent silicate glasses is shown in Figure 2.24.[109] The apparent activation energy is considerably larger in the low temperature region than at high temperatures. Hofmaier and Urbain[110] suggested that the higher than predicted activation energies encountered at lower temperatures may be attributed to the precipitation of a 'solid phase'.

The variation in ΔE with temperature indicates that viscous flow cannot be regarded as a simple activated process, as suggested by the absolute rate theory, but that it involves co-operative motion of more than one atom or molecule.[83] Indeed the temperature dependence of viscosity for many materials is beyond description by any of the standard

theoretical models. The empirical equations are found to be inconsistent with experimental data on glass-forming liquids at high viscosities.

For many glass-forming melts the following equation proposed by Fulcher gives a very good representation of the variation of viscosity with temperature over a wide temperature range,

$$\eta = A_F \exp\left[\frac{\Delta E_F}{R(T - T_o)}\right] \tag{2.22}$$

where A_F is a constant, ΔE_F the activation energy, R the gas constant, T the absolute temperature, and T_o a temperature correction for a given melt composition, required to fit data to a linear plot.[89]

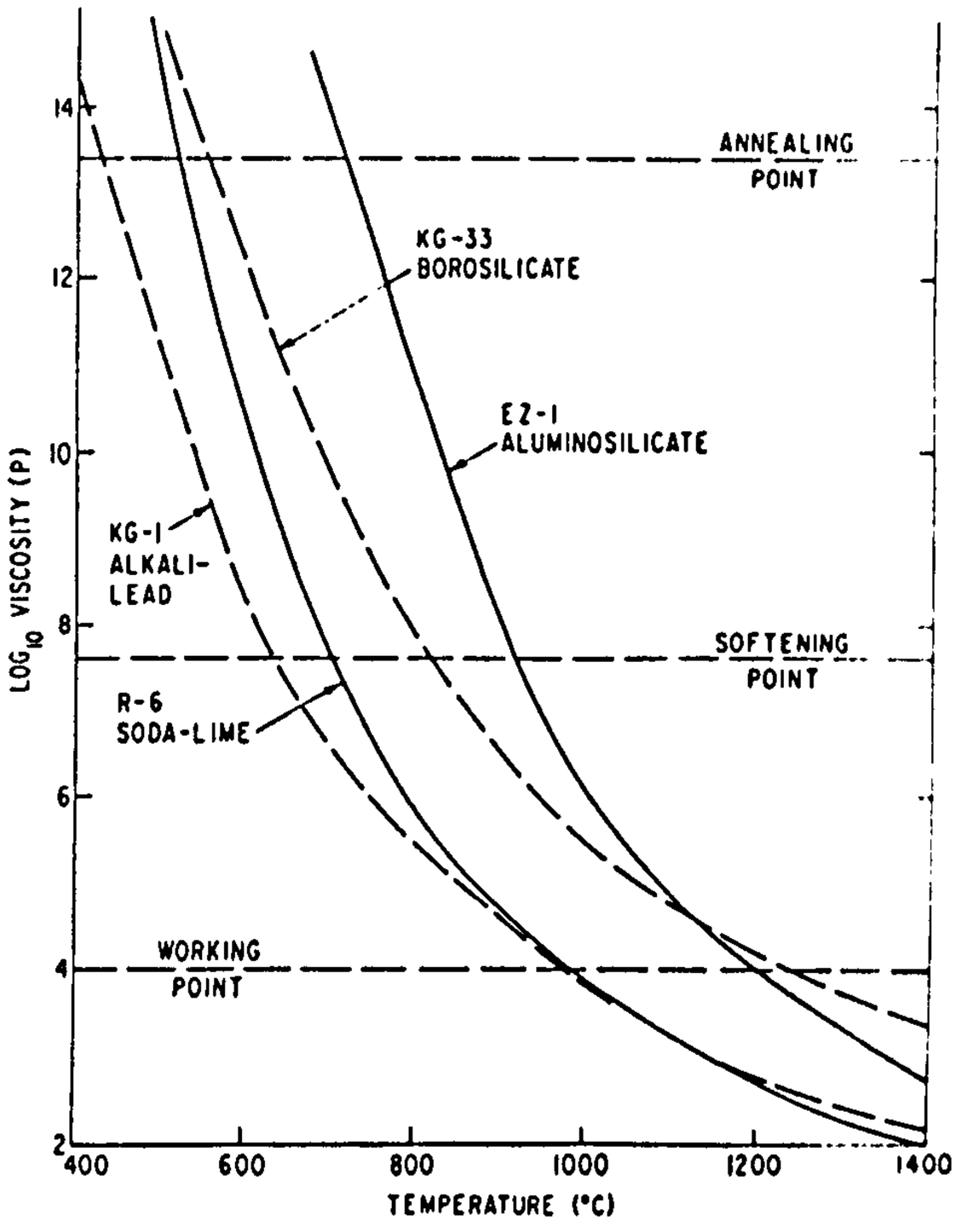

Composition wt%	SiO_2	B_2O_3	Al_2O_3	CaO	MgO	PbO	Na_2O	K_2O
Soda lime	72.6	0.8	1.7	4.6	3.6		15.2	
Aluminosilicate	55.0	7.0	15.0	21.0			1.0	1.0
Alkali lead	77.0			1.0		8.0	9.0	5.0
Borosilicate	68.0	24.0	1.0				7.0	

Figure 2.24 Viscosity-temperature relations of some silicate glasses[109]

2.17.2 Compositional dependence

Among inorganic oxide materials, the viscosity is often found to be highly sensitive to changes in composition. In the case of the silicates, the viscosity is almost invariably found to decrease with increasing concentration of modifying cations. For example, at

1700°C the viscosity of fused silica can be decreased by four orders of magnitude by the addtition of as little as 2.5mol% K_2O. As previously described in Section 2.15, the effect of the modifier addition is to introduce non-bridging oxygen atoms which serve as relatively weak links in the covalent network. In complex oxide glasses, the addition of modifying cations generally decreases the viscosity at any given temperature; the addition of silica or alumina serves to increase the viscosity. Furthermore, the addition of more than one type of alkali or alkaline earth ion results in a higher viscosity than would be expected with the same total concentration of single modifier (the 'mixed alkali effect').[83]

The compositional dependence of viscosity has been used to assess the slagging propensity of coal ashes; the ratio of the sum of basic oxides to the sum of acidic oxides is frequently used.[35] The ratio of basic to acidic oxides ($R_{b/a}$) is given by

$$R_{b/a} = \frac{Fe_2O_3 + CaO + MgO + K_2O + Na_2O}{SiO_2 + Al_2O_3 + TiO_2} \qquad (2.23)$$

The basic oxides are network modifiers and serve to break Si-O bonds, while the acidic oxides are network formers. Hence, high values of the base:acid ratio suggest that the viscosity is low and as a consequence the slagging propensity of the ash is high.

2.18 Measurement of viscosity

It is seldom possible to obtain the viscosity of a liquid melt over a wide range of temperatures using a single technique. There are two methods most frequently used by glass technologists to measure the viscosity of a material. The measurement of viscosity at high temperature involves the relative rate of rotation of two concentric cylinders under constant torque. Measurement over the lower viscosity range 10^{-2}-10^{3} Pa s is possible.[108] Higher viscosities (10^{15} Pa s is considered an upper limit) are measured by the rate at which a glass fibre elongates under a constant force. The viscosity (η) is then given by the formula

$$\eta = \frac{Lmgf}{3\pi R^2 v} \qquad (2.24)$$

where L and R are the length and radius of the glass fibre respectively, m the mass attached to the fibre, g the gravitational constant, v an instrumental reading proportional to the rate of elongation, and f is a calibration factor for the instrument.

The experimental methods for viscosity measurement are difficult, cumbersome and time-consuming. Several techniques, based upon the aforementioned principles, are available and reported viscosities frequently depend on the method of measurement. Thus there is a strong incentive to develop accurate methods of viscosity determination from theoretical considerations. Such estimations avoid direct experimental measurements.

2.18.1 Modelling viscosity

Several models of viscosity calculation have been applied to coal ash slags for the purpose of maintaining the flow of molten slag in wet bottom boilers. Such models are based on the bulk ash properties, particularly the relationship of viscosity to bulk chemical composition, and are limited to certain ranges of composition and coal rank. For example, the empirical model developed by Watt and Fereday[111]

$$\log\eta = (10^7 M)(T-150)^2 + C \qquad (2.25)$$

$$M = 0.00835\ SiO_2 + 0.00601\ Al_2O_3 - 0.109$$
$$C = 0.0415\ SiO_2 + 0.0192\ Al_2O_3 - 0.0276\ Fe_2O_3 + 0.0160\ CaO - 3.92$$

is based on a large number of experimental viscosity measurements for different compositions of coal ash melts, and results in a reasonable correlation for a limited range ($Al_2O_3 + Fe_2O_3 + CaO + MgO = 100$wt%) of UK coal ashes.

Ash deposits form when molten or partially molten particles of ash impinge and adhere to a heat transfer surface. It is the presence, chemical composition, quantity and viscosity of the surface liquid phase that governs the initial adhesion and subsequent sintering behaviour. The viscosity of the liquid phase plays an important role in the mechanism of viscous flow sintering as described by the Frenkel equation, Equation 2.19. The empirical nature of the Watt-Fereday relationship does not give sufficient insight into the flow behaviour of the liquid phase participating in deposit formation and growth, since the model is constrained by a specific range of composition. The

viscosity of component liquid phases, with chemical compositions dissimilar to the bulk ash, cannot be determined with confidence using this approach.

2.18.2 The Urbain model of viscosity

The geologist Urbain developed a theoretical model to estimate the viscosity of molten magmas and silicate-based metallurgical slags. The model has since been applied to a number of fields including ceramic processing, glass forming, and cement and steel production, where the viscosity of liquid phases is of importance. Urbain et al[112,113] derived an empirical formula relating ash chemical composition to viscosity. The theory is based on a description of the structure of an ash melt in terms of network forming, network modifying and amphoteric oxides. In essence, the Urbain calculation is based upon the statistical vacancy distribution and probability for the jump of one vacancy site to another within a silicate or an aluminosilicate melt. The relationship can be written as follows:

$$\eta = A\mathrm{T}\exp\left(\frac{10^3 B}{\mathrm{T}}\right) \tag{2.26}$$

where η is the viscosity, T the absolute temperature, and A and B two parameters with values which depend on the composition of the melt. A study of a variety of compositions in SiO_2-Al_2O_3-MO and SiO_2-Al_2O_3-M_2O ternary systems (where MO and M_2O respectively represent the di- and monovalent oxides) showed that the parameters A and B were linked through the following empirical relationship:

$$-\ln A = 0.2693B + 11.6725 \tag{2.27}$$

The calculation of the viscosity of a silicate melt at any given temperature thus consists of the determination of the parameter B. The parameter B is a complex function of the chemical composition and may be expressed by the following equation:

$$B = B_0 + B_1\mathrm{N} + B_2\mathrm{N}^2 + B_3\mathrm{N}^3 \tag{2.28}$$

where N = molar fraction of network forming oxide(s) (SiO_2, P_2O_5)[114]

$$B_i = a_i + b_i\alpha + c_i\alpha^2 \quad \text{for } i = 0, 1, 2, 3. \tag{2.29}$$

$$\alpha = \frac{(\sum \text{ mol fraction modifier})}{(\sum \text{ mol fraction modifier} + \sum \text{ mol fraction amphoteric})}$$

From experimental measurements the numerical values of B_i can be fitted by regression as a function of N (Equation 2.28), the molar fraction of network modifier, for values of

$\alpha = 0$, 0.5, and 1. Additional values of B_i can be interpolated for all other values of α by considering a relation of the second order, Equation (2.29). The parabolic equations so obtained are listed below. The units of B are degrees Kelvin.

$$B_o = 13.8 + 39.9355\alpha - 44.049\alpha^2$$
$$B_1 = 30.481 - 117.1505\alpha + 129.9978\alpha^2$$
$$B_2 = -40.9429 + 234.0486\alpha - 300.04\alpha^2$$
$$B_3 = 60.7619 - 153.9276\alpha + 211.1616\alpha^2$$

The model considers all oxide components of a system, excluding sulphur, with no compositional range constraints. The whole sequence of the calculation may be computerised to obtain an estimate of the viscosity over a range of temperatures. In comparison with experimental data, the Urbain method has been found to estimate the viscosity of metallurgical slags and other melts with reasonable precision, even when the sum of the major oxides (SiO_2, Al_2O_3, CaO) is less than 50%. To illustrate the accuracy of viscosity calculations using the Urbain method, the estimation of viscosity values are compared with experimental results as shown in Table 2.22 for mineral samples with compositions shown in Table 2.23.[112]

Table 2.22 A comparison of viscosity data from calculation and experiment[112]

SAMPLE	N (mole fraction)	α (mole fraction)	B (K)	T (°C)	measured viscosity (Pa s)	calculated viscosity (Pa s)
(1)	0.535	0.793	26.5	1300	23.5	21.9
				1400	7.1	8.5
(2)	0.651	0.671	34.0	1300	353.0	346.8
				1400	94.4	101.3

Table 2.23 Chemical composition of minerals (1) and (2)[112]

SAMPLE	SiO_2	Al_2O_3	Fe_2O_3	FeO	CaO	MgO	K_2O	Na_2O	MnO	TiO_2
(1)	50.7	14.5	4.9	9.1	8.8	4.7	0.8	3.2	0.2	1.7
(2)	60.7	17.5	3.5	2.7	5.5	3.4	1.2	4.2	0.1	0.9

Experimental and calculated values are in favourable agreement; the average deviation in the logarithm of viscosity is 2.5%.

The importance of the Urbain model to predict the viscosity of phases in coal or biomass ash systems lies in the application to ash deposition phenomena.[115] The initial

procedure in the evaluation is to determine the amount and composition of the phases present in the deposit. There are two methods in which this may be achieved. The first is a simple theoretical prediction of crystallisation behaviour using phase equilibrium diagrams. Using this technique, a hypothetical chemical composition of the residual liquid phase could be calculated for a given degree of crystallisation in the melt. To strengthen the theoretical predictions of liquid phase composition and quantity, an analytical technique such as computer controlled scanning electron microscopy (CCSEM) using energy dispersive microprobe analysis (EDS) can be used to determine the chemical composition and distribution of crystalline and amorphous phases in ashes and deposits. The average composition of the liquid phase may be obtained by analysis of the amorphous regions.

The original Urbain viscosity model has been modified by Kalmanovich and Frank[115] to provide a more comprehensive method of viscosity calculation, which is applicable to both simple oxide glasses and complex silicate melts. The parameter A in the Urbain model was re-evaluated and defined by the following relationship:

$$-\ln A = 0.281B + 11.8279 \qquad (2.30)$$

The corrected Urbain model was found to compare most favourably with the experimental data of Machin et al[116] for glasses in the system CaO-MgO-Al_2O_3-SiO_2, and the viscosity determinations of coal ash systems by Watt and Fereday.

2.19 Surface Tension

Surface tension, γ, is another measurable parameter in the sintering model proposed by Frenkel. In this model, sintering is assumed to commence with the deformation of particles under the influence of surface tension. The degree of sintering is enhanced by high surface tension. The surface tension also affects the interaction of molten ash with heat transfer surfaces.

The approach to equilibrium at constant temperature and pressure is always accompanied by a minimisation of the free energy. Thus liquids tend to adopt shapes that minimise their surface area and so the surface behaves as though it were in a state of tension. A force is required to extend a liquid surface. The surface, or interfacial, tension (γ) is thus defined as the reversible work dw_r required to increase the surface of the liquid by a unit area dA:[83]

$$dw_r = dA \tag{2.31}$$

By definition, the surface tension in units of mNm^{-1} is numerically equal to the surface energy in units of mJm^{-2}. The surface tension is a property of the free surface in equilibrium with the surrounding gas or vapour phase. The interfacial tension is a property of the interface between two condensed phases.[89] The relationship between surface and interfacial energies determines to a large extent the wetting behaviour of a liquid on a solid surface. These surface and interfacial properties have a decisive influence on liquid phase sintering, reaction kinetics, nucleation, and suspension of solid or liquid droplets in molten slags and glasses. If the solid-liquid interfacial tension (γ_{SL}) is high, the liquid tends to form a spherical bead on the surface of the substrate to minimise the total interfacial energy. If the solid-vapour surface tension (γ_{SV}) is high, the liquid tends to wet the solid to reduce the solid-vapour interface. The contact angle (θ), is the angle between the solid surface and the tangent to the liquid surface at the point of contact; the contact angle may vary between 0 (perfect wetting) and 180° (non-wetting), as illustrated in Figure 2.25.[83] The angle specifies the conditions for minimum energy according to the relation

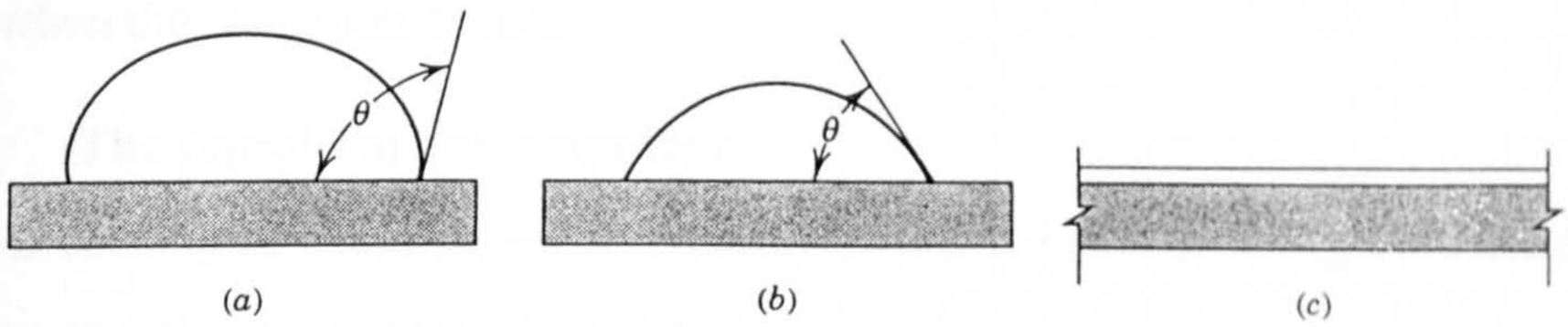

$$\gamma_{LV}\cos\theta = \gamma_{SV} - \gamma_{SL} \tag{2.32}$$

Figure 2.25 An illustration of (a) non-wetting ($\theta > 90°$), (b) wetting ($\theta < 90°$), and (c) spreading ($\theta = 0°$) of a liquid on a solid[83]

Oxide liquids have much lower surface energies than solid metals, and consequently oxide layers tend to wet metals on which they are deposited; contact angles vary between 0° and 50°.[83] Alkali-metal sulphates frequently constitute a liquid phase in coal ash deposits, and the molten sulphates readily wet and spread on the surface of boiler tubes. In reducing atmospheres, sulphates are reduced to sulphides which spread on any surface.[35]

2.20 Vapour pressure[117]

Vapour pressure is the pressure of a vapour in equilibrium with its condensed phase at a specified temperature. The precise location of a phase boundary, i.e. the pressures and temperatures at which two phases coexist, may be found by equating the chemical

potential of each phase; at equilibrium the chemical potential (μ) of a substance is the same throughout the sample, regardless of how many phases are present. Where the phases α and β are in equilibrium, $\mu_\alpha(p,T) = \mu_\beta(p,T)$ (2.33)

An equation for the phase boundary may be obtained by solving the equation for p (vapour pressure) in terms of T (temperature). For infinitesimal changes in each property of the Gibbs function ($G = H - TS$), $dG = Vdp - SdT$, (2.34)

since $H = U + pV$ where dU is replaced by the fundamental equation $dU = TdS - pdV$ for a reversible change in a closed system at internal equilibrium; where G is the Gibbs free energy, H the enthalpy, S the entropy, U the internal energy, and V the volume.

For infinitesimal changes in chemical potential $d\mu = V_m dp - S_m dT$ (2.35)

Equation (2.33) now becomes $V_{\alpha,m}dp - S_{\alpha,m}dT = V_{\beta,m}dp - S_{\beta,m}dT$ (2.36)

which rearranges into the Clapeyron equation:

$$\frac{dp}{dT} = \frac{\Delta S_m}{\Delta V_m} \qquad (2.37)$$

where $\Delta S_m = S_{\beta,m} - S_{\alpha,m}$ and $\Delta V_m = V_{\beta,m} - V_{\alpha,m}$ are the changes in molar entropy and molar volume when the transition occurs.

2.20.1 The liquid-vapour boundary

The molar entropy of vaporisation at a temperature T is equal to $\Delta H_{vap}/T$. Therefore the Clapeyron equation for the liquid-vapour boundary is:

$$\frac{dp}{dT} = \frac{\Delta H_{vap}}{T\Delta V_{vap}} \qquad (2.38)$$

The molar volume of a gas , $V_m(g)$,is very much greater than that of the liquid, and so one may write $\Delta V_{vap} \approx V_m(g)$. Moreover if the gas is ideal, $V_m(g) = RT/p$. These two approximations turn the exact Clapeyron equation into the Clausius-Clapeyron equation:

$$\frac{d\ln p}{dT} = \frac{\Delta H_{vap}}{RT^2} \qquad (2.39)$$

where $dp/p = d\ln p$. If it is also assumed that the enthalpy of vaporisation is independent of temperature, the Clausius-Clapeyron equation integrates to:

$$p = p^* e^{-C} \quad \text{with} \quad C = \frac{\Delta H_{vap}}{R}\left(\frac{1}{T} - \frac{1}{T^*}\right) \qquad (2.40)$$

where,
- p = vapour pressure at temperature T
- p^* = vapour pressure at temperature T^*
- ΔH_{vap} = enthalpy of vaporisation
- R = molar gas constant

Chapter Three

Samples

This chapter presents a record of samples obtained for characterisation, listing the supplier and providing details of sample origin. A broad range of biomass materials, indigeneous to Great Britain, were obtained, encompassing energy crops, agricultural wastes and forestry residues. Deposits, ashes and other residues derived from commercial and pilot plant operations using such feedstocks, were also acquired for this study. To add to the integrity of the project, pyrolysis chars prepared from a variety of biomass, were also provided as a result of a collaborative study with Strathclyde University, during which an exchange of technical data and samples occurred.

The samples have been grouped into three general categories and entered into Tables 3.1 (raw materials), 3.2 (deposits and process residues), and 3.3 (pyrolysis chars). The raw materials are shown in the photograph of Frame 3.1.

Frame 3.1 *The raw materials.*

Clockwise from left: chestnut chunk, willow chippings, sectioned poplar (bark, sapwood, twigs, stem cross-sections), crushed Danish pine, poultry litter (top right), shredded car tyre (bottom right), chopped straw, and RDF pellets and fluff (bottom left).

Table 3.1. Raw materials and respective suppliers

SAMPLE	SOURCE
Energy crops	
Poplar and willow coppice 'sticks' and chippings (1-4 years growth)	Silsoe Research Institute (SRI), Bedfordshire
Poplar and willow chippings (variable maturity, 1-4 years)	Long Ashton Research Station, Bristol
Agricultural residues	
Wheat straw, chopped	Mitsui Babcock Energy Ltd., Renfrew
Poultry litter	
Chicken and turkey litter	Fibropower Ltd., Eye, Suffolk
Forestry residues	
Chestnut chunk	Power Gasifiers International, Gloucester
Danish pine, crushed	Mitsui Babcock Energy Ltd.
Industrial wastes	
scrap tyres, shredded	Mitsui Babcock Energy Ltd.
Refuse derived fuel	
RDF pellets (Paisley)	Mitsui Babcock Energy Ltd.
RDF 'fluff' (Isle of Wight)	
Sewage Sludge	
Paisley treated sludge, dried	Mitsui Babcock Energy Ltd.
Thames treated sludge, wet	Thames Water Sewage Treatment Works

A range of pyrolysis chars were provided by B. McGhee and Dr P. Hall from the Department of Pure and Applied Chemistry at Strathclyde University. Char preparation involved the pyrolysis of Danish pine wood, straw, and RDFs (of Isle of Wight and Byker origin) in a Stanton Redcroft tubular furnace, heating each sample to temperatures of 500°C, 700°C and 900°C at 10°Cmin^{-1} in a nitrogen atmosphere. The raw materials were also subjected to a 1M HNO_3-treatment before pyrolysation.

Table 3.2 Deposits, ashes and other residues from commercial and pilot plant operations

SAMPLE	FUEL	PROCESS	BOILER SCALE (MWe)	SOURCE
Tube deposit Boiler dusts	scrap tyres	*Combustion*	25	Basic Energy Ltd.
Fouling (superheater) & slagging deposits	poultry litter	*Combustion*	12.5	Fibropower Ltd.
Slag	sewage sludge	*Gasification*		Warren Springs Laboratory, Stevenage
Hearth deposit Charcoal-rich residues	chestnut + RDF	*Gasification*	0.5	Power Gasifiers Int.
Cyclone material from wood gasification	willow	*Gasification*		TPS, Termiskar Processor, Sweden

Table 3.3 Pyrolysis chars

SAMPLE	**SOURCE**
Pyrolysis chars prepared at 500, 700 and 900°C*: Danish pine Straw Byker RDF Isle of Wight RDF	Department of Pure and Applied Chemistry, Strathclyde University, Glasgow

* precursors also subjected to a 1M HNO_3- treatment

Chapter Four

Experimental

4.1 Experimental procedures

4.1.1 Sample preparation of the raw materials

Each of the raw materials (RDF, straw, tyres, wood chippings) was of a grossly heterogeneous nature on a macroscopic scale, and of varying relative density and mass. To obtain a sample most representative of the batch, a 'cone and quartering' technique was employed. Thus an approximate 50g sample was obtained for characterisation.

4.1.2 Sampling of poplar and willow sticks from the Silsoe Research Institute

In order to ascertain the distribution of inorganic constituents and the bulk concentration of elements in various sections and tissue areas of the coppice, the poplar and willow sticks from the SRI were divided into nine categories of sample: twigs and leaves (from the top and bottom of the stem), main stem (top, mid-stem and bottom), bark (mid-stem and bottom), sapwood and heartwood (mid-stem). The letters A to E were used to label each section of the stick as illustrated in the diagram of Figure 4.1. Sample codes C1 to C4 were applied to the bark, sapwood and heartwood of the mid-stem fraction, also shown in Figure 4.1.

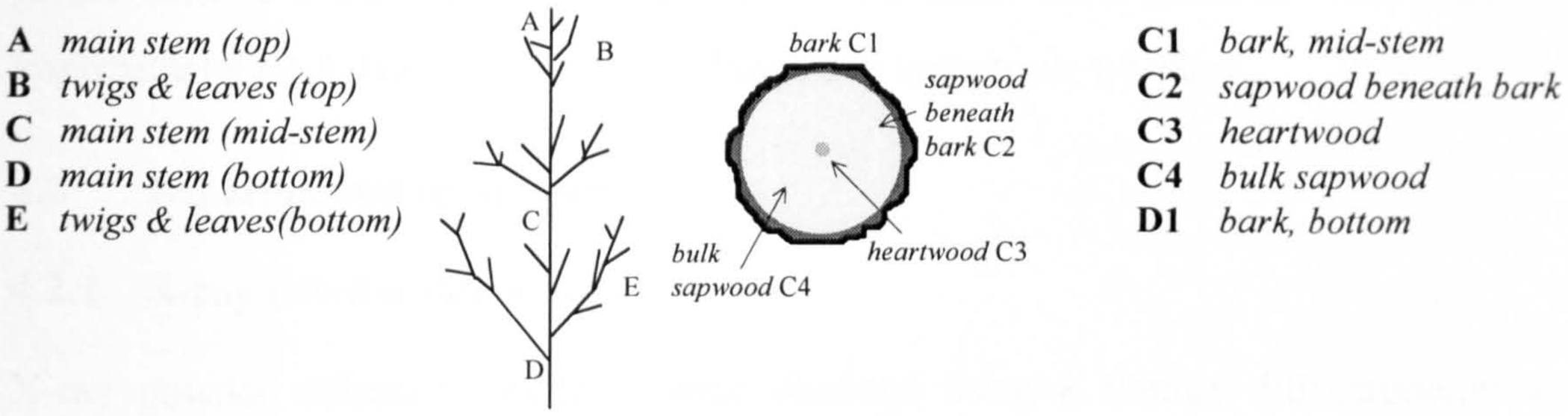

Figure 4.1 A diagram of a poplar/willow stick illustrating sample categories A to E (left) and a cross section of the main stem (right)

4.1.3 Moisture and ash determination

Approximately 10g of the raw material was oven-dried overnight. The sample was weighed prior to and after drying to obtain the moisture content. The dry sample was heated in air to a temperature of 500°C in a muffle furnace, holding at temperature for two hours, and subsequently heated to 815°C overnight in accordance with the British Standard method for high temperature ashing. The reduction in sample mass was used to calculate the ash content.

During high temperature ashing, much of the inorganic matter present in biomass materials will participate in a series of reactions, such as decomposition, oxidation and solid state interactions, at the high temperatures involved. Low temperature ashing is a process which has been developed to oxidise carbonaceous material, whilst the inorganic species remain in a relatively unaltered state. Activated oxygen atoms and free radicals produced by a plasma react with the carbonaceous matter, the temperature of the sample not exceeding 120°C.

To increase the rate of oxidation in the plasma, the surface area of the RDF pellets and the wood chips was increased by manual stripping and grinding.

4.1.4 Low temperature ashing

Between 1 and 2g of each raw material was evenly distributed in four silica boats, oven dried, weighed, and placed in a Tracerlab low temperature asher. The sample chamber, a glass tube, was pumped down to a pressure of 1mmHg (~130Pa), with an oxygen bleed of $8cm^3min^{-1}$. A power of 8 Watts (reflected power 2-3W) was applied to produce a sufficiently oxidising plasma, yet to avoid heating the sample in excess of 110°C.

The samples were frequently stirred to expose unreacted material to the plasma. The boats were weighed at regular intervals, and the ashing procedure continued until no

further change in mass was recorded. Wood and straw were found to react readily, in approximately 2-3 days; RDF, sewage sludge and tyres took 4-5 days.

4.2 Experimental techniques

4.2.1 X-ray powder diffraction

X-ray powder diffraction patterns were obtained using a Philips diffractometer and CuKα radiation to determine the crystalline phases present in the LTAs and deposits. The samples were prepared for the diffractometer by grinding a small quantity in a clean agate mortar to obtain a fine homogeneous powder; ~30mg of the powder was mixed with 1-2 drops of acetone to form a slurry which was spread uniformly over a single crystal (silicon) mount. The samples were scanned over the range $10° \leq 2\theta \leq 70°$. The diffraction patterns comprised a series of peaks of varying intensity, width and position (diffraction angle, 2θ) and were used to determine the crystalline phases present and to provide an indication as to the relative amount of each particular phase present. The identification of species from the powder diffraction pattern is based upon the diffraction angle 2θ, which is determined by the interplanar spacing of the crystal. With the aid of the Bragg equation ($n\lambda=2d\sin\theta$), the interplanar spacing (d) is readily calculated from the known wavelength (λ) of the source and the measured angle (2θ). The crystalline phases were identified by comparison of the interplanar spacings with those of standard compounds in the X-ray Diffraction Data File. The data in these files are in terms of d spacings and relative peak intensities. The samples contained several crystalline compounds, and therefore various combinations of the more intense peaks were used until a match was found.

4.2.2 Determination of the ash composition

Chemical analysis of LTAs and deposits were obtained by scanning electron microscopy (SEM) in conjunction with energy dispersive spectroscopy (EDS). The samples were prepared for the microscope as follows.

The deposits

A small quantity of a deposit, approximately 2-5g in mass, was ground to a fine powder in an agate mortar, with the exception of the RDF/chestnut deposit which required more vigorous grinding in a TEMA mill due to the outstanding strength of this material. The

ground sample was compacted into a 1mm×0.5mm pellet and fused onto an alumina tile lined with platinum foil, to avoid sample and substrate interaction, in a furnace at a temperature of 1650°C for 30 seconds. The sample was then vacuum impregnated in an epoxy cold setting resin mount, 25mm in diameter, for polishing.

Low temperature ash of the raw materials

Approximately 50mg of finely ground LTA was mixed with one drop of a 5% PVA solution, to serve as a binder, pressed into a 1mm×0.5mm pellet, and set in an epoxy resin mount under vacuum.

Once mounted, all the samples were ground to achieve a uniform surface using progressively finer SiC papers lubricated with ethanol, then polished using diamond lapping compounds to a ¼µm finish. A carbon coat was applied to the sample to prevent charging in the electron beam and to be undetectable when using EDS. The composition of the sample was determined using EDS on the Jeol JSM-35 and JSM-6400 scanning electron microscopes. The compositions were recorded by scanning multiple areas of 400µm×400µm throughout the LTA specimens, and by point analysis of the more homogeneous fused samples. An average composition of elements was obtained and converted to wt% oxide. ZAF-4 corrections were applied to the analysis conducted on the JSM-35, considering the atomic weight (Z), absorption (A) and fluorescence (F) of the sample, whilst Proza corrections were used on the JSM-6400 which account for, in addition to the aforementioned, the accelerating voltage and take-off angle. For samples containing atoms of low atomic number, Proza is the more effective correction method.

4.2.3 Microstructural analysis of the deposits

The microstructures of the deposits were examined optically and using scanning electron microscopy. A section of each deposit was mounted in a 25mm diameter mould with a low viscosity epoxy resin, ground and diamond polished to a ¼µm finish. The area of the sample cross-section was, on average, one centimetre square. Porous samples were impregnated in a vacuum desiccator. General information regarding the sample porosity, the morphology and distribution of crystalline and amorphous phases within the deposit, was obtained by optical examination in a Nikon microscope using reflected and polarised light. Subsequently the sample was carbon coated in preparation for the electron

microscope in which the sample could be examined at higher magnification and in greater detail. Qualitative analysis of components of the microstructure was obtained using Energy Dispersive Analysis of X-rays (EDAX) in the Jeol T-200 microscope. The distribution of elements between various phases was determined using the back-scattered imaging mode in which a phase of higher mean atomic number results in a more intense image.

In addition to the polished cross-sections, fragments of the deposits, including fractured surfaces, were examined to give an overall impression of the deposit microstructure in three dimensions. A fragment of the deposit was mounted on an aluminium stub with a polystyrene cement, and carbon coated in preparation for the electron microscope.

Distribution of inorganic species in wood

Strips of inner bark, sapwood and heartwood from dried samples of poplar, willow and chestnut were prepared for microstructural analysis in the SEM by mounting a section, ~4mm^2, onto an aluminium stub with polystyrene cement. A surface coating of gold, a few nanometres thick, was applied to the specimens to prevent charging in the electron beam. Qualitative analysis of the inorganic matter was obtained using EDAX in the Jeol T200 microscope.

4.2.4 Bulk density, true density and porosity of a tyre incinerator deposit

True density

The true density was obtained by a basic method of experimentation using a finely ground sample of the incinerator deposit, a density bottle and cyclohexane. A clean, dry density bottle was weighed (W_1), filled with cyclohexane (a solvent in which the material was not soluble), and re-weighed (W_2). The bottle was then emptied and dried, filled to approximately a quarter of its volume with the sample and re-weighed (W_3). More cyclohexane was decanted into the bottle with a drop of detergent until three quarters full; the bottle was placed into a vacuum desiccator for ~10 minutes, subsequently topped up with cyclohexane and re-weighed (W_4). The true density (ρ_T) was calculated using the formula:

$$\rho_T = \frac{W_3 - W_1}{(W_2 - W_1) + (W_3 - W_4)} \rho(\text{cyclohexane}) \qquad (4.1)$$

Bulk density

The bulk density was determined by another simple experiment. A piece of deposit was cut to yield a cube of approximate dimensions 1.5×1.5×1.5 cm^3, and the mass obtained by weighing in air. The volume was determined using Archimedes principal by submerging the sample in cyclohexane and measuring the volume of liquid displaced. The ratio of sample mass to volume gave the overall bulk density (ρ_B). The experiments were repeated several times and average values for the true and bulk densities obtained.

The true porosity

The true porosity (P - closed pores) was calculated using the following equation:

$$P = 1 - \left(\frac{\rho_B}{\rho_T}\right) \qquad (4.2)$$

4.2.5 Determination of the thermal conductivity of a car tyre incinerator deposit

The thermal conductivity of the tyre deposit was measured using a modified Lee's Disc apparatus in which a cylindrical sample (S), approximately 5cm in diameter and 8cm thick, was placed between copper discs and a heater (H) of similar dimensions. Each of the copper discs A, B and C were fitted with a thermocouple. The configuration is illustrated in Figure 4.2 below.

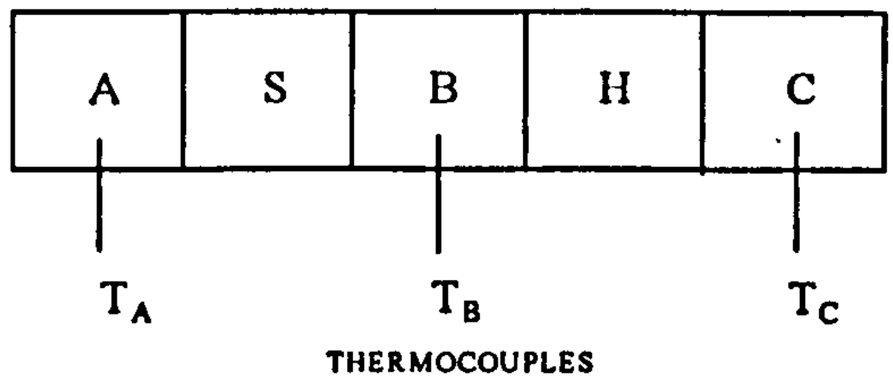

Figure 4.2 A schematic showing the arrangement of the heater (H), specimen (S), and copper discs (A, B and C) in the modified Lee's Disc apparatus

A current was passed through the heater disc until thermal equilibrium was attained. The temperature of the sample was taken as the mean of the disc temperatures on either side, $1/2(T_A + T_B)$ at equilibrium. The thermal conductivity of the sample was calculated by considering the steady state heat flow through the discs according to the following equations.

(*i*) For the steady state conduction of heat,

heat input = heat dissipated

$$IV = h(a_A T_A) + (a_S T_S) + (a_B T_B) + (a_H T_H) + (a_C T_C) \qquad (4.3)$$

(*ii*) For the sample disc in a steady state,

mean energy input and output - heat dissipated through surface = 0

$$hd[a_S \frac{1}{2}(T_A + T_B) + 2a_A T_A] - k2\pi r_S^2 (T_A - T_B) = 0$$

$$k = \frac{hd\left[a_S \frac{1}{2}(T_A + T_B) + 2a_A T_A\right]}{2\pi r_S^2 (T_A - T_B)} \qquad (4.4)$$

where, k = thermal conductivity; h = rate of heat dissipated per unit area; d = sample thickness; a_i = exposed area of disc; r_S = radius of sample; T_i = temperature of disc above ambient

A porous insulating aluminosilicate refractory sample ($k = 0.31 Wm^{-1} K^{-1}$) was used as a comparative reference standard.

4.2.6 Hot stage microscopy

A small quantity, approximately 30mg, of the LTA of each raw material was finely ground in an agate mortar and pressed onto the tip of a Pt/20%Rh-Pt/40%Rh thermocouple and attached to the stage of a low power optical microscope. The thermocouple was used as a resistance heater. Nitrogen gas was passed through the cell containing the thermocouple, and the temperature was steadily raised to 1500°C. The solidus and liquidus temperatures of the samples were determined by observing the behaviour of the ash particles at the thermocouple tip. The solidus was recorded at the temperature when the particles just began to consolidate, indicating the presence of the first layer of liquid on the surface of the particles. The liquidus temperature was taken when the sample was completely molten.

4.2.7 Distribution of particle size using a Malvern Analyser

The particle size distribution of the two boiler dust samples from a vehicle tyre incinerator (Basic Energy, Wolverhampton) were determined using a Malvern 3600 particle size analyser. The instrument consisted of a laser source, a glass sample cell, and a quadrangle array of sensors to detect the intensity of diffracted laser light at different angles of diffraction. Approximately 0.5g of each specimen was suspended in ethanol and kept in constant flux by a magnetic stirrer. The implicit assumption of this technique

is that each particle is of spherical geometry, and diffracts the incident laser beam through an angle ϕ; the smaller the particle the greater ϕ. Thus ϕ is related to particle size, and the intensity of the diffracted light at any given angle is related to the proportion of particles of that size.

4.2.8 Determination of char reactivity by thermal analysis (DTA)

The reactivity of the pyrolysis chars, derived from demineralised and as-received precursor materials (pine wood, RDF and straw), was assessed by differential thermal analysis (DTA) in a Stanton-Redcroft STA-780 Thermal Analyser. To compare the reactivity of one sample with another, each char was finely ground in a clean agate mortar to pass a 38μm sieve. Thus variations in reactivity due to differences in particle size were minimised. A 5mg sample in a platinum crucible was placed in the thermobalance and heated in air (flow rate $65cm^3min^{-1}$) to 900°C at a rate of $10°Cmin^{-1}$. Alumina was used as the reference material. Data was recorded as weight loss (thermal gravimetric analysis, TGA), rate of weight change (differential thermogravimetry, DTG), and as temperature differences (differential thermal analysis, DTA) between the sample temperature and that of the reference material.

Chapter Five

Results

An apparent paucity of information regarding the properties of biomass and waste materials has frequently resulted in poor technical and commercial performance of many processes. The data obtained in this study should be of value to potential designers, developers and operators of both plant and thermochemical processes which use biomass as an energy source. This chapter of results presents a characterisation of a diverse range of biomass materials, including deposits and residues formed under combustion and gasification conditions in small-scale commercial and pilot plant operations. The nature and extreme variability of the potential fuels has been investigated, highlighting the peculiarities and distinctive features of the individual material, especially those which may present technical problems.

The raw materials, deposits and residues were found to contain a wide variety of crystalline species, many of complex chemistry and stoichiometry. While each crystalline compound processed a unique structure and therefore a characteristic X-ray diffraction pattern, many of the patterns for the compounds concerned in this study were extremely complex. When two or more phases are present, the X-ray diffraction trace is a composite pattern, with relative peak heights corresponding approximately to the proportions of phases present. A complete interpretation and identification of the diffraction traces had, in some instances, proved to be difficult. While it has been possible to identify many of the major phases, some of the samples contained as yet unidentified crystalline phases.

5.1 A characteristation of fuel and deposits from the Elm Energy tyre incinerator plant operated by Basic Energy Ltd.

5.1.1 Scrap tyres

A sample of shredded car tyre was provided for this study by Mitsui Babcock Energy Ltd. The specimen contained rubber crumb and fibrous textile cords. It appeared that any steel components of the composite tyre structure would have been recovered prior to disposal of the carcass. The moisture and ash contents were found to be 2.3% and 6.9wt% respectively, on a dry ash basis. The composition of the tyre ash, presented in Table 5.1, was found to be lime rich with substantial quantities of Al_2O_3 and SO_3. An X-ray diffraction technique revealed that the major crystalline phases present in the low temperature ash were calcite ($CaCO_3$) and zincite (ZnO). Calcite was most certainly employed as an inorganic filler, or extender, in the tyre manufacturing process, and ZnO an activator designed to facilitate the chemical cross-linking mechanism for vulcanisation.

Table 5.1 Bulk ash composition of car tyre waste, after ferrous metal recovery

OXIDE	SiO_2	Al_2O_3	Fe_2O_3	CaO	MgO	K_2O	Na_2O	P_2O_5	MnO	SO_3	ZnO
wt %	2.7	27.4	0.0	44.4	0.0	0.0	0.0	0.7	1.5	23.3	1.5

5.1.2 Boiler tube deposit

A sample of deposit formed on the boiler tubes of a $25MW_e$ vehicle-tyre incinerator was obtained from Basic Energy Ltd., Wolverhampton. The tube deposit, approximately 15mm in thickness, was of a brown-grey colour with a fine (<1mm) powdery white layer adjacent to the tube metal surface. The entire sample was of an extremely friable nature. The build-up of deposits of this type on the reactor boiler tubes had considerably reduced heat transfer and hence boiler efficiency. The experimentally determined true density was found to be $3.2gcm^{-3}$ and the bulk density $1.1gcm^{-3}$, resulting in an overall calculated porosity of 66%. The thermal conductivity of the sample was measured using a modified Lee's disc apparatus and found to be $0.23Wm^{-1}K^{-1}$ at 383°K.

The boiler tube deposit was characterised in terms of the bulk ash composition, the nature of the crystalline constituents and the microstructure. The quantitative ash analysis is presented in Table 5.2. The deposit was found to contain two major oxides,

ZnO and SO_3, with SiO_2, Fe_2O_3 and CaO in secondary amounts.

Table 5.2 Bulk ash composition of a tyre incinerator tube deposit

OXIDE	SiO_2	Al_2O_3	Fe_2O_3	CaO	MgO	K_2O	Na_2O	P_2O_5	MnO	SO_3	ZnO
wt %	11.8	1.7	6.0	5.9	1.1	2.4	2.4	0.7	0.1	38.0	29.9

The crystalline constituents of the deposit were determined using an X-ray powder diffraction technique. The results, presented in Table 5.3, revealed the white inner layer adjacent to the tube surface to be primarily ZnO. The bulk of the sample was identified as a mixture of ZnO, $ZnSO_4$ (major phases), $CaSO_4$ and Fe_3O_4 (minor phases). The presence of an amorphous phase was also discernible.

Table 5.3 Crystalline phases present in a tyre incinerator tube deposit, identified by XRD

SAMPLE	CRYSTALLINE PHASE		
	major	**minor**	**trace**
white inner layer	ZnO *(zincite)*		$CaSO_4$ *(anhydrite)*
bulk	ZnO *(zincite)* $ZnSO_4$ *(zinkosite)*	$CaSO_4$ *(anhydrite)*	Fe_2O_3 *(magnetite)*

5.1.3 Microstructural examination of a tyre incinerator tube deposit

A microstructural examination of a 'fractured' surface and a polished cross-section of the deposit revealed a highly porous assembly of sintered ash particles. The deposit was mainly composed of glassy aluminosilicate ash particles, of spherical morphology, bonded together by a condensed peripheral layer of ZnO. Further infilling of the porosity had occurred with the formation of $CaSO_4$ and $ZnSO_4$ in the remaining voids. Characteristic features of the microstructure are captured in Frames 5.1 to 5.7.

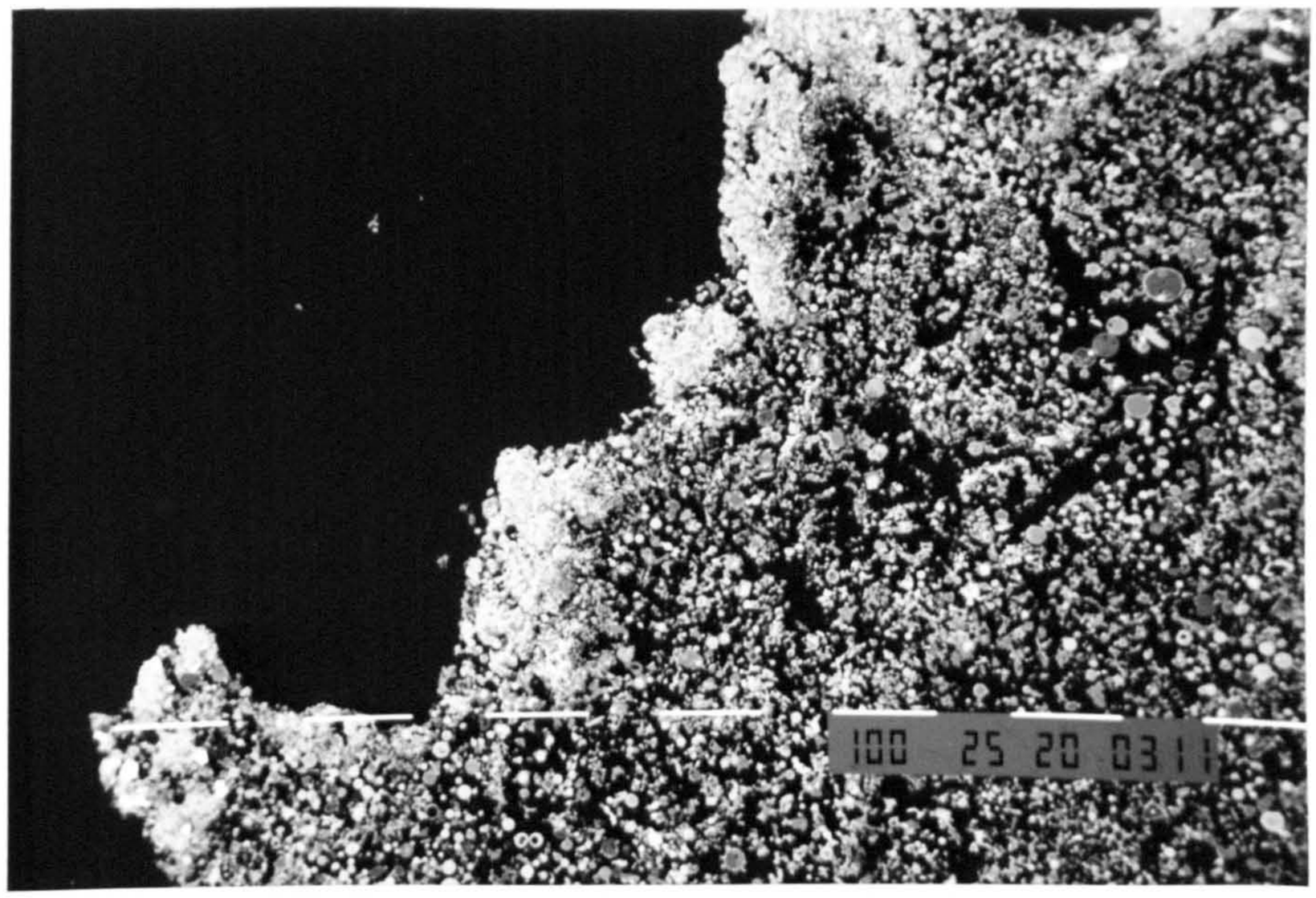

Frame 5.1. *Tyre incinerator deposit. 1 bar ≡ 100μm. Back scattered image.*

A polished section of the fouling deposit from a car tyre incinerator. A general view of the deposit showing the white layer adjacent to the tube surface.

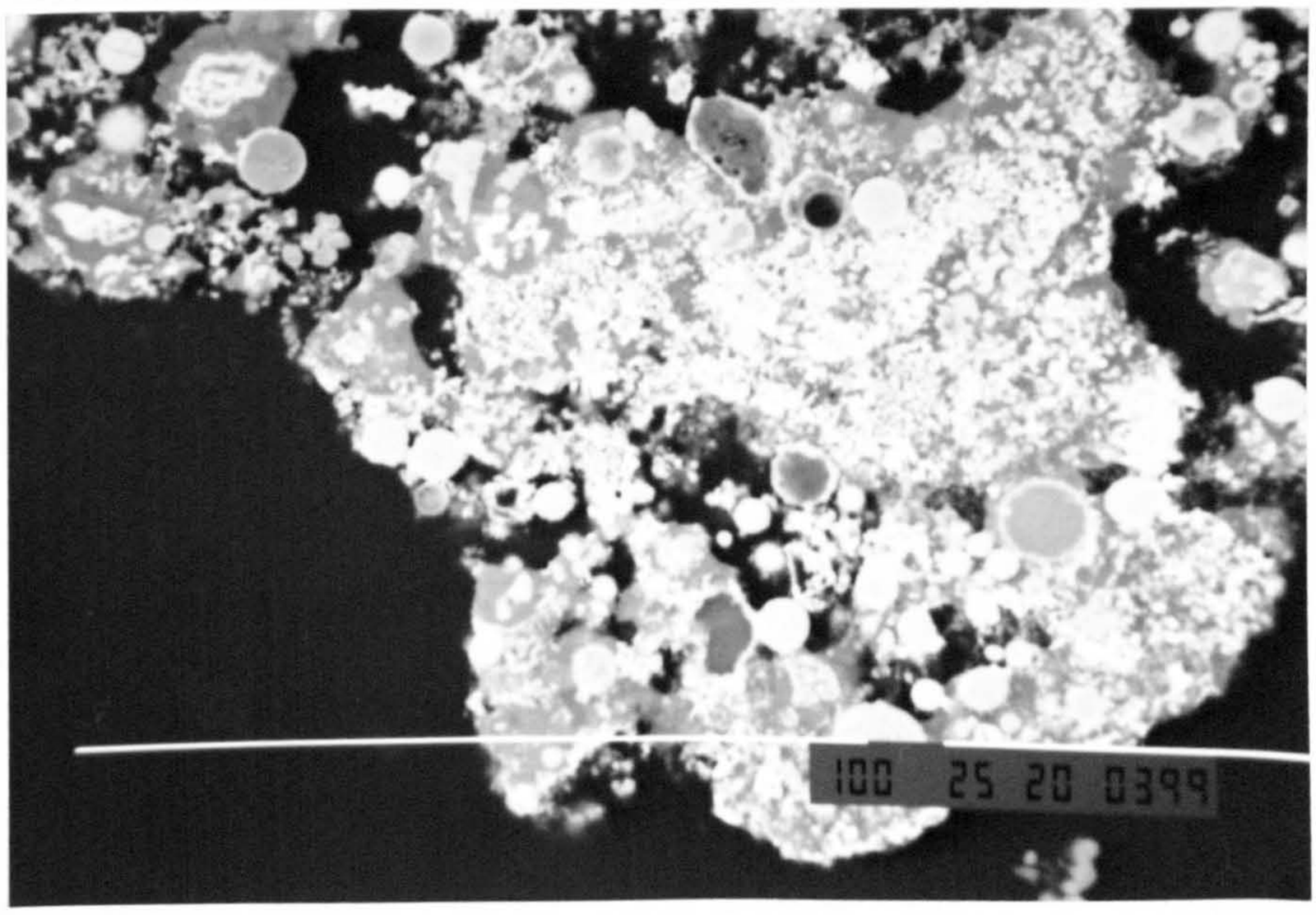

Frame 5.2. *Tyre incinerator deposit. 1 bar ≡ 100μm. BSI.*

The white layer of deposit adjacent to the tube surface consists predominantly of ZnO.

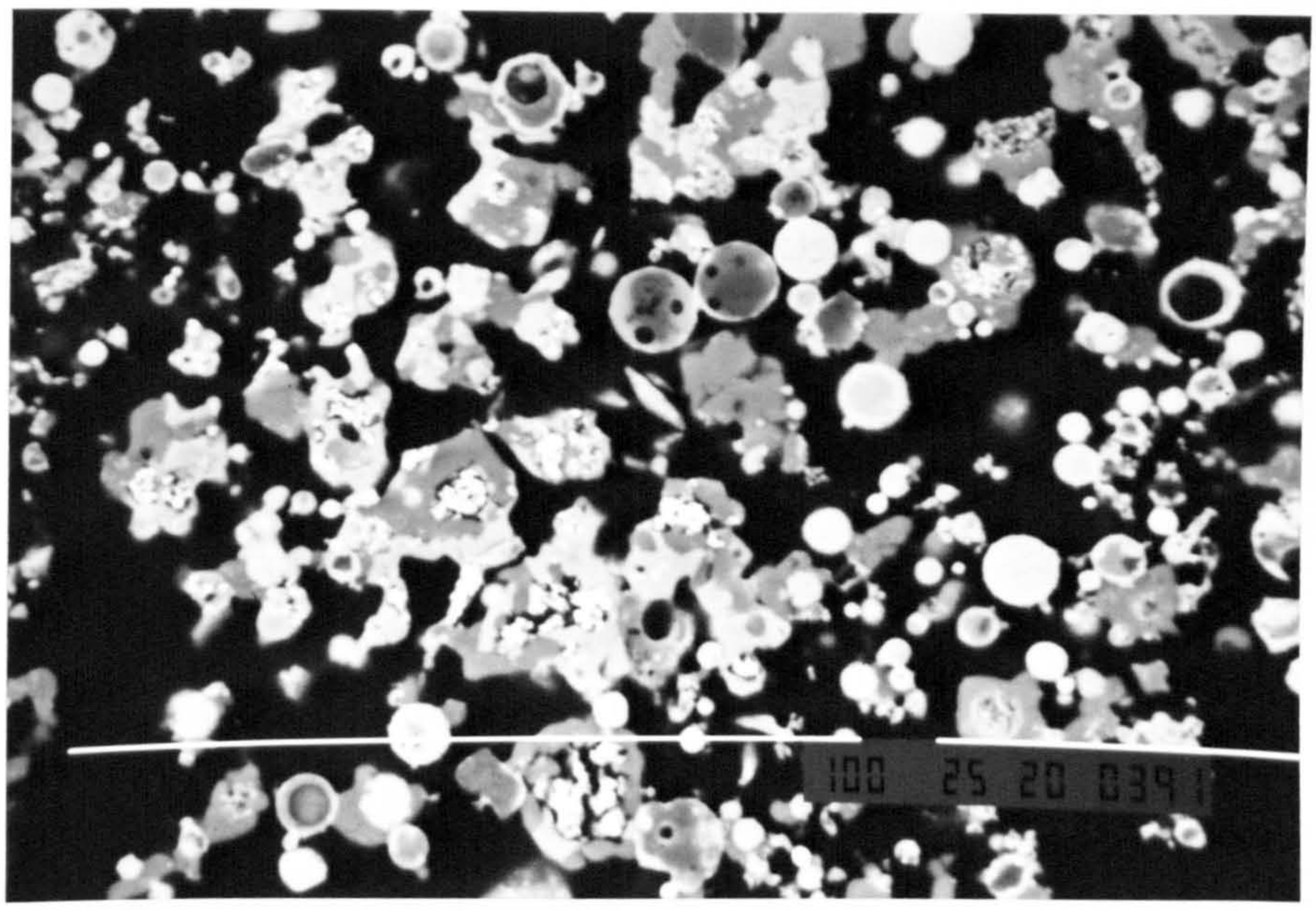

Frame 5.3. *Tyre incinerator deposit. 1 bar ≡ 100μm. Back scattered image.*

Shown above is a region within the bulk of the material illustrating the varied particle morphology and size.

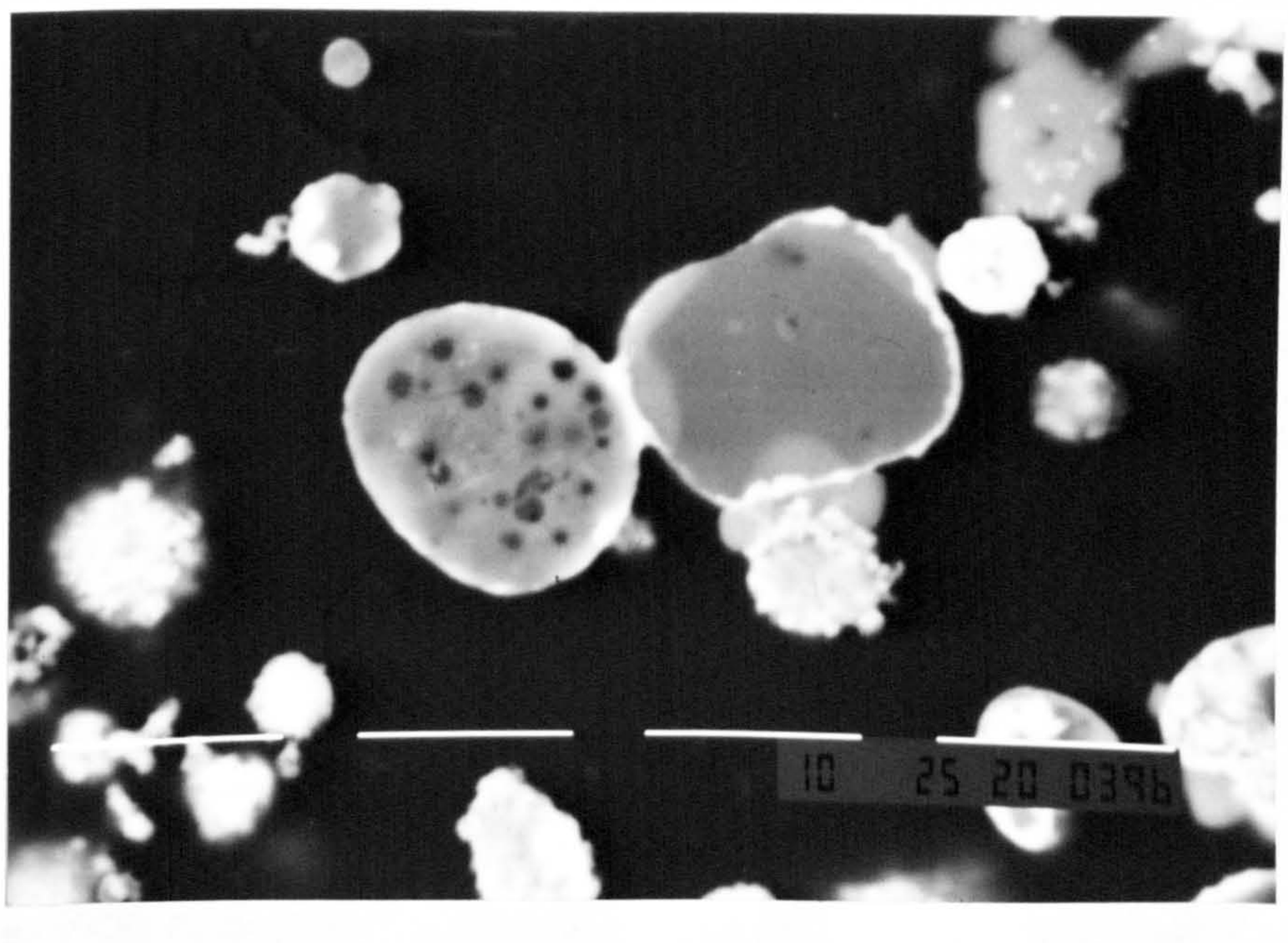

Frame 5.4 *Tyre incinerator deposit. 1 bar ≡ 10μm. BSI.*

The above micrograph illustrates the initial mechanism of adhesion. It is apparent that the bonding of two adjacent calcium aluminosilicate ash particles (dark grey) is facilitated by a peripheral coating of condensed ZnO, shown as a bright rim of approximate thickness 1μm. A distinct neck has formed between the particles. There is also evidence of another bonding medium, $CaSO_4$ (mid-grey).

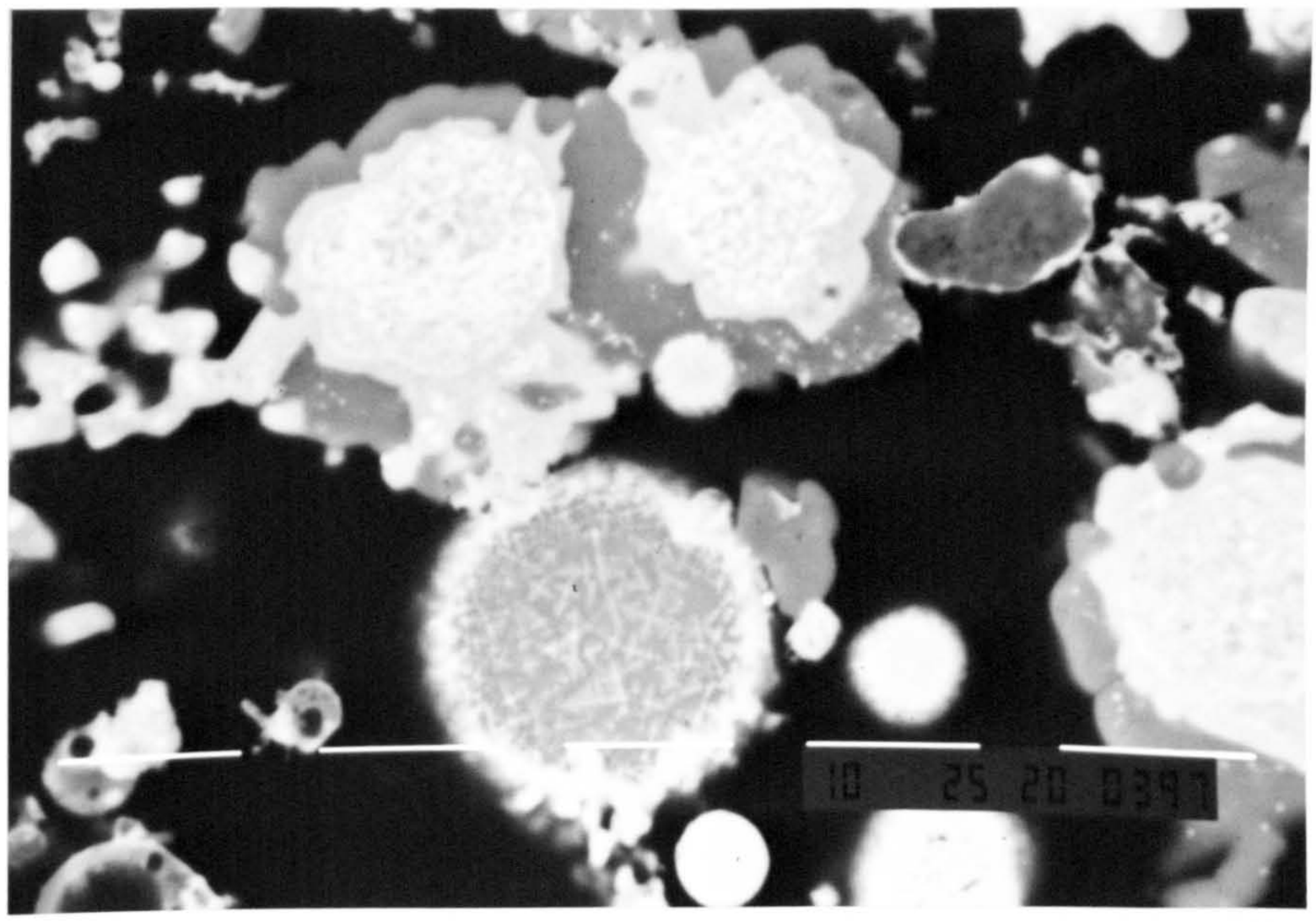

Frame 5.5. *Tyre incinerator deposit. 1 bar ≡ 10μm. BSI.*

Two relatively large particles of ZnO (centre, top) are shown in the above micrograph to be coated in a calcium-zinc-sulphate phase (pale grey), ~2-5μm in thickness, bonded together by $CaSO_4$ (mid-grey).

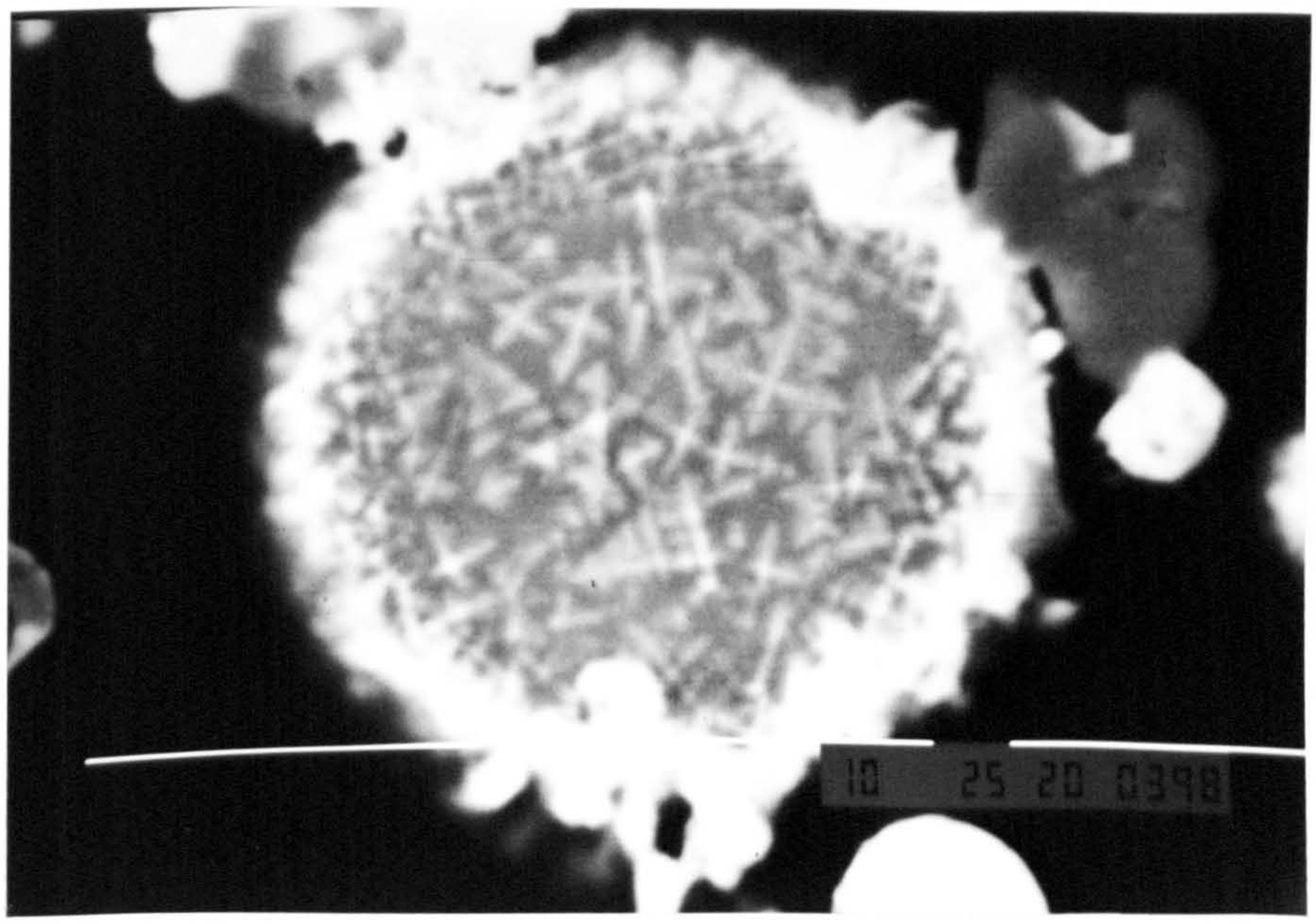

Frame 5.6. *Tyre incinerator deposit. 1 bar ≡ 10μm. BSI.*

Several particles within the deposit bulk contained elaborate iron-rich dendrites in a viscous silicate matrix, such as those illustrated in the above micrograph. At this high magnification the outer rim of ZnO is evidently composed of sub-micron particles formed by condensation from the vapour phase.

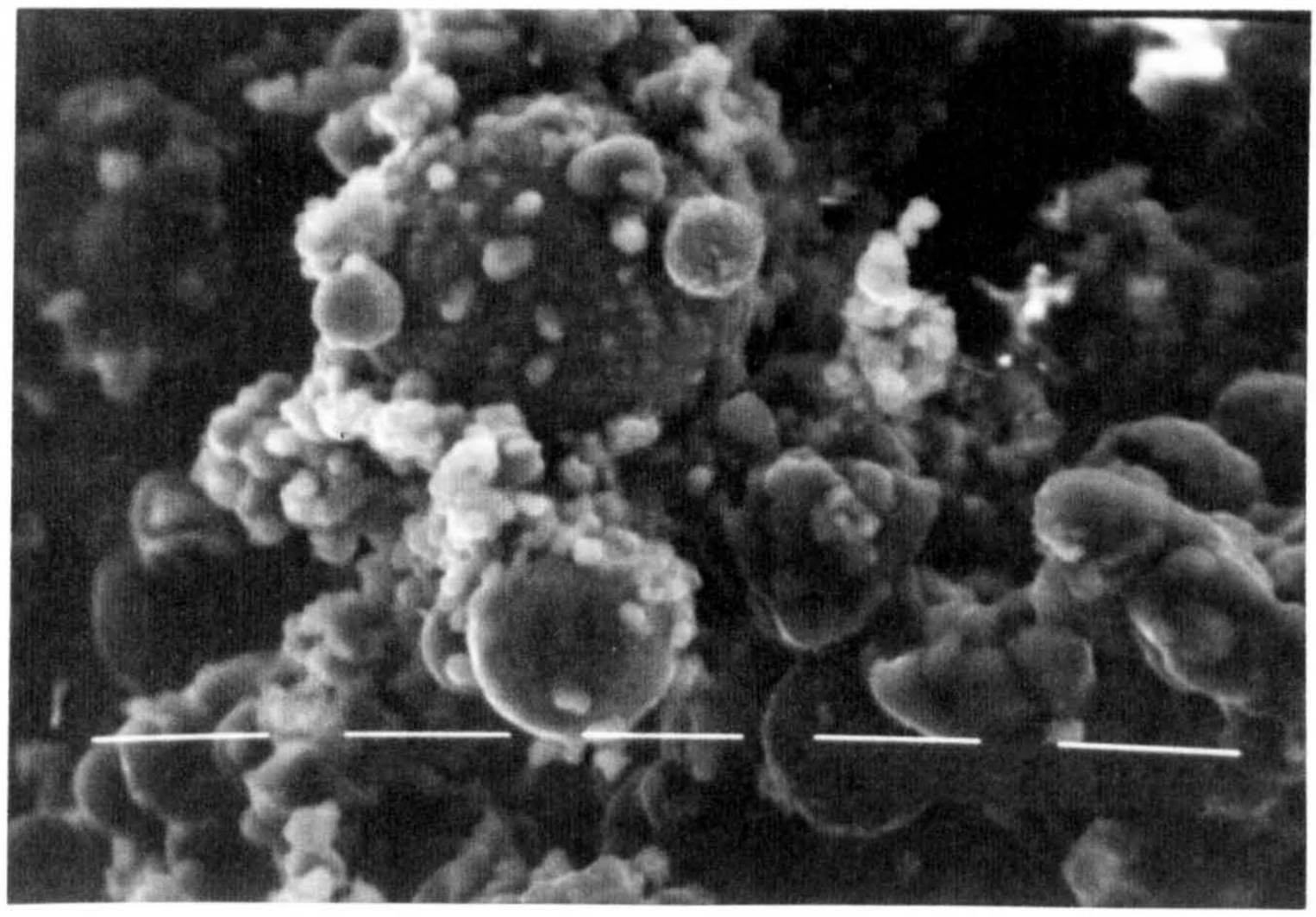

Frame 5.7. *Tyre incinerator deposit* *1bar ≡ 10μm. SEI*

A secondary electron image of a 'fractured' surface within the bulk of the deposit. Shown above is an assembly of mostly spherical particles. A silicate sphere (centre-top), approximately 30μm in diameter, is shown to be partially coated in ZnO spheres. Other ash particles are seen lightly adhering to the surface. Several particles coated in $CaSO_4$ are shown centre right.

5.1.4 Proposed mechanism of deposit formation and growth

From the results it may be inferred that the problems of deposit formation in the Elm Energy incinerator were largely attributable to the inorganic filler materials, ZnO and $CaCO_3$, in the composite tyre structure. ZnO, readily reduced by carbon at the combustion temperatures to a highly volatile zinc vapour, was the first phase to have deposited on tube metal surfaces. In an oxidising environment, at high temperatures, ZnO formed which subsequently condensed in the cooler boiler reaches on tube surfaces and gas borne particles. The fouling of the tyre incinerator was initiated by the deposition of a thin layer of condensed ZnO vapours which clearly encapsulated other ash particles, the majority also coated in a thin layer of ZnO. Calcite decomposes at temperatures in excess of 850°C to form CaO and CO_2.

During pyrolysis of the tyre, the hydrocarbons are aromatised, by a Diels-Alder type reaction, to form mono- and polycyclic aromatic liquid species. Reaction of the aromatic hydrocarbons with organic sulphur, of the rubber vulcanisation system, produces PASH (sulphur-polycyclic aromatic hydrocarbons). On combustion the PASH form SO_x gases, which combine with solid CaO and ZnO/Zn vapours to form the respective sulphate: $CaSO_4$ and $ZnSO_4$. At high oxygen fugacities, sulphur in the gas would primarily have been in the form of SO_2 and the overall reaction would likely have been either of the following

$$Zn_{(g)} + SO_{2(g)} + O_{2(g)} \rightarrow ZnSO_{4(S)}$$

$$ZnO_{(s)} + SO_{2(g)} + \tfrac{1}{2}O_{2(g)} = ZnSO_{4(s)}$$

The sulphates have relatively high vapour pressures and enter the gas phase only to recondense on cooler surfaces in the convective heat transfer regions of the boiler. The condensed sulphates constitute a low-melting and hence sticky surface layer which encapture other types of impinging gas borne particle. The agglomeration of ash particles coated in a layer of condensed ZnO vapour was assisted by the continued condensation of sulphate to form an adhesive matrix.

5.1.5 A characterisation of boiler dust samples

Two samples of boiler dust, one labelled 'zinc oxide powder', from the hoppers and baghouse of a waste car tyre incinerator were received from Basic Energy Ltd. These residues have a potential market value, for the ZnO can be reclaimed and effectively recycled to the tyre industry. The compositions of the boiler dusts are shown in Table 5.4. The dust was found to consist of two predominant oxides, ZnO (42wt%) and SO_3 (39wt%) with smaller amounts of silica (8wt%), lime (6wt%) and soda (7 wt%). The zinc oxide powder was grey in colour and found to contain only 72wt% ZnO with 11wt% SO_3, 4wt% SiO_2 and 5wt% Na_2O.

Table 5.4 The composition of ash samples from a car tyre incinerator

OXIDE (wt%)	SiO_2	Al_2O_3	Fe_2O_3	CaO	MgO	K_2O	Na_2O	P_2O_5	TiO_2	SO_3	ZnO
Boiler dust	8.3	1.0	2.2	6.0	0.5	2.0	7.2*	0.4	1.1	29.4	42.0
Grey powder	3.8	1.8	2.2	2.2	0.0	1.3	5.4*	0.4	0.1	11.2	71.8

** The Na K peak lies within the background noise level of the Zn L peak, with the latter substantially greater in magnitude. Difficulties may therefore arise in the analysis of Na_2O, although in this instance a correction has been applied.*

The major crystalline components of the boiler dust were identified as zinc oxide and a zinc sulphate, with anhydrite and magnetite in minor proportions. The results are tabulated in Table 5.5.

Table 5.5 Crystalline phases present in tyre incinerator ashes, identified by XRD

SAMPLE	CRYSTALLINE PHASE		
	major	minor	trace
Boiler dust	ZnO *(zincite)* $Zn_3O(SO_4)_2$	$CaSO_4$ *(anhydrite)*	Fe_2O_3 *(magnetite)*
Grey powder	ZnO *(zincite)*		traces of other unidentified compounds

Microstructurally, the boiler dust and the deposit samples were very similar in that the boiler dusts consisted of mostly spherical ash particles coated in a thin layer of condensed ZnO. A rim of $CaSO_4$ was also discernible around some particles, although deposition at lower temperatures resulted in much less interparticle bond formation. Thus a relatively free flowing powder was produced compared to the sintered nature of the boiler deposit. Typical microstructural features of the boiler dusts are illustrated in Frames 5.8 and 5.9.

The formation of ash deposits on the heat transfer surfaces of scrap tyre incinerators continues to be a major operational problem for their disposal by this route. Indeed, during the course of the project, the plant at Wolverhampton was forced to close down after poor technical and commercial performance, and failure to operate to specification, following severe ash deposition on convector heat transfer surfaces. No immediate solution to this problem seems imminent as the relative ease of reduction of ZnO vapours with carbon at the combustion temperatures and the high volatility of zinc vapours will always lead to the condensation of these species somewhere in the system.

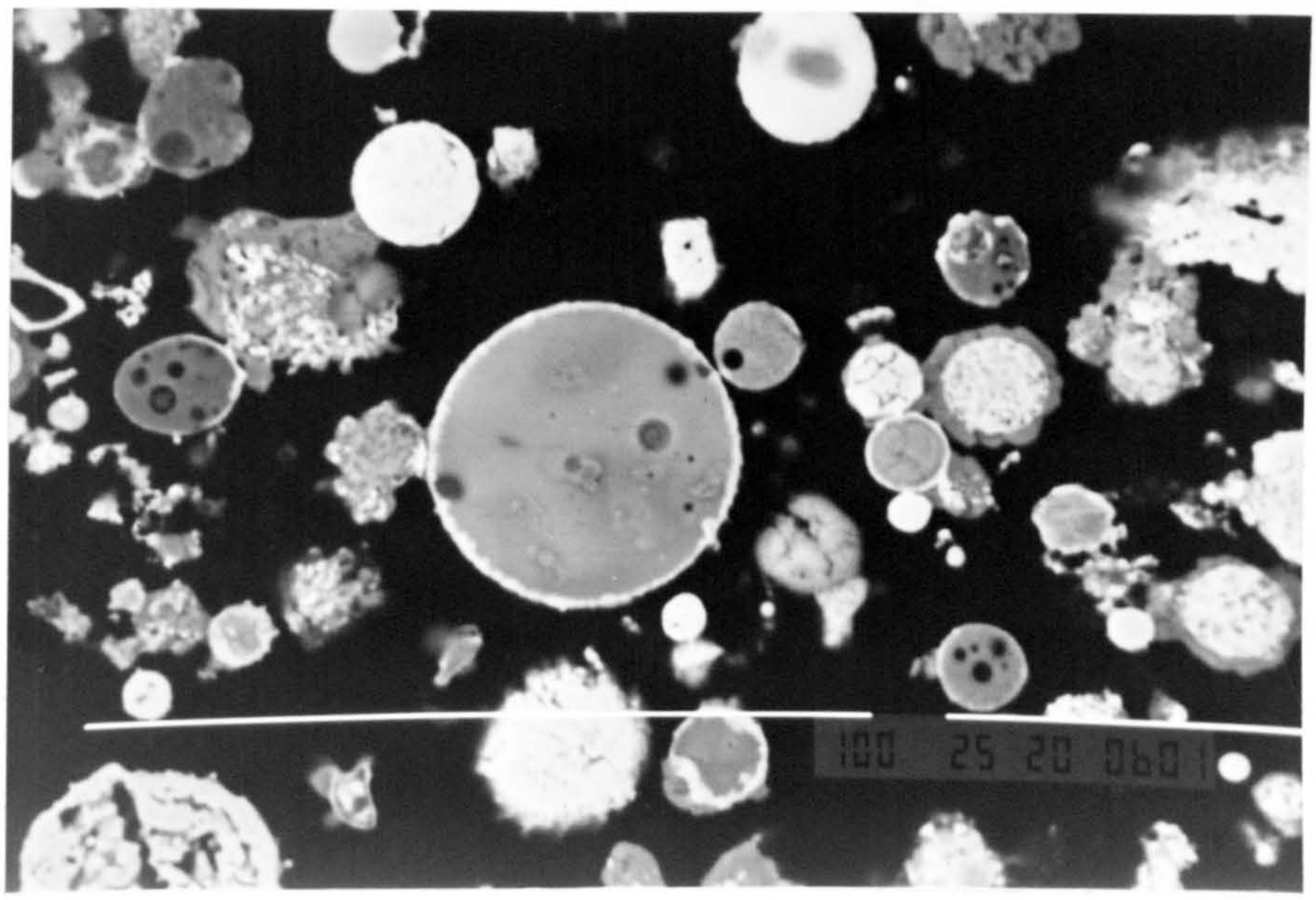

Frame 5.8. *Boiler dust.* *1bar ≡ 100μm.BSI*

A polished cross-section of the boiler dust from the waste tyre incinerator at Wolverhampton. The above microstructure bears a resemblance to that of the tube deposit, however the boiler dust contains little evidence of particle-particle interaction.

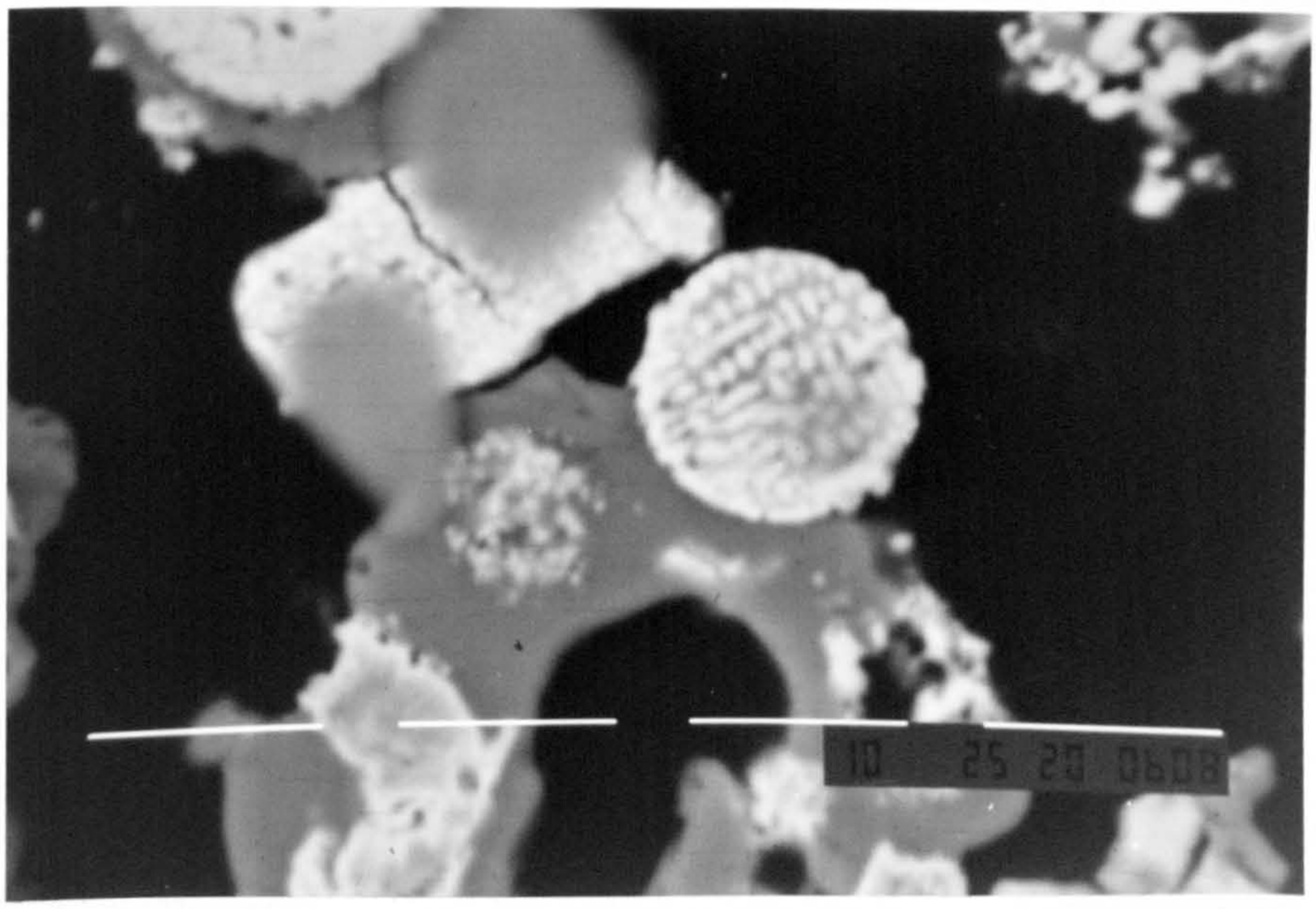

Frame 5.9. *Boiler dust.* *1bar ≡ 100μm.BSI*

A particle containing iron-rich dendrites, coated in ZnO and bonded to a once tacky mass of $CaSO_4$.

5.2 A characterisation of fuel and deposits from Eye power station

5.2.1 Background to poultry litter combustion at Eye

Samples of poultry litter fuel, a superheater deposit and two boiler slags were provided for this study by Fibropower Ltd from the Eye Power Station, Suffolk. The 12.5MW_e Eye plant, the world's first power station fuelled by poultry litter, was commissioned in July 1992. The boiler is a three pass, natural convection system, with two banks of superheaters and an economiser. The plant design (Aalborg) was based on a straw combustor, where the fuel produces an ash characteristically rich in lime and potash. As designed, the boiler contained no sootblowers to clean the heat transfer surfaces. It was anticipated that slagging and fouling could be eliminated by restricting gas temperatures to 950°C. The plant experienced problems with ash deposition from start-up, with excessive slagging of the boiler furnace walls and blockage of the convective superheater passes. A maximum of five days operation could be attained before the plant had to be shut down for manual cleaning. A shot cleaning system had been provided to clean the superheaters and economiser, however this method proved to be ineffective with shot and deposits lodging between the horizontal tubes. The addition of steam sootblowers to the boiler furnace was a major improvement, with the continuous operation of the plant extended to 30 days before manual cleaning was again necessary. A schematic diagram of the plant, indicating the positioning of the sootblower and shot cleaning systems, is shown in Figure 5.1.

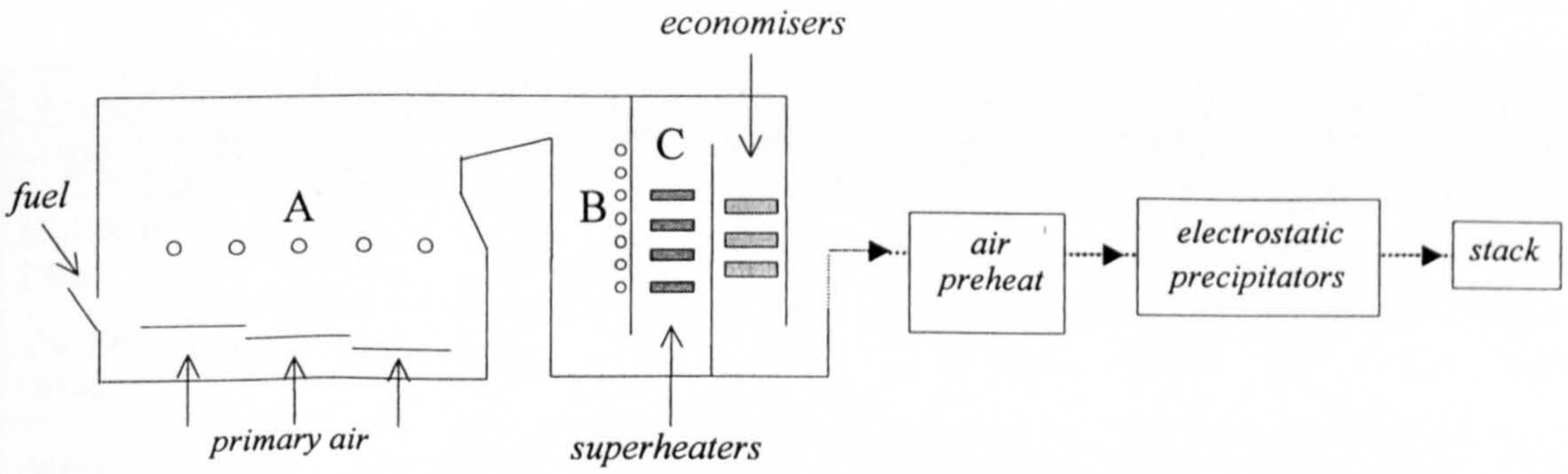

A: front wall sootblowers B: retractable sootblowers C: shot cleaning facility

Figure 5.1 A schematic diagram of Eye Power Station

5.2.2 Poultry litter

Poultry litter is composed of droppings, feathers and bedding material (up to 10-15% straw or wood shavings). The feedstock for the Fibropower boiler is generally a combination of chicken and turkey litter in a ratio of 2:1, however the supply of a consistent quality and constitution of fuel is not guaranteed. Samples of poultry litter, including different livestock bedding, were received from Fibropower Ltd: the chicken litter comprised wood shavings and droppings, while the turkey litter included a straw based material. The fuel was characteristically high in moisture; chicken litter was found to contain 51.3% moisture, and turkey litter substantially greater at 59.4%. Once dried, the material was friable and fibrous. The ash contents of the chicken and turkey litter samples were 13.6wt% and 15.0wt% respectively, on a dry ash basis. The composition of the LTA of each sample comprised four major oxides: CaO, K_2O, P_2O_5, and SO_3. A striking feature of the poultry litter ash composition was the considerable quantity of the volatile alkali oxide K_2O (chicken litter 17wt%, turkey litter 24wt%). Even at an early stage of the characterisation, it would seem hardly surprising from a knowledge of the ash composition that the Eye plant had experienced problems with ash deposition. The ash compositions of turkey and chicken litter were similar with respect to all oxides with the exception of lime, potash and soda. Table 5.6 presents a comparison of the oxide compositions. The ash compositions of a cereal straw (ash content 2.4wt% dab) and pine sawdust (2.7wt% ash dab), constituents of the poultry litter, are also included.

Table 5.6 The composition of poultry litter LTA samples

OXIDE (wt%)	SiO_2	Al_2O_3	Fe_2O_3	CaO	MgO	K_2O	Na_2O	P_2O_5	MnO	TiO_2	SO_3
Chicken litter	3.5	0.8	0.7	24.7	5.0	17.0	4.5	29.4	0.6	0.1	13.8
Turkey litter	5.3	0.6	0.8	17.3	5.7	24.0	2.6	30.5	0.4	0.1	12.8
Straw	71.3	1.0	0.0	10.3	1.9	11.4	0.4	3.8	0.0	0.0	0.0
Pine sawdust	34.6	19.8	4.3	29.4	2.1	3.4	1.4	2.2	2.1	0.6	0.0

The chicken and turkey litter ashes also contained chloride, 1.2 and 2.0wt% respectively. The crystalline phases, identified by X-ray diffraction, present in the poultry litter samples and in straw and pine wood are presented in Table 5.7.

Table 5.7 Crystalline phases present in the poultry litter low temperature ashes

SAMPLE	CRYSTALLINE PHASE		
	major	**minor**	**trace**
Chicken litter	$Ca_5(PO_4)_3(OH)$ (*hydroxylapatite*)	K_2SO_4 (*arcanite*)	NaCl
Turkey litter	$Ca_5(PO_4)_3(OH)$ (*hydroxylapatite*)	K_2SO_4 (*arcanite*)	
Straw	SiO_2 (*quartz*)	$CaMg(CO_3)_2$ (*dolomite*) KH_2PO_4 (*potassium-orthophosphate*)	$CaCO_3$ (*calcite*)
Pine sawdust	SiO_2 (*quartz*)	$CaHPO_4$ (*calcium-orthophosphate*)	

A complete interpretation of the diffraction patterns had proved difficult.

5.2.3 High temperature microscopy

The ash fusion characteristics of the poultry litter samples, a cereal straw and pine wood were investigated using hot stage microscopy. The observations have been recorded in Table 5.8.

Table 5.8 Fusion behaviour of poultry litter, straw and pine wood

SAMPLE	TEMPERATURE (+/-10°C)			
	Solidus	**First visible liquid** *(30-40% liquid)*	**Appreciable softening** *(70-80% liquid)*	**Liquidus**
Chicken litter	820	940	1030	1140 *fluid melt*
Turkey litter	800	800	950	1100 *fluid melt*
Straw	780	900	1050	1200 *viscous melt*
Wood	650	1090	1300	1350 *fluid melt*

5.2.4 Superheater tube deposit

A sample of a fouling deposit, of approximate dimensions 15×8×7cm, from the boiler at Eye was examined. The impression of two primary superheater tubes, approximately 0.1m apart (centre-to-centre), was discernible with an arrowhead configuration of deposit between the tubes indicating an up-draught pass. The bulk of the tube deposit was of a brown-grey colour; a thin (~2mm) fine grained white layer was observed adjacent to the tube surface. The deposit was of low porosity and substantial strength.

A shot cleaning system had previously been employed to dislodge deposits from the superheaters. It was evident from a macroscopic examination of the sample that a chunk of deposit material displaced by the shot cleaning action had merged with an underlying deposit that had formed a bridge between the lower horizontal banks of two superheater tubes. Iron pellets were found embedded in the deposit. Shot cleaning of the superheaters proved to be ineffective at Eye since the shot would only clean exposed upper surfaces, while much of the deposit would accumulate underneath the tubes in an up-draught pass system. Subsequently the boiler was fitted with sootblowers to remove wall slags and the fouling deposits in the economisers and superheaters.

The crystalline phases present in the fouling deposit were determined using an X-ray powder diffraction technique. The white inner layer adjacent to the tube surface was found to be a sulphate of potassium (arcanite, K_2SO_4). The bulk of the deposit was also primarily K_2SO_4 with a potassium calcium phosphate [$K_3CaH(PO_4)_2$] and KCl in minor and trace proportions respectively. The bulk composition of the superheater tube deposit, determined by EDS, comprised four oxides of substantial proportions: SO_3 (~36wt%), K_2O (34wt%), CaO (12wt%) and P_2O_5 (11wt%). Silica, magnesia, and soda constituted the remaining ash chemistry at 2.2, 2.5, and 1.9wt% respectively. The results are presented in Table 5.9.

Table 5.9 Bulk ash composition of a superheater tube fouling deposit from Eye plant

OXIDE	SiO_2	Al_2O_3	Fe_2O_3	CaO	MgO	K_2O	Na_2O	P_2O_5	MnO	TiO_2	SO_3
wt %	2.2	0.2	0.4	12.3	2.5	34.0	1.9	10.6	0.2	0.1	35.6

The compositions of deposits formed in various regions of the boiler early in 1994, while severe fouling was still experienced, are tabulated in Table 5.10. The data was provided by Fibropower Ltd. While the problem of extensive fouling in the boiler has

largely been overcome by the addition of sootblowers, the current deposit, with enhanced K_2O and SO_3 concentrations highlights the problems to be anticipated for such fuels with a high alkali metal oxide content.

Table 5.10 Fuel ash and deposit compositions, data from Fibropower Ltd.

OXIDE (wt%)	SiO_2	Al_2O_3	Fe_2O_3	CaO	MgO	K_2O	Na_2O	P_2O_5	MnO	TiO_2	SO_3
Fuel	9.8	1.8	1.5	23.1	8.1	9.5	2.3	26.4	0.4	0.1	6.8
Grate ash	9.9	1.2	1.1	24.9	8.8	13.6	3.1	26.5	0.4	0.1	5.4
Superheater deposit	12.4	1.1	1.3	22.8	9.8	10.7	3.2	30.1	0.4	0.1	0.2
Economiser deposit	15.6	0.7	1.5	17.5	9.1	13.4	2.4	18.9	0.2	0.1	15.8
Precipitator dust	6.4	0.8	0.7	16.9	8.3	16.1	3.0	22.9	0.4	0.1	14.0

The fusion properties of the superheater deposit were investigated using high temperature microscopy. The first trace of liquid formation (the solidus temperature) was observed at 850°C, with complete fusion (liquidus) at 1060°C with the formation of a low viscosity melt. The low solidus temperatures for the superheater deposit and the poultry litter fuel LTA would suggest that molten or partially molten ash particles would be produced during the combustion process. The cumulative effect of the low solidus temperature, short fusion range and relatively high vapour pressures of potassium salts and P_2O_5 would be the inevitable formation of phosphate bonded deposits in such a system.

5.2.5 Microstructural analysis of the superheater deposit

The deposit microstructure was indeed consistent with the predictions based upon ash chemistry and high temperature microscopy. The deposit consisted of ash particles, the majority of spherical calcium-potassium phosphate, coated and embedded in a K_2SO_4 matrix to give a dense structure. The condensation of K_2SO_4 on the surface of ash particles and on tube surfaces in the convective regions of the boiler played a crucial role in the encapture and consolidation of ash to form a sintered deposit of substantial strength.

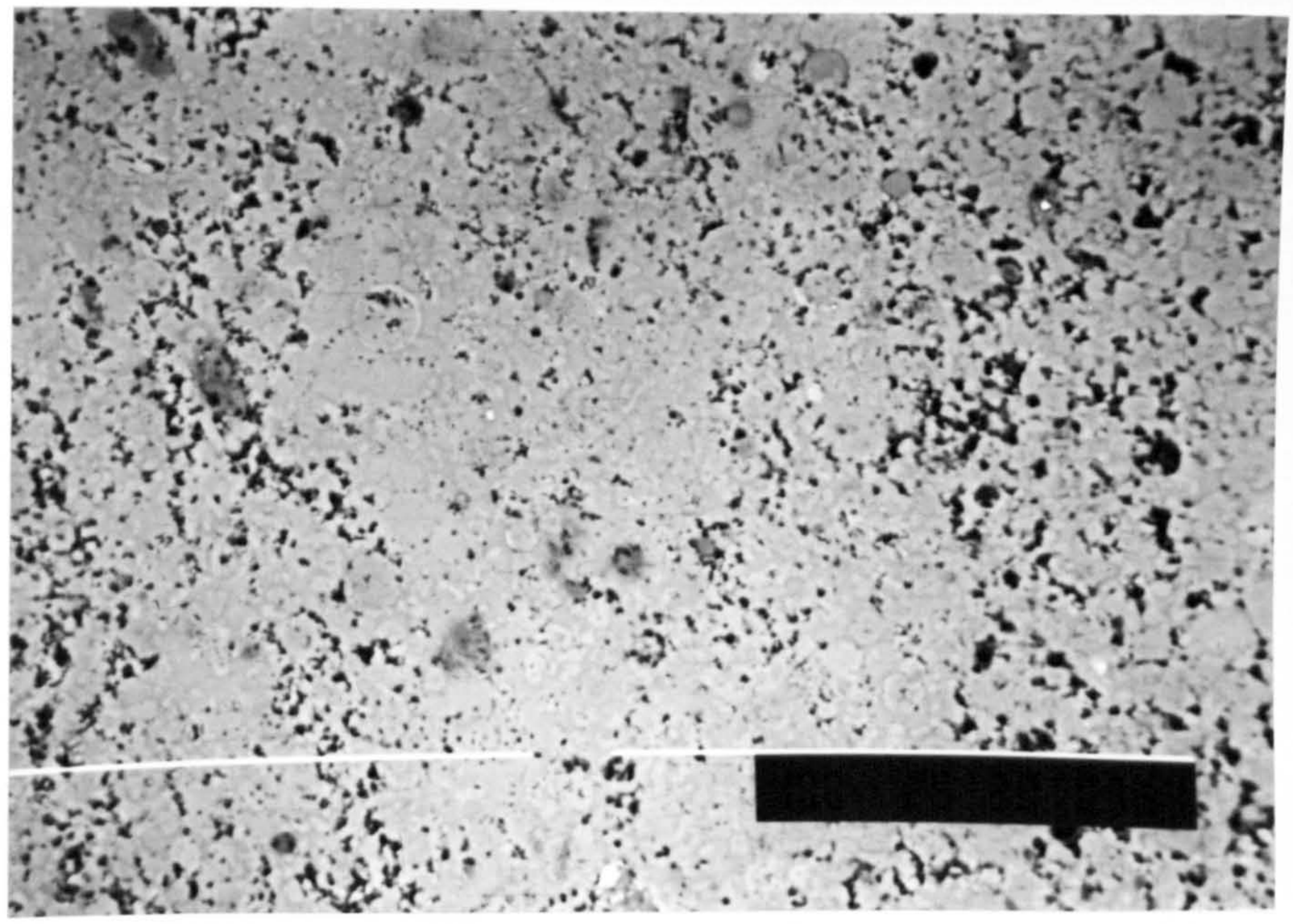

Frame 5.10. *Eye superheater deposit.* *1 bar ≡ 100μm. BSI*

A cross-section of a deposit sample from the superheater tubes of the Eye boiler. Shown in the micrograph above is a region within the bulk of the deposit, characteristic of the entire microstructure. Very little variation in back-scattered electron intensity was observed. Spherical ash particles were barely distinguished amid the K_2SO_4 matrix.

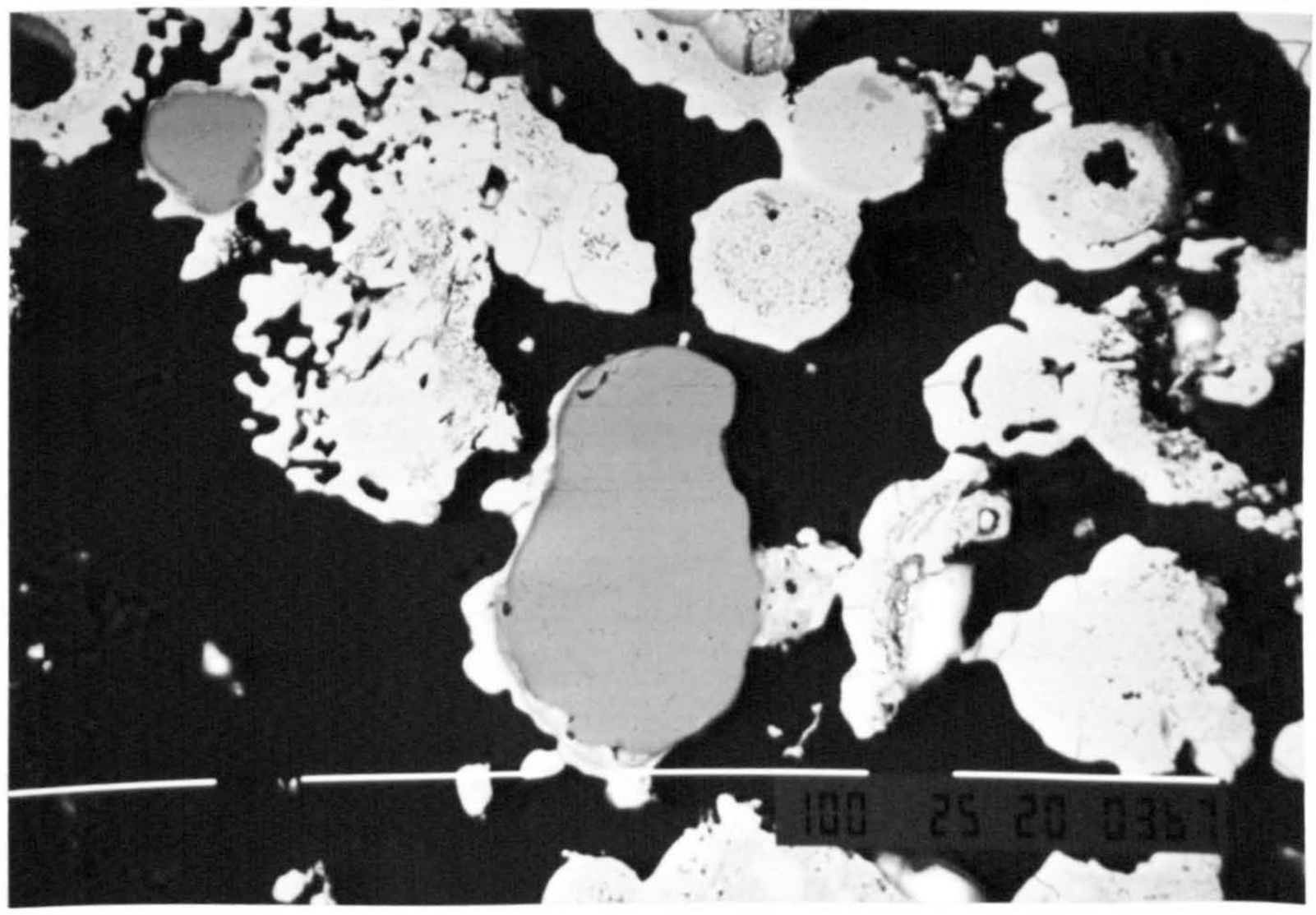

Frame 5.11. *Eye superheater deposit.* *1 bar ≡ 100μm. BSI.*

A quartz particle, 100-150μm in size, is shown in this micrograph to be partially coated in a layer of K_2SO_4, of approximate thickness 10-20μm. Two spherical calcium-potassium phosphate particles (centre, top) were mutually bonded by the K_2SO_4 phase.

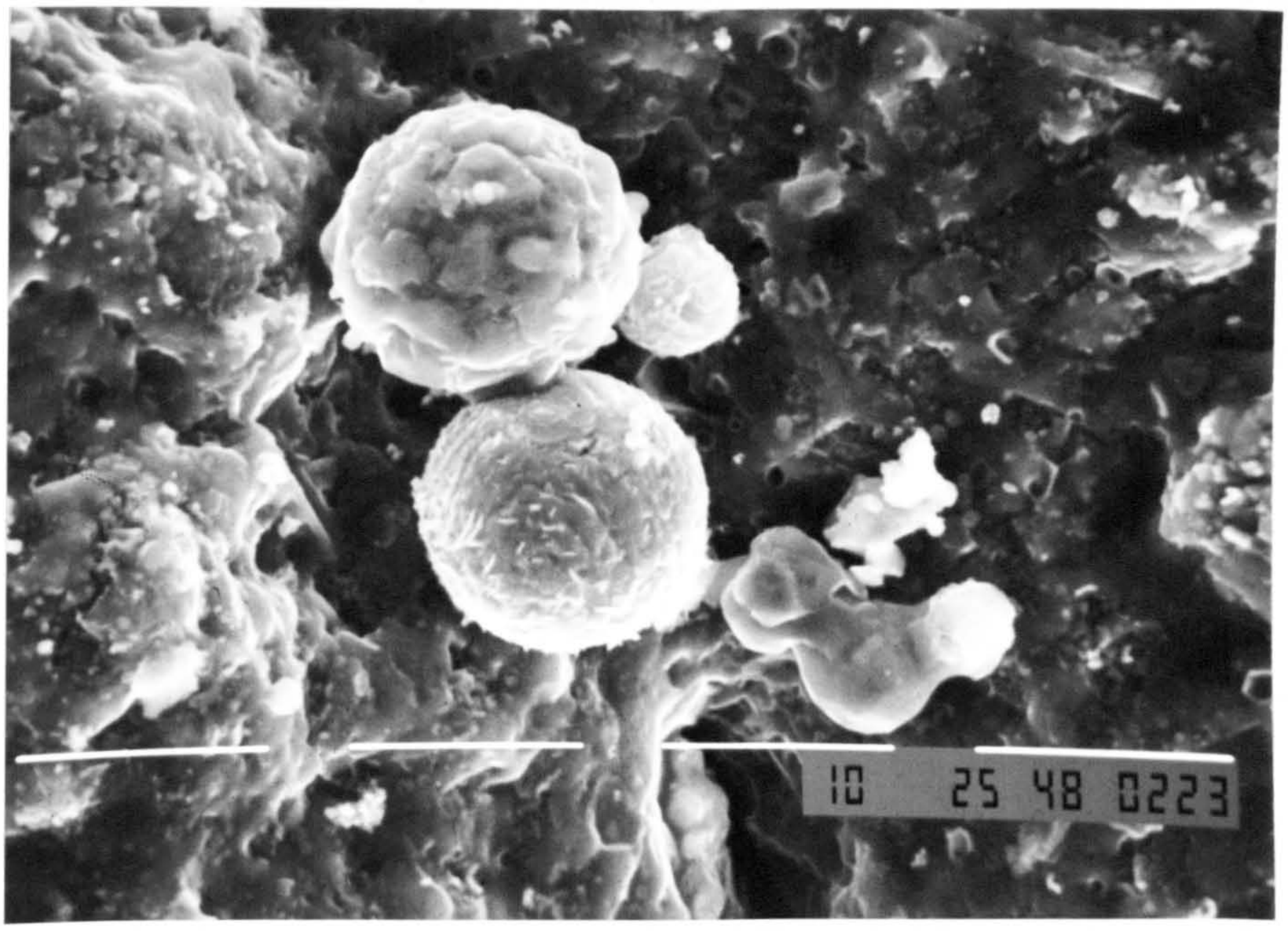

Frames 5.12. *Eye superheater deposit* *1 bar ≡ 10μm. SEI*

An image of the deposit surface. Shown above are several spherical particles mutally bonded by a K_2SO_4 phase. Necks between particles average 2μm. The background of the micrograph indicates that the role of K_2SO_4 was very much that of an adhesive/glue.

5.2.6 The boiler deposits, Eye II and III

Two samples of slag from a refractory lined section of the front wall of the Eye boiler were also examined.

As the poultry litter fuel did not ignite readily, oil burners were employed at Eye as a supplementary fuel to support combustion. Once combustion was established and self-sustaining, the burners were extinguished. To expand the combustion zone and increase power output, a refractory panel ($6.12 \times 2.66 m^2$ and 65mm in thickness) of an aluminosilicate composition was installed, and restrained by welded metal anchors, 150mm apart. The effect of the addition of the refractory to the boiler system was to increase the local gas temperatures. Consequently, within several days of operation, a slag deposit of approximate dimensions $2.0 \times 1.5 \times 0.2 m^3$ had accumulated, requiring manual removal. The location of the refractory and slagging deposits is illustrated in the schematic diagram of Figure 5.2.

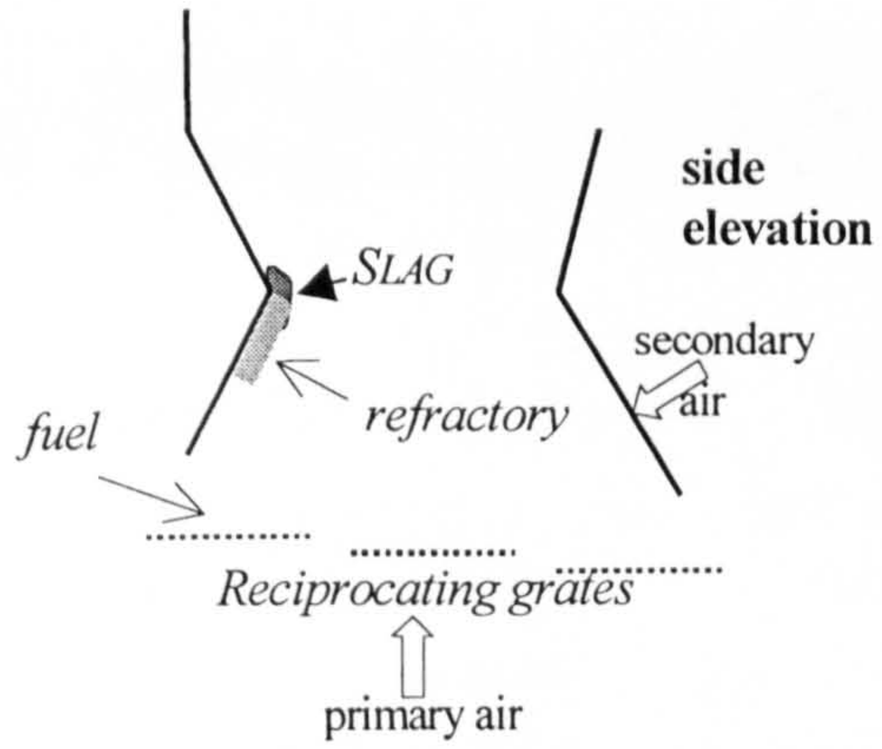

Figure 5.2 Location of the slagging deposits and the refractory furnace lining

5.2.7 Chemical analysis of Eye II and Eye III

Slag sample Eye II, 5cm thick, was observed to have a definite fireside surface. The fireside region possessed a high degree of porosity, and consequently was of a more friable and brittle nature than the rest of the deposit. On arrival the friable section of the deposit had separated from the more dense material. The refractory side of the deposit was more heterogeneous in appearance and contained material of varying colour, including light-mid brown, russet, and grey, with numerous large open pores. On a macroscopic scale, the structure of the deposit was distinctly layered with varying degrees of porosity. The refractory-side material had developed great strength, and a hammer and chisel were required to remove a sample for analysis. The refractory and fireside regions were characterised independently.

The second slagging deposit (Eye III), from the same location (depicted in Figure 5.2), was of a more uniform texture relative to the former, with no friable material and hence no perceptible fireside surface. The slag contained varying degrees of surface porosity, the pores ranging in size from <1mm to 1cm.

The EDS compositions of the slags (Eye II and III) are presented in Table 5.11. The refractory and fireside regions of Eye II were found to share much the same composition containing P_2O_5 (an average of 32wt%), CaO (25wt%), K_2O (17wt%) and SiO_2 (12wt%) in major proportions. Eye III was also of a similar constitution, with the exception of the silica content which was approximately twice that of Eye II at 22wt%.

Table 5.11 Chemical composition of the boiler slags Eye II and III

OXIDE (wt%)	SiO_2	Al_2O_3	Fe_2O_3	CaO	MgO	K_2O	Na_2O	P_2O_5	MnO
Eye II fireside of deposit	13.9	1.2	1.2	24.8	6.0	17.4	3.0	31.5	1.1
refractory-side of deposit	10.2	1.1	1.4	26.4	5.9	18.1	3.1	33.4	0.4
Eye III	21.8	1.8	1.7	21.8	5.4	17.3	2.3	27.9	0.5

XRD analysis of the slagging deposits produced very similar diffraction patterns, containing identical major and minor phases. The major phase common to Eye II (refractory and fireside) and Eye III was a potassium-calcium phosphate ($KCaPO_4$). The standard pattern given in the Powder Diffraction Data File is a close match, but not an exact fit to d-spacing values of the sample traces. It is believed that other ions, such as sodium, may substitute for potassium thereby altering the dimensions of the unit cell. The minor phases identified in each trace were forsterite ($2MgO.SiO_2$), quartz and kalsilite ($KAlSiO_4$), a member of the nepheline group of tridymite-type structures.

Adhering to the surface of the refractory side of Eye II was a small region, approximately $1cm^2$ and <1mm thick, of white refractory material. The XRD analysis of the refractory detected mullite as the dominant phase.

5.2.8 High temperature microscopy

The ash fusion characteristics of the slagging deposits were investigated using hot stage microscopy. From a knowledge of the ash chemistry, the boiler slags exhibited similar solidus and liquidus temperatures, averaging 1075°C and 1205°C respectively. The results are presented in Table 5.12. Contrary to the behaviour of the slags at high temperature, the superheater tube deposit was observed to have relatively low solidus and liquidus temperatures reflecting the presence of an ample quantity of potash. A liquid phase was observed at 850°C and the material completely molten at 1060°C.

Table 5.12 High temperature microscopy observations of deposits Eye II and III

SAMPLE	TEMPERATURE (+/- 10°C)		
	Solidus	**Appreciable liquid** *(70-80% liquid)*	**Liquidus**
Eye I Superheater fouling deposit	850	950	1060 *fluid melt*
Slagging deposits: **Eye II**, fireside	1090	1150	1220 *viscous melt*
Eye II, refractory-side	1060	1140	1190 *viscous melt*
Eye III	1070	1180	1210 *viscous melt*

5.2.9 Microstructural analysis

The microstructure of Eye II (refractory and fireside) and Eye III contained similar features. All the samples, observed in the back scattered imaging mode, showed evidence of fusion, with crystal growth from a viscous silicate liquid phase. The phases were identified using EDAX and quantitative point analysis (EDS). The crystallisation of the molten slag formed $KCaPO_4$ crystals, potassium phosphate crystals, laths and angular particles of a calcium phosphate, all within an eutectic mixture of forsterite ($2MgO.SiO_2$) and a silicate matrix. While the microstructure was indeed a complex assembly of phases, the nature was entirely consistent with that of the crystallisation of a multi-component K_2O-CaO-P_2O_5-SiO_2 system, as predicted from the relevant phase equilibrium diagrams. Characteristic features of the microstructure of Eye II are shown in Frames 5.13 to 5.17 and the microstructure of Eye III in 5.18.

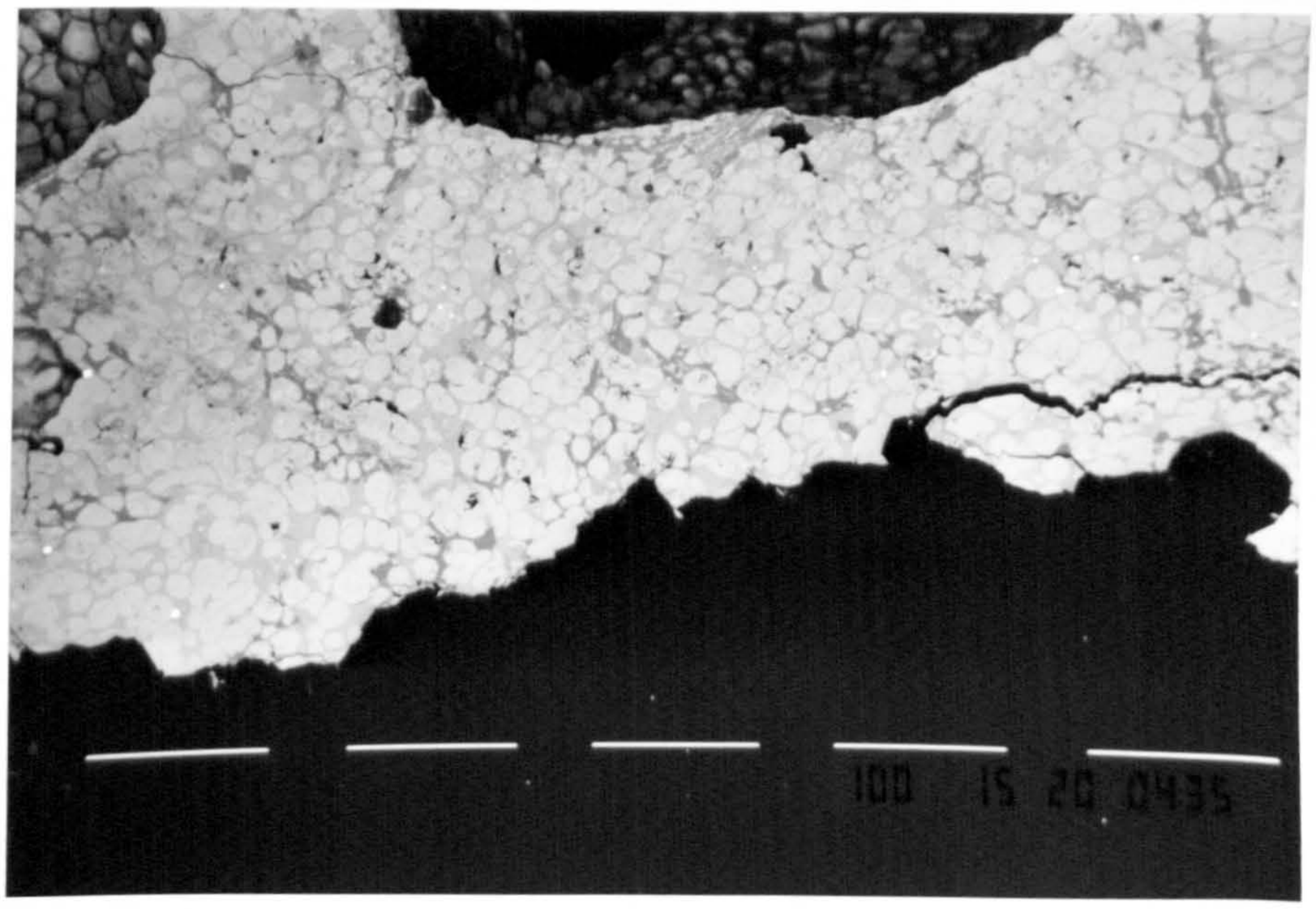

Frame 5.13 *Eye II, fireside. 1 bar ≡ 100μm. BSI*

An image of a cross-section of the fireside region of boiler slag Eye II at low magnification, illustrating the heterogeneity of the microstructure.

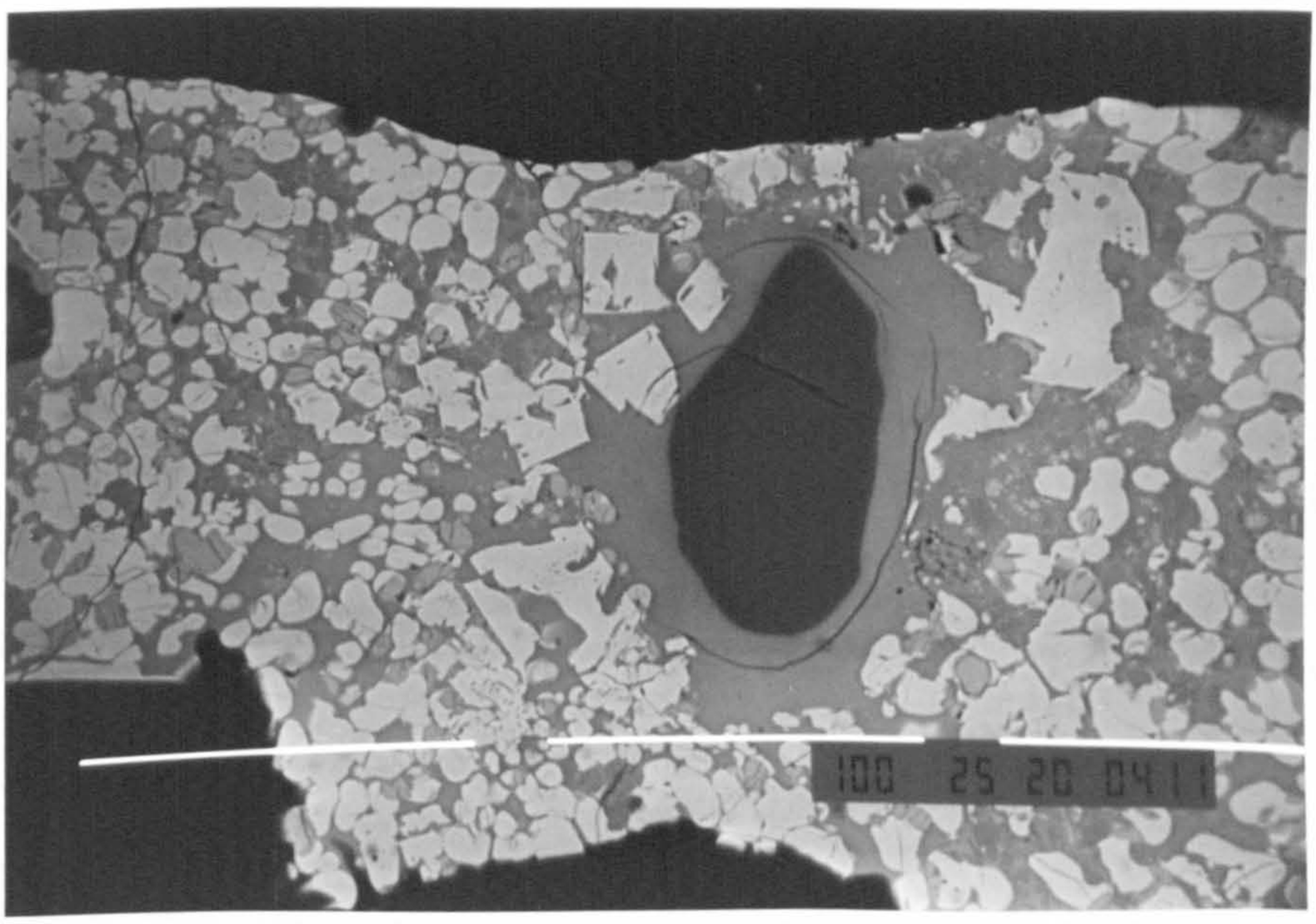

Frame 5.14 *Eye II, fireside. 1 bar ≡ 100μm. BSI*

A quartz particle (dark grey), approximately 100μm in size, and in the immediate vicinity a solution rim of a once present highly viscous silicate liquid.

Frame 5.15 *Eye II, fireside. 1 bar ≡ 100μm. BSI*

The microstructure is composed of rounded crystals (light grey, bright rim, ~10μm) of a potassium calcium phosphate, potassium phosphate crystals (mid-grey, ~5μm and less), laths and angular particles (~30μm in size) of a calcium phosphate, and a fine eutectic mixture of forsterite dendrites in a silicate matrix (dark grey).

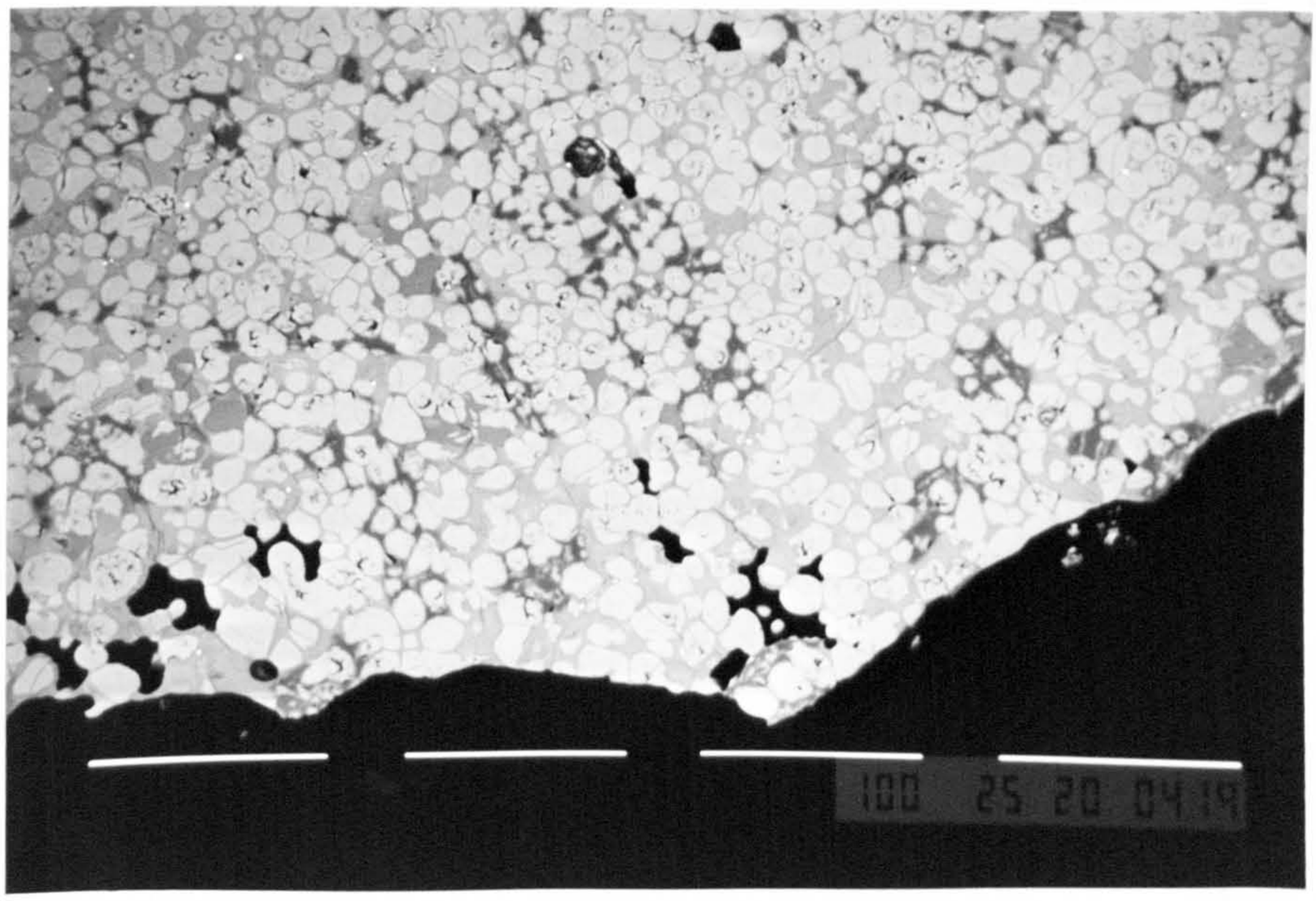

Frame 5.16 *Eye II, refractory side. 1 bar ≡ 100μm.*

A general view of the refractory-side deposit microstructure, which appears coarser and more homogeneous than its fireside counterpart.

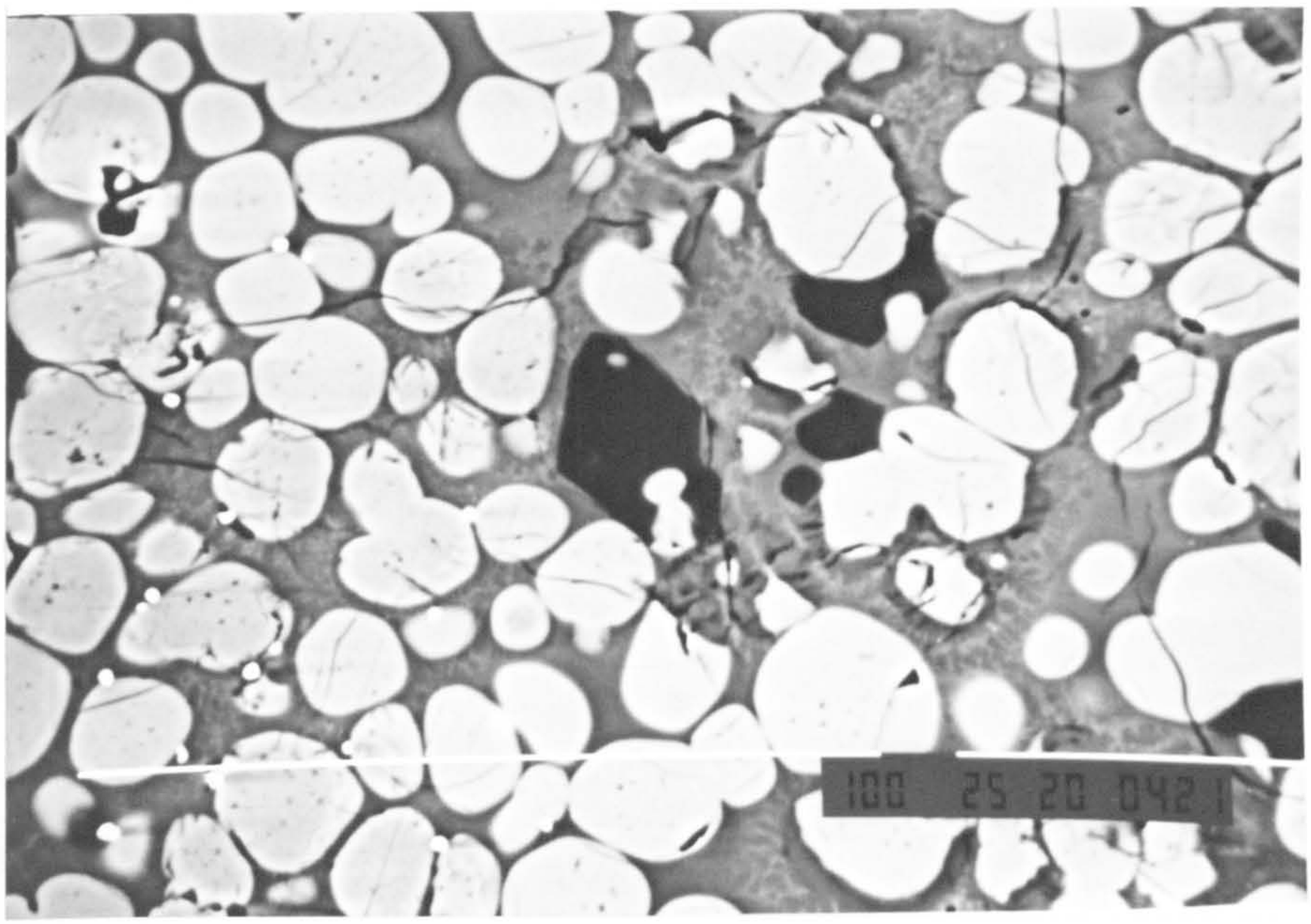

Frame 5.17 *Eye II, refractory side. 1 bar ≡ 100µm.*

Shown in the above micrograph are bright phosphate crystals ($KCaPO_4$) of approximate size 15µm in a silicate matrix. Fine dendrites of forsterite can just be distinguished between phosphate grains. The microstructure also features particles of $KAlSiO_4$ (dark grey).

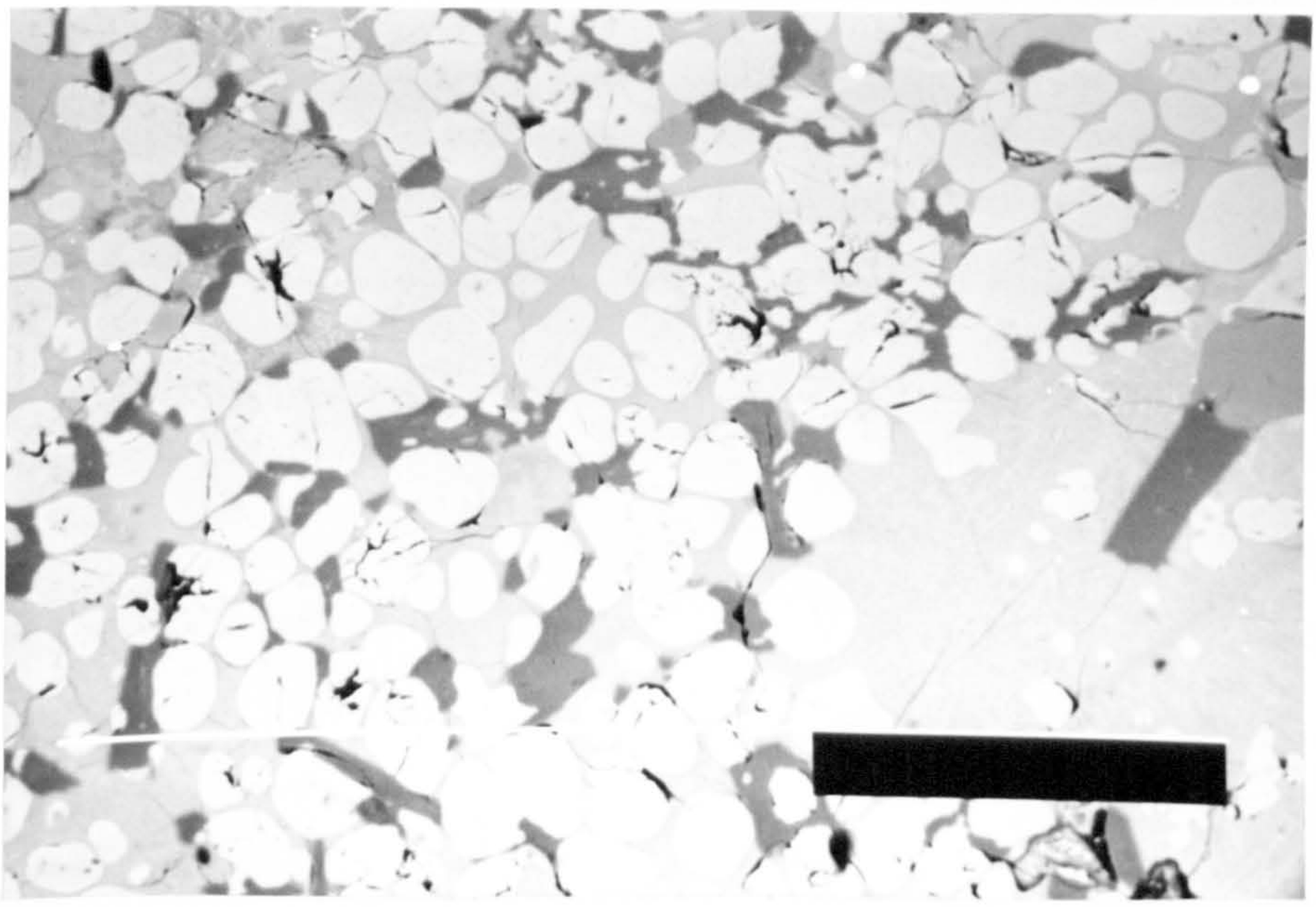

Frame 5.18 *Eye III.1 bar ≡ 100µm.*

The microstructure of the second boiler slag, Eye III, is somewhat coarser than that of Eye II with $KCaPO_4$ grain sizes averaging 25µm.

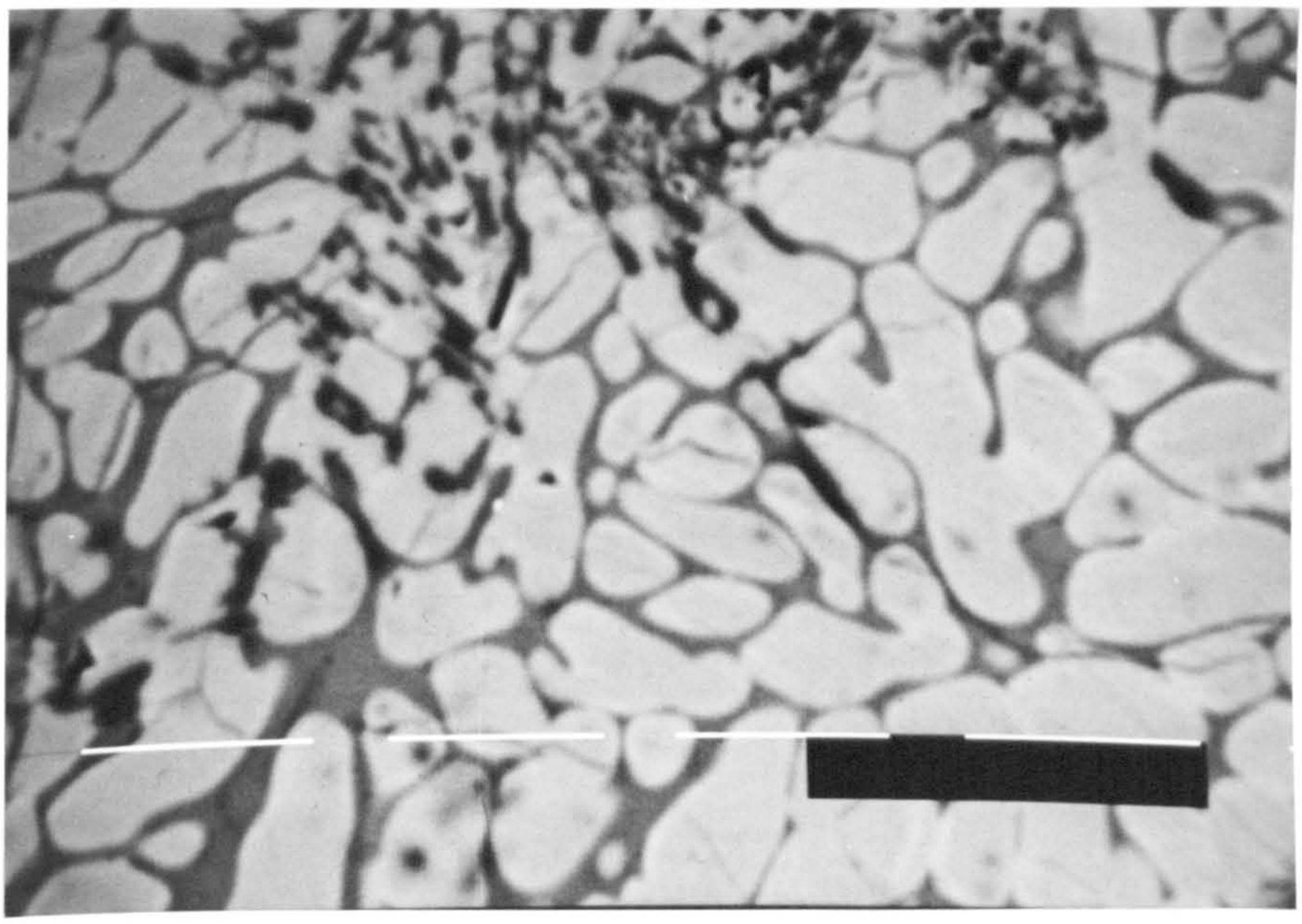

Frame 5.19 *Eye III.1 bar ≡ 100μm. BSI*

Evidence of diffusion and growth of adjacent $KCaPO_4$ crystals into one another at the expense of the matrix. The dark grey phase in the above micrograph again appears to be that of $KAlSiO_4$.

5.3 A characterisation of sewage sludge and gasification residues

5.3.1 Sewage sludge

Samples of dried and treated sewage sludge (~75% moisture) were obtained from a Paisley and a Thames Valley sewage treatment plant, respectively. The ash content of the sludges were found to be relatively high, compared to most biomass and conventional fuels, at 26wt% (Paisley) and 33wt% (Thames) on a dry basis. The chemical composition of the LTA of the sludges is presented in Table 5.13. The ash was essentially an aluminosilicate system appreciably rich in lime and phosphate. The differences in composition between the two samples is marked with the Paisley sludge containing a considerably greater quantity of silica, and less alumina. The other major difference regards the P_2O_5 content, which is notably higher in the Thames sample (15wt%) compared with the Paisley (9wt%), reflecting the increased amounts of water

softening phosphate compounds used in detergents in the South of England to combat the harder water.

Table 5.13 Chemical composition of sewage sludge LTA samples

OXIDE (wt%)	SiO_2	Al_2O_3	Fe_2O_3	CaO	MgO	K_2O	Na_2O	P_2O_5	MnO	TiO_2
Thames sewage sludge	32.1	24.7	3.0	20.0	1.9	1.4	0.4	15.3	0.0	1.3
Paisley sewage sludge	46.0	12.3	5.0	19.8	3.4	0.9	2.1	8.9	0.5	1.1

The trace element analysis of Thames Water sewage sludge was obtained from NEI using induced coupled plasma spectroscopy (ICPS). The results are presented in Table 5.14.

Table 5.14 Trace element analysis of Thames Water sludge ash

Element	Pb	Cd	Hg	V	Zn	Ni	As	Mo	Cu	Co	Cr
µg/g	211	2	< 2	12	567	32	10	5	829	3	62

X-ray diffraction analysis of the sewage sludge LTA revealed that the samples contained identical crystalline components: quartz and calcite ($CaCO_3$). The Thames LTA also consisted of kaolin ($Al_2O_3.2SiO_2.2H_2O$) and calcium phosphate ($Ca_3(PO_4)_2$) in minor proportions. The high temperature ash of the Thames sample consisted of quartz and whitlockite [Ca,Mg) $_3(PO_4)_2$]. A broad 'halo', indicative of an amorphous or glassy phase was present in both sample traces. An examination of the sewage sludge LTA in an electron microscope, featured aggregates (100-500µm in size) of nondescript morphology reflecting the treatment procedures of the precursor material to remove grit, sediment and other solid contaminants from wastewater.

The fusion behaviour of the LTA samples was studied in a hot stage microscope. The solidus and liquidus temperatures of the Paisley ash were 950°C and 1270°C respectively. The first trace of liquid formation (the solidus temperature) in the Thames LTA was observed at 880°C, with complete fusion at 1300°C. Both samples produced a viscous liquid on fusion with evidence of crystallisation on cooling.

5.3.2 Ash deposit from sewage sludge gasification

A deposit of sewage sludge ash, perhaps better described as a clinker, was provided by the Warren Springs Laboratory, Stevenage. The deposit had formed in a down draught gasifier, although the precise location was unknown. The fuel for the trials had been a 50/50 mixture of sewage sludge pellets and filtrate fines of local origin. The deposit, a dense fused mass, was dark-brown in colour and contained very few surface pores. A hammer and chisel were required to remove a suitably sized sample for analysis. The bulk chemical composition of the slag was determined by EDS; the results are shown in Table 5.15. The gasifier deposit was enriched in Fe_2O_3 (at 22 wt%) and SO_3 (12 wt%), relative to the fuel ash, and found to contain two other principal constituents: SiO_2 (21 wt%) and CaO (24 wt%), with appreciable amounts of P_2O_5 (11 wt%).

Table 5.15 Bulk chemical composition of the sewage sludge ash deposit

OXIDE (wt%)	SiO_2	Al_2O_3	Fe_2O_3	CaO	MgO	K_2O	Na_2O	P_2O_5	TiO_2	SO_3
Gasfier deposit	20.8	5.8	22.2	23.9	1.1	0.6	1.4	10.8	1.2	12.3

The nature of the crystalline constituents of the sinter was investigated using XRD. A pyroxene [pyroxyferroite, $(Fe,Ca)SiO_3$)], maghemite (γ-Fe_2O_3) and troilite (FeS) were found to be present in minor proportions, with no apparent amorphous phase. It may be inferred that the deposit was formed in a reducing atmosphere within the reactor. A complete interpretation of the diffraction pattern remained incomplete, with the other major phase or phases as yet unidentified. The fusion properties of the deposit were investigated using high temperature microscopy. The observed solidus and liquidus temperatures were found to be similar in value to those of the sludge ash, at 980°C and 1290°C respectively, with the formation of a relatively low viscosity melt.

5.3.3 Microstructural examination of the deposit

The microstructure of the deposit, examined in cross-section in an electron microscope, was entirely heterogeneous in nature, a multi-phase system with strong evidence of crystal growth from a liquid/glassy phase. The microstructure consisted of laths of a calcium phosphate, extending up to a millimetre in length, euhedral crystals of a spinel, dispersed precipitation of FeS, and acicular crystals of $(Fe,Ca)SiO_3$, with very little matrix material apparent. The presence, and morphology, of these crystals would

suggest that the deposit had been completely molten at an early stage of formation. The microstructue is shown in Frames 5.20 to 5.21.

EDS point analysis was performed, using the JSM-6400 electron microscope, in order to identify the nature of the crystalline constituents of the microstructure. The results are presented in Table 5.16.

Table 5.16 Composition of crystals of different morphology in a gasifier deposit

Wt % ELEMENT	Si	Al	Fe	Ca	P	Ti	S
Laths	-	-	5	63	32	-	-
Euhedral	-	13	76	-	-	10	-
Acicular	29	8	31	32	-	-	-
Angular	-	-	61	-	-	-	39

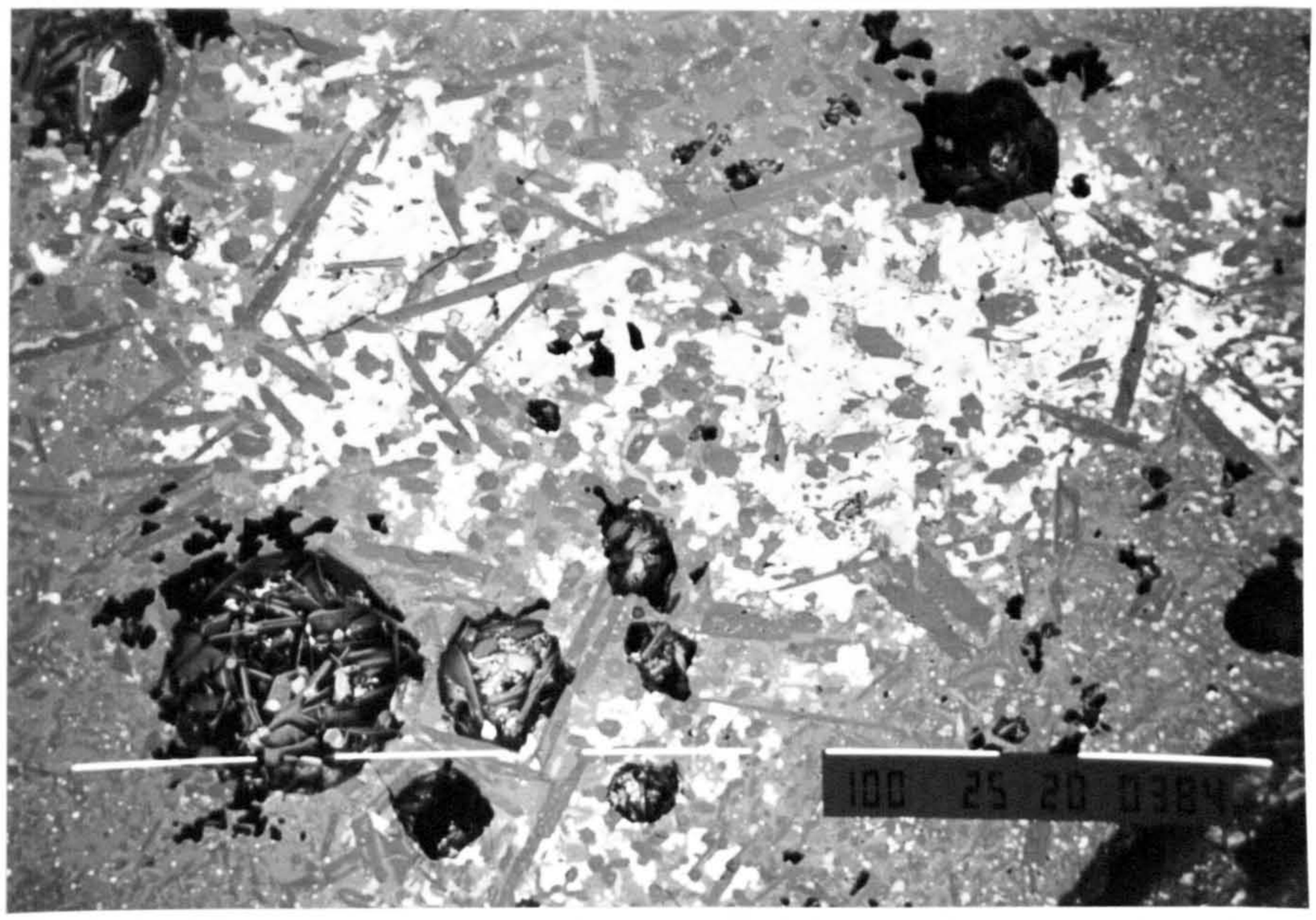

Frame 5.20 *Warren Springs gasifier deposit 1 bar ≡ 100μm. BSI*

A back scattered low magnification image of a polished cross-section through a sample of the sewage sludge gasifier deposit. A general view of the microstructure, highlighting the extensive growth of calcium phosphate laths amid bright regions of FeS within the deposit bulk and on pore surfaces.

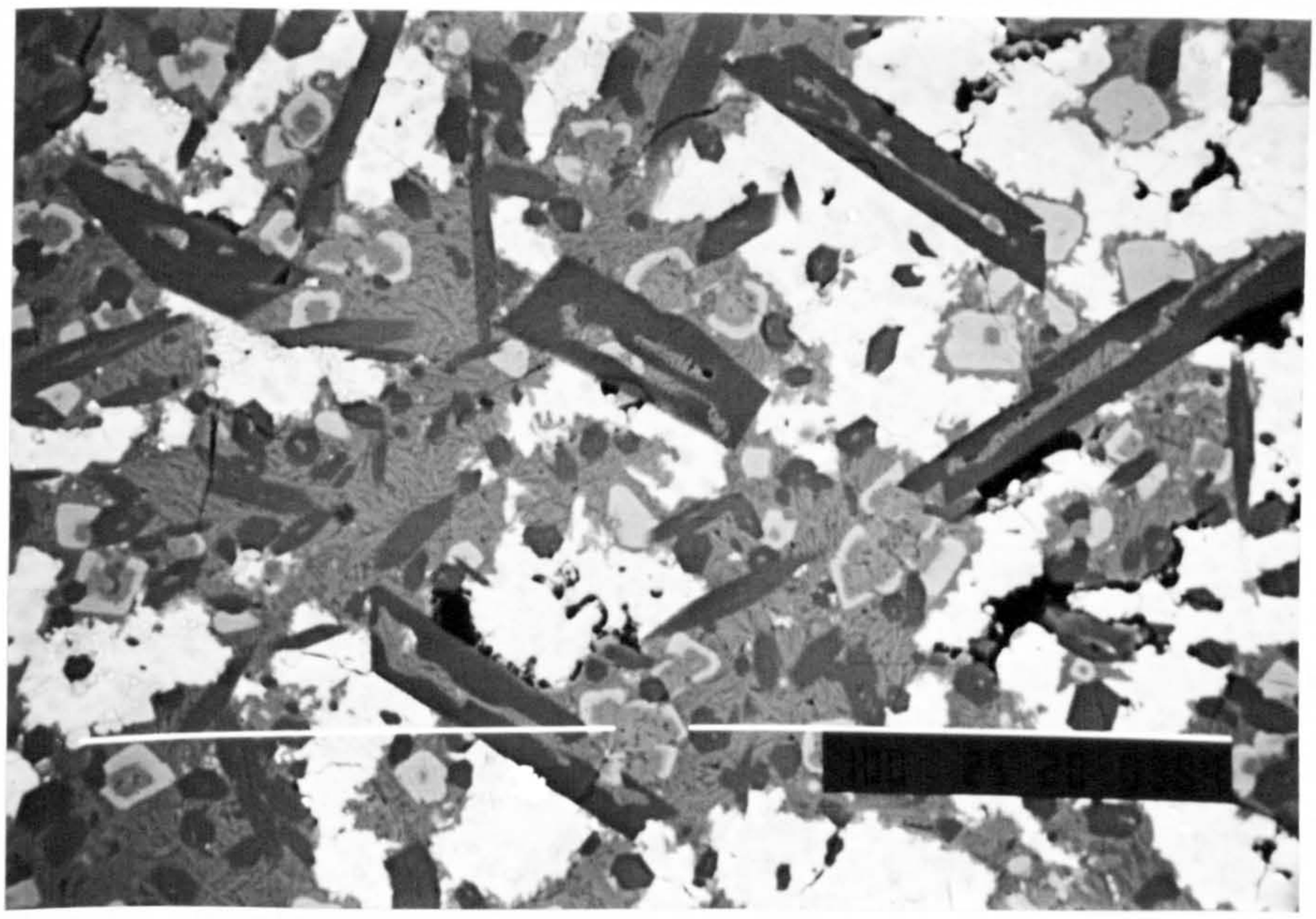

Frame 5.21 *Warren Springs gasifier deposit 1 bar ≡ 10μm. BSI*

Shown in the above micrograph are angular laths of a calcium phosphate (dark grey), an extensive precipitation of FeS (light grey), zoned euhedral crystals (pale grey, <20μm in size) of a spinel containing Fe, Al and Ti, and acicular crystals of $(Fe,Ca)SiO_3$ (mid-grey, <10μm in length).

5.4 A characterisation of short rotation coppice

The development of energy crops cultivated by short rotation coppice techniques is now actively encouraged in Britain and is a beneficiary of the NFFO mechanism for subsidising such activities.

5.4.1 Poplar and willow coppice from the Silsoe Research Institute

Poplar and willow coppice, colloquially termed 'sticks', of four years growth were obtained from the Silsoe Research Institute (SRI), Bedfordshire. The coppice had been planted in the spring of 1988. The poplar sticks were selected from an outside stockpile which had been exposed for approximately six months after the winter harvest. The willow had been harvested more recently; leaves and catkins were present on the branches. The sticks were sampled by taking sections along the main stem, including separate fractions of bark, sapwood and heartwood. The objective of study was to ascertain the distribution of inorganic constituents in sections and tissue areas of the as-harvested coppice, as it may have some bearance on the variation in fuel quality and method of sampling and comminution employed.

The sticks, approximately 4m in length, were divided into nine categories of sample: twigs and leaves (from the top and base of the stem), main stem (sections of the top, bottom and mid-stem), bark (from the mid-section and the base), sapwood and heartwood (mid-stem). The letters A to E were allocated to each section of the stick as shown in Figure 4.1 of Chapter Four. The sample codes C1 to C4 were applied to the major tissues of the stem.

5.4.2 Characterisation of poplar coppice from SRI

The moisture and ash contents (determined by a high temperature ashing procedure to remove volatile and organic matter) of each section of the main stem, and the major tissues (bark, sapwood, and heartwood) of poplar coppice are shown in Tables 5.17 and 5.18 respectively, in addition to the bulk ash (LTA) composition of the sectioned coppice. The bulk moisture contents of the sectioned stem were found to be fairly constant throughout. However, a trend towards decreasing ash content from top to bottom of the main stem was observed. The twigs and topmost section of the main stem possessed greater ash contents, at 3.6 and 2wt% respectively, than the mid- (1.3wt%)

and base-stem (1wt%) bulk samples. The samples differed with respect to the bark-sapwood ratios, which were found to decrease towards the base of the stem. The heartwood, physiologically dead tissue, was found to occupy less than 5% of the main stem radius.

The bulk chemical compositions of the sectioned poplar stick contained four principal constituents: CaO, K_2O, P_2O_5, and SO_3, with an appreciable quantity of MgO (averaging 5wt%). The notable variations in bulk ash composition from the top to bottom fractions of the poplar sticks were a decrease in CaO content from 46wt% at the top to 31wt% at the bottom, with a subsequent enrichment in K_2O (20-25wt%) and P_2O_5 (12-20wt%) concentrations.

Table 5.17 Chemical composition, moisture and ash contents of sectioned poplar coppice cultivated at the SRI

OXIDE (wt%)	TOP		MID-STEM	BOTTOM (unbranched)
	A main stem	**B** twigs	**C** main stem	**D** main stem
SiO_2	0.8	1.2	1.5	1.8
Al_2O_3	0.1	0.3	0.5	0.4
Fe_2O_3	0.4	1.1	0.5	0.6
CaO	46.0	52.5	39.3	31.2
MgO	5.4	5.8	5.0	4.8
K_2O	19.5	15.0	20.1	24.8
Na_2O	0.9	1.2	1.2	1.1
P_2O_5	11.7	10.2	12.8	20.1
MnO	0.1	0.4	0.2	0.1
TiO_2	0.1	0.1	0.1	0.2
SO_3	15.1	12.2	18.8	14.8
Moisture (%)	*45.0*	*42.7*	*47.0*	*45.6*
Ash content, d.a.b. (wt%)	*2.1*	*3.6*	*1.3*	*1.0*

The moisture contents of the major tissues of the mid-stem fraction of poplar were found to vary considerably from the bark (at around 60%) to the adjacent sapwood

(40%) and central heartwood (35%). The variations in ash contents across the main stem were more pronounced. The bark was considerably richer in inorganic material than the corresponding wood, with an ash content (4wt%) approximately four times that of the sapwood (0.6wt%) and heartwood (1wt%). Such observations are consistent with the knowledge that the phloem (inner bark) of the plant vascular system provides a mode of transport for photosynthetic products as well as principal mineral nutrients.[120] The chemical variations across the stem were striking, with the bark of the mid-section containing 59wt% lime in marked contrast to the adjacent sapwood (22wt%) and heartwood (24wt%). Conversely, K_2O, P_2O_5 and SO_3 concentrations increased from bark to sapwood.

Table 5.18 Chemical composition of major tissues of poplar coppice

OXIDE (wt%)	MID-STEM				BOTTOM
	C1 bark	**C2** sapwood beneath bark	**C3** heartwood	**C4** bulk sapwood	**D1** bark
SiO_2	2.0	1.1	0.8	0.9	1.2
Al_2O_3	1.9	0.3	0.2	0.2	0.3
Fe_2O_3	1.0	0.3	0.3	0.5	1.1
CaO	57.4	22.2	23.9	26.1	52.3
MgO	7.0	4.2	6.1	5.6	4.8
K_2O	7.7	28.3	24.8	20.8	13.7
Na_2O	1.3	1.0	0.9	0.8	1.2
P_2O_5	15.3	18.8	17.7	17.1	10.1
MnO	0.2	0.1	0.1	0.2	0.2
TiO_2	0.2	0.1	0.0	0.1	0.1
SO_3	6.1	23.6	25.2	28.0	14.9
Moisture (%)	*58.7*	*38.2*	*32.8*	*35.2*	*62.0*
Ash content, d.a.b. (wt%)	*3.9*	*0.6*	*1.0*	*0.6*	*3.8*

X-ray diffraction analysis of the LTA of the sectioned poplar coppice revealed the nature of the inorganic species present in the wood. The principal crystalline phases present in the bark alone were identified as calcium oxalate (CaC_2O_4) and a phosphate

of potassium ($K_2PO_3NH_2$). These phases were also present in the twigs, reflecting the high proportion of bark relative to sapwood. No trace of amorphous material was apparent in the diffraction pattern. Syngenite [$K_2Ca(SO_4)_2.H_2O$] and calcite ($CaCO_3$) were found to be present in the sapwood and heartwood, in addition to amorphous material, signified by a broad 'halo' in the diffraction pattern.

Table 5.19 Crystalline phases present in poplar LTA fractions, identified by XRD

SAMPLE	CRYSTALLINE PHASE		
	major	**minor**	**trace**
Bark	CaC_2O_4 *(calcium oxalate)*	$K_2PO_3NH_2$ *(potassium-amidophosphate)*	
Twigs	CaC_2O_4 *(calcium oxalate)*	$K_2PO_3NH_2$ *(potassium-amidophosphate)*	
Sapwood beneath bark	CaC_2O_4 *(calcium oxalate)*	$K_2PO_3NH_2$ *(potassium-amidophosphate)*	$CaCO_3$ *(calcite)*
Sapwood	$CaCO_3$ *(calcite)*	$(K_2Ca(SO_4)_2.H_2O$ *(syngenite)*	
Heartwood	$(K_2Ca(SO_4)_2.H_2O$ *(syngenite)*	$CaCO_3$ *(calcite)*	

A microstructural (SEM) examination of the woody tissues revealed the presence of calcium oxalate crystals in the bark. Two distinct types of calcium oxalate crystal were identified, those of multifaceted 'rosette' and rhomboidal crystal morphologies (Frames 5.22 and 5.23). The crystalline morphology may have been influenced by the presence of certain ions in solution, which can have a profound effect on the morphology of growth. Indeed an EDS point analysis of the crystals revealed that a trace of sodium (2wt%) was present in the calcium oxalate crystals of rosette-type morphology, while the rhomboidal calcium oxalate crystals were found to contain approximately 2wt% potassium. Crystals were not observed in the heartwood and bulk sapwood samples. The growth kinetics, composition and habit of crystals precipitated from solution can be altered by physical conditions, and by the growth medium which may contain other solutes or suspended material. The conditions which lead to crystal nucleation and growth in plant cells, however, are not completely understood.

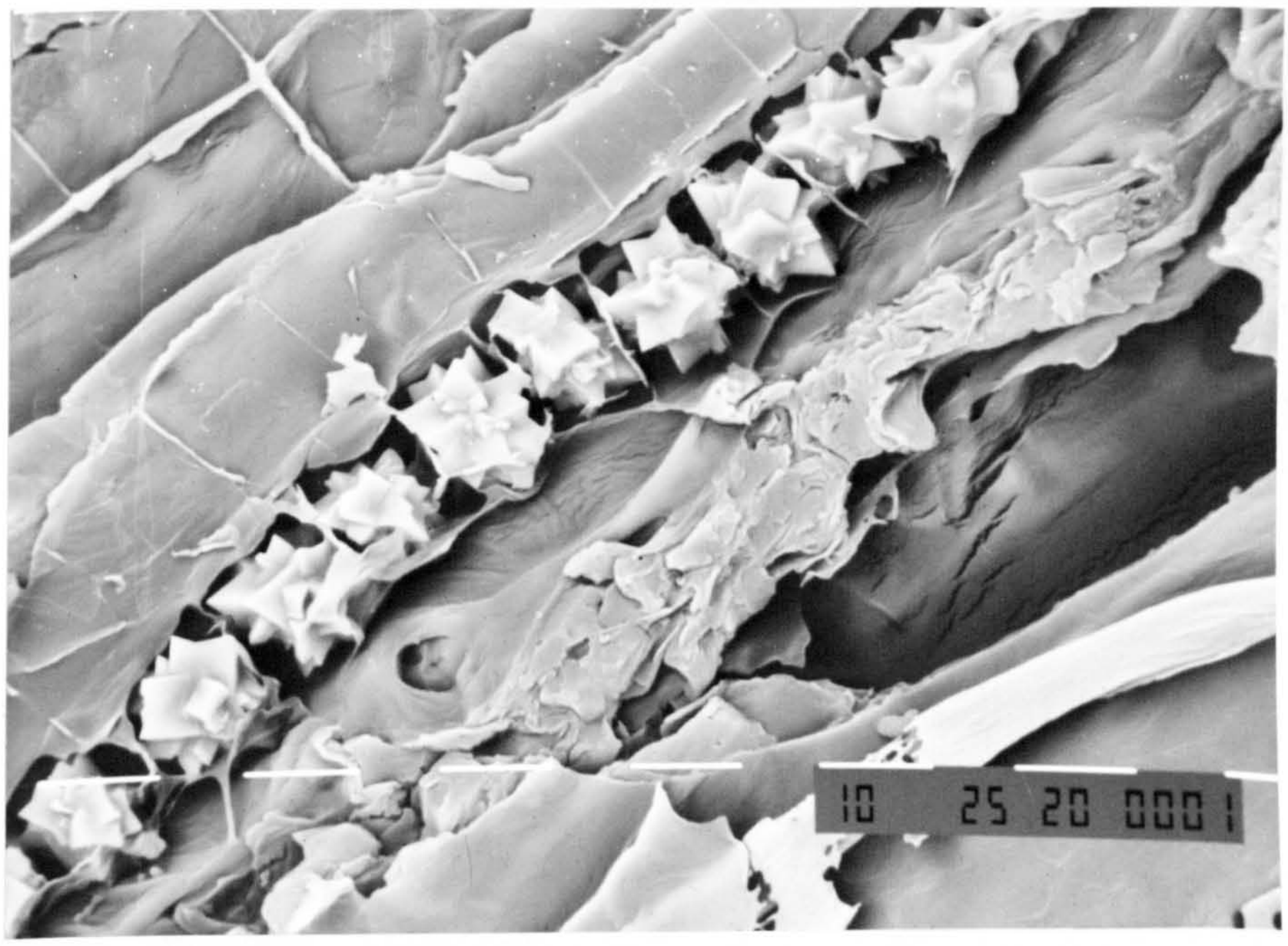

Frame 5.22 *Poplar bark C1. 1 bar ≡ 10μm. BSI.*

A back scattered image of an inner layer of poplar bark. Shown above is an array of multi-faceted calcium oxalate crystals (~10μm in size) nestled in a ribbon of vertical parenchyma cells that run longitudinal to the stem length. The apparent morphology suggests that these crystals were precipitated from solution.

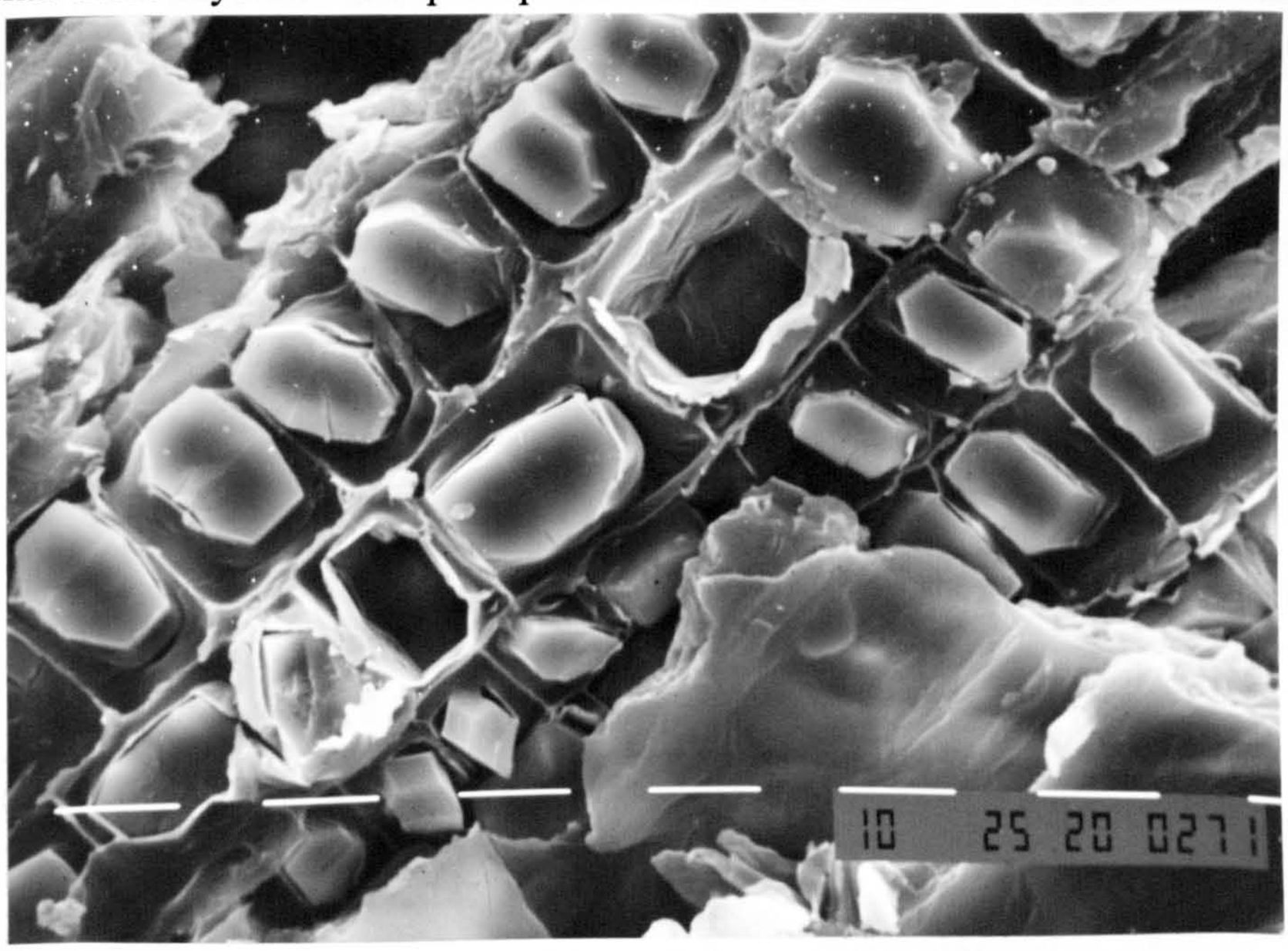

Frame 5.23 *Poplar bark C1. 1bar ≡ 10μm. SEI.*

Shown in the above micrograph are polyhedric calcium oxalate crystals (~10μm in size) in enchambered parenchyma cells. There appears to be one crystal per cell, each secured within a membrane or thin layer of wall material.

5.4.3 Willow coppice from SRI

The willow sticks were subjected to similar methods of sampling and characterisation as the poplar. The moisture, ash and chemical compositions of the stem fractions are presented in Table 5.20. The bulk moisture content of the willow stem averaged 29%, less than that of the poplar. No apparent trend was observed in the ash contents of the sectioned stem which remained approximately 1wt% throughout the stem length. The twigs and leaves/catkins were found to contain the most ash at 3.5 and 2.4wt% respectively.

Table 5.20. Chemical composition, moisture and ash contents of sectioned willow coppice cultivated at the SRI

Oxide (wt%)	TOP			MID-STEM	BOTTOM	
	A main stem	B leaves, catkins	B twigs	C main stem	D main stem	E twigs, leaves
SiO_2	1.5	2.9	3.9	9.3	3.1	2.3
Al_2O_3	0.3	0.2	0.6	0.4	0.3	0.6
Fe_2O_3	0.4	0.6	0.9	0.5	0.4	0.7
CaO	55.6	22.4	47.9	51.5	68.9	65.9
MgO	2.4	4.0	3.5	2.6	2.5	1.7
K_2O	10.5	21.8	10.1	14.6	8.5	6.7
Na_2O	1.3	2.3	3.4	1.2	0.9	1.2
P_2O_5	10.2	24.6	15.3	21.4	9.5	9.0
MnO	0.2	3.3	0.3	0.2	0.2	0.2
TiO_2	0.2	0.1	0.1	0.0	0.0	0.2
SO_3	17.4	17.9	14.0	7.3	5.7	11.6
Moisture (%)	*30.4*	*20.1*	*14.6*	*27.9*	*29.9*	*23.7*
Ash content, d.a.b. (wt%)	*1.1*	*2.4*	*3.5*	*0.9*	*1.3*	*3.8*

The LTA of various parts of the coppice contained four dominant oxides in varying proportions: CaO (51-69wt%), K_2O (8-15wt%), P_2O_5 (9-25wt%) and SO_3 (6-17wt%). Again, in a similar trend to poplar, the lime content of the ash was observed to increase towards the base of the stem from 56wt% CaO at the top to 69wt% at the bottom, at the

expense of K_2O and SO_3. The leaves and catkins were found to be enriched in K_2O (22wt%), P_2O_5 (25wt%) and SO_3 (18wt%), with an appreciable concentration of MnO (3.3wt%). The leaves of a plant are the most favourable sites for the precipitation of inorganic material. It would thus appear that calcium ions have a more complex function than nutrition alone.

The moisture and ash contents and chemical compositions of the major tissues (bark, sapwood and heartwood) of the mid-stem fraction are shown in Table 5.21. The moisture content was found to decrease from the bark (38%) to the heartwood (27%). The ash contents of the tissues were found to range from 5wt% for the bark, to 0.7wt% for the heartwood and a mere 0.2wt% for the sapwood.

Table 5.21 Chemical composition of the major tissues of willow coppice

Oxide (wt%)	**MID-STEM**				**BOTTOM**
	C1 bark	C2 sapwood beneath bark	C3 heartwood	C4 bulk sapwood	D1 bark
SiO_2	1.6	7.8	6.0	7.8	5.6
Al_2O_3	0.2	1.3	0.3	0.3	0.4
Fe_2O_3	1.1	0.8	0.7	0.7	0.4
CaO	75.7	34.3	31.7	32.2	78.6
MgO	1.4	3.8	5.6	4.6	1.4
K_2O	3.9	18.5	24.3	24.7	3.9
Na_2O	1.1	1.6	1.7	1.8	0.6
P_2O_5	4.8	21.0	19.5	17.8	3.7
MnO	0.4	0.3	0.2	0.1	0.2
TiO_2	0.3	0.1	0.1	0.2	0.0
SO_3	9.5	10.4	9.9	9.9	5.2
Moisture (%)	*37.7*	*29.1*	*27.4*	*29.6*	*34.4*
Ash content, d.a.b. (wt%)	*5.0*	*0.5*	*0.7*	*0.2*	*5.5*

Willow bark was found to be rich in lime, containing an outstanding 76wt% CaO. The lime content of the ash was found to decrease abruptly from the bark to the

neighbouring sapwood (34wt% CaO) and heartwood (32wt% CaO). SiO_2 and P_2O_5 were found to be most abundant in the sapwood beneath the bark, at 8wt% and 21wt% respectively. The bulk sapwood was enriched in potash, which comprised 25wt% of the ash.

The nature of the inorganic material in the major tissues of the willow coppice was determined by X-ray diffraction. Calcium oxalate was identified as the major phase in the bark and the sapwood. The interpretation of the diffraction pattern presented numerous difficulties, with some crystalline phases as yet unidentified. An SEM examination of the woody tissues revealed two types of calcium oxalate crystal morphology to co-exist in the bark, as previously encountered in poplar. Multifaceted rosette-type calcium oxalate crystals were observed in the outer strips of bark, and crystals of polyhedric morphology were found to be present in the inner layers of bark. The multifaceted calcium oxalate crystals (shown in Frame 5.23) appeared to lack an ordered arrangement as observed in the poplar bark; instead the crystals were found to occupy random parenchyma cells. The polyhedric crystals of calcium oxalate were far more abundant than those of multifaceted morphology, in marked contrast to poplar bark. The polyhedric crystals formed densely packed arrays, as illustrated in Frame 5.24.

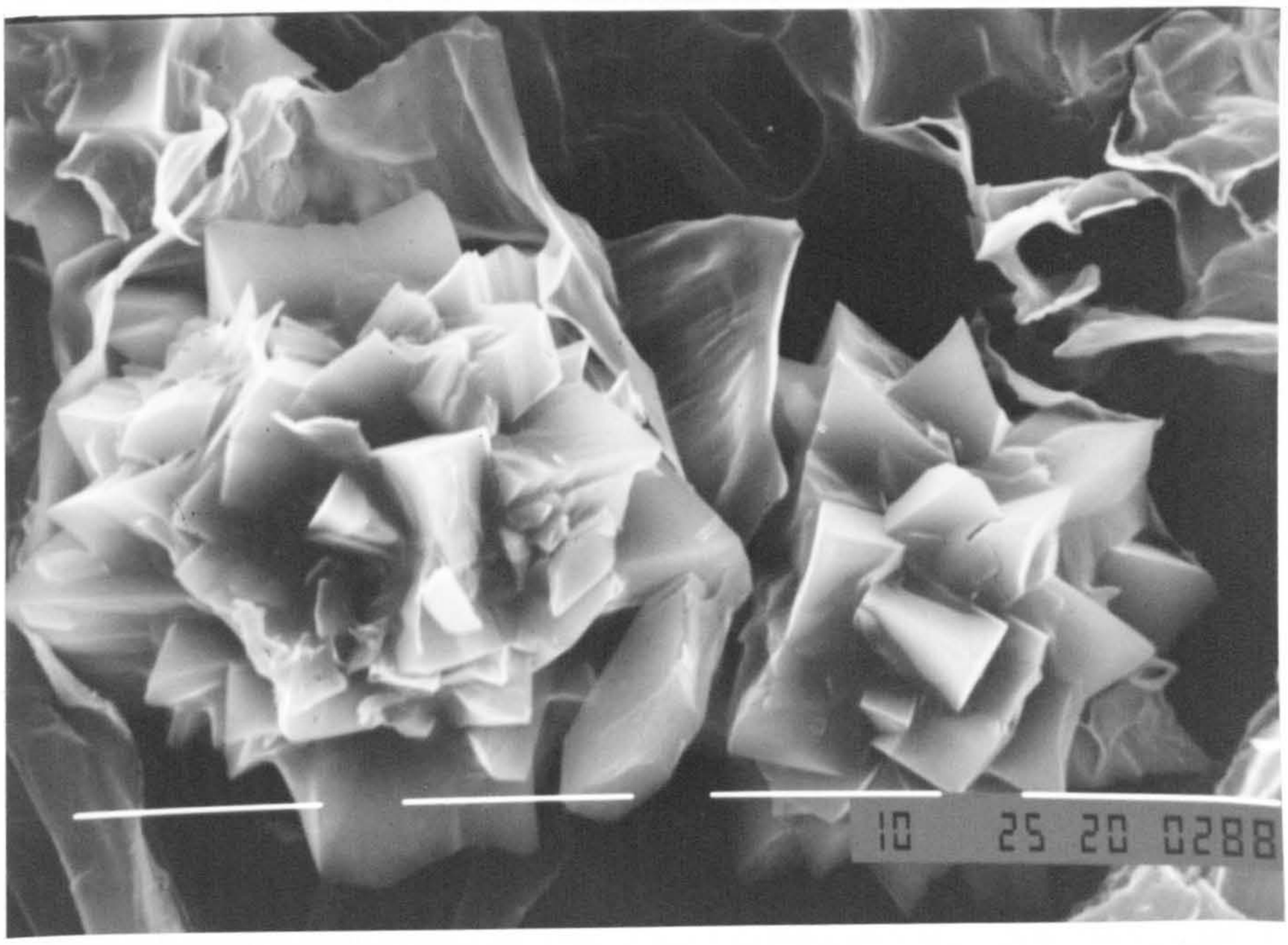

Frame 5.23 *Willow bark. 1 bar ≡ 10μm. SEI.*

Randomly distributed multifaceted calcium oxalate crystals (~25μm in size) in the outer layers of willow bark.

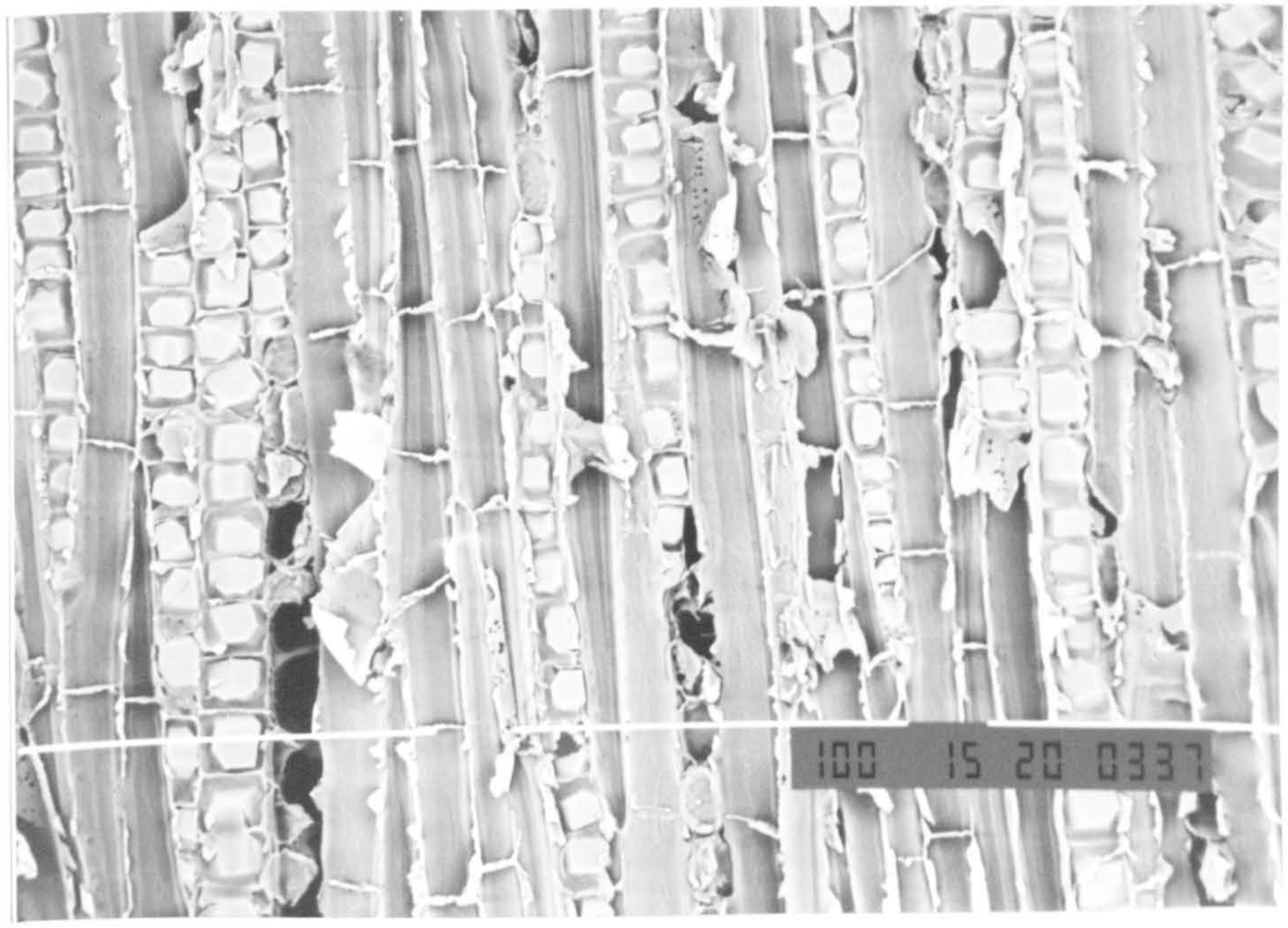

Frame 5.24 *Willow bark. 1 bar ≡ 100μm. BEI.*

Columns of rhomboidal calcium oxalate crystals (~10μm) occupying vertical parenchyma cells of the inner bark.

5.4.4 Poplar and willow coppice from the Long Ashton Research Station

Willow and poplar chippings, harvested at various stages of maturity in the range of one to four years growth, were obtained from the Long Ashton Research Station, Bristol. The moisture and ash contents of the chippings have been determined, in addition to the bulk chemical composition of the low temperature ash. The results are presented in Table 5.22. The moisture contents of samples I (mixed poplar and willow of one years growth) and II (two year old willow) were found to be a mere 6 % indicating that the samples had been dried. Moisture contents of 42% for three year old willow and 56% for mixed three and four year poplar were perhaps closer to their post-harvest values.

Table 5.22 Bulk ash compositions of poplar and willow coppice cultivated at the Long Ashton Research Station, Bristol

OXIDE (wt%)	**I** *(mixed 1yr old poplar and willow)*	**II** *(2yr old willow)*	**III** *(3yr old willow)*	**IV** *(mixed 3 and 4yr old poplar)*
SiO_2	9.7	18.5	4.8	4.3
Al_2O_3	1.8	2.3	0.4	0.5
Fe_2O_3	1.0	1.3	0.5	0.8
CaO	33.0	35.0	32.4	45.7
MgO	4.7	4.0	8.0	5.5
K_2O	19.0	16.3	20.0	14.1
Na_2O	1.9	0.9	4.0	1.6
P_2O_5	14.5	12.6	16.4	13.1
MnO	0.3	0.3	0.2	0.2
TiO_2	0.3	0.2	0.2	0.2
SO_3	13.6	8.6	13.2	13.9
Moisture (%)	*6.1*	*6.4*	*42.2*	*56.0*
Ash content, d.a.b. (wt%)	*2.2*	*1.9*	*1.5*	*1.8*

The bulk ash contents were observed to decrease with maturity, from 2.2wt% to 1.5wt% over a three year growth period, reflecting the decrease in bark-to-sapwood ratio in the main stem. The predominant components of the LTA of both poplar and willow of one to four years growth were found to be CaO, K_2O, P_2O_5 and SO_3, with appreciable

amounts of SiO_2 and MgO. Willow coppice of two years growth was substantially richer in silica at 18.5wt% than the slightly more mature three year old willow (4.8wt% SiO_2). The alumina content was also observed to decrease considerably with increase in age from 2.4wt% to a mere 0.4wt% Al_2O_3. Other notable differences in ash composition between two and three year old willow include an increase in MgO, K_2O, P_2O_5 and SO_3 concentrations with increase in age. The poplar coppice cultivated at Long Ashton was found to be considerably richer in CaO than the willow species.

The nature of the inorganic material in the Long Ashton poplar and willow species was determined using an X-ray diffraction technique. The results are presented in Table 5.23. The principal crystalline constituents of willow of two years growth were identified as quartz (the major phase), calcium oxalate (CaC_2O_4) and a potassium phosphate ($K_2PO_3NH_2$), minor components. The silica generally deposited within plant tissues has been found by a variety of authors to be amorphous, often in the form of granulated lumps or as a lining of the cell walls.[23,118] In the case of young willow, quartz may be in part responsible for an increased strength and weather resistance. Quartz becomes a minor component of three year old willow, with calcium oxalate the major phase. For the species of poplar cultivated at Long Ashton, calcium oxalate was identified as the major crystalline phase, and potassium-amidophosphate ($K_2PO_3NH_2$) the minor phase.

Table 5.23 Crystalline phases present in poplar and willow species (Long Ashton samples)

SAMPLE	CRYSTALLINE PHASE		
	major	**minor**	**trace**
II *2 yr willow*	SiO_2 *(quartz)*	CaC_2O_4 *(calcium oxalate)*	$K_2PO_3NH_2$ *(potassium-amidophosphate)*
III *3 yr willow*	CaC_2O_4 *(calcium oxalate)*	SiO_2 *(quartz)*	
IV *3 & 4 yr willow*	CaC_2O_4 *(calcium oxalate)*	$K_2PO_3NH_2$ *(potassium-amidophosphate)*	

5.4.5 A comparison of poplar and willow species cultivated at different sites

Unlike the major cell wall components such as cellulose and lignin, the nature and amount of the inorganic material has been reported to vary to a great extent with the environmental conditions under which the wood is cultivated. The variability of poplar and willow coppice in terms of a fuel and ash residue was investigated by conducting a comparative characterisation of the same species grown at different sites.

Poplar and willow chippings were obtained from the Silsoe Research Institute, Bedfordshire. The willow coppice had been cultivated on-site at Silsoe, whereas the poplar had been grown at Swanbourne, Buckinghamshire (an out-post of the SRI). The bulk chemical compositions are given in Table 5.24, along with the Long Ashton poplar and willow ash compositions for comparison. The willow grown at Silsoe (Bedfordshire) was found to be remarkably rich in lime at 64wt%, far richer in lime than the corresponding willow of Long Ashton (Bristol), which contained 32wt% CaO. Consequently the Long Ashton willow contained greater proportions of K_2O, P_2O_5 and SO_3. Another notable difference in ash chemistry between the willow species from Brisol and Bedfordshire was the SiO_2 content, which was appreciably higher in the Long Ashton willow grown at Bristol. The ash fusion behaviour of the willow ashes was expected to be distinctly different on account of the variation in ash chemistry.

The chemical compositions of the poplar coppice LTA samples from Swanbourne and Bristol were found to be similar. The notable differences in composition were the K_2O and SO_3 concentrations. The poplar coppice from Long Ashton, Bristol, was richer in SO_3 than the Swanbourne counterpart. Consequently the Swanbourne poplar contained a greater proportion of K_2O.

The differences in ash composition would seem to reflect the different soil conditions of the two sites and this would be a major variable in fuel quality for potential energy recovery processes.

Table 5.24 Bulk ash compositions of poplar and willow chippings cultivated in different regions of Britain

OXIDE (wt%)	POPLAR *Bedfordshire*	POPLAR *Bristol*	WILLOW *Swanbourne*	WILLOW *Bristol*
SiO_2	6.0	4.3	1.6	4.8
Al_2O_3	1.4	0.5	0.4	0.4
Fe_2O_3	1.0	0.8	1.0	0.5
CaO	43.6	45.7	63.5	32.4
MgO	5.4	5.5	3.3	8.0
K_2O	20.5	14.1	10.2	21.0
Na_2O	1.9	1.6	1.2	4.0
P_2O_5	12.2	13.1	10.8	13.4
MnO	0.1	0.2	0.3	0.2
TiO_2	0.2	0.2	0.1	0.2
SO_3	7.7	13.9	7.7	13.2
Moisture (%)	*47.7*	*56.0*	*29.7*	*42.2*
Ash content, d.a.b. (wt%)	*1.3*	*1.8*	*1.4*	*1.5*

The ash fusion characteristics of the coppice chippings from the SRI and Long Ashton were investigated using high temperature microscopy. The observations have been recorded in Table 5.25. As anticipated, from a knowledge of the ash chemistry, the fusion behaviour of the Silsoe and Long Ashton ashes was observed to be very different. The willow LTA from the SRI displayed high solidus and liquidus temperatures of 950°C and 1500°C respectively, indicating the temperatures at which the first liquid phase was detected and the temperature for complete fusion. In contrast, the willow from Long Ashton (Bristol) showed less favourable fusion properties; a liquid phase was observed at 600°C (the solidus) and the ash was completely molten by 1380°C. The much higher solidus and liquidus temperatures of the Silsoe sample appeared to reflect the increased amount of lime (64wt%), a refractory component at this concentration, contained in the ash.

Table 5.25 Fusion behaviour of the poplar and willow LTA from different sources

SAMPLE	TEMPERATURE (+/-10°C)			
	Solidus	First visible liquid *(30-40% liquid)*	Appreciable softening *(70-80% liquid)*	Liquidus
Willow (Silsoe,Bedfordshire)	950	1420	1490	1500
Willow (Long Ashton III, Bristol)	600	1000	1260	1380
Poplar (Silsoe, Swanbourne)	770	850	1400	1490
Poplar (Long Ashton IV, Bristol)	800	1010	1350	1440
Poplar sapwood (Silsoe, Swanbourne)	680	800	900	1380
Poplar bark (Silsoe, Swanbourne)	900	1150	1480	1500

The poplar species from Swanbourne (SRI) and Bristol (Long Ashton) were found to exhibit rather similar ash fusion properties with solidus temperatures of 770°C and 800°C, and liquidus temperatures of 1490°C and 1440°C, respectively. The poplar bark alone, being considerably richer in lime than the neighbouring sapwood, was observed to display comparable ash fusion properties to the lime-rich willow ash from Silsoe, i.e. high solidus (900°C) and liquidus (1500°C) temperatures. The sapwood LTA was found to exhibit much lower solidus (680°C) and liquidus (1380°C) temperatures as a consequence of the decrease in lime content from bark to sapwood and the subsequent enrichment in K_2O.

5.4.6 Cyclone ashes from TPS, Sweden

Two samples of cyclone ash, labelled 0530 and 1220, from a gasification trial of willow were obtained from Termiskar Processor AB (TPS), Sweden. The ashes consisted of a fine black dust, with a mean particle size of 15-20μm, as determined by a Malvern particle size analysis. The sample of cyclone material labelled 0530 was found to contain 46.5wt% ash, while the ash content of sample 1220 was 58.6wt%. The chemical compositions of the ashes, presented in Table 5.26, were seen to consist primarily of CaO and MgO. Since MgO was not found to be a major constituent of

willow ash, the MgO may have originated from the use of dolomite [$CaMg(CO_3)_2$] as a tar cracking catalyst.

Table 5.26 Bulk chemical composition of the cyclone ashes (TPS Termiskar Processor)

OXIDE (wt%)	SiO_2	Al_2O_3	Fe_2O_3	CaO	MgO	K_2O	Na_2O	P_2O_5	MnO	SO_3
Sample 0550	5.2	1.6	1.4	55.6	29.2	1.8	0.3	2.6	0.9	0.8
Sample 1220	4.0	1.4	0.8	53.8	29.5	2.0	0.6	4.9	0.6	1.5

A microstructural examination of a polished cross-section of the cyclone ashes showed no sign of particle-particle interaction which might have indicated incipient fusion or sintering of the ash. This was a most encouraging observation.

5.5 A characterisation of RDF, chestnut and gasification residues from Power Gasifiers International

Fuel, deposits and gasifier residues were obtained from Power Gasifiers International, Gloucester. The gasifier had been operating on a mixed feed of chestnut chips and RDF pellets (an ETSU/DTI funded project), with the aim of establishing the maximum amount of RDF which could be incorporated in the feed before operational difficulties were encountered. It was reported that up to 50% RDF could be added to the chestnut before serious problems arose.

5.5.1 Chestnut and RDF

Chestnut chippings had originated from a local forest where traditional coppicing techniques had been employed for more than 200 years to provide fuel and construction material for the neighbouring community. In comparison with poplar and willow chippings from Silsoe and Long Ashton, the chestnut had reached a more advanced stage of maturity with increased sapwood/heartwood-to-bark ratios.

Samples of RDF from two separate sources, Byker and the Isle of Wight, were supplied by Mitsui Babcock Energy Ltd. The Byker RDF was in the form of densified pellets, 3-5cm in length and 2-2.5cm in thickness. The Isle of Wight refuse had been processed to a much finer material which had the consistency of wool or fluff, reflecting the

cellulosic content of the fuel. Developments in the UK have largely focused on the production of pelletised RDF aimed at the industrial boiler market. Although the composition of RDF is expected to differ with respect to the location and season of collection, the characterisation of the RDF samples supplied by Babcock accompanies this section to serve as a general guide to the properties and high temperature behaviour of RDF residues.

The moisture and ash contents of the chestnut chunks were found to be 13% and 0.46wt% (dab), respectively. In contrast, the refuse derived fuels possessed significantly higher ash contents; the RDF pellets of Byker origin contained 10.9wt% ash (4.8% moisture), and the Isle of Wight RDF 'fluff' contained 12.6wt% ash (4.8% moisture). Bulk chemical compositions of the chestnut and RDF LTAs are given in Table 5.27. The ash chemistry of chestnut was found to be rather different to that of the coppice willow and poplar samples of this study. The chestnut ash was found to be abundant in SO_3, at 33wt%, yet contained relatively low concentrations of CaO (22wt%) and P_2O_5 (4wt%) in contrast to the poplar and willow ashes. Perhaps the most striking feature of the chemical composition was the considerable proportion of MnO (7.5wt%) in the chestnut ash, most unlike that previously encountered in the coppice woods in which MnO was found in only trace quantities (<0.5wt%). The chestnut ash was red-brown in colour on account of the considerable transition metal ion content.

The bulk chemical compositions of the RDF LTA samples contained three dominant oxide components: SiO_2, Al_2O_3 and CaO. The ash compositions of the Byker and Isle of Wight RDF were found to be similar with respect to all constituents, the Byker ash being slightly richer in SiO_2 and Al_2O_3, at the expense of CaO, than the Isle of Wight counterpart. Both RDF ashes also contained appreciable quantities of TiO_2, at approximately 3wt%. The presence of such constituents in the ash was thought to have been derived principally from inorganic fillers used in paper and plastic products. Thus the assumption was confirmed by X-ray diffraction of the LTAs, which revealed the presence of the following phases common to both Byker and Isle of Wight samples: quartz (SiO_2), kaolinite ($Al_2O_3.2SiO_2.2H_2O$), calcite ($CaCO_3$) and rutile (TiO_2). All these materials are used extensively as fillers in paper, plastics, rubbers, and paints.

Table 5.27 Bulk chemical composition of the chestnut and RDF ashes (LTA)

OXIDE (wt%)	SiO_2	Al_2O_3	Fe_2O_3	CaO	MgO	K_2O	Na_2O	P_2O_5	MnO	TiO_2	SO_3
Chestnut	5.1	1.3	1.0	21.8	5.1	17.7	3.1	3.9	7.5	0.4	33.1
Byker RDF	43.2	31.1	2.4	15.4	2.5	1.6	2.6	1.0	0.0	2.8	0.0
Isle of Wight RDF	40.7	23.6	2.3	23.2	1.8	2.0	2.7	0.6	0.0	3.1	0.0

The knowledge that RDF was essentially a cellulose-based material, containing 80-90wt% paper and paperboard, led the author to briefly investigate the nature of a variety of paper products during the initial stages of the project when the supply of other samples was wanting. The ash contents of tissue and newsprint were found to be negligible at 0.4 and 0.8wt% (dab) respectively, however for card (4-10wt%), quality paper (18-20wt%) and magazine paper (19-24wt%) the ash contents were found to be significant, reflecting the increased additions of filler materials to enhance the texture, print quality and aesthetic properties of the product. For example, Croxley Script was found to contain 19wt% ash (dab) and consisted of kaolin ($Al_2O_3.2SiO_2.2H_2O$), an illite {muscovite $K_2Al_4[Si_6Al_2O_{20}](OH)_4$}, quartz, gypsum ($CaSO_4.2H_2O$) and rutile ($TiO_2$). The plate-like morphology of the filler particles, typical of the clays, is illustrated in the micrograph of Frame 5.25.

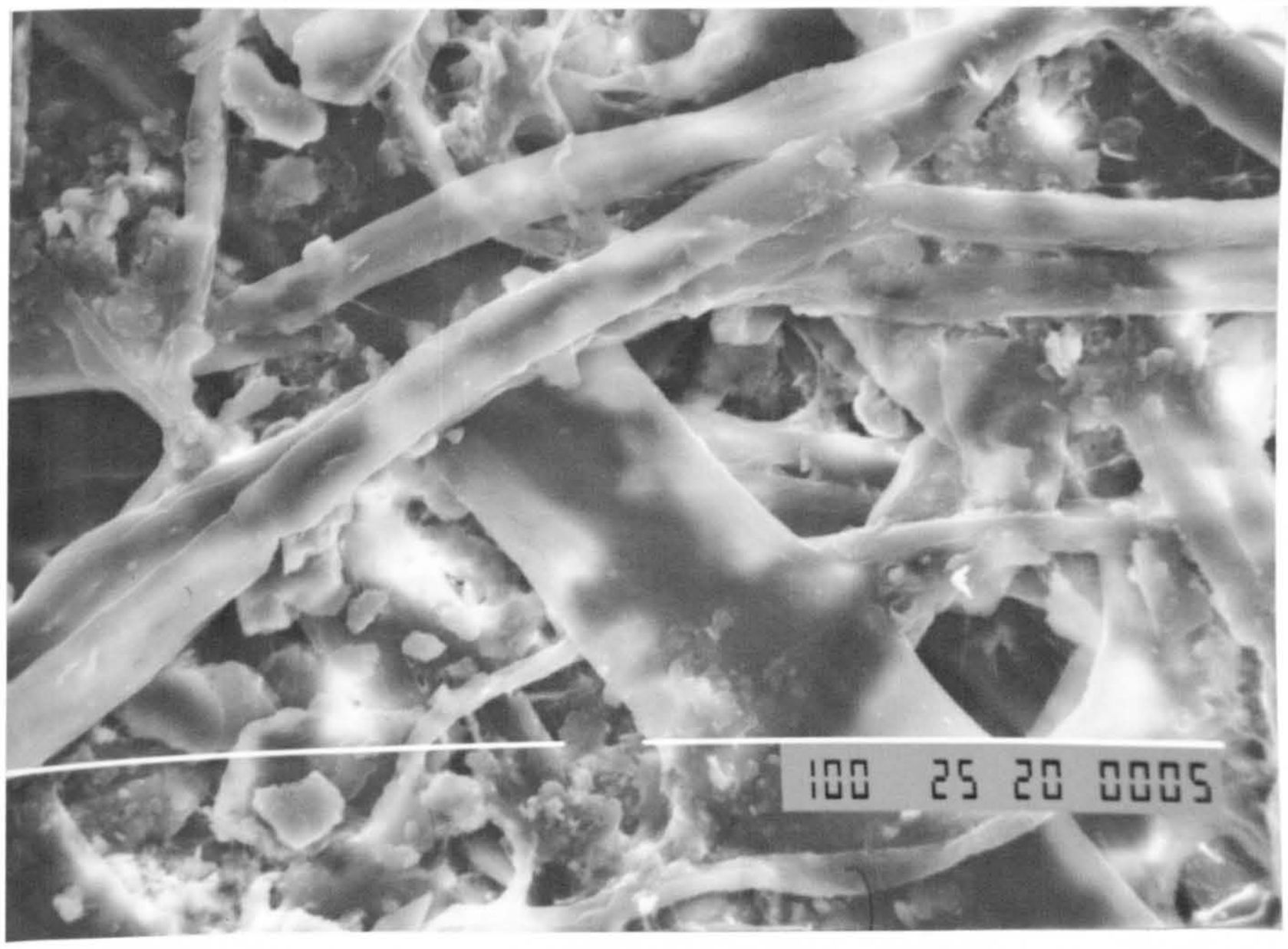

Frame 5.25 *Croxley Script* *1 bar ≡ 100μmSEI*

Inorganic filler particles (10-40μm) of plate-like morphology, interspersed within a network of cellulose fibres which constitute the paper structure.

Quartz and calcium oxalate (CaC_2O_4) were found to be present in the chestnut LTA, with little evidence of amorphous material from the X-ray diffraction trace. A complete interpretation of the diffraction pattern was not straightforward, and the nature of a crystalline phase containing sulphur remained elusive. The results are presented in Table 5.28.

Table 5.28. Crystalline phases present in chestnut and RDF LTA

SAMPLE	CRYSTALLINE PHASE		
	major	**minor**	**trace**
chestnut	CaC_2O_4 *(calcium oxalate)*	SiO_2 *(quartz)*	
Byker RDF	SiO_2 *(quartz)* $Al_2O_3.2SiO_2.2H_2O$ *(kaolin)*	$CaCO_3$ *(calcite)* TiO_2 *(rutile)*	traces of other unidentified compounds
Isle of Wight RDF	SiO_2 *(quartz)* $Al_2O_3.2SiO_2.2H_2O$ *(kaolin)* $CaCO_3$ *(calcite)*		TiO_2 *(rutile)*

The ash fusion characteristics of the chestnut and RDF ashes were investigated by high temperature microscopy; the results are presented in Table 5.29. The chestnut LTA was observed to have the longest fusion range, with the first trace of liquid at 880°C and complete fusion at 1500°C. The high temperature behaviour of the chestnut ash would have been difficult to predict without a more detailed knowledge of the ash chemistry. It would appear that the extended fusion range may have been due to the presence of a complex sulphate. Once mixed with RDF, the behaviour of the inorganic material in chestnut at high temperatures would have little bearing on the system as a whole on account of the very low ash content relative to RDF.

Table 5.29. Fusion behaviour of chestnut and RDF LTA

SAMPLE	TEMPERATURE (+/-10°C)			
	Solidus	First visible liquid *(30-40% liquid)*	Appreciable softening *(70-80% liquid)*	**Liquidus**
Chestnut	880	1020	1340	1500
Byker RDF	980	1090	1150	1220 *viscous melt*
Isle of Wight RDF	900	1040	1090	1200 *viscous melt*

The RDF samples were found to exhibit comparable ash fusion characteristics, consistent with the similarities in their ash chemistry. However, the solidus and liquidus temperatures of the Byker RDF ash were higher than those of the Isle of Wight, reflecting the increased quantities of SiO_2 and Al_2O_3, and the subsequent reduction in the fluxing potential of CaO in the Byker LTA.

5.5.2 The hearth deposit

The characterisation of a gasifier slag, received from Power Gasifiers Int., was conducted with respect to the chemistry and microstructure. The deposit had been removed from the hearth of a down-draught gasifier, in the vicinity of the air nozzles. The deposit was grey-black in colour, highly sintered yet partially vitrified, and of great strength. A diamond saw was required to section the material for analysis. The bulk chemical composition of the deposit is presented in Table 5.30. The constitution of the slag was essentially that of an aluminosilicate with a substantial quantity of lime (28 wt%) and fair proportion of Fe_2O_3 (6 wt%). X-ray diffraction analysis revealed the presence of three crystalline phases in the slag, those of gehlenite ($2CaO.Al_2O_3.SiO_2$), wollastonite ($CaO.SiO_2$) and anorthite ($CaO.Al_2O_3.2SiO_2$). A broad 'halo' in the diffraction pattern marked the presence of an amorphous (glassy) phase(s).

Table 5.30. Bulk chemical composition of a hearth deposit (Power Gasifiers)

OXIDE (wt%)	SiO_2	Al_2O_3	Fe_2O_3	CaO	MgO	K_2O	Na_2O	P_2O_5	MnO	TiO_2	SO_3
Hearth deposit	40.3	11.2	6.4	28.5	2.3	2.3	2.4	2.6	1.3	2.2	0.6

5.5.3 Microstructural examination of the hearth deposit

Microscopic examination of a polished cross-section of the hearth deposit revealed that the sample was predominantly crystalline, with wollastonite laths, euhedral crystals of diopside and discrete particles of copper metal, all embedded within a calcium-aluminosilicate matrix. It was evident that the slag had been fluid at operational temperatures with crystallisation from a molten aluiminosilicate. The strength of the deposit was undoubtedly attributable to the mass of interlocking needle-like wollastonite crystals. The microstructure was heterogeneous, changing with respect to the morphology, distribution, relative association and orientation of the various crystalline phases. Inhomogeneity of the aluminosilicate matrix was indicated by variations in back scattered electron intensity observed as streaks in the glass. Such heterogeneity of microstructure from a small section of deposit would suggest that the observations may not be characteristic of the entire sample.

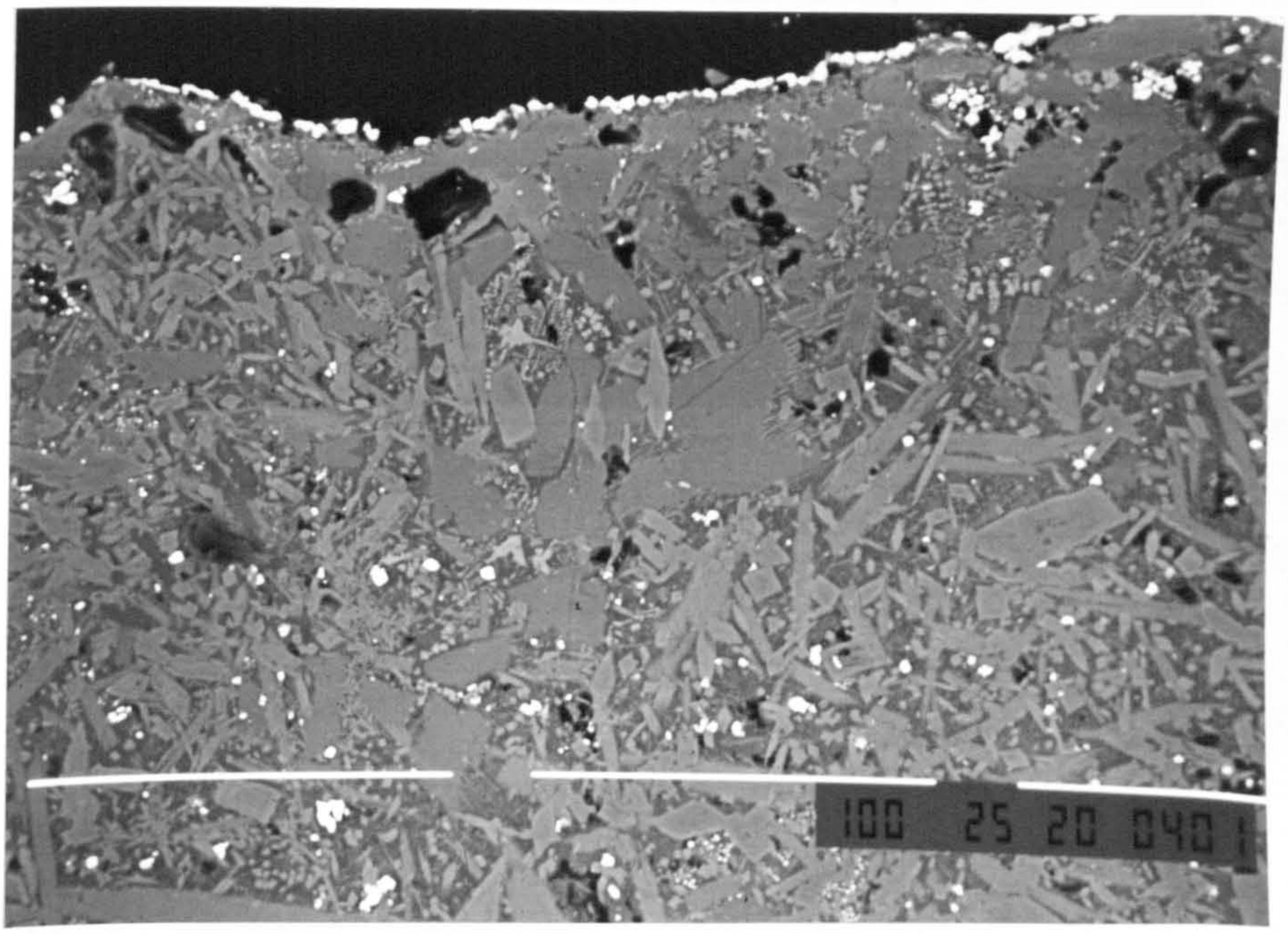

Frame 5.26. *Hearth deposit (Power Gasifiers) 1 bar ≡ 100μm. BSI*

The above micrograph illustrates the heterogeneity of the deposit microstructure in cross-section. A multiphase system of variable crystal morphology. Copper metal (bright phase) is found within the microstructure and lining pore surfaces, evidently deposited from the vapour phase.

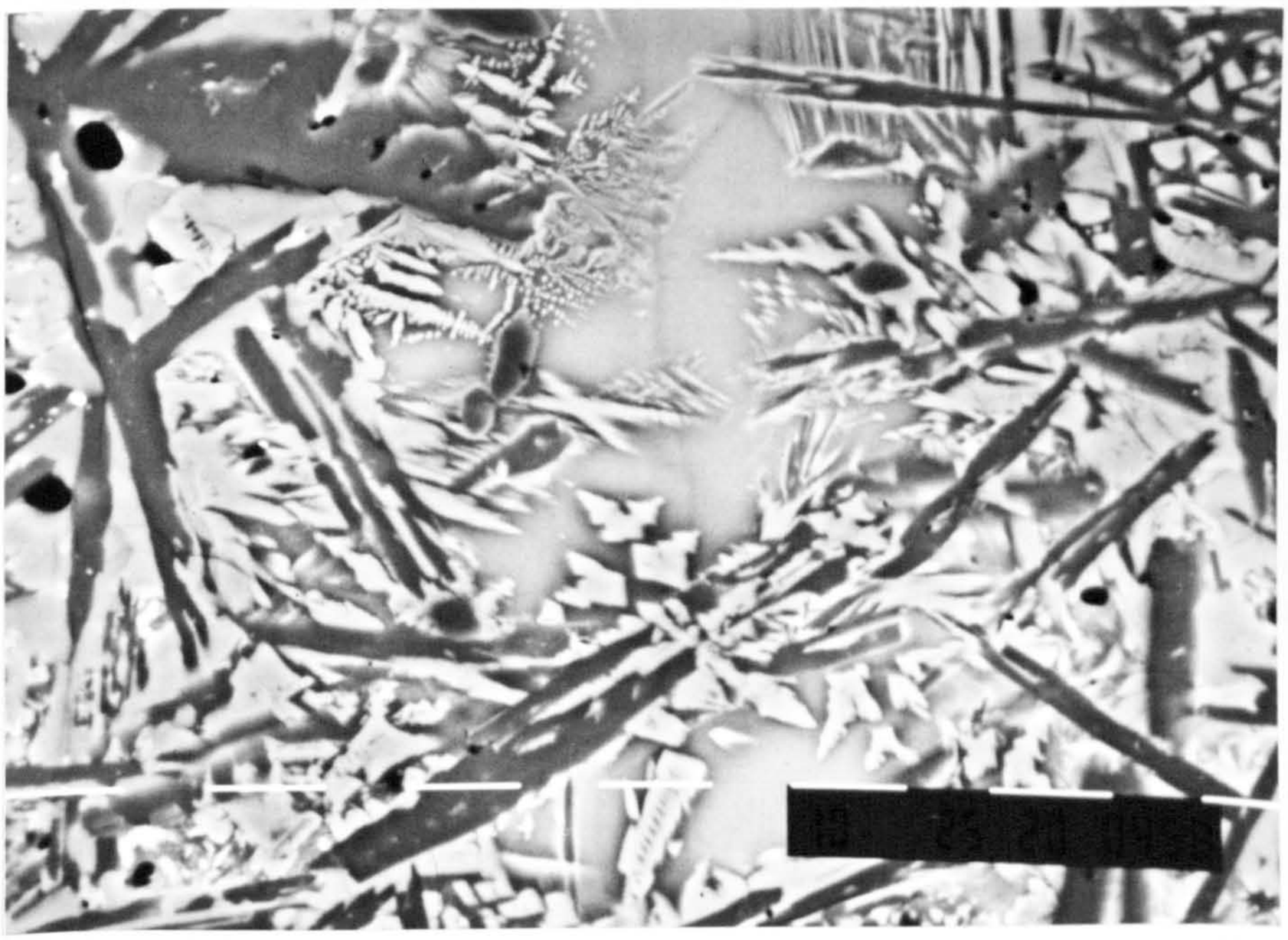

Frame 5.27. *Hearth deposit (Power Gasifiers) 1 bar ≡ 10μm. BSI*

Another region of the sample in which the presence of a dendritic phase suggests that the growth medium was highly viscous. The microstructures of Frames 5.26 and 5.27 are indicative of an inhomogeneous matrix.

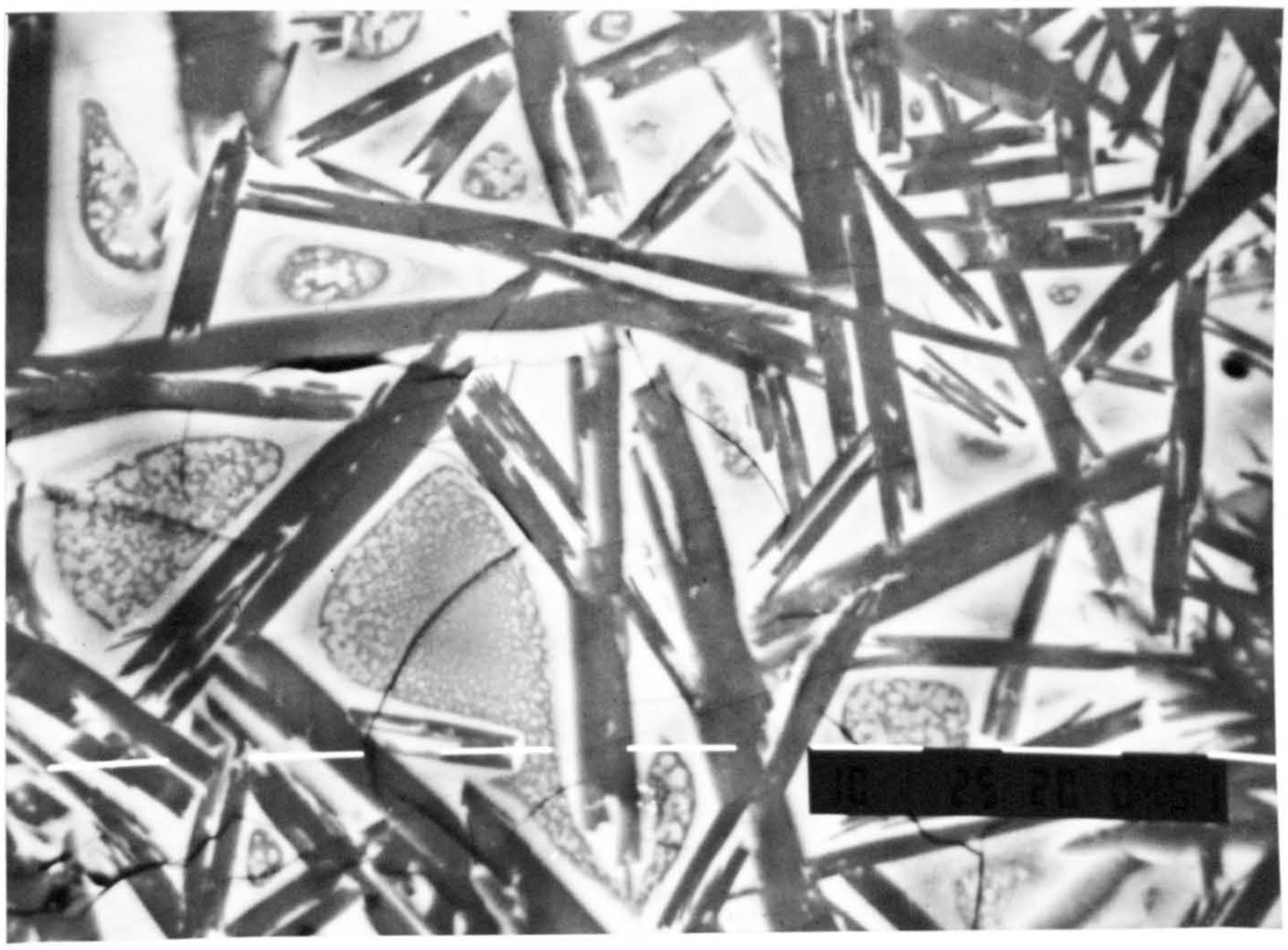

Frame 5.28. *Hearth deposit (Power Gasifiers) 1 bar ≡ 10μm. BSI*

The microstructure contains interlocking wollastonite laths (dark-grey). Multiphase 'particles' have formed in the concentration gradient between wollastonite crystals, and illustrate the complex nature of the solidification process.

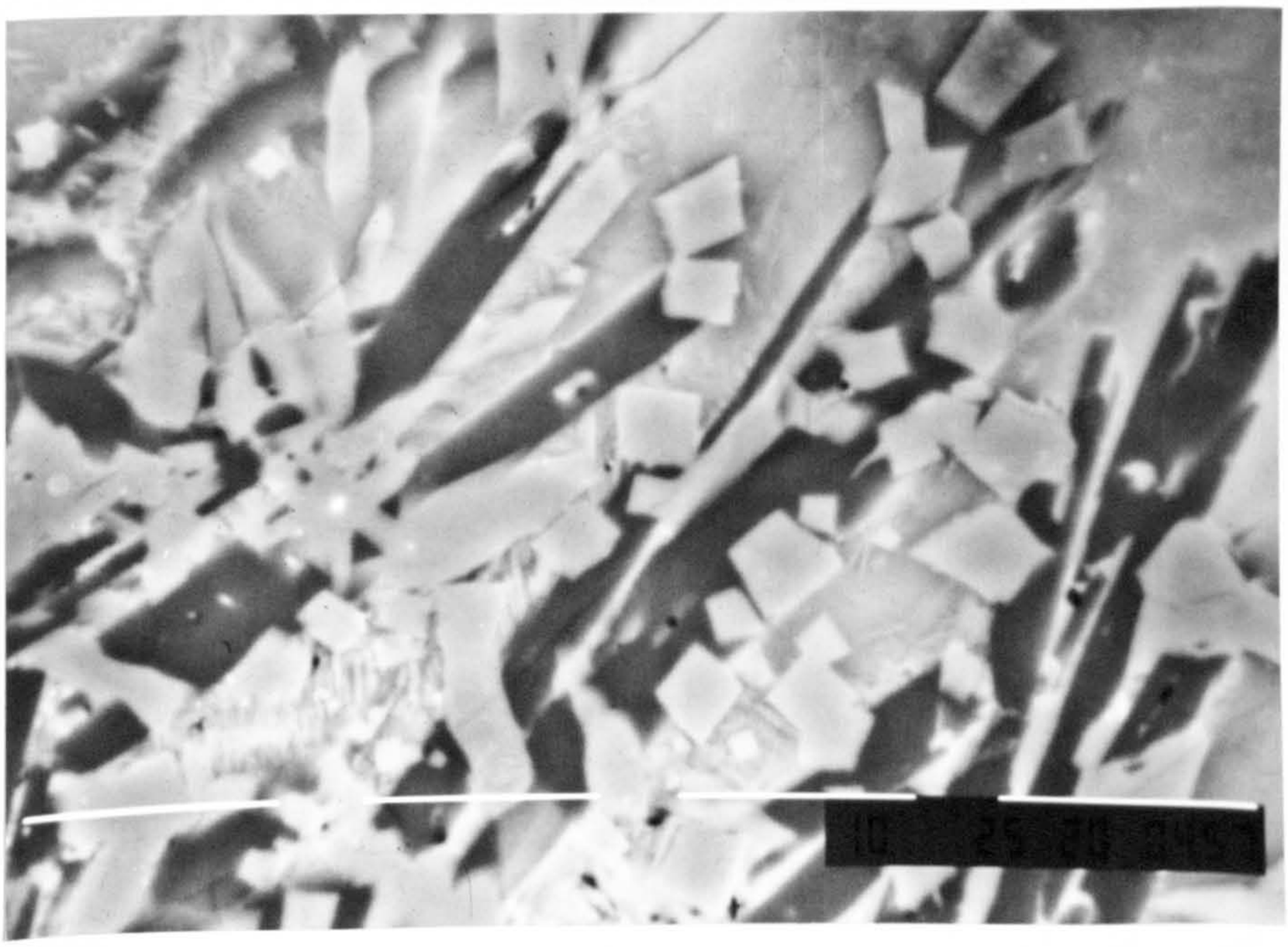

Frame 5.29. *Hearth deposit (Power Gasifiers) 1 bar ≡ 10μm. BSI*

The microstructure includes wollastonite laths (dark-grey), and euhedral crystals of diopside (<10μm in size) which are characteristically zoned with an iron-rich surface, in an amorphous aluminosilicate matrix. The matrix also contains K, Ca, Ti, Mn, and Fe.

5.5.4 The char-rich gasification residues

Power Gasifiers International provided two bottom ash residues from a 50kW$_e$ down draught gasifier fueled solely by chestnut or by a mixed feed of chestnut and 30% RDF. The deposits could only be described as char-rich, highly porous and friable. A characterisation of the gasification residues was undertaken with respect to moisture and ash contents, ash chemistry and char reactivity (in air). The chestnut and chestnut/30%RDF gasification residues were found to have moisture contents of 75% and 45% respectively, reflecting absorbed water from the ash quenching sluice. The ash content of the residue formed during the co-firing of chestnut and 30% RDF was 18.7wt%, considerably higher than that from chestnut alone (2.7wt%). The bulk ash compositions of the residues are presented in Table 5.31. During the gasification process, the chestnut residue had become enriched in SiO_2 (22wt%), Al_2O_3 (5wt%), Fe_2O_3 (6wt%), CaO (33wt%), and surprisingly Na_2O (5wt%), in relation to the fuel ash itself. As expected, a fair proportion of the more volatile species, K_2O and SO_3, had not been retained in the bottom ash residue. The addition of 30% RDF to the chestnut chunk resulted in a pronounced increase in the quantities of silica (30wt%) and alumina (15wt%) in the gasification residue. Consequently, the majority of the remaining ash components had been reduced in concentration.

Table 5.31. Compositions of chestnut and chestnut/30%RDF gasification residues

OXIDE (wt%)	SiO_2	Al_2O_3	Fe_2O_3	CaO	MgO	K_2O	Na_2O	P_2O_5	MnO	TiO_2	SO_3
Chestnut residue	21.9	4.9	5.9	33.2	5.4	9.1	4.6	2.9	3.5	0.8	7.8
Chestnut/ 30%RDF residue	29.6	14.8	1.8	30.7	3.5	3.6	6.6	2.3	0.5	2.1	4.6

The principal crystalline phases of the LTA of the chestnut and chestnut/30%RDF gasification residues were identified by X-ray diffraction as quartz and portlandite [$Ca(OH)_2$].

The effect of RDF additions to the chestnut fuel on the reactivity, with respect to oxygen, of the char-rich gasification residues was investigated using differential thermal analysis (DTA). The results were recorded in terms of a plot of ΔT (the difference between the sample temperature and the reference temperature) versus temperature (a differential thermogram), where the peak temperature of the major exothermic reaction

($C + O_2 \rightarrow CO_2$) was regarded as a measure of the char reactivity (see section 5.6.1). Both samples were of identical mass and were ground to pass a 38μm mesh sieve in order that differences in reactivity due to exposed char surface area were minimised. The chestnut derived char produced a major exotherm at 495°C, while the char from a mixed fuel containing 30% RDF gave a maximum exothermic peak at 535°C, indicating a reduction in reactivity with the addition of the RDF. The chestnut/RDF gasification residue was marginally less reactive, the peak temperatures differing by 40°C.

5.6 Results of a collaboration with Strathclyde University

Throughout the project, an exchange of technical data and samples occurred, with B McGhee and Dr P Hall at Stathclyde University (Department of Pure and Applied Chemistry). The work at Strathclyde had concentrated on the pyrolysis and gasification mechanisms of biomass and RDF, in addition to the reactivity of chars prepared under different conditions.

Pyrolysis char samples derived from straw, Danish pine, and RDF (Byker and Isle of Wight) precursors were obtained from Strathclyde University. The chars had been prepared by heating these materials in a fixed bed reactor at a rate of 10°C min^{-1} to 500°C, 700°C, and 900°C in a nitrogen atmosphere, sustaining the respective peak temperature for one hour. The char yield, ultimate analysis and chemical composition were determined at Strathclyde.

5.6.1 Characterisation of pyrolysis chars by DTA

In the present study, the relative reactivities of the pyrolysis chars were assessed by differential thermal analysis (DTA). In this technique, the difference in temperature between the sample and reference material was measured and plotted against sample temperature to give a differential thermogram such as that shown in Figure 5.3.

Differential thermal analysis maxima and minima (peaks) result from both physical changes and chemical reactions induced by temperature changes in the sample. The maxima observed in the thermograms are the result of heat evolution from the sample and are thus exothermic processes. Minima at the beginning of each trace correspond to the endothermic vaporisation of absorbed water.

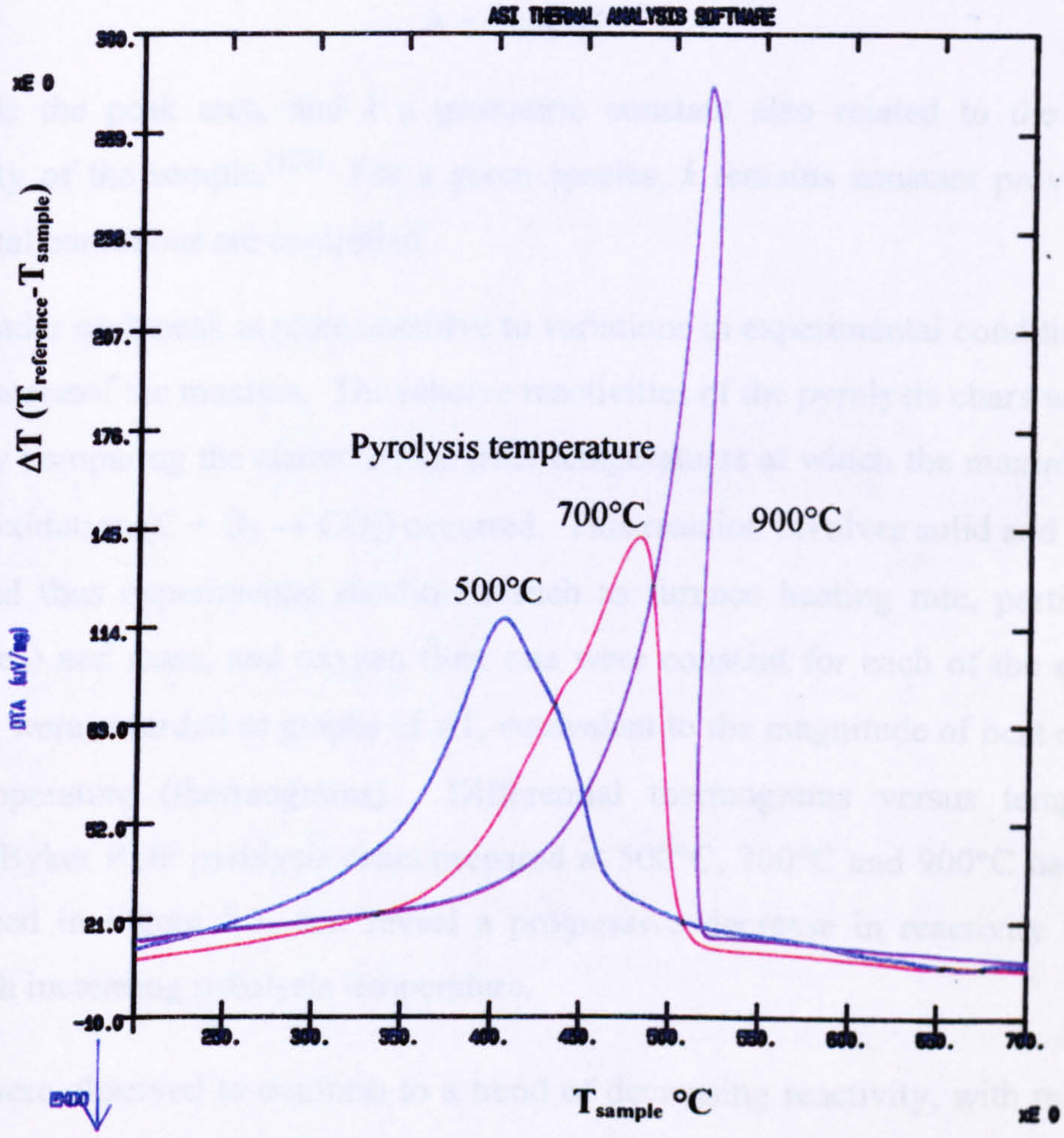

Figure 5.3 Differential thermograms, ΔT ($T_{reference}$-T_{sample}) versus sample temperature (T_{sample}) for Byker RDF chars prepared at 500°C, 700°C and 900°C

The area beneath each peak is a measure of the total heat evolved or absorbed during the chemical reaction or physical change. Peak areas depend upon the sample mass, *m*, the enthalpy change, ΔH, of the process, and certain geometric and heat conductivity factors. These variables are related by the equation

$$A = - km\Delta H$$

where A is the peak area, and *k* a geometric constant also related to the thermal conductivity of the sample.[120] For a given species, *k* remains constant provided the experimental conditions are controlled.

The area under each peak is more sensitive to variations in experimental conditions than the temperaturesof the maxima. The relative reactivities of the pyrolysis chars were thus assessed by comparing the characteristic peak temperatures at which the maximum rate of carbon oxidation ($C + O_2 \rightarrow CO_2$) occurred. This reaction involves solid and gaseous species, and thus experimental conditions such as furnace heating rate, particle size (surface area) and mass, and oxygen flow rate were constant for each of the samples. The results were recorded as graphs of ΔT, equivalent to the magnitude of heat evolved, versus temperature (thermograms). Differential thermograms versus temperature graphs for Byker RDF pyrolysis chars prepared at 500°C, 700°C and 900°C have been superimposed in Figure 5.3, and reveal a progressive decrease in reactivity towards oxygen with increasing pyrolysis temperature.

All chars were observed to conform to a trend of decreasing reactivity, with respect to oxygen, with increasing pyrolysis temperature. The peak temperatures of the major DTA exotherms, representing carbon oxidation, are given in Table 5.32 for each of the precursors and char preparation conditions. The temperature of carbon oxidation was found to differ by 45-75°C between chars pyrolysed at temperatures of 500°C and 700°C, and by 20-70°C between pyrolysis temperatures of 700°C and 900°C. RDF chars were found to be more reactive than those of straw and wood. The increase in reactivity may be in part ascribed to the significantly greater ash contents of the RDF samples and the action of alkali ions as oxidation catalysts for carbon.

Table 5.32 Oxidation temperatures of pyrolysis chars

PRECURSOR	PYROLYSIS TEMPERATURE (+/- 5°C)			
	500	700	900	acid-treated* 900
Danish pine wood	470	515	535	595
Straw	430	475	500	620
Byker RDF	405	480	520	565
Isle of Wight RDF	425	480	550	585

** 1M HNO_3 treatment*

5.2.6 Effect of acid treatment

A 1M HNO_3 treatment of the biomass precursor was performed at Strathclyde with subsequent pyrolysation. Data from Strathclyde revealed a reduction in ash content of the acid-treated materials. As expected, the composition of the ashes were notably reduced in CaO, MgO and K_2O. As shown in Table 5.32, the chars produced from the HNO_3-treated materials were less reactive (with respect to oxygen) than their untreated counterparts.

The nature of the crystalline phases present in the range of Byker RDF pyrolysis chars was investigated by XRD of the LTA. Quartz was found to be the major phase at all pyrolysis temperatures. Calcite, present in the sample prepared at 500°C, was absent at 700°C and above; reaction of the decomposition product, CaO, with SO_2 would have produced $CaSO_4$ which appeared as anhydrite at 700°C and 900°C. The initial decomposition of talc, $Mg_6(Si_8O_{20}](OH)_4$, was also found to have occurred by 700°C, with the probable formation of $MgSiO_3$ by 900°C.

The HTA prepared from Byker RDF contained quartz, gehlenite ($2CaO.Al_2O_3.SiO_2$) and nepheline [$(Na,K)AlSiO_4$]. The presence of both these aluminosilicate phases, not present in the LTA of Byker RDF may seem improbable, yet clearly reflects the complex nature of reactions (including those of the solid state) occurring at high temperatures during the preparation of HTAs.

Table 5.33 Crystalline phases present in Byker RDF as a function of pyrolysis temperature

CRYSTALLINE PHASE	PYROLYSIS TEMPERATURE °C			
	500	**700**	**900**	**HTA***
Major	SiO_2 (*quartz*) $CaCO_3$ (*calcite*)	SiO_2 (*quartz*)	SiO_2 (*quartz*)	SiO_2 (*quartz*)
Minor	TiO_2 (*rutile*) $Mg_6[Si_8O_{20}](OH)_4$ (*talc*)	TiO_2 (*rutile*) $CaSO_4$ (*anhydrite*)	TiO_2 (*rutile*) $CaSO_4$ (*anhydrite*)	$2CaO.Al_2O_3.SiO_2$ (*gehlenite*) $(Na,K)AlSiO_4$ (*nepheline*)
Trace	$CaSO_4$ (*anhydrite*)		$MgSiO_3$	$MgSiO_3$

* HTA at 900°C

5.6.2 Microstructural examination of pyrolysis chars

The influence of pyrolysis temperature on char morphology was investigated by SEM. Microstructural examination of chars prepared from Danish pine (Frames 5.30 to 5.32) and straw (Frames 5.33 to 5.35) has shown that the rapid evolution of volatile matter during pyrolysis yields carbonaceous residues with cellular structures closely resembling those of the original materials. The high specific surface area will give these chars a high reactivity, with additional catalytic activity from the presence of alkali ions (Ca^{2+}, K^{+}). Chars from the RDFs were prepared from pellets (Byker) and 'fluff' (Isle of Wight). The microstructures (Frames 5.36 to 5.41) show remarkable similarity despite the difference in RDF processing. The chars have a fibrous structure originating from the high proportion of paper and card in RDF. Cellulose is the chief component of wood and plant fibres, and thus paper derived wastes. The structure of cellulose, a high molecular weight carbohydrate $[(C_6H_{10}O_5)_n]$, consists of bundles of H-bonded chains (>1000 glucose units per molecule), which twist to form rope-like structures.[119] Resistance to thermal degradation in the absence of oxygen is likely to be high. In addition, the RDF char micrographs reveal fragments of glass, a soda-lime silicate (Frame 5.38) and filler particles (Frame5.41). Fragments of aluminium and copper metals were also detected.

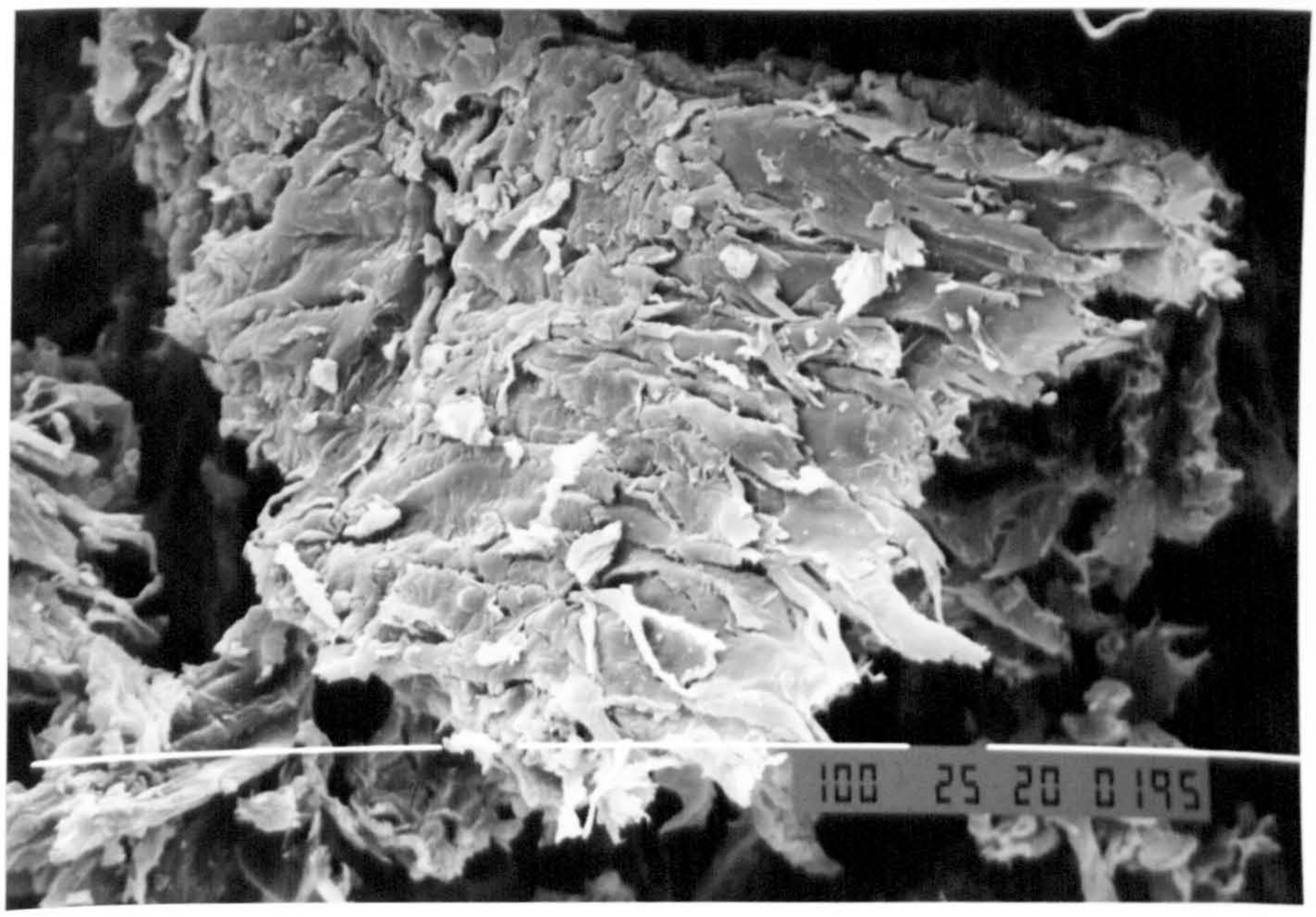

Frame 5.30. *Danish pine pyrolysis char 1 bar ≡ 100μm. SEI*

Microstructure of Danish pine char prepared at 500°C in an atmosphere of N_2.

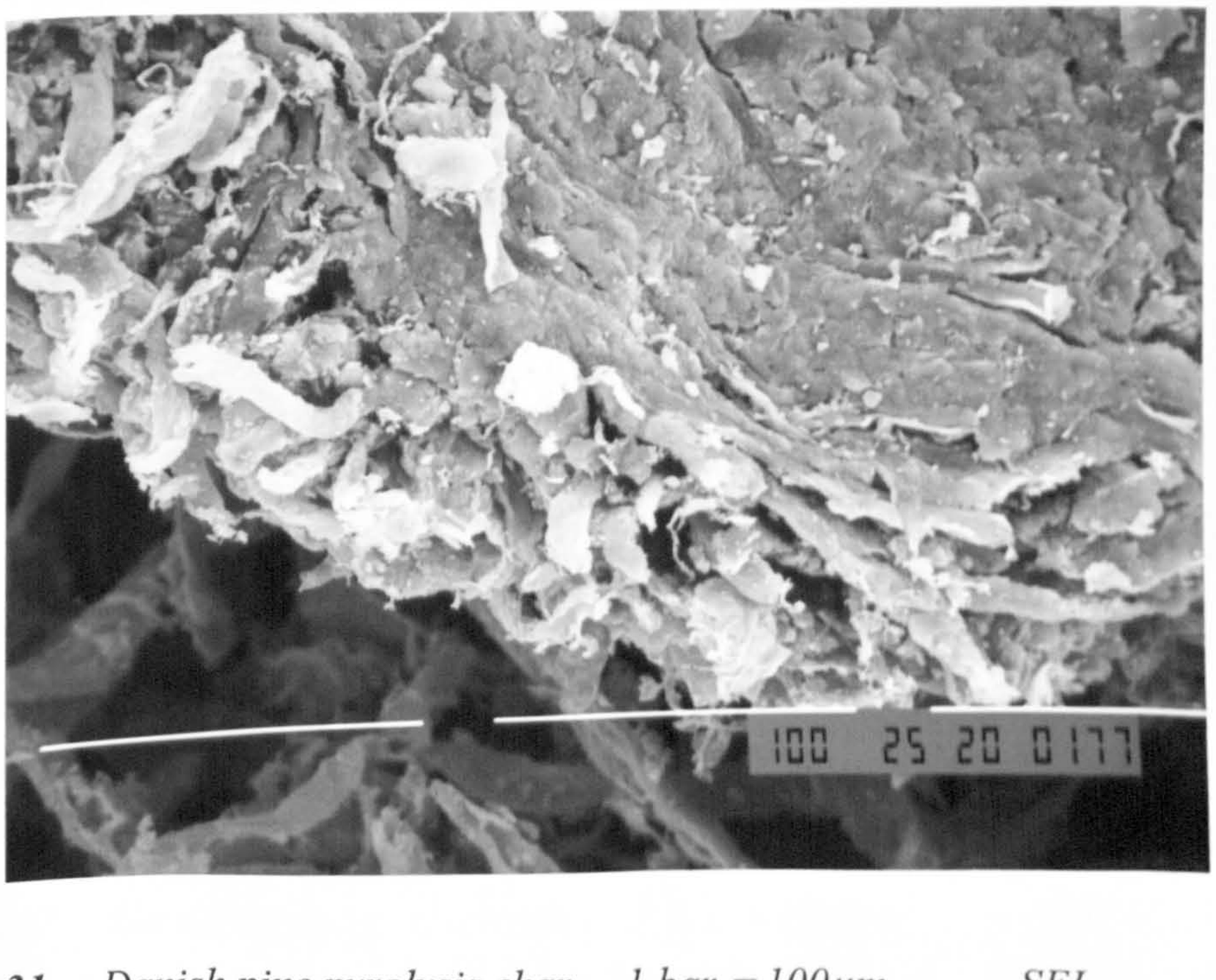

Frame 5.31. *Danish pine pyrolysis char 1 bar ≡ 100μm. SEI*

Microstructure of pine char prepared at 700°C. The higher pyrolysis temperature has made little difference to the apparent char morphology.

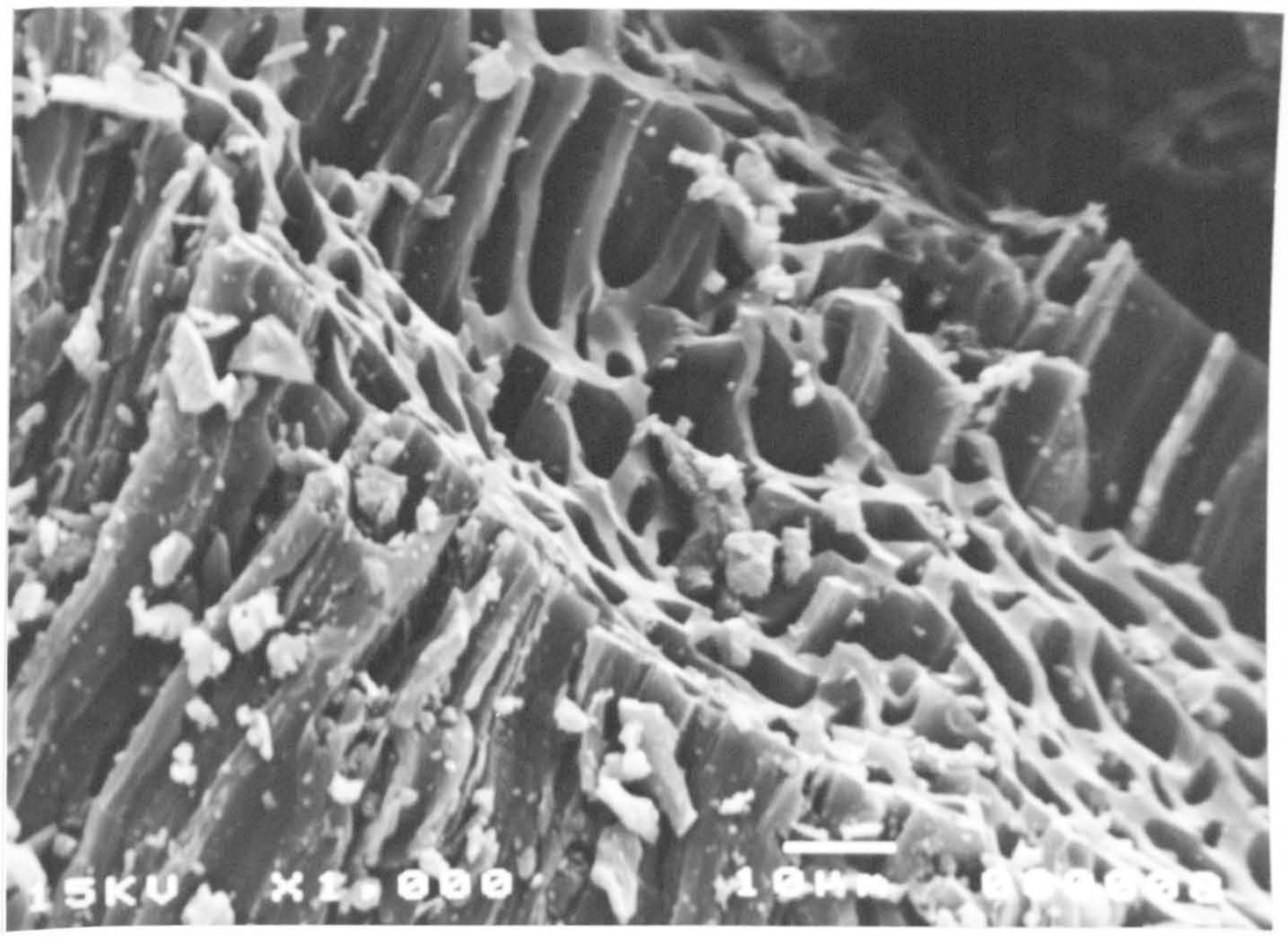

Frame 5.32. *Danish pine pyrolysis char 1 bar ≡ 100μm. SEI*

Cellular structure of pine char retained at pyrolysis temperature 900°C.

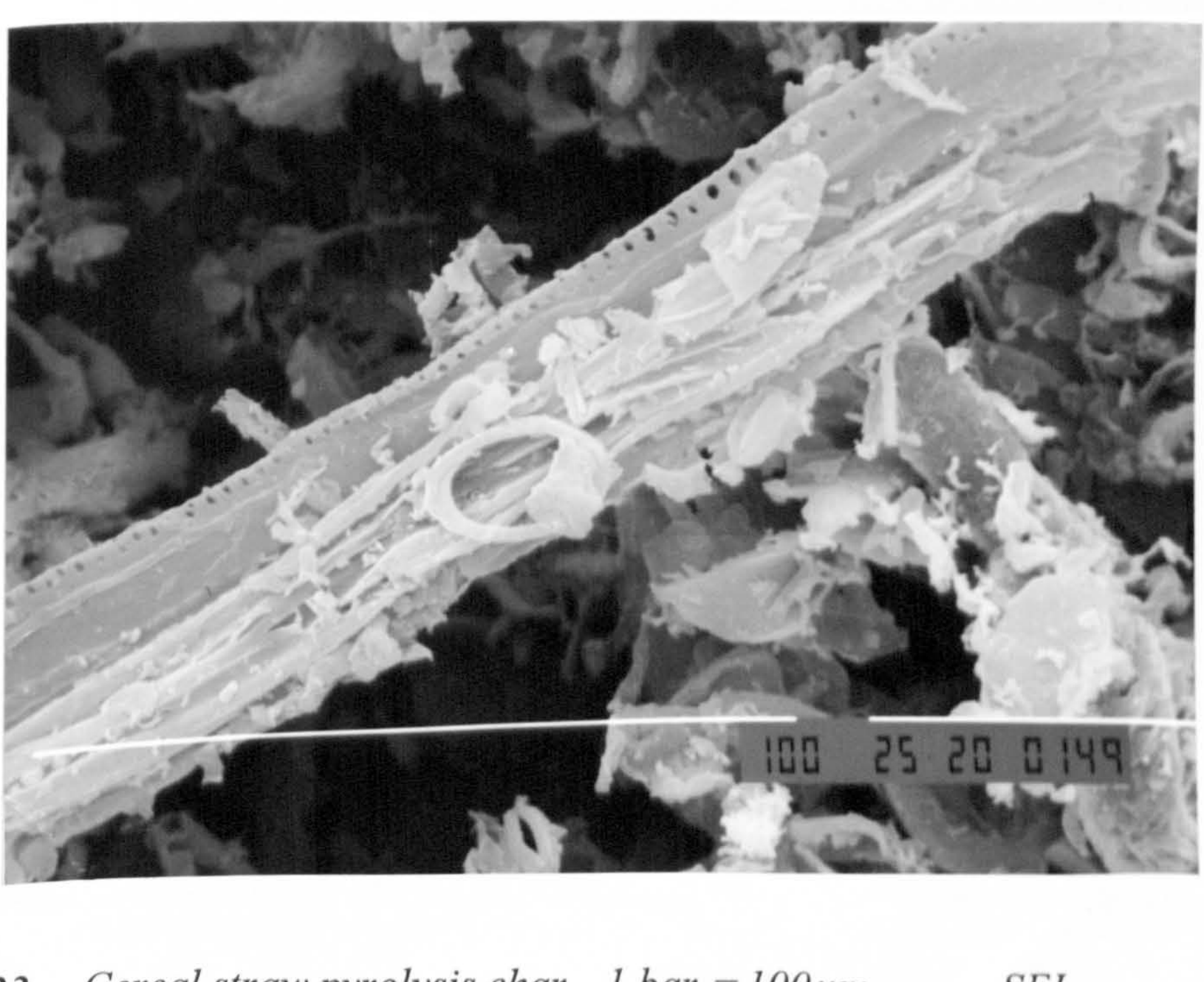

Frame 5.33. *Cereal straw pyrolysis char 1 bar ≡ 100μm. SEI*

Microstructure of straw char prepared by pyrolysis in an atmosphere of N_2 at 500°C. Cellular structure just visible.

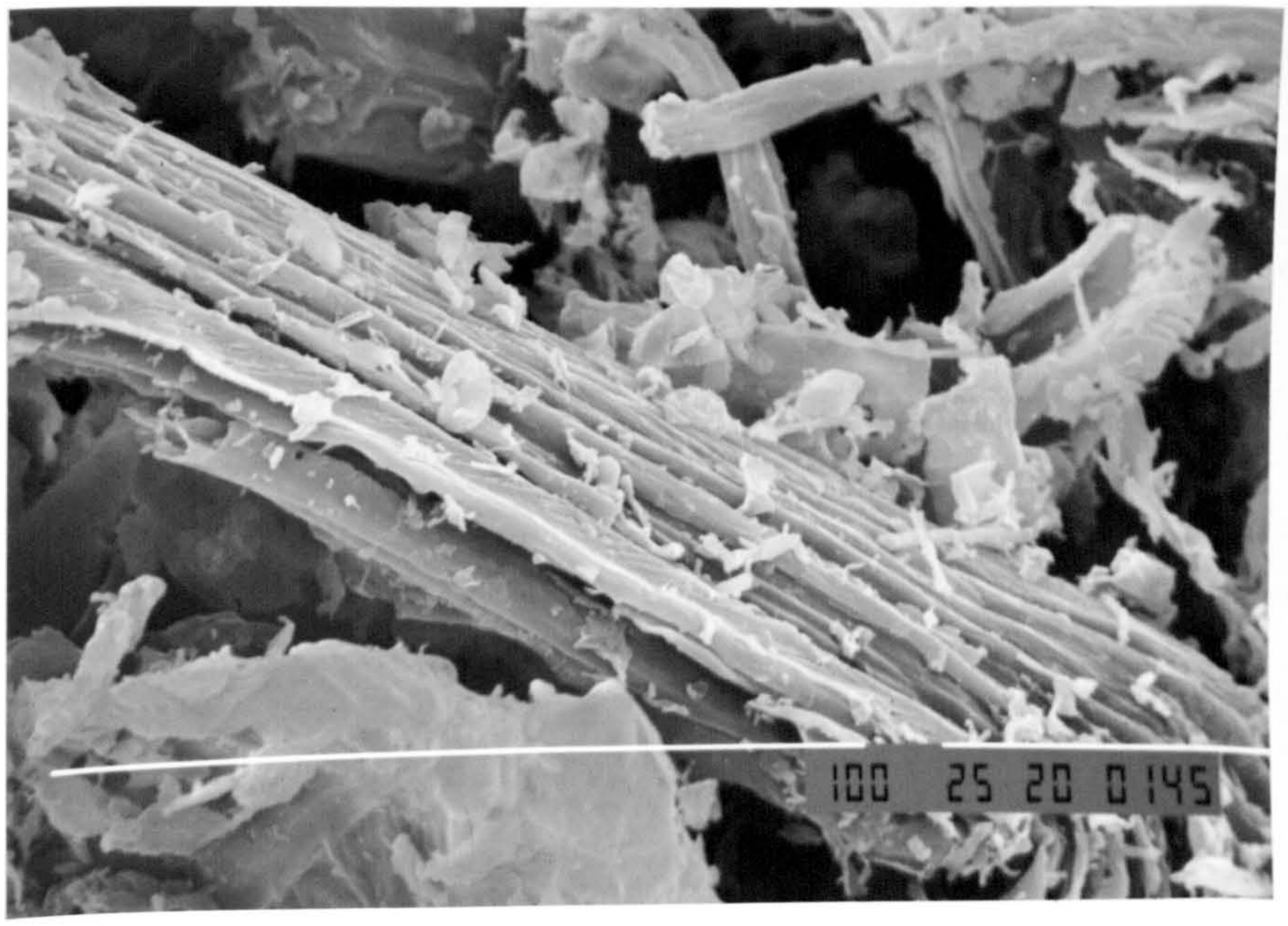

Frame 5.34. *Cereal straw pyrolysis char 1 bar ≡ 100μm. SEI*

Cellular structure of straw char retained at pyrolysis temperature 700°C.

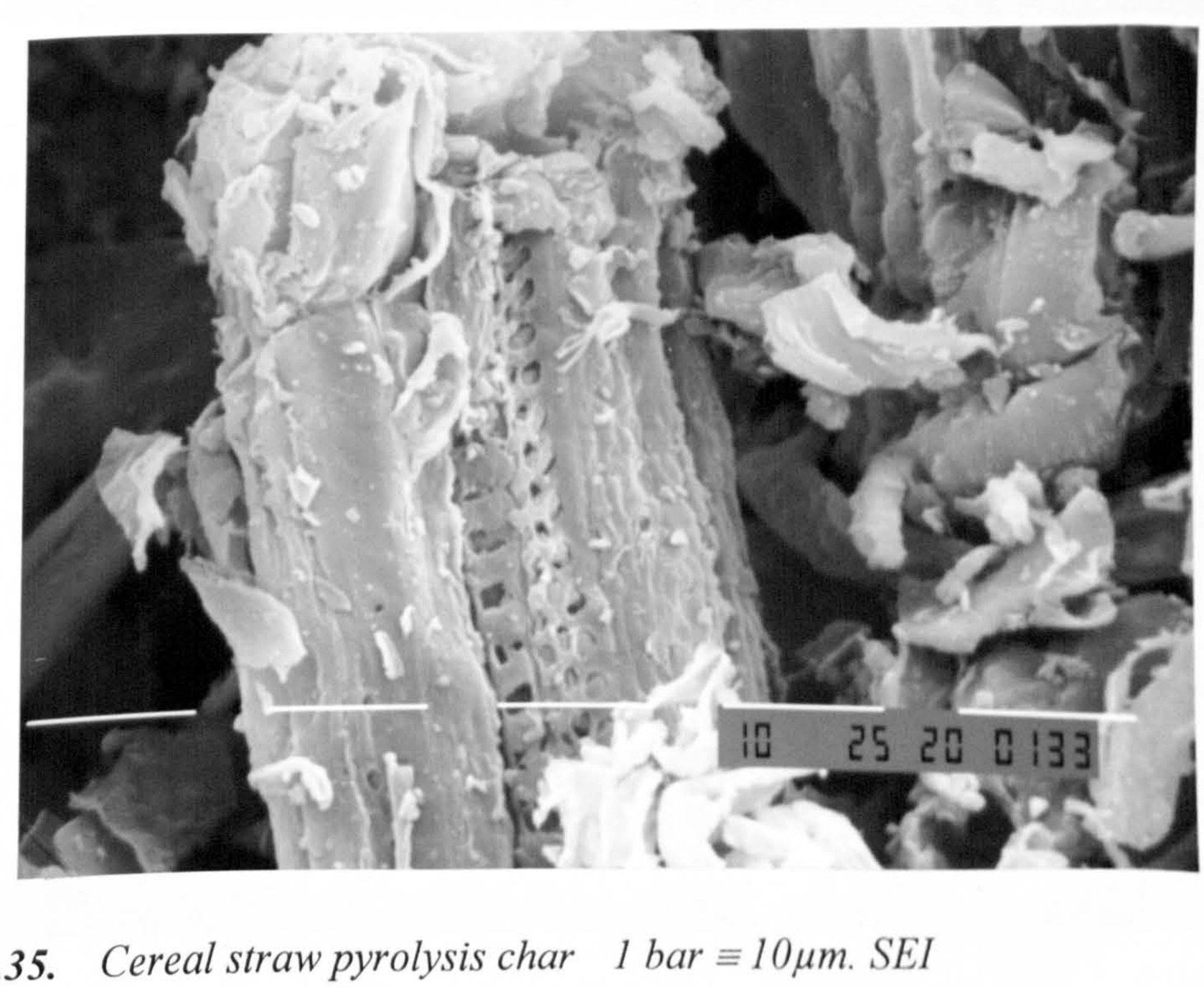

Frame 5.35. *Cereal straw pyrolysis char 1 bar ≡ 10μm. SEI*

Microstructure of straw char prepared at 900°C revealing the cellular structure of the raw material.

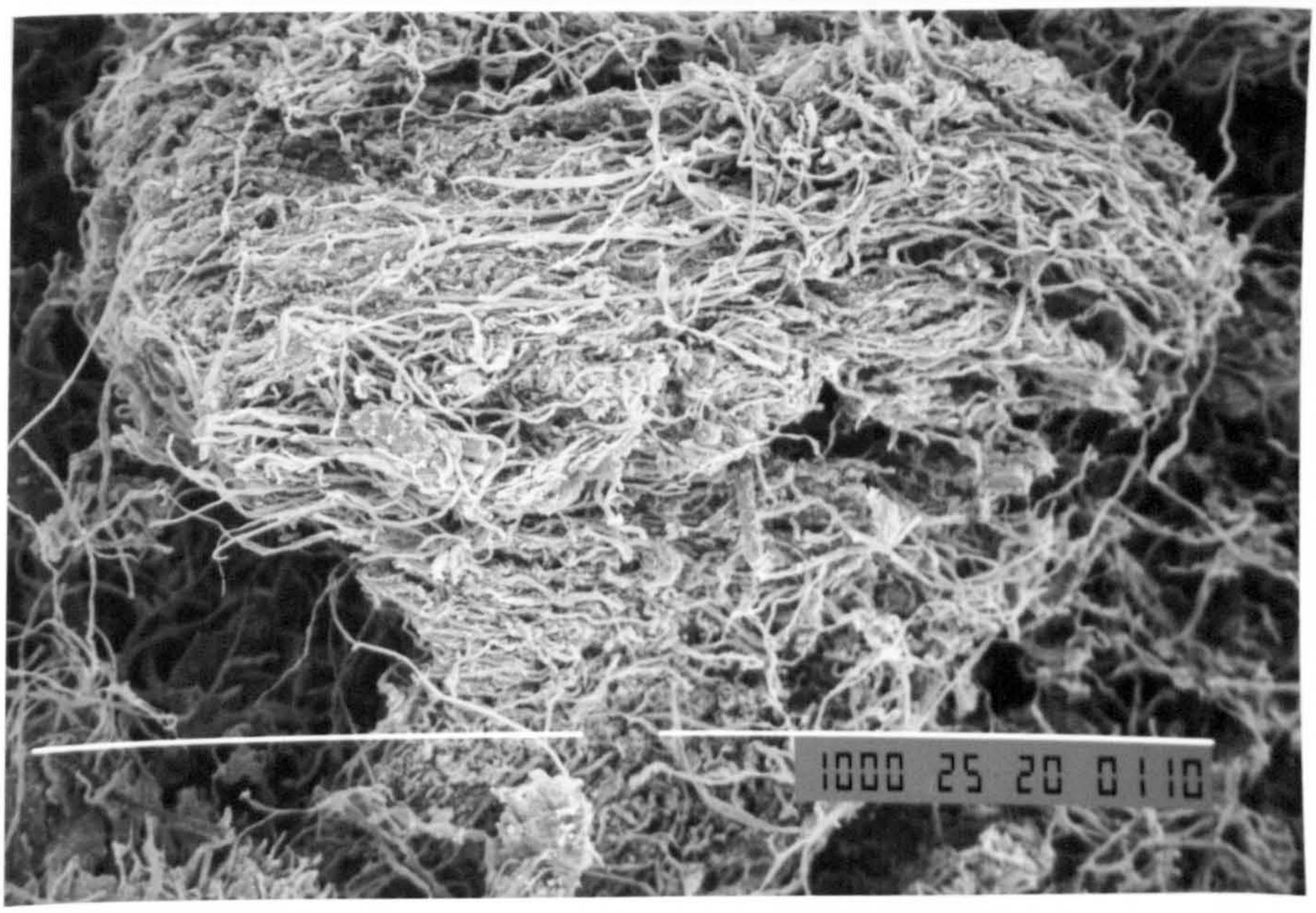

Frame 5.36. *Isle of Wight RDF pyrolysis char* *1 bar ≡ 1mm.* *SEI*

Microstructure of pyrolysis char prepared from Isle of Wight RDF 'fluff' at 500°C. The char retains the fibrous structure of the high cellulose content of the original material.

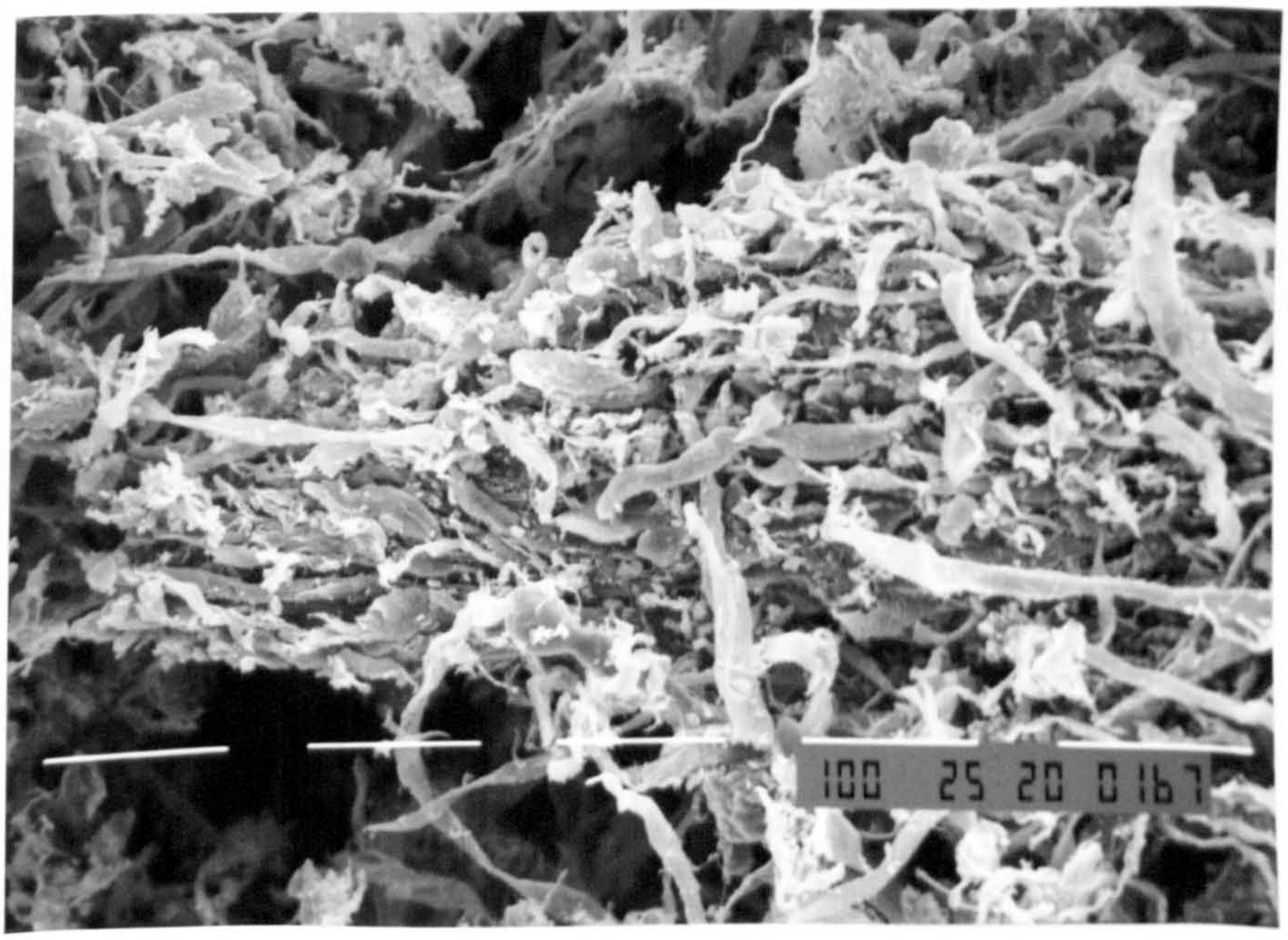

Frame 5.37. *Isle of Wight RDF pyrolysis char* *1 bar ≡ 100μm.* *SEI*

Microstructure of Isle of Wight RDF char prepared at 700°C showing fibrous structure.

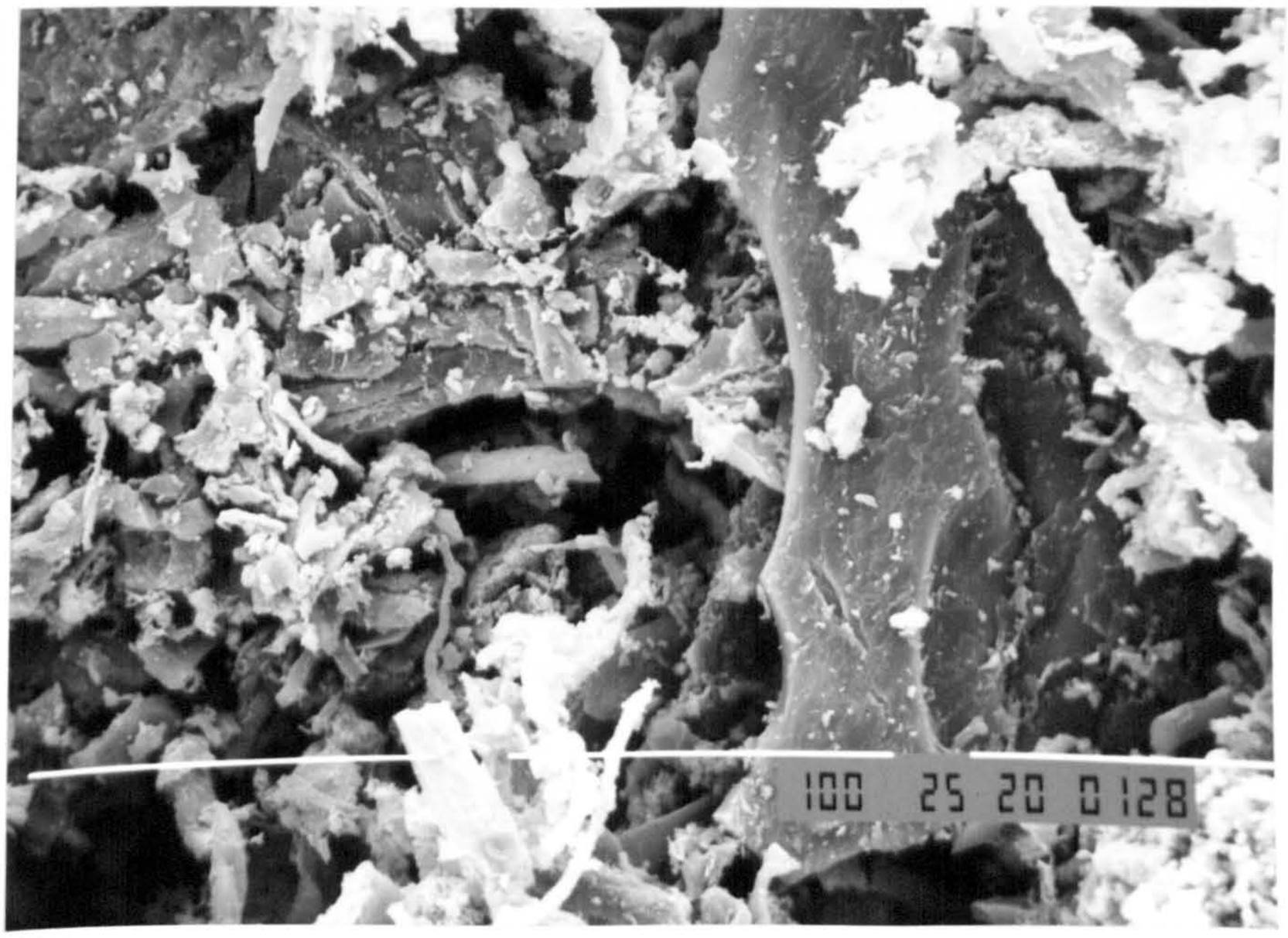

Frame 5.38. *Isle of Wight RDF pyrolysis char 1 bar ≡ 100μm. SEI*

Fragment of soda-lime glass (typical conchoidal fracture) embedded in char from Isle of Wight RDF prepared at 900°C.

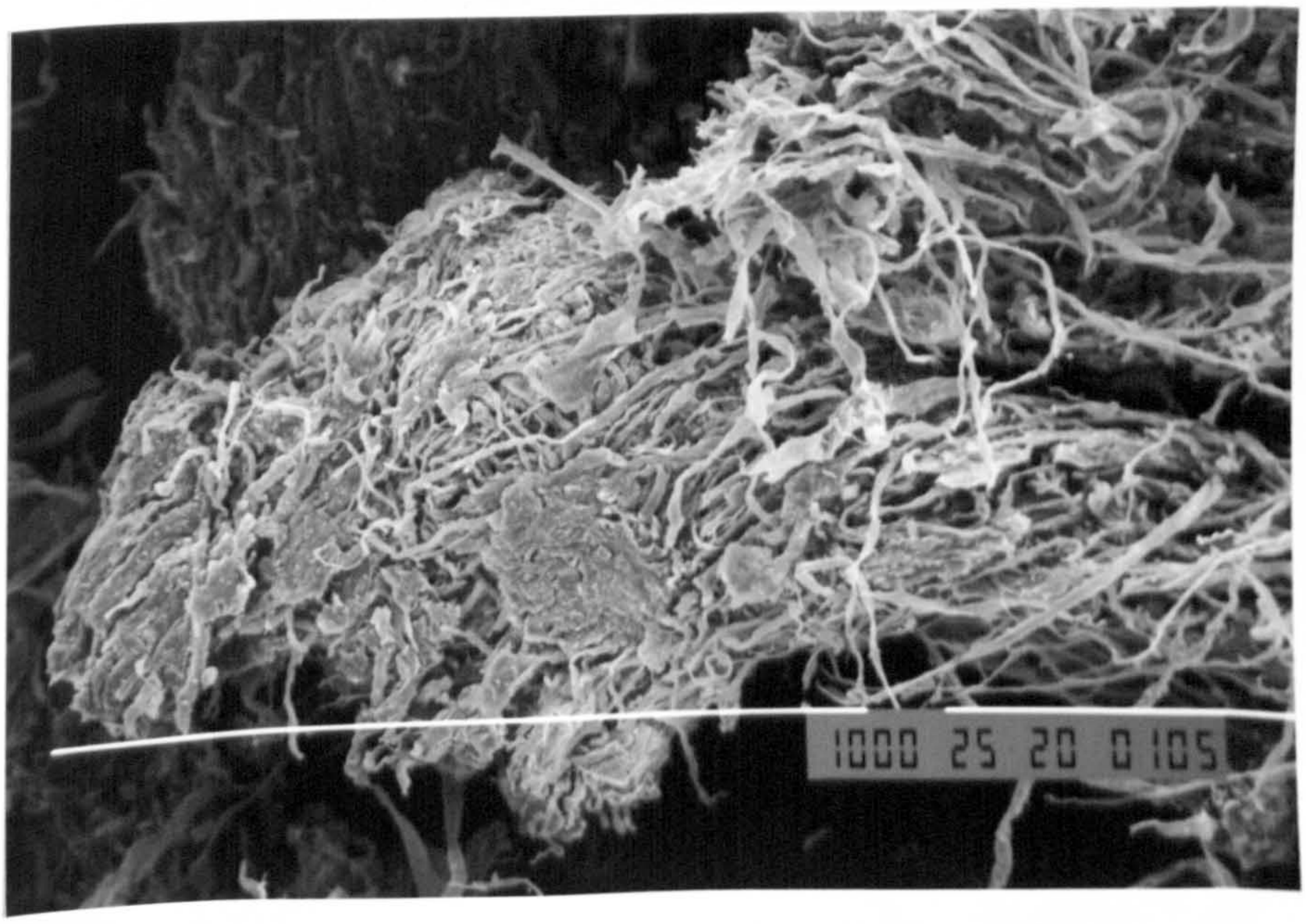

Frame 5.39. *Byker RDF pyrolysis char 1 bar ≡ 1mm. SEI*

Microstructure of Byker RDF char prepared at 500°C in N_2 showing inorganic filler particles in a matrix of cellulose fibres.

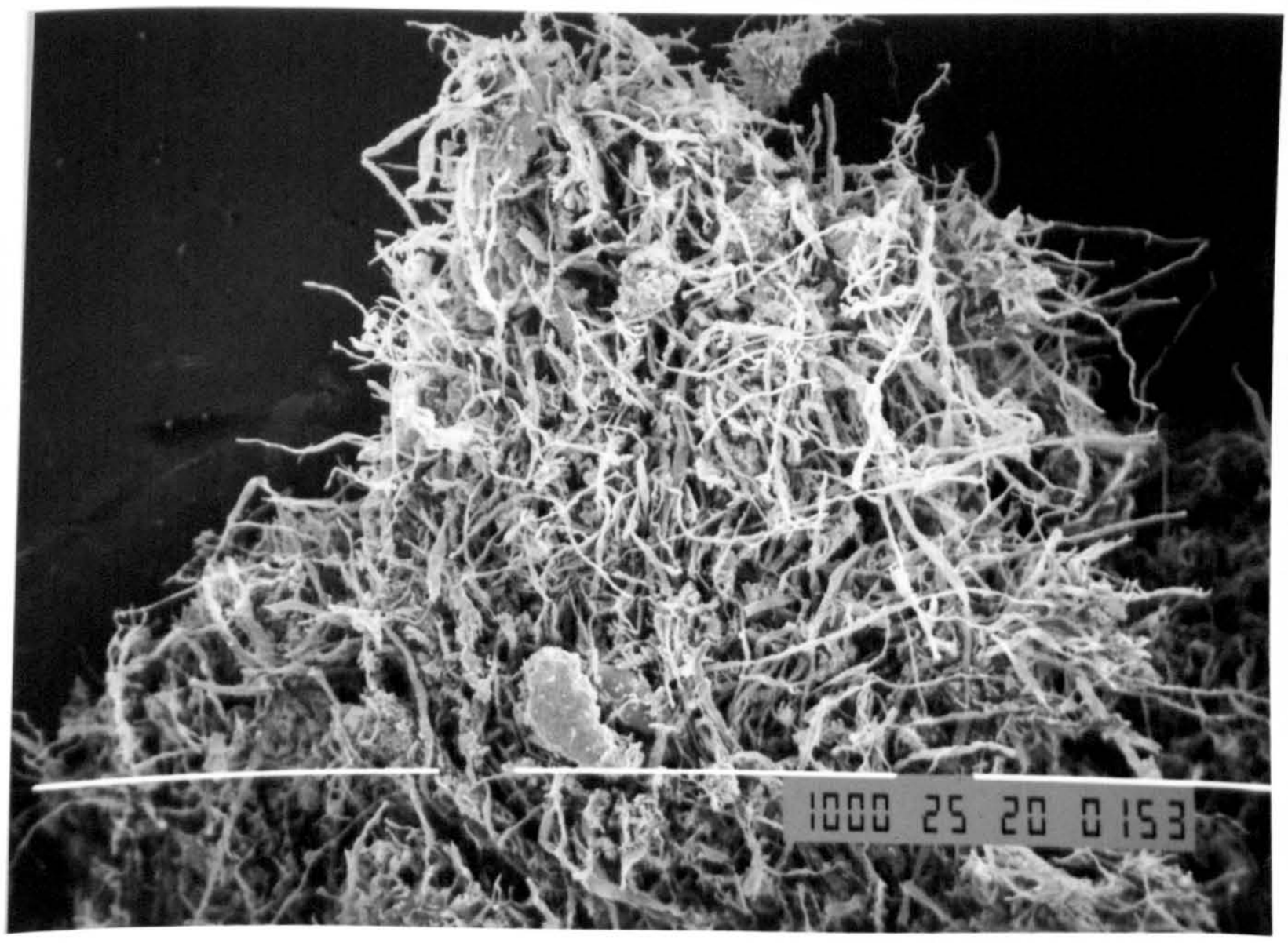

Frame 5.40. *Byker RDF pyrolysis char* *1 bar ≡ 1 mm. SEI*

Structure of Byker RDF char prepared at 700°C. The microstructure is very similar to that of Isle of Wight char despite the difference in RDF processing (pellets versus shredded 'fluff').

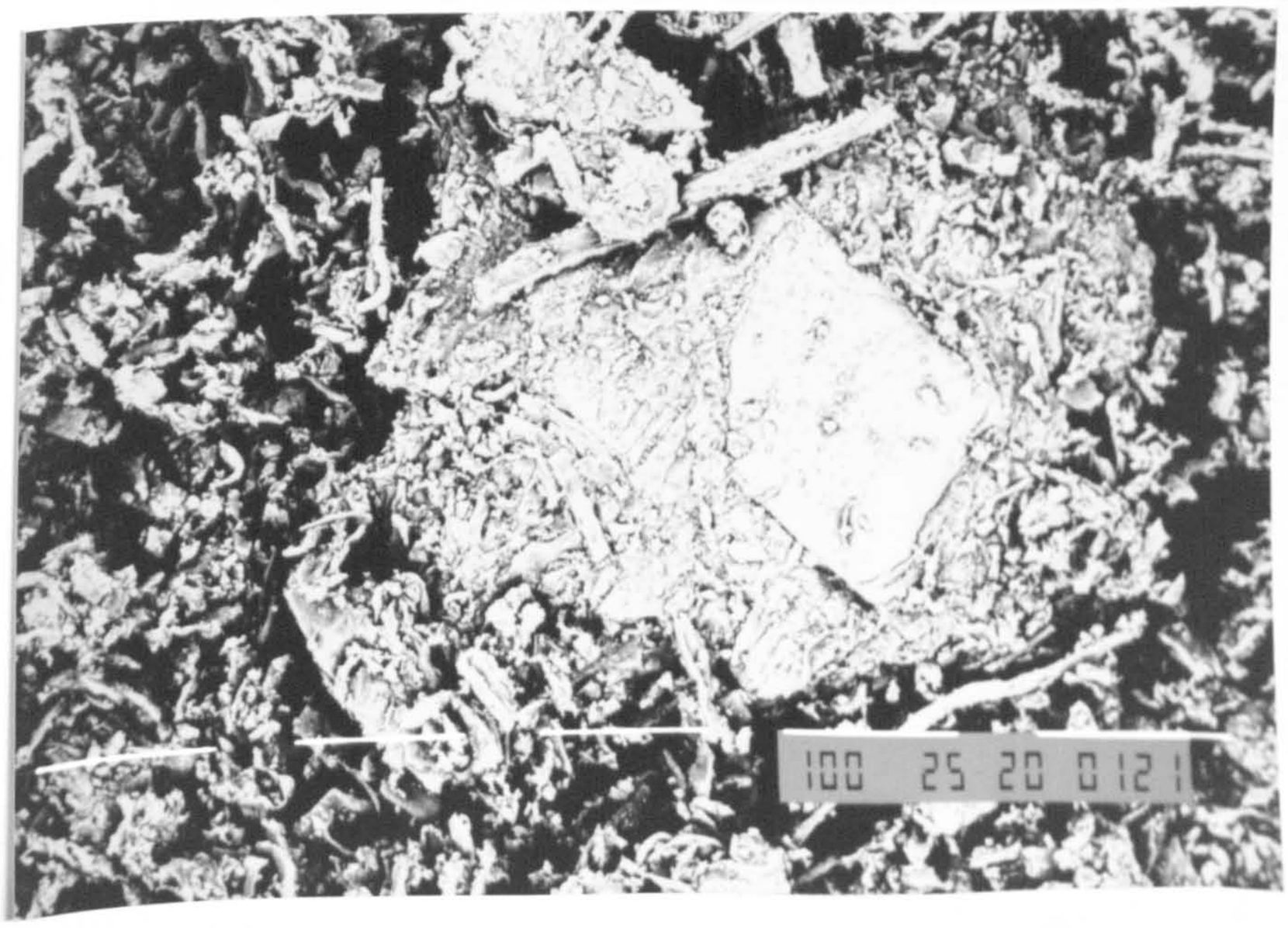

Frame 5.41. *Byker RDF pyrolysis char* *1 bar ≡ 100μm.* *BSI*

Microstructure of Byker RDF char prepared at 900°C showing a large (~200μm) aluminosilicate fragment (clay origin) in the carbonaceous matrix.

Chapter Six

Discussion

Few European countries have an energy policy, yet the provision of energy is recognised as fundamental to our living standards. The oil crisis of the mid-1970's was a costly lesson to those countries heavily dependent on oil imports, and with two-thirds of the world's oil originating from a region of great political instability, most European governments have been keen to develop electrical power industries which use a spread of primary energy sources.

With present technologies it seems unlikely that biomass could ever produce electrical power at costs approaching those from coal or natural gas. However, the added problems of waste disposal, and ever increasing CO_2 emissions from the combustion of fossil fuels, have encouraged most countries to provide tax incentives and subsidies to encourage the use of biomass and wastes as energy sources.

The technology to accommodate such diverse energy sources has yet to be developed. Such plant must be designed to run without interruptions for prolonged periods. This assumes that the problems associated with the ashes and residues from a combustion or gasification process can be managed and controlled. Thus a knowledge of the high temperature behaviour of combustion/gasification residues is prerequisite to the design and operation of such plant.

Having characterised a diverse range of biomass materials, it is now appropriate to consider the results of the preceding chapter with two principal objectives in mind. The

first objective is to predict the high temperature behaviour of the inorganic matter under combustion and gasification conditions, on a theoretical basis using thermodynamic data, phase equilibria studies and viscosity calculations. The accuracy and reliability of such predictions can then be ascertained by a direct correlation with observed ash behaviour in commercial and pilot plant operations. The second is to elucidate the mechanisms of deposit formation by an interpretation of the deposit microstructure. This approach to predicting ash behaviour at high temperature, in particular the propensity of deposit formation, should be of value to potential designers and operators of both plant and processes which use biomass as an energy source.

The adherence and subsequent bonding/consolidation of ash particles at the temperatures of interest is largely due to the presence of a liquid phase, which may be formed by the fusion or surface melting of the inorganic material, or by an eutectic reaction resulting from the chemical interaction of several ash species. To summarise the theory of Section 2.16 regarding deposit formation, the transfer of material via a viscous liquid phase is the predominant mechanism of sintering in combustion and gasification systems. In the systems concerned the degree of sintering, and hence the increase in strength of a deposit, is critically influenced by the liquid viscosity (an inverse relationship is described by the Frenkel Equation). Thus particular attention has been ascribed to the prediction of solidus temperatures, at which a liquid phase is first to appear on heating under equilibrium conditions, in particular the marked dependence of the viscosity of the residual liquid on temperature and composition.

The subject of viscosity has been pursued for a number of years, and whereas the kinetic theory is acknowledged as satisfactory for gases, no comparably successful theory has been found for liquids. One result of this has been the derivation of a plethora of empirical relationships which are used to predict the viscosity of a melt as a function of temperature. Many of these expressions are lacking in mathematical rigour and have limited ranges of applicability. However, the Urbain theoretical model of viscosity is far more attentive to structural detail in silicate and phosphate melts than others, and relates the chemical composition to viscosity with no compositional constraints. For this reason the Urbain method of viscosity calculation, discussed in Section 2.18.2, has been applied to this study.

6.1 Combustion of scrap tyres - the Elm Energy plant

The Ellingham diagram, a plot of the standard Gibbs free energy of formation of metal oxides versus temperature, provides immediate information about the free energy of reaction between any one element and the oxide of any other. All the reactions illustrated involve the consumption of one mole of oxygen in the formation of an oxide ($2x/yM + O_2 \rightarrow 2/yM_xO_y$) with an associated entropy decrease. With reference to the Ellingham diagram of Figure 6.1. it is evident that the reduction of ZnO by solid carbon would be thermodynamically favourable at combustion/gasification temperatures, by virtue of the following reaction:

$$2ZnO_{(s)} + 2C_{(s)} = 2Zn_{(g)} + 2CO_{(g)}$$

The reaction is favoured at high temperatures due to the increase in entropy associated with the formation of two moles of CO gas and zinc vapour. The standard free energy lines for the formation of ZnO and CO intersect at ~950°C, at which temperature the standard free energy change for the above reaction is zero. With increasing temperature the reduction of ZnO by carbon becomes increasingly more favourable. At combustion temperatures of 1000°C, for example, the reduction of ZnO would proceed spontaneously if the oxygen partial pressure of the system was less than 10^{-17}, equivalent to a CO/CO_2 ratio of <50/1 or a H_2/H_2O ratio of <40/1. At this temperature zinc, with a boiling point of 907°C[121], would assume the vapour phase.

In the cooler regions of a boiler, and in an oxidising environment, zinc would be a less stable vapour species and could reoxidise according to the following reaction:

$$Zn_{(g)} + 1/2O_{2(g)} = ZnO_{(s)}$$

ZnO would condense on heat transfer surfaces and on gas borne particles.

The combustion of PASH (sulphur-polycyclic aromatic hydrocarbons), tyre pyrolysis products, would introduce oxides of sulphur (SO_2 and SO_3) into the gaseous atmosphere of the reactor. The ratio SO_2:SO_3 is dependent upon the oxygen partial pressure of the system. Zinc vapour may also react with the sulphur oxide species, which at high oxygen fugacities would be present in the form of SO_2 in the product gas, and hence the pertinent reactions may be written as follows:

$$Zn_{(g)} + SO_{2(g)} + O_{2(g)} = ZnSO_{4(s)}$$

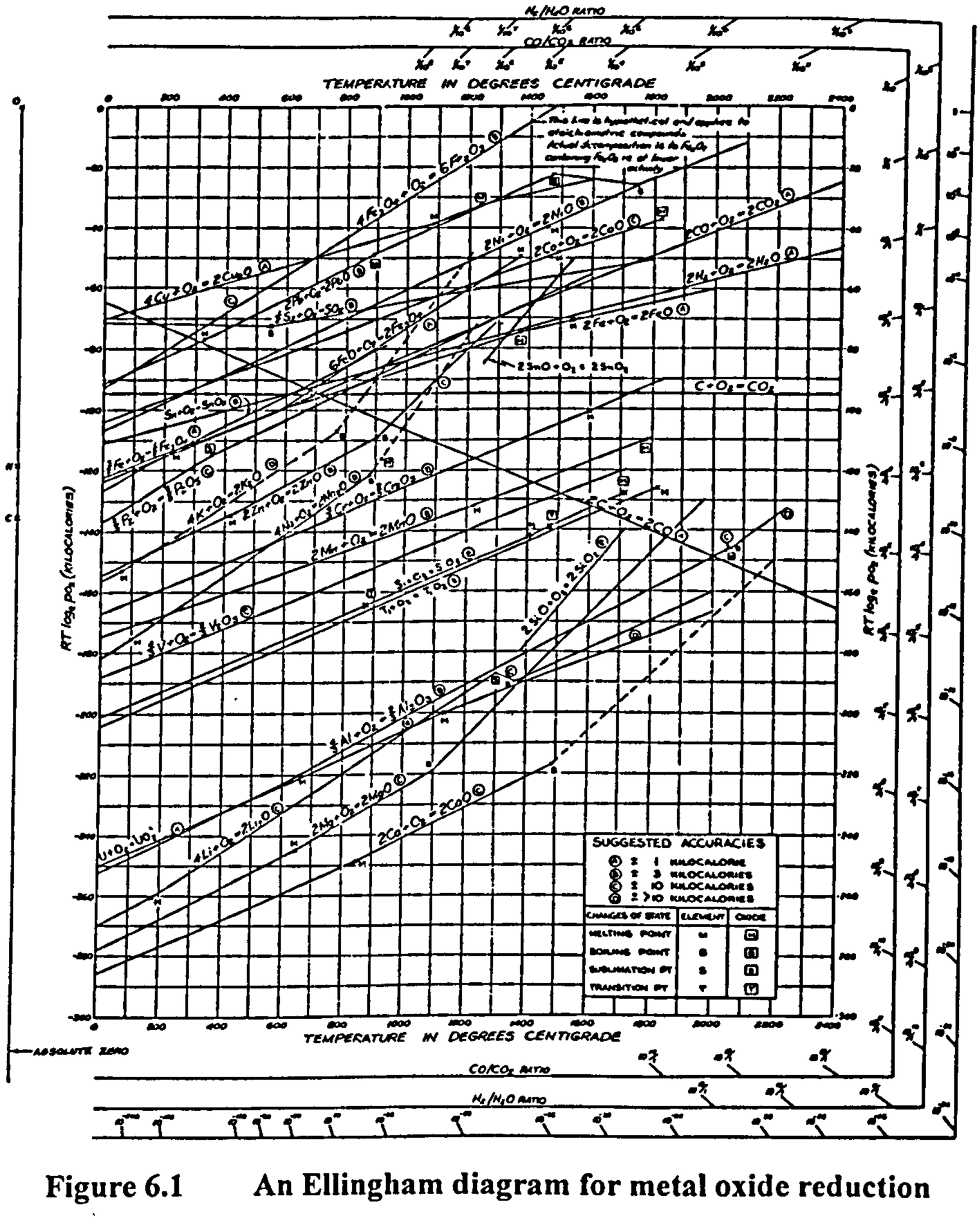

Figure 6.1 An Ellingham diagram for metal oxide reduction

The sulphation of lime, a decomposition product of $CaCO_3$, may also take place between entrained CaO particles and SO_2 gas. The reaction sequence may be summarised as:

$$CaCO_{3(s)} \rightarrow CaO_{(s)} + CO_{2(g)}$$

$$CaO_{(s)} + \quad SO_{2(g)} + \tfrac{1}{2}O_{2(g)} \rightarrow CaSO_{4(s/l)}$$

The sulphates are also expected to condense on tube surfaces and gas borne ash particles in the convective regions of the boiler. The condensed species, ZnO and $CaSO_4$, have high melting points (1975°Cand 1673°C respectively), while $ZnSO_4$ is said to decompose above 600°C. It is unlikely that eutectic liquids would be present at temperatures to be experienced in convective zones. Therefore, the formation of sulphate bonded deposits could occur by condensation/reaction of the sulphate directly from the vapour phase onto ash particle surfaces.

6.1.1 The tube deposit

A microstructural examination of a polished cross-section of the tube deposit from the Elm Energy car tyre incinerator revealed a highly porous assembly of sintered ash particles. As a consequence of the extensive porosity, the material was extremely friable and of low thermal conductivity. Fouling of the superheater tube was initiated by the deposition of a layer of ZnO, approximately 1mm in thickness, which evidently served to encapsulate other ash particles, the majority also coated in a thin layer of ZnO. The microstructure of the deposit bulk was characterised by amorphous/glassy aluminosilicate ash particles, of spherical morphology, bonded together by a condensed layer of ZnO. Further infilling of porosity had occurred with the formation of $CaSO_4$ and $ZnSO_4$ in the remaining voids. The condensed sulphates also played a significant role in particle bonding by the formation of an adhesive matrix.

It must be assumed that combustion temperatures in excess of 1200°C were experienced to account for the observed spherical morphology of the aluminosilicate ash, assumed to be of clay origin, and the nature of the particle-particle bonding. The surface of a liquid (or solid) has a higher energy than that of the bulk material, due to the presence of unsatisfied or distorted bonds, therefore the liquid strives to attain a state of minimum free energy by reducing its surface area. Since a sphere is the geometric configuration which has the smallest surface area for a given volume, molten ash particles assume a spherical form. A number of ash spheres were also observed to contain an intricate mesh of iron-rich crystals. The dendritic nature of the crystals indicates that the iron-rich species must have precipitated from a highly *viscous* silicate liquid. The latent heat of fusion, which represents the energy that is evolved as the disordered liquid structure transforms to a more stable crystal structure, must be removed from the solid-liquid interface before solidification is completed. In this case the recipient of the latent heat is a viscous molten silicate in which the mobility of molecular species is lower than in a liquid. In an attempt to increase the rate of evolution of the latent heat, a nucleus would develop protruberances which extend into the viscous melt. Heat would be removed more effectively from the tip of the protrusion than from the surrounding regions, and thus a dendrite arm would develop in the viscous environment and grow preferentially. An extensive network of secondary and tertiary dendrite arms would thus serve as a more efficient conductor of the latent heat to the undercooled melt.

To conclude, the problems of deposit formation in the Elm Energy plant were largely attributable to the inorganic fillers, such as ZnO, $CaCO_3$, and clay based materials, in the rubber compounds within the complex tyre structure. The formation of ash deposits on the heat transfer surfaces of scrap tyre incinerators continues to be major operational problem for their disposal by this route. Indeed during the course of the project, the Elm Energy plant was forced to close down after poor technical and commercial performance, and failure to operate to specification. At present, waste vehicle tyre incinerators are no longer operational in Britain. No immediate solution to this problem seems imminent as the relative ease of reduction of ZnO by carbon at the combustion temperatures, and the high volatility of zinc vapours will always lead to the condensation of these species somewhere in the system.

6.2 Short rotation coppice

The development of arable crops, farmed by short rotation coppicing techniques, as potential fuels for energy recovery processes is actively encouraged by both the EU and UK Government energy policies. Poplar and willow are decidedly the most suitable species for this method of cultivation providing high yields and a favourable net energy balance. The poplar and willow arable coppice for this study was obtained from Silsoe as the entire stem and foliage ('stick') and as chipped material. The chippings were reserved for a bulk ash analysis in order to compare the ash characteristics of poplar and willow species, and to invesigate the effect of different soil conditions on ash composition and hence fuel quality. The sticks were separated into fractions with the objective of ascertaining the distribution of inorganic material in sections and major tissues of the coppice sticks, and may have some bearance on the variation in fuel quality and the methods of sampling/comminution employed.

6.2.1 The coppice sticks

The moisture contents of the major tissues of a cross-section of the main stem were found to vary considerably from the bark (at around 60%) to the adjacent sapwood (40%) and heartwood (35%). The variations in ash content across the main stem were even more pronounced. The bark was considerably richer in inorganic constituents than the corresponding wood, with an ash content (4wt%), approximately four times that of the sapwood and heartwood. This comes as some surprise in view of the general

function of the elements of the vascular system, which provide a channel for the distribution of nutrients (mineral and organic) throughout the organism. In essence, the vascular system is composed of two distinct tissues; the xylem (sapwood, heartwood) and the phloem (inner bark). Inorganic matter moves from the soil into the xylem vessels of the root and is thereafter transported to the shoot/growing regions. Ions required for the growth and metabolism of the root cells are retained, surplus ions being released into the transpiration or root pressure stream. Xylem transport of minerals is essentially a unidirectional stream from the root to leaves/shoots. The concentration of salts established in the xylem fluid is many times that in the soil solution. Transport of the products of photosynthesis (sucrose in the majority of species) from the leaf down through the stem to the root is via the *phloem*. The inner bark is undisputedly the main channel for the transport of organic materials, and the sapwood is the major pathway for inorganic salts and metal chelates.[112,123] Thus the tissues of the xylem would be expected to possess a greater ash content than the phloem.

The heartwood represents xylem that has become superfluous for transport and reserve storage functions and from which nutrients may profitably be withdrawn for reutilisation elsewhere. Thus the heartwood is expected to possess the least moisture and ash contents of all the woody tissues of the vascular system. This assumption does indeed correlate with the experimental observations.

During a microstructural examination of the woody tissues of the poplar and willow species, inorganic matter was only found in the parenchyma cells of the phloem in the form of calcium oxalate crystals. Two distinct crystal morphologies were observed: multifaceted 'rosettes' and rhomboidal crystals, each evidently precipitated from solution. The crystal morphology may have been influenced by the degree of supersaturation of the salt solution and/or by the presence of inorganic impurities which can have a profound effect on the morphology of growth.

In the present study the observed enrichment of inorganic material in the bark may be explained, somewhat tentatively, by the withdrawal of calcium oxalate from the leaves to the phloem (i) as the organs senece as a means of nutrient storage, or (ii) to deter the invasion of wood boring/rotting insects and micro-organisms, indeed the morphology of the multifaceted calcium oxalate crystals would suggest such a function. The salts may also have been transfered laterally from the xylem for such purposes. Over relatively

minor distances, the inorganic species can travel within and between cells by diffusion and by cytoplasmic movement supplemented by active transfer across cell membranes.[122]

The implication of an ash-enriched tissue, which can effectively be stripped from the bulk wood, is of relevance to combustion/gasification systems in that processes which eliminate the bark significantly reduce the ash content and hence the rate of ash deposition. The difference between the ash content of wood and bark residues is further compounded by the increased probability of bark contamination, as experienced during timber production and forestry management practices which often introduce gross impurities such as soil, gravel and sand to the cork. Consequently the ash content is increased and represents a major variable in fuel quality. However, the removal of the bark from the wood core not only creates another operation in the comminution process, but also generates a waste. Although the ash content largely determines the rate of deposition, it is the composition of the ash that has a more profound influence on the slagging and fouling propensity of the process.

6.2.2 Prediction of slagging propensity

The ash chemistry of the major woody tissues of the stem were strikingly different. The poplar bark was rich in lime at 57wt%, in marked contrast to the sapwood (22wt%). Consequently, K_2O, P_2O_5 and SO_3 concentrations increased from bark to sapwood. In a discussion of slagging propensity, the influence of SO_3 can largely be ignored under the assumption that it is present as sulphate, for example $CaSO_4$ will be present as a solid and show little reaction with molten oxides. With the exception of SO_3, the ash contained three major oxides CaO, K_2O and P_2O_5, which together comprised over 80wt% of the bark LTA and ~67wt% of the remaining wood ash. For the purpose of this study, we may assume that the minor components of the ash have only a small effect on the ash behaviour, and normalise the composition to that of a three component mixture. However, apart from the KPO_3-$Ca(PO_3)_2$ pseudobinary within the CaO-P_2O_5-K_2O system, there is no other data available for this ternary system. The ash compositions were normalised and plotted on an equilateral triangle with each apex representing 100wt% of CaO, K_2O and P_2O_5, as shown in Figure 6.2. The composition of the bark was found to lie nearer the CaO-P_2O_5 binary eutectic boundary than the

pseudobinary. Thus it appears that a relatively basic binary system may provide some information regarding the ash fusion behaviour of the bark residues.

CaO and MgO in isolation are refractory oxides, but both have similar fluxing properties with phosphate melts, and for the purpose of this study may be assumed to be equivalent. (CaO+MgO) and P_2O_5 constituted approximately 82wt% of the bark ash. The composition of the poplar bark was normalised to that of two components and plotted on the $CaO-P_2O_5$ binary system, as shown in Figure 6.3.[124] On cooling from the binary melt, under equilibrium conditions, solidification would commence at 2020°C (the liquidus) with the nucleation of CaO. With decreasing temperature, CaO would continue to precipitate as the residual liquid becomes progressively enriched in P_2O_5. Due to the refractory nature of CaO at such concentrations, the viscosity of the residual melt is expected to decrease as the

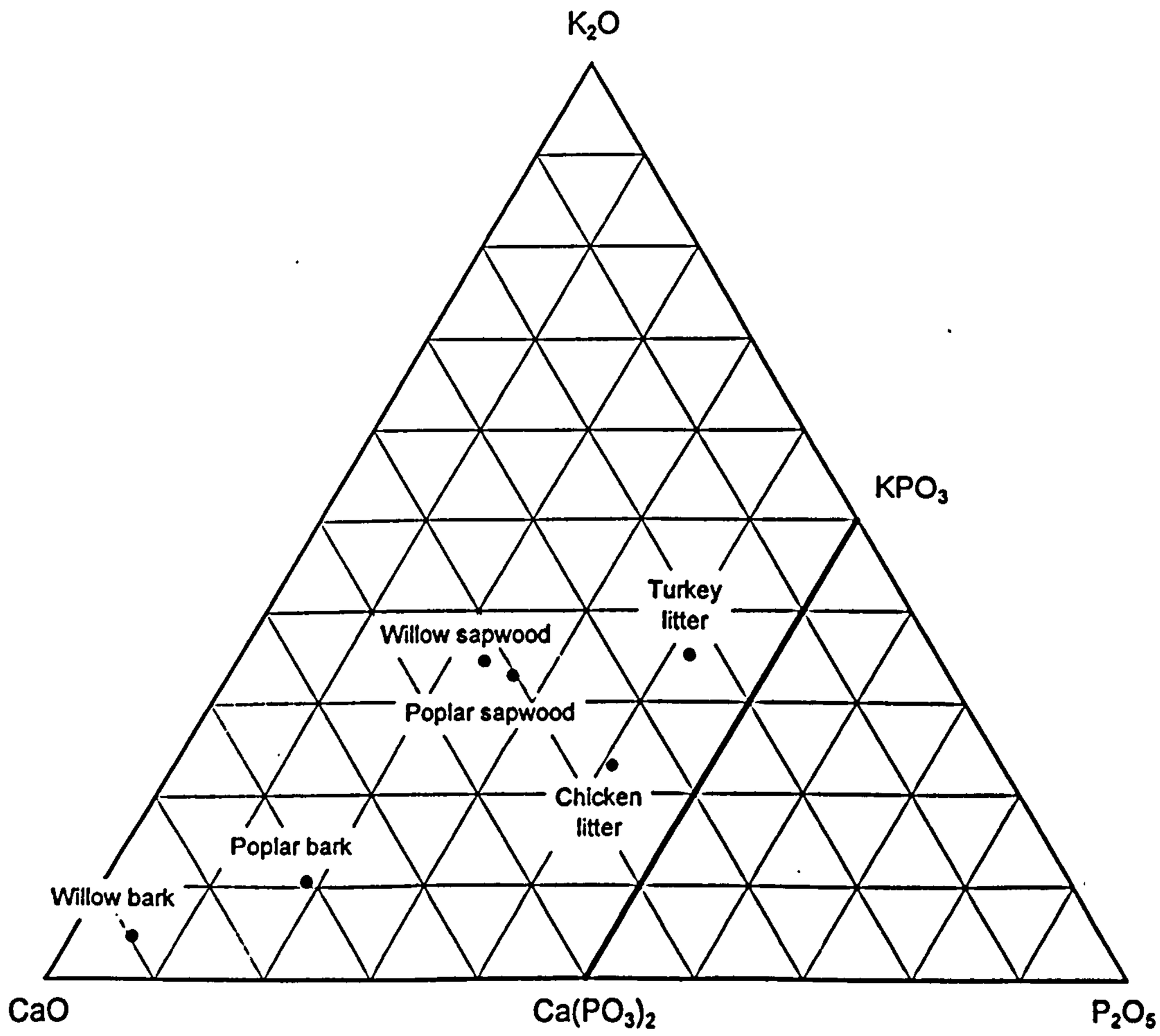

Figure 6.2 Normalised LTA compositions plotted on the the $CaO-P_2O_5-K_2O$ system

concentration of CaO is depleted. At 1630°C, all the liquid (~38% by the Lever Rule) is consumed as $4CaO.P_2O_5$ by virtue of the following peritectic reaction:

$$L + CaO \rightarrow 4CaO.P_2O_5 + CaO$$

The peritectic reaction takes place on the surface of CaO, and is thus a heterogeneous reaction. A solid phase of $4CaO.P_2O_5$ nucleates and grows as CaO dissolves. Non-equlibrium solidification of the peritectic reaction would result in the presence of a residual liquid below 1630°C if the primary phase had insufficient time in which to dissolve. Furthermore if, at the peritectic, the phase $4CaO.P_2O_5$ forms a continuous layer over the CaO precipitate the reactants (L + CaO) would be effectively separated by a solid coating of $4CaO.P_2O_5$. Under non-equilibrium conditions, the reaction does not have time to reach completion, since solid state diffusion is ~10^9 times slower than in a

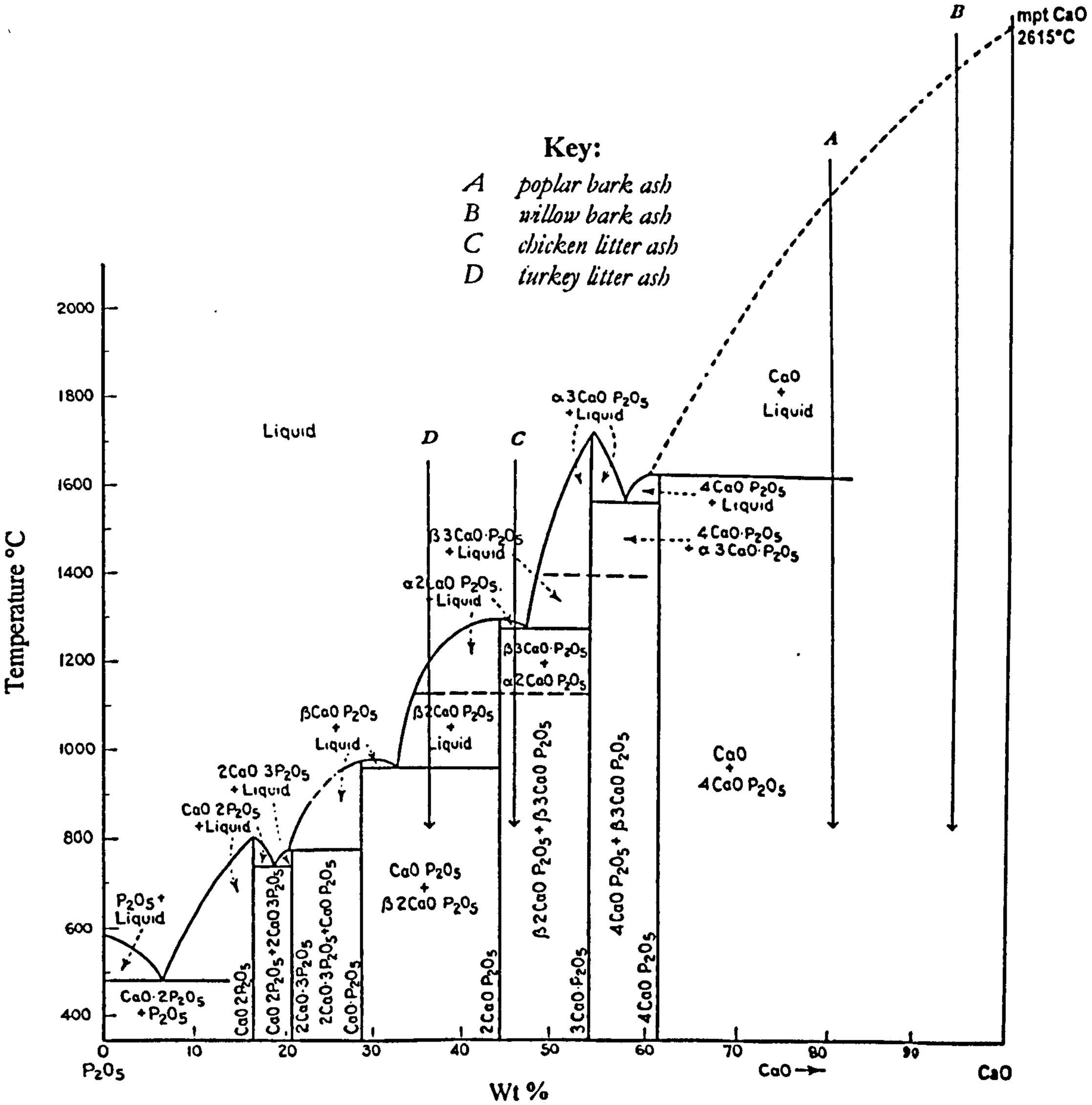

Figure 6.3 Binary equilibrium phase diagram for system the $CaO-P_2O_5$[124]

liquid, and the composition of the residual liquid would continue to follow the liquidus to the eutectic point at 1560°C, at which temperature the last trace of liquid would solidify as $3CaO.P_2O_5$ via the eutectic reaction:

$$L \rightarrow 4CaO.P_2O_5 + \alpha 3CaO.P_2O_5$$

Without more extensive equilibrium data available, one may speculate that the effect of K_2O on the $CaO\text{-}P_2O_5$ binary system would not be expected to alter the phases of the CaO-rich region of the $CaO\text{-}P_2O_5$ equilibria, although it is anticipated that the liquidus, peritectic and eutectic temperatures would be reduced by up to 100°C by an addition of 13wt% K_2O due to its fluxing properties in phosphate melts. In this approach, the implicit assumption has been made that the presence of other constituents in the ash have little influence on the ash fusion behaviour. However, the experimentally determined solidus and liquidus temperatures (900°C and 1500°C respectively) of poplar bark were found to be appreciably lower than those predicted, reflecting the network modifying characteristics of K_2O and Na_2O present in the bulk ash.

The Swanbourne willow bark was also found to be lime-rich, containing an outstanding 76wt% CaO, with K_2O, P_2O_5 and SO_3 constituting the remaining ash chemistry. On account of the high lime content of the willow ash, there appears to be less element of speculation in using the $CaO\text{-}P_2O_5$ binary system to predict ash fusion behaviour. The liquidus curve of the CaO-rich region of the $CaO\text{-}P_2O_5$ binary system was extrapolated to the melting point of lime. The predicted liquidus of the willow ash when normalised is thus estimated as 2200°C, notably higher than that of the poplar bark ash. The equilibrium solidification is much the same as described for the poplar bark, with only 15% of a liquid phase present at the peritectic, reflecting the increased precipitation of lime from the melt.

The xylem tissues (sapwood and heartwood) were found to be considerably richer in K_2O, at 21wt% and 25wt% respectively, than the neighbouring bark (8wt% K_2O). The binary system $CaO\text{-}P_2O_5$ would not provide an accurate description of the wood ash high temperature behaviour. However, one may speculate that the constitution of the wood ash, with an increased $K_2O{:}P_2O_5$ ratio, would favour the formation of liquids at lower temperatures than the more refractory lime-enriched bark. The wood ash melt is also expected to have a much lower viscosity than that of the bark ash. These

assumptions are based upon the experience of K_2O as a network modifier in phosphate melts and glasses.

With a distinct lack of thermodynamic and viscosity data to represent the bark and wood ash systems, an Urbain viscosity calculation has been applied to the bulk LTA composition, in order to illustrate the effect of K_2O on the viscosity of the respective melts. The graph of Figure 6.4 shows the presents the results of the Urbain calculation as a function of temperature. The viscosity of the sapwood is seen to be reduced by an order of magnitude in relation to the bark, reflecting the ability of K_2O to disrupt the ultraphosphate framework by increasing the number of non-bridging oxygen ions in the melt. Such viscosity predictions must be treated with great caution since the Urbain model is only known to work well with melts containing significant silica contents.

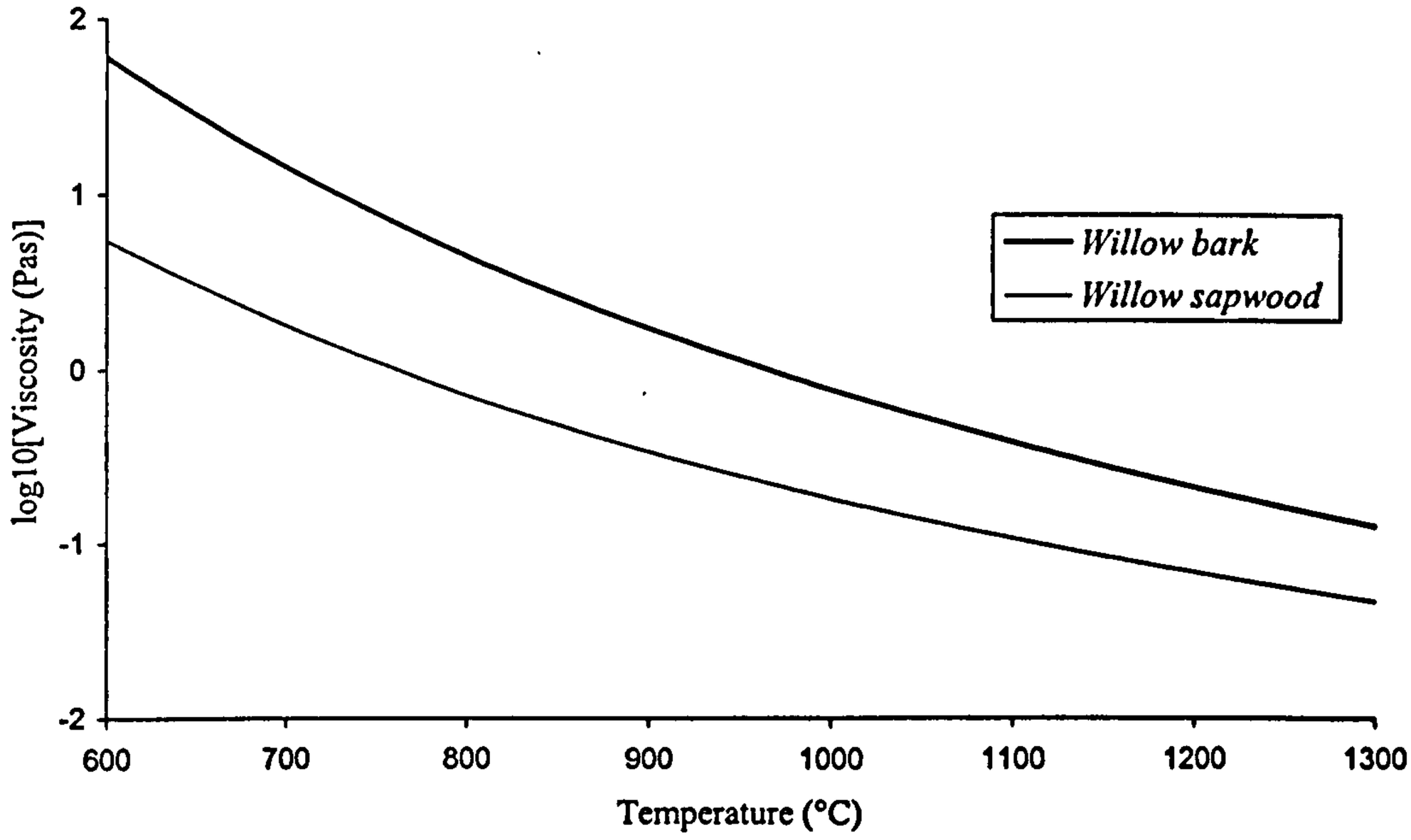

Figure 6.4 Urbain viscosity as a function of temperature for willow bark and sapwood LTA compositions

Although the ash content of the bark is four to five times that of the wood, the chemical composition is more refractory in character, suggesting a reduced slagging propensity. The increased solidus and liquidus temperatures (experimental and predicted) relative to the wood ash reflect the abundance of CaO in the bark. The calculated viscosity of the bulk and residual melts is approximately an order of magnitude greater than the wood ash and thus the tendency of a deposit to consolidate and gain strength is much reduced. The bark residue is thus beneficial to the high temperature ash properties of the fuel by raising the temperature at which liquids form and by increasing the viscosity of such

melts, thereby reducing the driving force for viscous flow sintering processes in deposits.

6.2.3 The poplar and willow chippings

In contrast to the bulk anatomy of woody stems, which predominantly consist of cellulose and lignin, the nature and concentration of the inherent inorganic material has been reported to vary with the particular conditions of the growth media. The ash characteristics of the poplar and willow species cultivated at different sites was investigated. The willow grown on-site at Silsoe (Bedfordshire) was found to be richer in lime (at 64wt%) than the willow from Long Ashton (at 32wt% CaO). Consequently the Long Ashton willow contained greater proportions of K_2O, P_2O_5 and SO_3. The Silsoe willow ash is more refractory in nature relative to the Long Ashton sample and thus a marked difference in ash fusion behaviour is anticipated. The results suggest that the Bedfordshire soil was more alkaline than that of the Bristol region, providing a nutrient medium rich in exchangeable Ca^{2+} ions. The difference in ash composition would seem to reflect the respective soil conditions and this would be a major variable in fuel quality for potential energy recovery processes.

Uptake of ions by plant roots has been shown to consisit of two phases: adsorption and absorption (accumulation). The adsorption phase is a physicochemical phenomena, is non-metabolic and is predominantly concerned with cations. The most generally accepted concept for the path which ions take from the soil to the root postulates an intervening liquid phase represented by the soil solution. The process is one of exchange in which H^+, generated by respiration, is released into the soil solution in return for essential cations; anions also essential for plant metabolism are exchanged for OH^- and HCO^{3-}. The renewal of such species is maintained in the soil by chemical decomposition and by microbial action.

Soils are complex physical, chemical and biological systems. The availability of inorganic matter for plant nutrition is conditional in the first instance upon the chemical composition of the local parent rocks, and of the minerals of natural waters.[123] Weathering of rock minerals yields soluble nutrient ions and clay particles. The latter species confer upon the soil a capacity to bind cations such as Na^+, K^+, Mg^{2+}, and Ca^{2+} by adsorption. In consequence such adsorbed cations account for most of the

exchangable ions in soils. By contrast the anions Cl^-, NO_3^- and SO_4^{2-} are effectively free species in the soil solution, dependent upon the rate of decomposition of the soil organic matter, and are thus readily leached from the soil. The mechanism of phosphate ion dissolution in the soil solution is more complex in nature due to the inherent insolubility of most naturally occuring phosphates, for example apatite. The PO_4^{3-} is, to some extent, adsorped at organic soil particle surfaces and may replace hydroxyl and silicate ions in clay structures, and react with Fe^{3+} and Al^{3+} ions forming soluble complexes. Exchangable phosphate is however only of significance in acidic soils of low Ca^{2+} content, where the soluble phosphate concentration is maintained by continuous release from almost insoluble, more complex, phosphates.

The uptake of a particular species is invariably selective; the relative concentrations of ions inside cells of the xylem differ, often strikingly, from their relative concentrations in the soil media. However, the adsorption of a particular ion is often markedly affected by the presence of other ions in the soil solution; for example Ca^{2+} and Mg^{2+} ions are often observed to compete with one another in the process of adsorption.

Turning to prospective boiler performance, the Long Ashton willow coppice is expected to be more problematic in terms of the ash residues than its Silsoe counterpart. This assumption is based upon the ash chemsitry, which contains higher concentrations of K_2O than the more refractory lime-rich Silsoe willow. The ability of K_2O to reduce the temperature of liquid formation and indeed the viscosity of liquids present, the consequence of which is to increase the tendency of particles to agglomerate via a viscous flow sintering mechanism, is profound.

Although the phase equilibria in the K_2O-P_2O_5 system has not been studied in any great depth, an analogy with the K_2O-SiO_2 system (Figure 6.5[125]) would suggest that the solidus and liquidus temperatures could be reduced by some 200°C by the network modifying properties of K_2O. The predicted increase in slagging propensity with an increase in K_2O content is veritably reflected by the results of the high temperature microscopy of the ashes, which indicated a decrease in solidus and liquidus temperatures for the Long Ashton willow by up to 250°C relative to the Silsoe ashes.

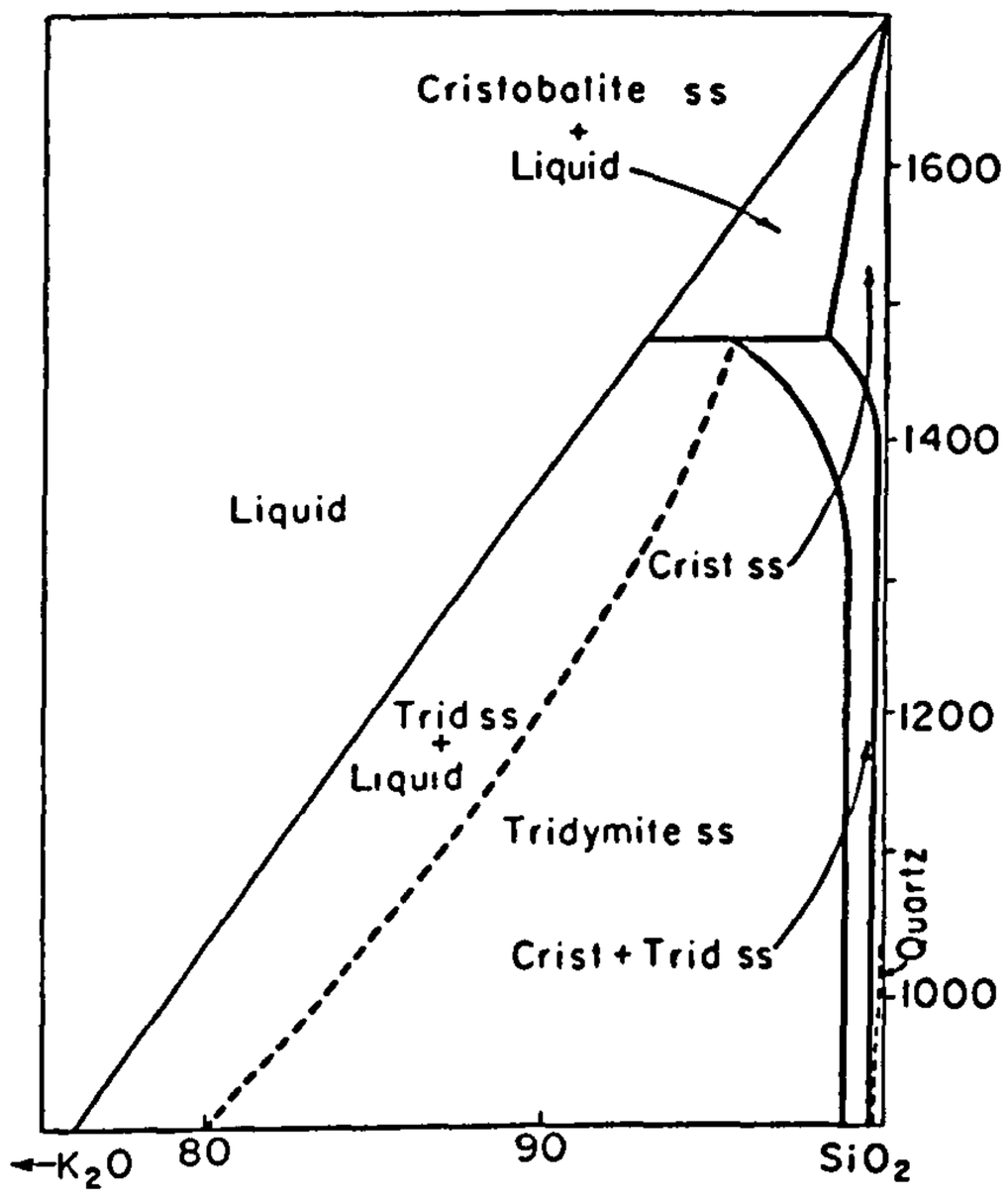

Figure 6.5 K_2O-SiO_2 system[125]

The determination of phase equilibria by experimental means can be a lengthy process. However, phase equilibria in multicomponent systems can now be predicted from thermodynamic data by employing a computer generated free energy minimisation technique. Computer programs are available, such as the systems run by NPL (National Physical Laboratory). This type of approach would in itself constitute a major, potentially valuable, study.

6.2.4 TPS cyclone ash

The results of the characterisation of the cyclone dust samples were somewhat encouraging. The constitution of the ashes were found to be refractory in nature, attributable to the major components CaO and MgO. A microstructural examination of the samples in cross-section revealed no evidence of particle-particle interaction and therefore no indication of incipient fusion or sintering of the ash. The TPS plant incorporated a tar cracker with a dolomite ($CaCO_3.MgCO_3$) catalyst. Since MgO was not found to be a major constituent of willow ash, it is probable that the appreciable quantities of MgO in the ash were derived from the dolomite catalyst. Indeed, the CaO:MgO ratios, although greater than one, indicate that dolomite may be present in the ash, bearing in mind that the willow ash is itself CaO-rich. The products of the decomposition (pyrolysis) of wood, or for that matter any carbonaceous fuel, are comprised of a char, gases and condensable hydrocarbons or tar vapours. The tar yield

is related to the volatile matter in the fuel, which for woody biomass is relatively high. The effective and thorough cracking of the tars to non-condensible, combustible gaseous products is a prerequisite if the product gas is to be compressed to feed a gas turbine. A cause for concern in the TPS gasifier is the fate of the condensible hydrocarbon products of wood pyrolysis. The deposition of the tars on heat transfer surfaces in the boiler would serve to encapture gas borne ash particles. The nature of boiler deposits that may form are likely to be organically bound refractory ash particles.

6.3 Poultry Litter

6.3.1 The fuel

The poultry litter was characterised by a CaO and P_2O_5 rich ash, with appreciable quantities of K_2O and SO_3. The ash is therefore sold as a fertilliser. X-ray diffraction analysis of the LTA revealed the presence of two crystalline phases, hydroxyapatite [$Ca_5(PO_4)_3(OH)$] and arcanite (K_2SO_4). Hydroxyapatite is a compound of great stability with regard to decomposition, and exhibits relative insolubility in aqueous, acidic and alkaline solutions. The compound is the principal inorganic constituent of bone. To encounter such a stable compound, with respect to hydrolysis and pH, in a poultry litter LTA suggests that a probable origin of hydroxyapatite is in the feed matter. Calcium and phosphorus are essential nutrients for most fowl (the metabolism of phosphorus is largely related to that of calcium), and their body matter is generally found to be saturated in calcium salts, principally to precipitate calcite ($CaCO_3$) in the formation of egg shells. However, hydroxyapatite does not appear to have been absorbed by the body, and thus its presence as a nutritional additive of the feed is questionable. A plausible, if somewhat disturbing, explanation is that hydroxyapatite was derived from bone matter in ground animal remains. Thus nutritional practices do not appear to have changed in response to adverse publicity.

6.3.2 Prediction of slagging propensity

The composition of chicken and turkey litter consists of four major oxides: CaO, K_2O, P_2O_5, and SO_3. If one assumes that SO_3 and K_2O are combined as K_2SO_4, then the remaining oxides are essentially CaO and P_2O_5 and the slagging propensity can be considered as a 'simple' binary system.

The $CaO-P_2O_5$ system

Chicken litter

The equilibrium solidification sequence is as follows:

at 1270°C, the liquidus temperature L → $\alpha 2CaO.P_2O_5$

at 1255°, the solidus L → $\alpha 2CaO.P_2O_5 + \beta 3CaO.P_2O_5$

At temperatures below the solidus, the liquid is entirely consumed and the eutectic mixture is composed of 85% $\alpha 2CaO.P_2O_5$ and 15% $\beta 3CaO.P_2O_5$.

Turkey litter

at 1160°C, liquidus L → $\alpha 2CaO.P_2O_5$

at 1120°C, phase change L → $\beta 2CaO.P_2O_5$

at 950°C, binary eutectic L → $CaO.P_2O_5 + \beta 2CaO.P_2O_5$

Below 950°C, equilibrium phases present are 54% $CaO.P_2O_5$ and 45% $\beta 2CaO.P_2O_5$.

As one can see from Figure 6.3, there are many different compounds in the $CaO-P_2O_5$ system, highlighting the complex nature of calcium phosphate crystal chemistry. With increasing P_2O_5 concentrations, the eutectic temperatures progressively decrease to 480°C at 6.5wt% CaO. Due to the heterogeneous nature of the fuel, regions rich in phosphate could have liquids present at much lower temperatures than indicated by the bulk composition.

6.3.3 Straw ash characteristics

The wheat cereal straw was characterised by a silica-rich ash (71wt% SiO_2), with the silica present predominantly as quartz. The deposition of silica in grasses, including cereals, undoubtedly conveys strength and stiffness to the stem structures. The straw LTA was found to contain three major components: SiO_2, CaO and K_2O which together comprised 93wt% of the ash. When the composition is normalised to these three components and plotted on the K_2O-CaO-SiO_2 ternary phase equilibrium diagram of Figures 6.6(a) and (b)[126], the composition of the straw LTA is found to lie in the silica-rich corner of the ternary system, within the compatibility triangle bounded by SiO_2, $K_2O.2CaO.9SiO_2$, and $K_2O.4SiO_2$. Equilibrium crystallisation of the melt would begin with the nucleation of tridymite at the liquidus temperature of ~1160°C. The solidification sequence would involve a binary eutectic reaction ($L \rightarrow SiO_2$(tridymite)$+K_2O.2CaO.9SiO_2$) at ~1100°C,

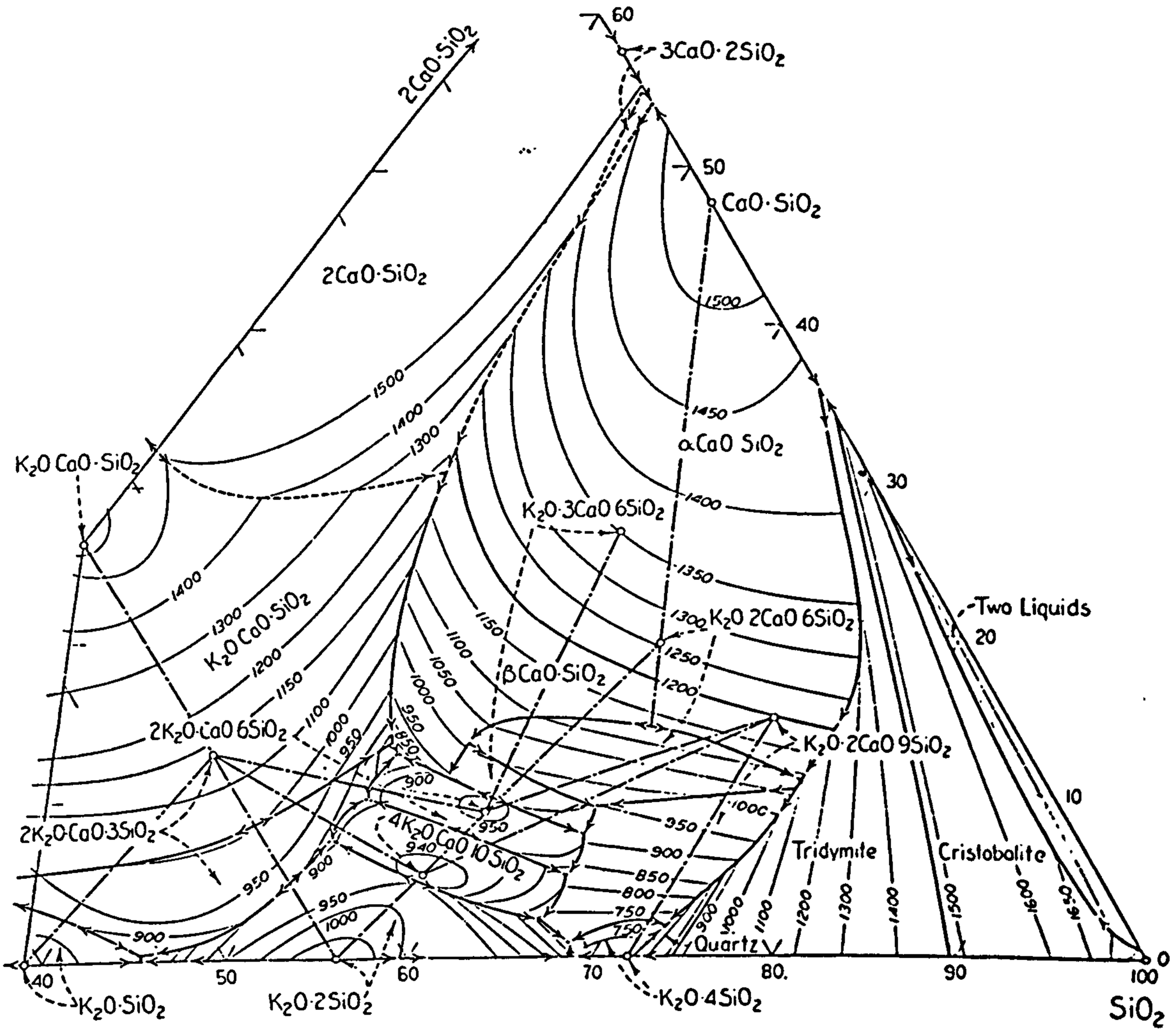

Figure 6.6(a) K_2O-CaO-SiO_2 phase equilibrium diagram[126]

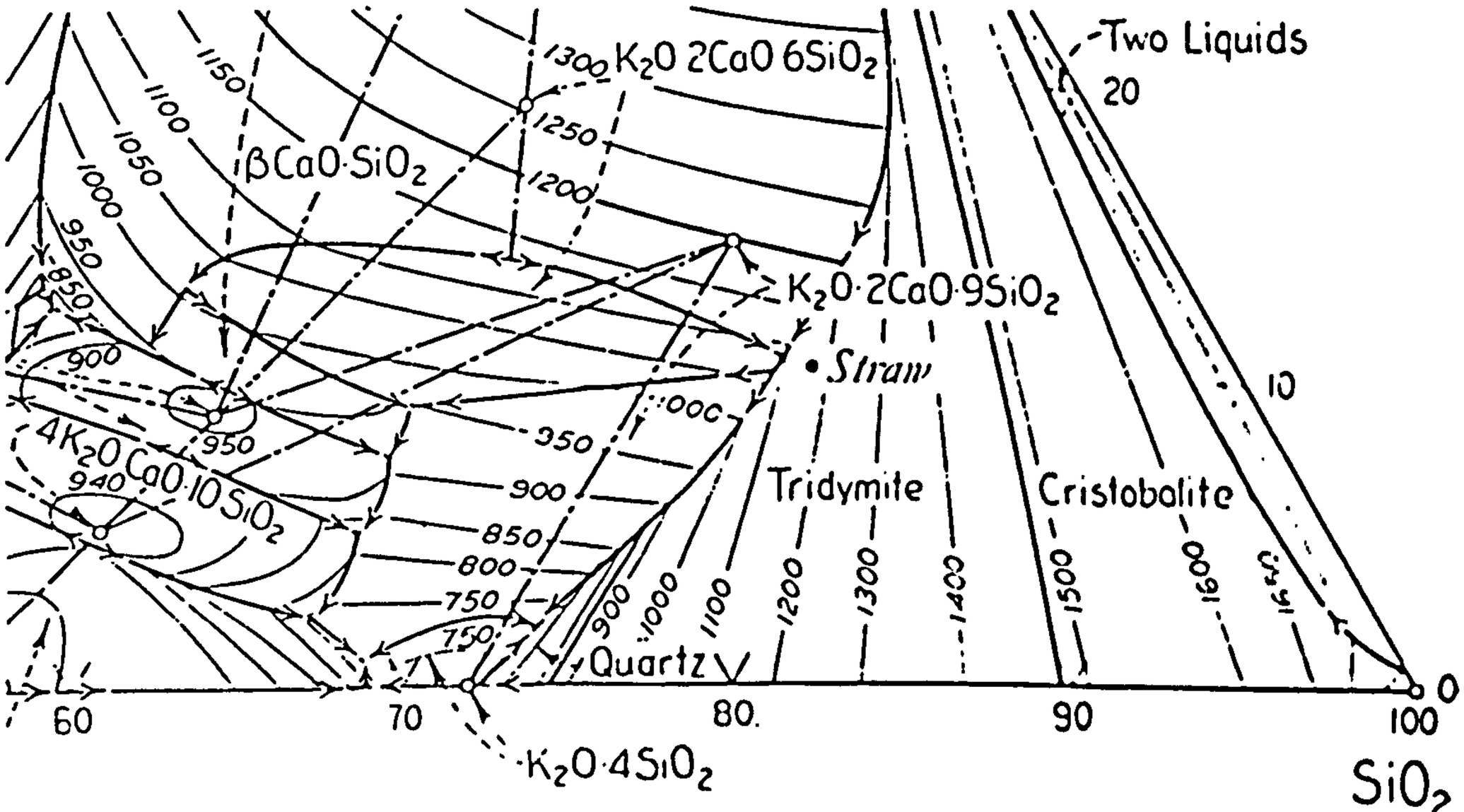

Figure 6.6(b) Silica-rich section of the K_2O-CaO-SiO_2 system

proceeding to the ternary eutectic reaction at ~725°C during which all the remaining liquid (~13.6%) is consumed:

$$L \rightarrow SiO_2(quartz) + K_2O.2CaO.9SiO_2 + K_2O.4SiO_2$$

The calculated Urbain viscosity of the eutectic liquid, of composition 72.5wt% SiO_2, 1.7wt% CaO and 25.8wt% K_2O, is ~1.66×10^9 Pa s at 725°C. The consequence of increased concentrations of straw in the chicken litter would be to increase the viscosity of liquid phases present and thus decrease the slagging propensity of the ash. The viscosity of the bulk ash melt as a function of temperature has been determined using the Urbain method, and the results of the calculation are shown Figure 6.7. At any one temperature, the viscosity of the straw ash melt is at least three to four orders of magnitude greater than that of the chicken litter ash system, reflecting the increase in covalent bonding of the silica-rich framework of the straw ash melts. The Urbain viscosity-temperature relationships are based upon a fixed composition, and although the composition of a residual liquid phase is variable, the graphs provide valuable information on the sensitivity of the viscosity at any one temperature to the ash composition, in particular the alkali and silica content.

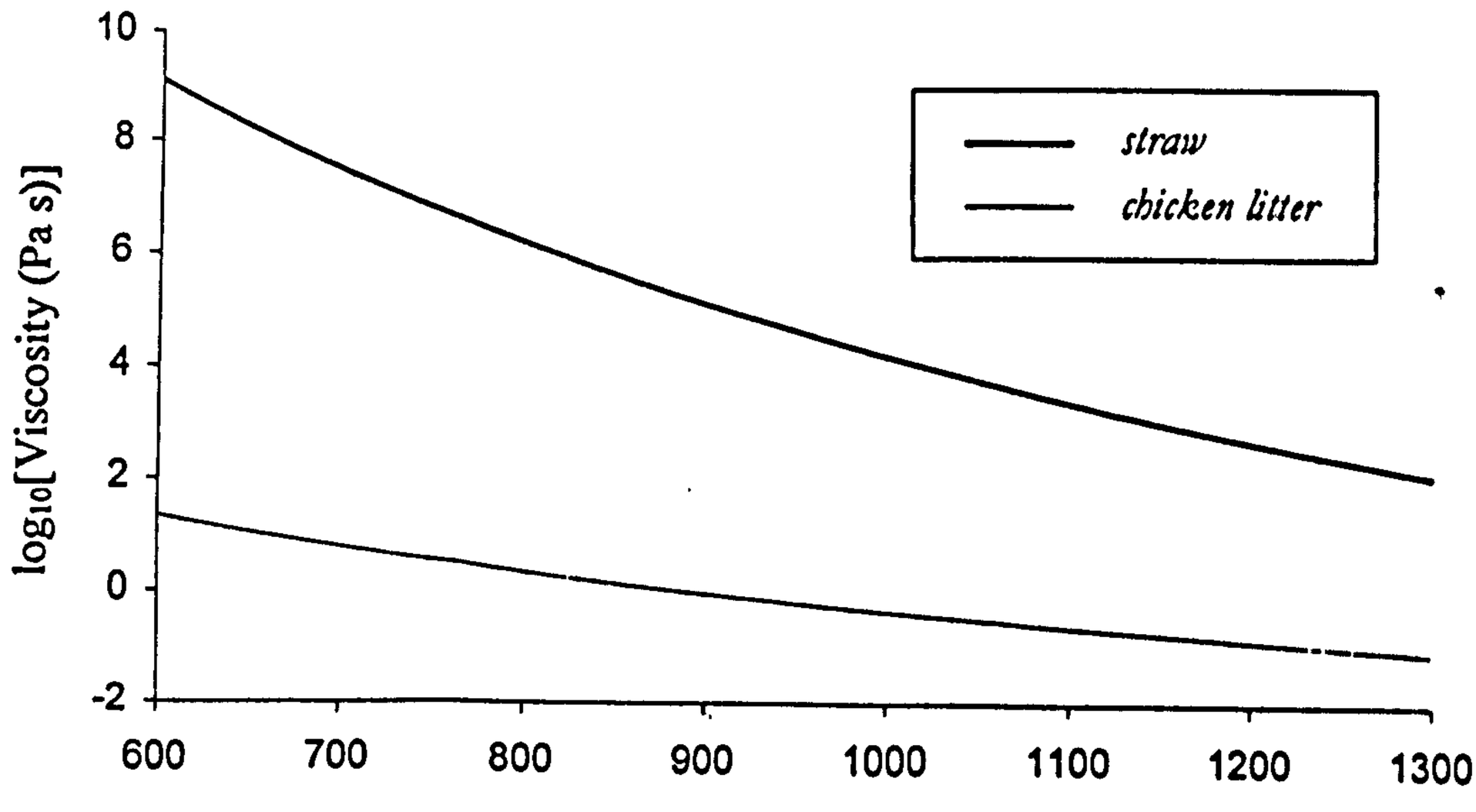

Figure 6.7 **Urbain viscosity as a function of temperature for straw and chicken litter LTA compositions**

6.3.4 Danish pine

The most appropriate system of phase equilibria to describe the high temperature behaviour of pinewood ash is the CaO-Al_2O_3-SiO_2 ternary. These three oxides comprise over 85% of the bulk ash composition. When the normalised composition is plotted on the CaO-Al_2O_3-SiO_2 phase diagram, as in Figure 6.8[94], the ash is seen to lie within the primary field of anorthite with a liquidus temperature of 1345°C. The equilibrium solidification sequence is as follows:

at the liquidus, 1340°C	$L \rightarrow CaO.Al_2O_3.2SiO_2$
at 1270°C	$L \rightarrow CaO.Al_2O_3.2SiO_2 + 2CaO.Al_2O_3.SiO_2$
at the solidus, 1265C	$L \rightarrow CaO.Al_2O_3.2SiO_2 + 2CaO.Al_2O_3.SiO_2 + CaO.SiO_2$

The microstructure of the solid would consist of a heterogeneous polycrystalline assembly of primary anorthite, the secondary anorthite + gehlenite, and ternary anorthite + gehlenite + pseudowollastonite eutectic reaction products. The quantity of liquid present at the solidus may be calculated from the tie-triangle [anorthite-gehlenite-eutectic(ternary)]. Thus ~75% of a liquid phase of composition 41.0wt% SiO_2, 38.5wt% CaO and 20.5wt% Al_2O_3 would be first to appear on fusion. A liquid of this composition would have a viscosity of ~23.65Pa s at the ternary eutectic temperature, as estimated using an Urbain method of viscosity calculation.

High temperature microscopy observations suggest that the solidus temperature of the pinewood LTA is essentially 600°C lower than the predicted solidus; such a difference is inherently due to the network modiyfing characteristics of MgO (2wt%), K_2O (3wt%), Na_2O (1wt%), MnO (2wt%), and Fe_2O_3 (4wt%). The nature of Fe^{3+} ions in glasses and melts is rather ambiguous, although the Urbain method can be used to calculate the viscosity of the bulk melt using either valency state. In the reduced state, Fe^{2+} exhibits increased fluxing properties compared to the 3+ oxidation state, and consequently is of pertinence to gasification processes in which the atmosphere is predominantly reducing.

It has been reported that the constitution of the poultry litter fuel is subject to variation and the supply of a consistent quality feed is not guaranteed. Other waste biomass and farming residues, including horse bedding (principally sawdust) and duck litter, is also added to the fuel. Gross mixing of the boiler feed occurs in the fuel halls. Each material will have a unique constitution and further work would be required to establish

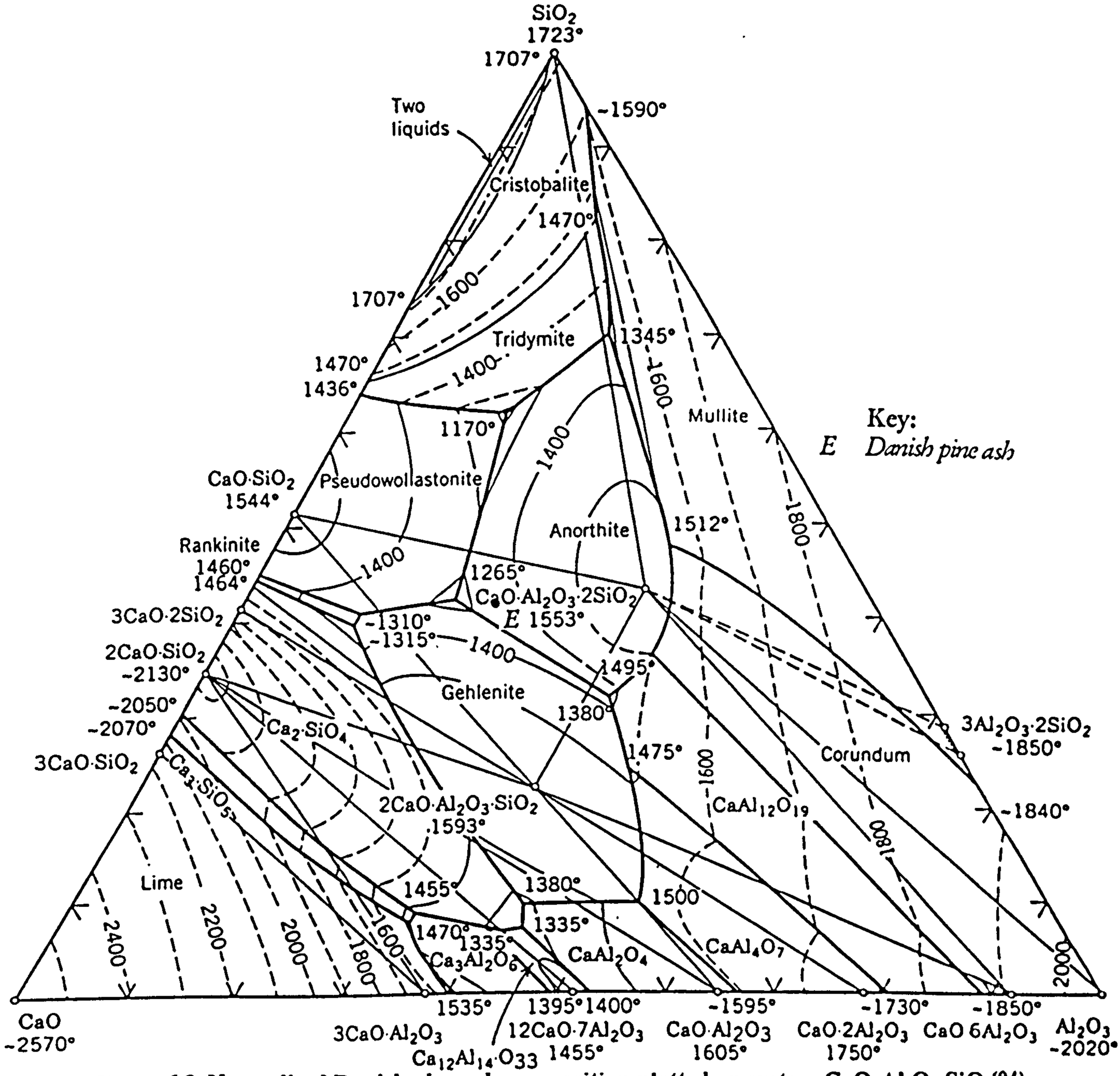

Figure 6.8 Normalised Danish pine ash composition plotted on system CaO-Al_2O_3-SiO_2[94]

the range of ash compositions to be encountered and their relative and mutual slagging and fouling propensities. Increasing the concentration of pinewood in turkey litter would inevitably increase the slagging propensity with the formation of relatively low viscosity liquids at 650°C or so.

6.3.5 The Eye boiler slags

One of the problems encountered at the Eye power station has been the higher than anticipated moisture content of the fuel. On entering the boiler the fuel must first be dried before combustion can commence. A consequence of this has been a higher than

acceptable level of unburned carbon in the ash leaving the grate. A recent modification to the boiler has been the installation of a refractory panel which receives radiant heat from the combustion zone, but which can also radiate this heat onto the incoming wet fuel. It was thus hoped that drying would occur more readily and that combustion would start at an earlier stage on the grate. The consequence of such an addition to the furnace was twofold: the first was to increase gas temperatures and hence power output, and the second was to increase the slagging propensity of the inorganic matter in the fuel, the two being inextricably linked. The results of a characterisation of the boiler deposits (Eye II and III) are in support of the above predictions with evidence of the crystallisation of liquid slags following ash deposition. The EDS compositions of the Eye II and III slags were similar to the bulk composition of the fuel itself, with the exception of silica which was found to be of increased concentration in the deposits. The slags contained similar microstructural features. The phase most characteristic of each deposit was that of $KCaPO_4$, also identified as the major phase by X-ray powder diffraction. A distinct coarsening of the microstructure was observed from the fireside to the refractory surface of Eye II. The microstructure of Eye III contained even larger $KCaPO_4$ grains, with evidence of their coalescence during growth, suggesting that either higher temperatures were experienced during deposit formation, or that the deposit had remained in the furnace for a longer period of time to permit the diffusion of K^+, Ca^{2+}, and PO_4^{2-} species through the viscous melt to the phase boundary.

The driving force for particles to undergo a coarsening process is the reduction of interfacial energy associated with increase in crystal size (Ostwald ripening). For a system in which the dispersed particles exhibit some solubility in the surrounding matrix (liquid or solid), particles greater than a critical size grow at the expense of the sub-critical sized crystals, which dissolve. The variation in particle size represents a concentration gradient (variation in chemical activity) from particle to particle. The dissolution of small particles contributes solute to the matrix, the solute is then forced to migrate through the matrix under the influence of the concentration gradient, and to then precipitate on the surface of larger particles.

The rate of growth of particles in a viscous medium is limited by ion mobility and thus there is a tendency for the growth process to be controlled by material-transfer processes. For a crystalline phase to increase in size, material must be transported to the

crystal-melt interface, and in so-doing must acquire an activation energy to detach itself from the attractions of neighbouring ions. The motion of ions in condensed matter is thus a thermally activated process. Since transport-limited kinetics are assumed, the temperature dependence is largely determined by the exponential temperature dependence of diffusion. The historical basis for the effect of temperature on the rate of the growth process is the Arrhenius equation, in which it is found that the diffusion coefficient (D) is given by $D = D_o exp[-\Delta G/RT]$, where ΔG is the activation energy, D_o a constant, and R the gas constant. Thus at higher temperatures the chemical driving force for the activated process increases as the thermal energy to motivate diffusional process and reaction kinetics increases. In a multicomponent melt, in which regions of heterogeneity exist, the diffusion coefficient is expected to vary. For example, in silicate glasses, as the amount of modifying cations are increased, the activation energy for their diffusive transport increases, and the diffusion coefficient increases. These changes presumably reflect the break up of the network and a decrease in the average interionic separation. Divalent cations diffuse much more slowly at a given temperature than monovalent cations, being more strongly bonded to the network structure, and their activation energies are generally much larger.

The microstructure of the fireside region of the deposit Eye II featured quartz grains surrounded by a solution rim of a high silica glass. Characteristic microstress cracks were observed; the cracks were caused by the α-β quartz transformation at 572°C. Although quartz is generally inert up to the melting point of 1723°C, rounding of the edges of quartz grains could occur at temperatures of ~1250°C[83], with the formation of a solution rim. With an increase in temperature, the quantity of the high-silica glass around the quartz grains would increase. No evidence of transformations into tridymite or cristobalite polymorphs was apparent, hence conditions of equilibrium were not established to permit the occurance of these reconstructive transformations which are known to be very slow. In the refractory region of Eye II and in Eye III, quartz grains were not observed, and thus assumed to have dissolved. In the presence of modifying cations, such as K^+, Na^+, Ca^{2+} and Mg^{2+}, the melting point of quartz would be significantly reduced. The bulk compositions of the Eye boiler slags contained substantial quantities of CaO (22-26wt%) and K_2O (17-18wt%), in addition to ~6wt% MgO and ~3wt% Na_2O. With reference to the studies of Kalmanovich[93] the melting

point of quartz could easily be reduced by 200-300°C by the cummulative fluxing influence of such alkali and alkaline earth metal species.

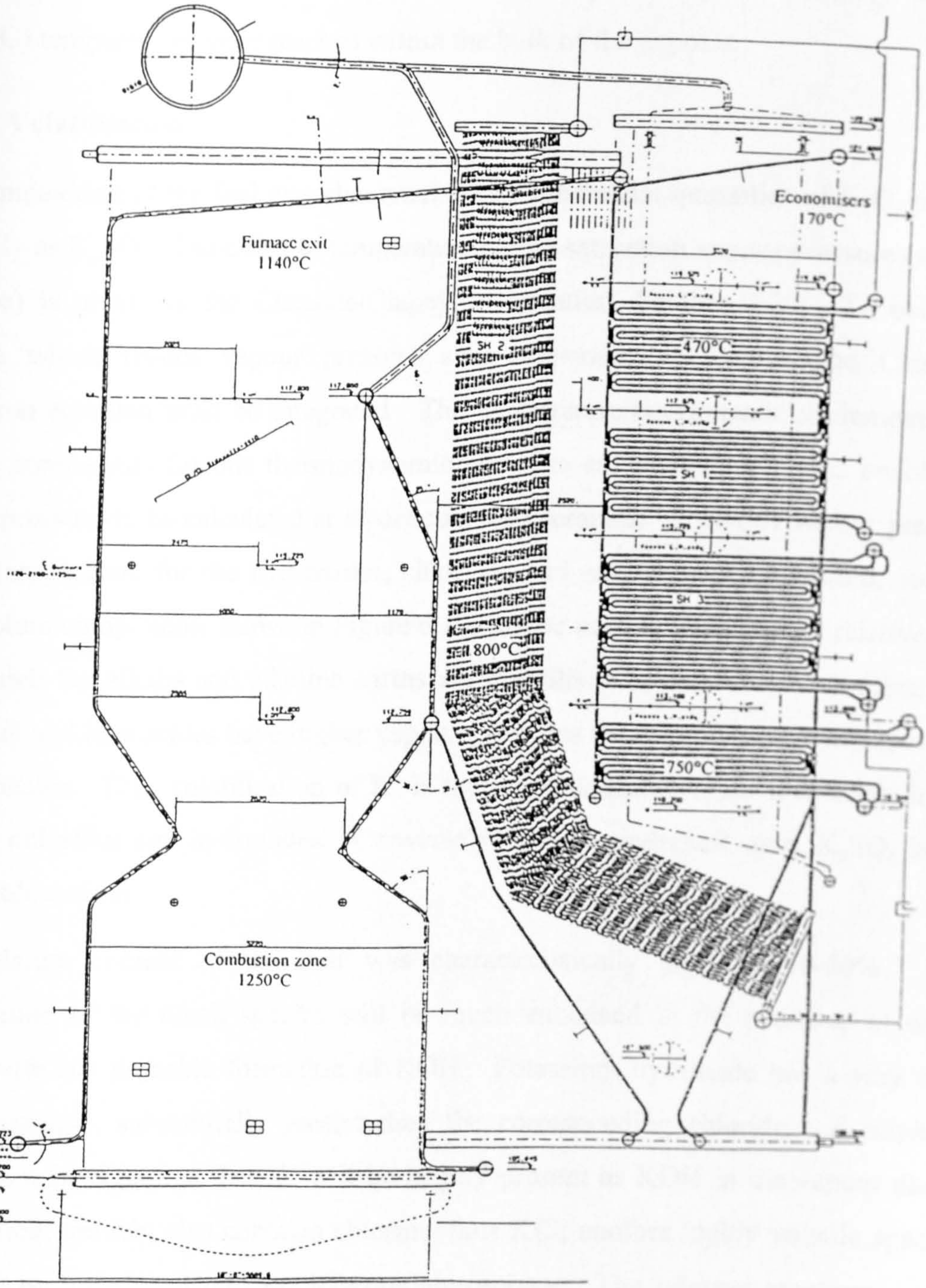

6.9 Eye boiler design temperature specifications

The design temperature specifications of the Eye boiler are indicated in the graphic projection of the plant construction in Figure 6.9. Microstructural evidence suggests that local gas temperatures in the region of deposit formation were 150-200°C higher than the design temperature for the furnace (1250°C). As a deposit accumulates, the temperature gradient between the refractory lined water wall and the outer surface

increases due to the insulating properties of the deposit. Therefore it is reasonable to assume that, with increased ash deposition, solidus (1075°C), and possibly liquidus (1205°C) temperatures were reached within the bulk of the deposit.

6.3.6 Volatilisation

The composition of the fuel was characterised by substantial quantities of K_2O, present primarily as K_2SO_4. The effect of temperature on the saturation vapour pressure (vapour pressure) is given by the Clausius-Clapeyron equation, Section 2.20. To obtain a formula which relates vapour pressure and temperature explicitly, the Clausius-Clapeyron equation must be integrated. The temperature coefficients of elements and volatile compounds for this thermodynamic equation are published[46], and enable the vapour pressure to be calculated at a particular temperature. A plot of vapour pressure versus temperature for the hydroxides, chlorides and sulphates of potassium, sodium and calcium compounds, shown in Figure 6.10, can be used to illustrate the relative ease with which the alkalis and alkaline earths are volatilised at combustion temperatures. Chlorides and hydroxides have higher vapour pressures than their corresponding oxides and sulphates. Thus volatilisation of K^+ is thermodynamically more favourable in the form of chlorides and hydroxides. Conversely, in the condensed state, K_2SO_4 is the most stable species.

The moisture content of the fuel was characteristically high, at 50-60%. The volatilisation of the alkali species will be much enhanced in the presence of water vapour with the probable formation of KOH. Potassium hydroxide has a very high vapour pressure, substantially greater than the corresponding chloride and sulphate. Therefore it is suggested that K^+ will be largely present as KOH in the vapour phase. Furthermore, the fuel also contains chlorine, thus KCl, another highly volatile species, may also be introduced into the gaseous atmosphere. The relevant reactions are as follows:

$$K_2SO_{4(s)} \rightarrow K_2SO_{4(l)}$$

$$K_2SO_{4(l)} \rightarrow K_2O_{(l)} + SO_{3(g)}$$

$$K_2O_{(l)} + H_2O_{(g)} \rightarrow 2KOH_{(g)}$$

$$K_2O_{(l)} + Cl_{2(g)} \rightarrow 2KCl_{(g)} + \tfrac{1}{2}O_2$$

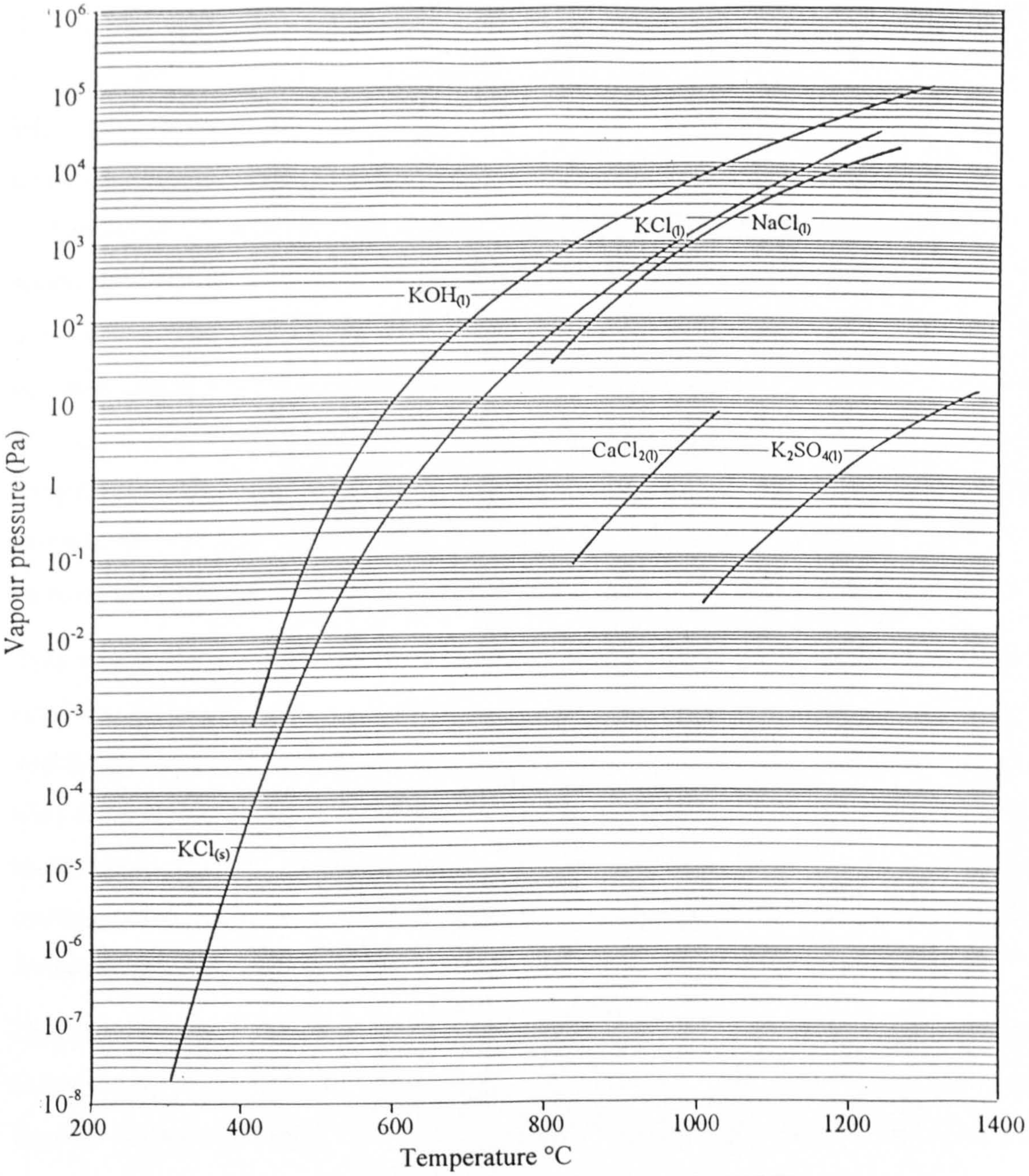

Figure 6.10 Vapour pressure versus temperature for KOH, KCl, K_2SO_4 NaCl and $CaCl_2$

The volatilised alkali species, transported via vapour diffusion, may condense on heat transfer surfaces and on gas borne particulates, or may react with SO_2/SO_3 to form K_2SO_4 in the cooler boiler reaches.

The LTA was also found to contain hydroxyapatite. Hydroxyapatite does not readily lose OH from the crystal lattice, and remains stable up to 1000°C.[105] Above 1500°C the compound decomposes into a mixture of tricalcium phosphate and tetracalcium phosphate.

$$Ca_{10}(PO_4)_6(OH)_2 \rightarrow 2Ca_3(PO_4)_2 + Ca_4P_2O_9 + H_2O$$

The melting points of the phosphates produced on decompostion are high, $Ca_3(PO_4)_2$ (1730°C) and $Ca_4P_2O_9$ (~1630°C from the phase diagram of Figure 6.3) and are thus inherently stable at high temperatures. If the solid products are elutriated by the combustion gases, condensation of K_2SO_4 on the surface of particles would increase the probability of adhesion to a tube surface or on collision with another ash particle. Any solids elutriated by the product gases would be relatively small, discrete particles. Once a bond has been established between two particles, with reference to the Frenkel equation (Section 2.16.3) the driving force for the sintering process will be dependent on the particle size and on viscous flow through the sulphate medium. Although the temperatures are much lower in the convective passes than in the radiant zones of the furnace, the comparatively small size of particles transported by the flue gas would increase the propensity of sintering, once an initial bond had formed between particles.

Two deposition mechanisms appear to exist. The volatile alkali species can either condense homogeneously from the flue gas forming partially molten or solid phases which can subsequently adhere to cooler surfaces; or nucleate on a substrate, such as a tube surface or entrained ash particle, with growth directly from the vapour phase. Both mechanisms probably operate and will be dependent upon concentration, temperature, melting points of the condensed alkali phases, and the availability of suitable substrates for heterogeneous nucleation.

Higher combustion temperatures will increase the volatilisation of alkali species and subsequently lead to enhanced deposition of K^+, Na^+, Ca^{2+}, Mg^{2+} and SO_4^{2-} occur on heat transfer surfaces in the boiler. Thus gas temperatures are critical variables in this process.

6.3.7 The superheater deposit

As predicted from thermodynamic data, K_2SO_4 was indeed found to condense on superheater tubes and on the surface of ash particles in the convective regions of the boiler. The microstructure of the deposit was characterised by spherical calcium-potassium phosphate particles engulfed in a matrix of K_2SO_4. Fouling of the convective passes of the Eye boiler was initiated by the condensation of K_2SO_4 on tube surfaces and on gas borne ash particulates. The viscid surface layer of sulphate on boiler tubes served to encapture all manner of impinging ash particle. Increased ash deposition via

the aforementioned mechanism would increase the temperature of the local environment due to the reduced heat transfer capability through the deposit. Sintering, in the presence of a viscous sulphate phase would ensue, forming a consolidated deposit of considerable strength. It appears that some particles exhibit partial solubility in the sulphate liquid. Thus condensed K_2SO_4 has played a crucial role in deposit formation in the convective passes of the boiler by presenting a captive surface to which ash particles initially adhere, and by promoting ash sintering.

The superheater deposit was found to have a short fusion range, with a low solidus temperature of 850°C. If the insulating properties of the deposit are such that the surface approaches the temperatures of the flue gas, it may be assumed that the formation of a liquid phase would facilitate ash sintering resulting in a deposit of greater strength and tenacity. The formation of fouling deposits during the combustion of these fuels appears to be inevitable, and thus frequent sootblowing may be the only solution to ash sintering and the development of deposit strength.

The progressive condensation of K_2O from the vapour phase is expected from the superheaters to the economisers and precipitators. However, reduced temperatures in the economiser region would result in a deposit of inferior strength and increased porosity since the driving force for sintering would be greatly reduced by the decrease in temperature.

The relatively high vapour pressures of potassium salts and P_2O_5 would imply that the subsequent condensation of these species in convective regions would always be a problem in combustion systems with the inevitable formation of deposits. To preclude excessive volatilisation of potassium salts and P_2O_5, the combustion temperatures must be kept to a minimum.

6.4 Sewage Sludges

The most appropriate method of sewage sludge disposal is a sensitive issue, and a nightmare for local authorities. The discharge of sewage sludge in the Estuaries of Britain is to be prohibited in the very near future. Agriculture is expected to remain the principal disposal route for the sludge, although the appreciable phosphate content of the sludge has ensured that this rate-limiting nutrient is in abundant supply for high biological productivity in waters. The trace element content of sewage sludges also

raises environmental and health issues. The gasification of sewage sludge has also encountered problems associated with phosphate species which have been found to contribute to the problems of deposit formation.

The ash contents of the sewage sludge ashes were found to be relatively high compared to most biomass and conventional fuels, averaging 30wt% (d.a.b). An increased rate of ash deposition is thus expected. The sewage sludge ash is essentially an aluminosilicate with appreciable amounts of CaO and P_2O_5. The Thames ash was found to contain quartz (SiO_2), calcite ($CaCO_3$), kaolin ($Al_2O_3.2SiO_2.2H_2O$) and a calcium phosphate ($Ca_3(PO_4)_2$). Sewage sludges are also reported to contain debris from the wear of roads such as gravel and road base materials which are all fundamentally aluminosilicates. As a first approximation, the behaviour of the major inorganic components at high temperatures may be described by the interaction of species within the $CaO-Al_2O_3-SiO_2$ system. The EDS composition of each LTA has been normalised to three components and plotted on the ternary phase system $CaO-Al_2O_3-SiO_2$[94], shown in Figure 6.11.

6.4.1 Thames sewage sludge

The Thames ash lies in the compatibility triangle bounded by anorthite ($CaO.Al_2O_3.2SiO_2$), gehlenite ($2CaO.Al_2O_3.SiO_2$) and pseudowollastonite ($CaO.SiO_2$), and has a liquidus temperature of ~1510°C. From the crystallisation path it is evident that on cooling the melt under equilibrium conditions, anorthite would be the first phase to crystallise, and the residual liquid phase would become increasingly rich in lime with decreasing temperature. The fluxing properties of CaO would serve to maintain the fluidity of the residual melt with decreasing temperature. The viscosity has been estimated using the Urbain model based upon the $CaO-Al_2O_3-SiO_2$ system. At ~1320°C, the liquid composition would reach a point on the binary eutectic boundary and the primary solidification of anorthite would cease. At this point the eutectic reaction

$$\text{Liquid} \rightarrow \text{anorthite} + \text{gehlenite}$$

would commence. With decreasing temperature, the eutectic mixture of anorthite+gehlenite would continue to precipitate and the composition of the residual liquid phase would move along the phase boundary. Solidification would be complete when the liquid composition reached the ternary eutectic point at 1265°C, where three

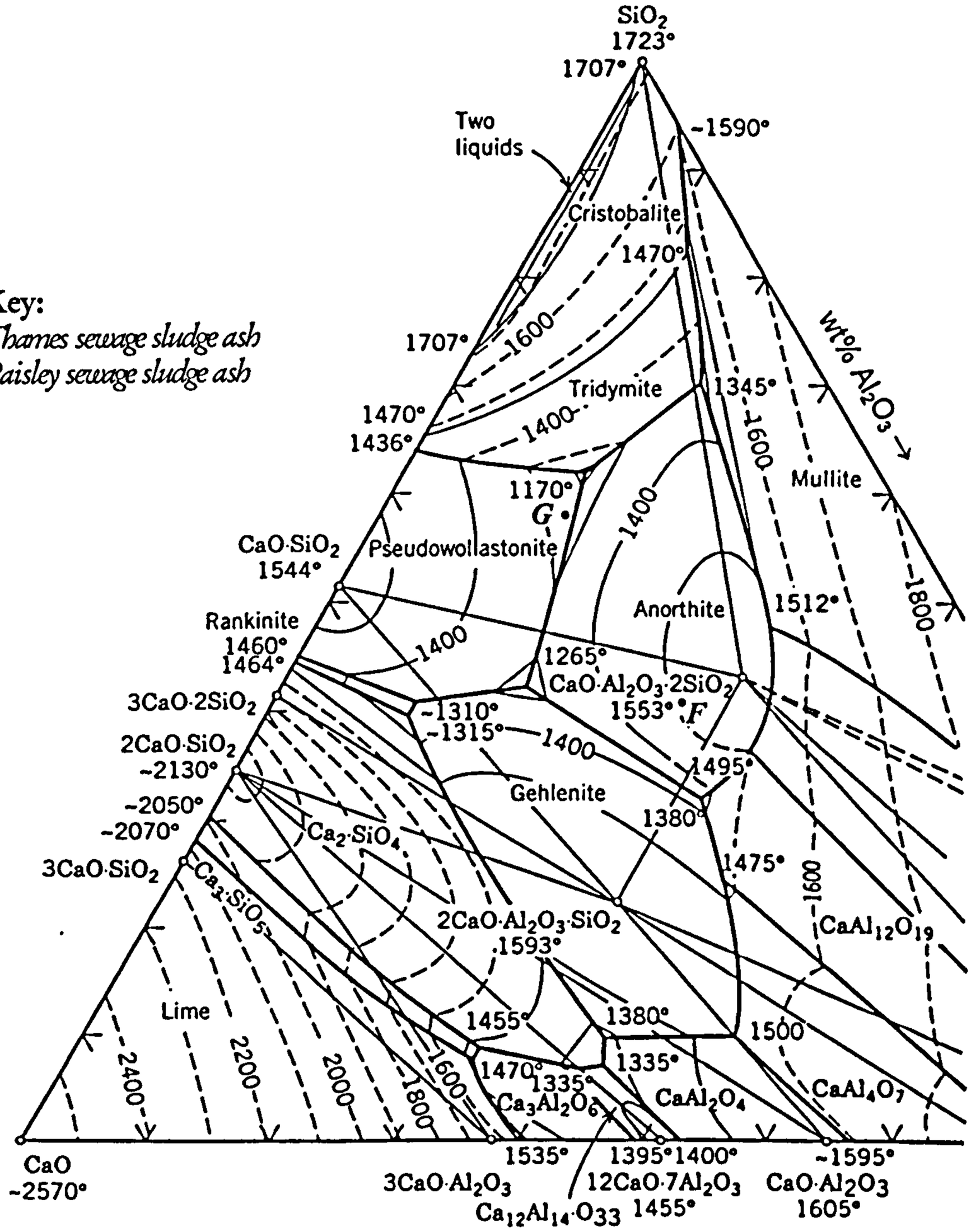

Figure 6.11 Normalised Thames Water and Paisley sewage sludge ash compositions plotted on system CaO-Al_2O_3-SiO_2

adjacent phases would be in equilibrium with the liquid phase. The ternary eutectic reaction may be written as follows:

Liquid → anorthite + gehlenite + pseudowollastonite

The ternary eutectic indicates the composition of, and temperature at which the very last liquid phase would be present during solidification. Conversely, and of more significance to this study, the point of invariance denotes the temperature/composition at which the first liquid phase would appear on fusion. The percentage of liquid that would be the first to appear during the fusion of the Thames ash can be calculated from the tie-triangle anorthite-gehlenite-ternary eutectic. Thus, ~ 26% of a liquid phase of

eutectic composition (42wt% SiO_2, 38wt% CaO and 20wt% Al_2O_3) would be present at 1265°C. The viscosity of a liquid of this composition has been calculated as ~ 14Pa s at 1265°C. The formation of a liquid phase of such a low viscosity could have major implications for the sintering of residues during the gasification of sewage sludge from the Thames Valley Treatment Plant.

6.4.2 Paisley sewage sludge

The normalised composition of Paisley ash lies within the primary field of pseudowollastonite and the compatibility triangle anorthite-pseudowollastonite-silica, alongside the anorthite-pseudowollastonite eutectic trough. On cooling the melt below ~1245°C (the liquidus temperature), the phase diagram predicts little crystallisation of pseudowollastonite. At ~1230°C the liquid composition would reach the binary eutectic boundary and precipitation of anorthite + pseudowollastonite would begin. The eutectic reaction (L → anorthite + pseudowollastonite) would progress, rejecting increased amounts of excess silica into the residual liquid which would consequently become more viscous. At 1170°C solidification would be complete by virtue of the ternary eutectic reaction:

$$L \rightarrow \text{anorthite} + \text{pseudowollastonite} + \text{silica}$$

At the ternary eutectic, 80% of a liquid phase, of composition 62wt% SiO_2, 15wt% Al_2O_3, and 23wt% CaO, would solidify. A liquid of this composition would have a viscosity of ~1.776×10^3 Pa s at 1170°C. Equilibrium in systems rich in silica is seldom attained in practice. The rate of atom/molecular diffusion within a melt varies exponentially with temperature, and thus the degree of transformation and the type of product obtained are dictated by the rate of cooling through the various phase fields. The mobility of molecular species in a high viscosity liquid phase is severely limited and very slow reaction rates are to be anticipated. Thus, on solidification, a departure from equilibrium behaviour is predicted with the viscous residual melt adopting the metastable condition of the vitreous state.

This analysis has revealed two very different predictions of slagging behaviour. Based upon this particular theoretical approach, the differences predicted in ash behaviour are attributable to the variable proportions of SiO_2, the network former, and CaO, the network modifier. The phase equilibria study predicts that the increased CaO:SiO_2 ratio in the Thames ash sample would result in the formation of an eutectic liquid of lower

viscosity and at a lower solidus temperature compared to Paisley ash. With reference to the Frenkel equation and the influence of viscosity on viscous flow sintering, the Thames sample would be expected to have a greater slagging propensity than its Paisley counterpart.

The Thames and Paisley ash compositions contained, in addition to SiO_2, Al_2O_3 and CaO, appreciable quantities of P_2O_5. These four components constituted 92wt% of the former and 87wt% of the Paisley ash. The applicability of the ternary phase diagram $CaO\text{-}Al_2O_3\text{-}SiO_2$ to predicting the fusion characteristics of the sewage sludge ashes is therefore limited, and the quaternary system of $CaO\text{-}Al_2O_3\text{-}SiO_2\text{-}P_2O_5$ would provide the basis for a more realistic analysis.

Only parts of the $CaO\text{-}Al_2O_3\text{-}SiO_2\text{-}P_2O_5$ quaternary diagram have been reported. The crystallisation paths of four component systems are three dimensional, with phase field occupying volumes, not areas, in space. In order to represent the quaternary system in two dimensions, planes of constant compositions of an arbitrary component, for example P_2O_5, are required and for which no such data has been published.

The Thames sewage sludge LTA was found to contain a condensed calcium phosphate, $Ca_3(PO_4)_2$. One may attempt to estimate the constitution of this sample in terms of the crystalline phases present. Let us assume that all the P_2O_5 in the ash is present as the phosphate $Ca_3(PO_4)_2$, in which the mole ratio of the oxides $CaO:P_2O_5$ is 3:1, therefore

$$\frac{\text{wt\% CaO}}{56\text{g}} = \frac{15.3\text{wt\% } P_2O_5 \times 3}{142\text{g}} \Rightarrow \%\text{CaO}=18.1\text{wt\% (1.9wt\% excess CaO in ash)}$$

$$\Rightarrow \%\ Ca_3(PO_4)_2=(18.1\text{wt\% CaO}+ 15.3\text{wt\% } P_2O_5) =33.4\text{wt\%}$$

The phosphate, in isolation, is relatively stable with regards to high temperature, with a melting point of 1730°C and thus is an appropriate apex of the $Ca_3(PO_4)_2\text{-}Al_2O_3\text{-}SiO_2$ section of the quaternary. The normalised composition, 37wt% $Ca_3(PO_4)_2$, 27.4wt Al_2O_3, 35.6wt SiO_2, lies within the primary field of anorthite ($CaO.Al_2O_3.2SiO_2$) with a liquidus temperature of ~1350°C as shown in Figure 6.12.[127]

The composition of anorthite lies on the basal plane of the $CaO\text{-}Al_2O_3\text{-}SiO_2$ system, as illustrated in Figure 6.13, thus as anorthite crystallises from the normalised composition, the residual liquid would become enriched in P_2O_5. Lack of sub-solidus information for this system precludes any further analysis of the crystallisation behaviour.

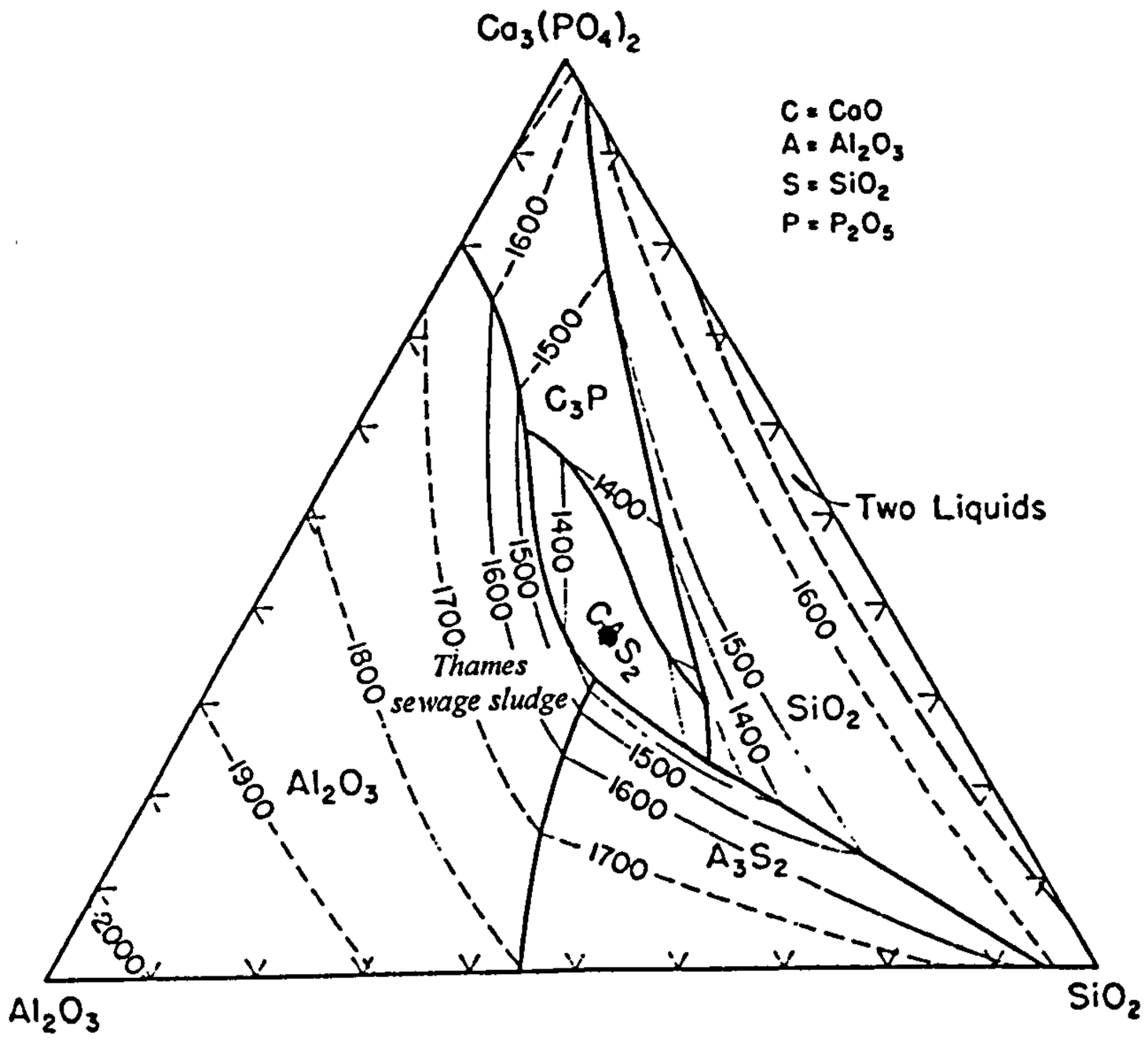

Figure 6.12 $Ca_3(PO_4)_2$-Al_2O_3-SiO_2 system[127]

The experimentally determined solidus and liquidus temperatures were found to be several hundred degrees lower than the predicted temperatures based upon simple phase equilibria. These differences may be accounted for by the presence of the additional network modifying species, such as K_2O, Na_2O, MgO and FeO, that have fluxing properties within glass-forming SiO_2 and P_2O_5 based melts. The function of these fluxes is to disrupt the continuity of the silicate/ultraphosphate network, thereby reducing the viscosity of the melt, and the liquidus and the solidus temperatures. The role of the network modifier depends on valence and co-ordination number, and on the relative bond strengths. For example, the fluxing effect of the alkalis is increased as the cation radii become smaller. Thus soda is more effective in reducing the melting point than potash. The mixture of fluxes in the sewage sludge ashes will have a cumulative effect in reducing the viscosity. In practical applications this phenomenon is experienced in the production of glazes, which are complex multicomponent systems, in comparison to most glasses which contain only four or five oxide constituents.

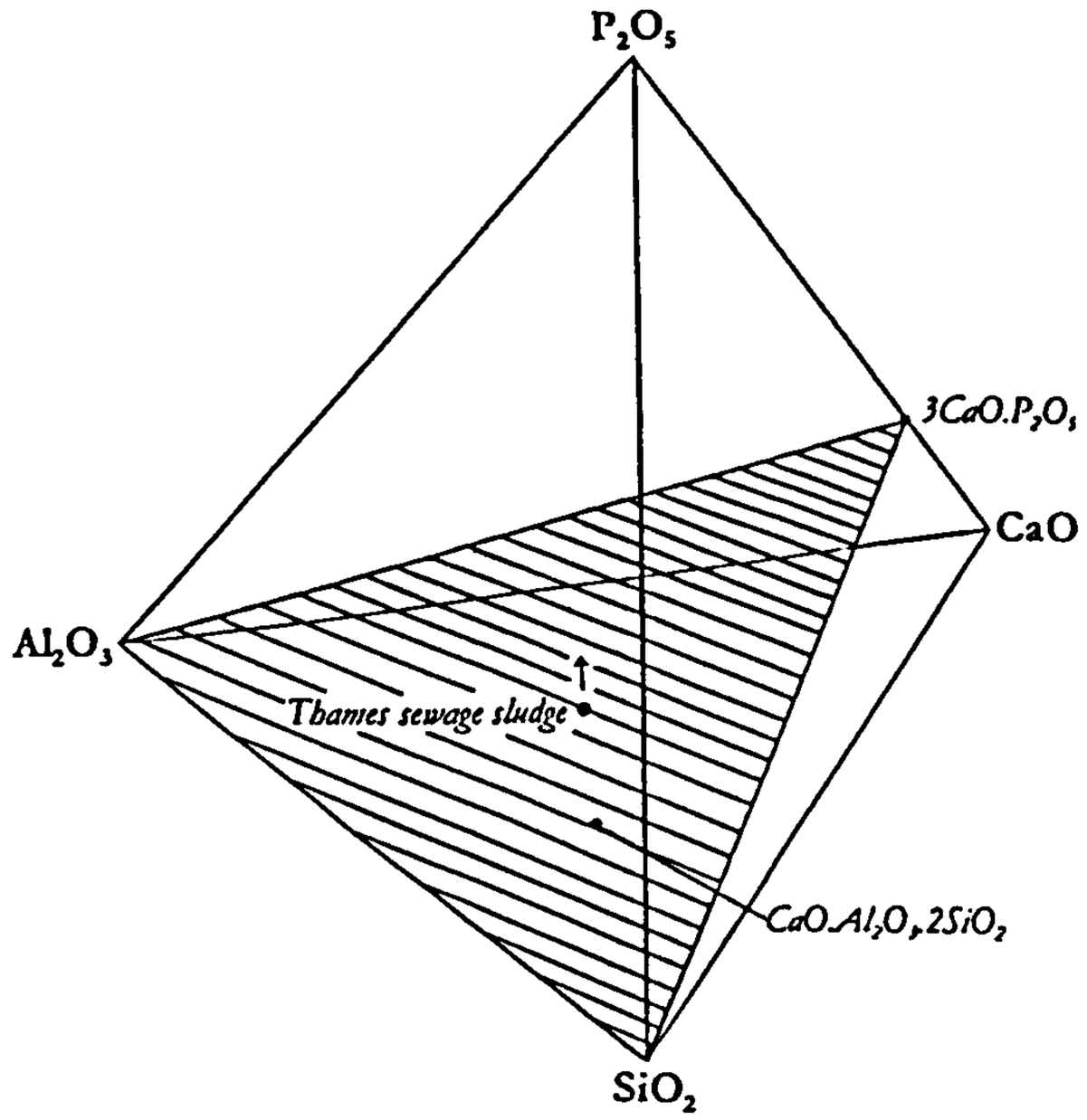

Figure 6.13 $CaO-Al_2O_3-SiO_2-P_2O_5$ system; arrow indicates initial crystallisation path of Thames sewage sludge LTA

The sludge from the Thames Water sewage facility contained a condensed calcium phosphate $Ca_3(PO_4)_2$. It is suggested that the phosphate was derived from water softening compounds employed in detergents and is a manifestation of the sewage treatment process. Detergents contain 5-12wt% of phosphate-based water softening compounds, and may contribute up to half the phosphate loads on sewage treatment facilities. The function of the phosphate group (PO_4^{3-}) and related anionic froms (HPO_4^{2-} and H_2PO^{4-}) in detergent compositions is to form soluble phosphate complexes from Ca^{2+} and Mg^{2+} ions, that contribute to water hardness. The reactions of Na_3PO_4, a traditional water softening constituent of detergents, are given below:[5]

$$3MgSO_4 + 2Na_3PO_4 \rightarrow Mg_3(PO_4)_2 + 3Na_2SO_4$$

$$5Ca(HCO_3)_2 + 4Na_3PO_4 + H_2O \rightarrow {}^1/_2Ca_{10}(PO_4)_6(OH)_2 + 10NaHCO_3 + Na_2HPO_4$$

Although largely superseded by polyphosphates, the principal reactions are essentially the same. Approximately 90% of the soluble phosphates can be removed during a tertiary sewage treatment in which lime, sodium aluminate and/or ferric salts are added to the wastewater with the precipitation of the respective insoluble metal phosphates, such as the $Ca_3(PO_4)_2$ identified in the Thames sample. The increased use of polyphosphate compounds in detergents in the South of England is a consequence of the extensive sedimentary carbonate rock masses, such as chalk and limestone, used for water storage in the Southern region. Carbonate rocks consist primarily of calcite

$CaCO_3$ with up to 25% dolomite ($CaCO_3$. $MgCO_3$) which are rapidly eroded when exposed to water containing dissolved CO_2:

$$CaCO_{3(s)} + CO_2 + H_2O \rightarrow Ca^{2+}_{(aq)} + 2HCO^{3-}$$

$$MgCO_{3(s)} + CO_2 + H_2O \rightarrow Mg^{2+}_{(aq)} + 2HCO^{3-}$$

The higher the concentration of calcium and magnesium ions in the water, the harder the water is said to be.

6.4.3 Fouling propensity

Waste body phosphorus is expelled in the urine predominantly as $NaNH_2HPO_4$. The compound is not expected to be particularly stable at combustion temperatures and its decomposition would be accompanied by the evolution of ammonia, P_2O_5 vapours and the volatile alkali species Na_2O, by virtue of the following reaction:

$$2NaNH_2HPO_4 \rightarrow Na_2O + NH_3 + P_2O_5 + O_2$$

Alkali and phosphate bonded fouling deposits are to be anticipated.

6.4.4 The Warren Springs Gasifier Deposit

The bulk chemical composition of the Warren Springs gasifier slag was found to be enriched in Fe_2O_3 (at 22wt%) and SO_3 (12wt%) relative to the fuel ash, and contained two other principal constituents: SiO_2 (21wt%) and CaO (24wt%), with appreciable amounts of P_2O_5. To account for the high concentrations of Fe_2O_3 in the slag, it is suggested that the iron was introduced as a 'contaminant' via an oxidised steel component within the gasifier. Predictions based upon the CaO-Al_2O_3-SiO_2 and the CaO-Al_2O_3-SiO_2-P_2O_5 phase equilibrium diagrams were complicated by the unexpected enrichment of iron present in two valency states: the reduced ($Fe^{2+}S$) *and* the oxidised ($Fe_2^{3+}O_3$) state, as revealed by X-ray diffraction analysis. It is not uncommon for a number of transition metal cations to exist in molten (metallurgical) slags and glasses in variable valency states, their relative proportions depending on the temperature, pressure, composition and oxygen potential of the system.[89] Thus high oxygen partial pressures would favour the formation of maghemite. However troilite (FeS) was found to be present in relative abundance suggesting that conditions within the gasifier were predominantly reducing.

The system FeS-FeO is a simple binary with a eutectic at 930°C and no known solid solutions, as shown in Figure 6.14.[128] Thus the oxidation of FeS would be

accompanied by the formation of a liquid phase at 940°C (the solidus). The melting point of FeS (the liquidus) would also be significantly reduced with an increase in oxygen partial pressure. West[80] postulated that the liquid produced by the oxidation of pyrrhotite was responsible for the initial bonding of ash particles in the British Coal Pressurised Fluidised Bed Gasifier. The Fe-S-O liquid phase was found to readily wet ash particles, and subsequent oxidation and reaction with clay particles resulted in the formation of a more substantial iron-rich aluminosilicate bond. It is anticipated that the formation of a Fe-S-O liquid phase at gasification temperatures would play a role of crucial importance in the process of sintering and agglomeration of ash particles during the gasification of Fe containing sewage sludges.

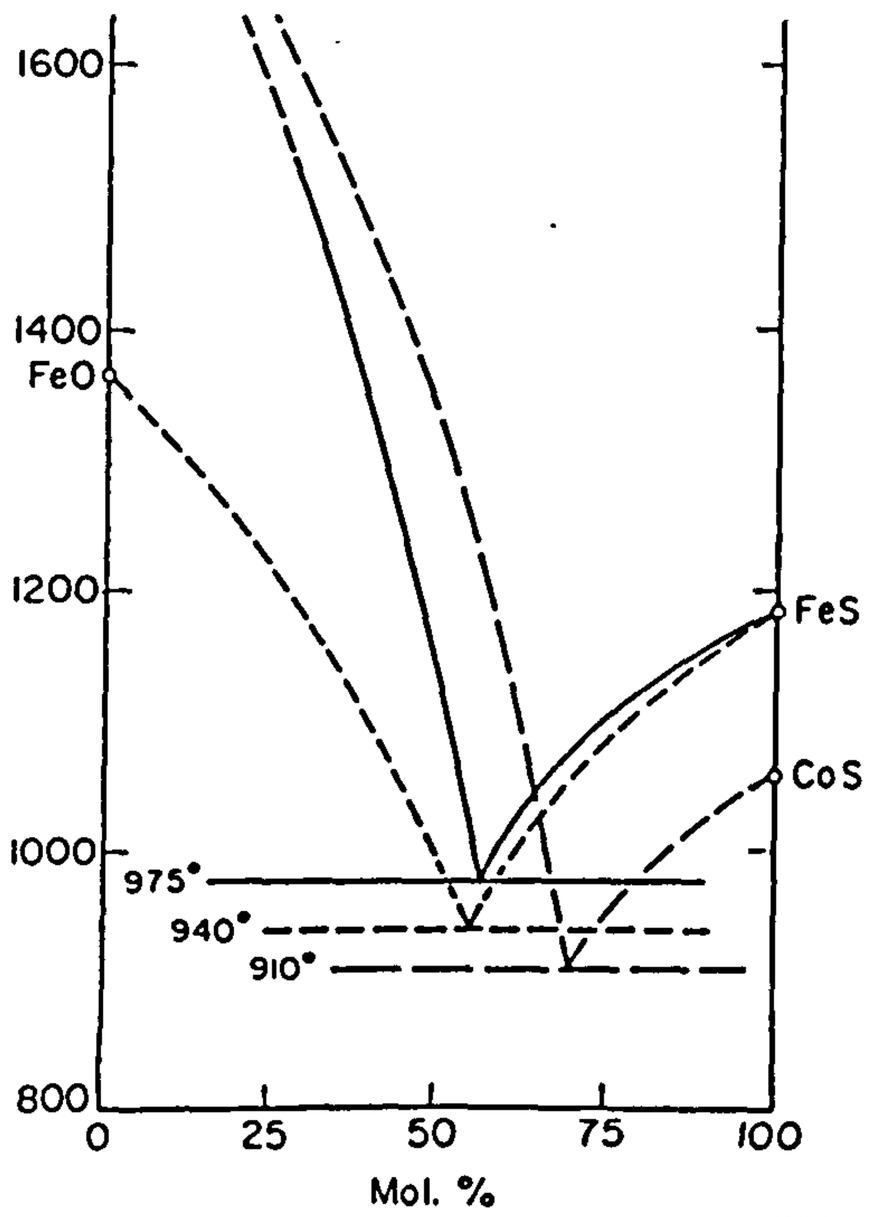

Figure 6.14 FeS-FeO system[128]

The microstructure of the Warren Springs gasifier slag was grossly inhomogeneous in nature, and characterised by the presence of a number of predominantly crystalline phases of varying composition and morphology, including laths of a calcium phosphate, independent euhedral crystals of a spinel, dispersed aggregates of FeS, and acicular crystals of a pyroxene [$(Fe,Ca)SiO_3$]. The chemical nature and well developed habit of these crystalline products would strongly suggest that the deposit had been molten at an early stage of formation. It is envisaged that the temperature of the local environment would undoubtedly have exceeded the solidus temperature (980°C), perhaps approaching that of the liquidus temperature (1290°C). An appreciable quantity of liquid would thus have been formed, from which the nucleation and growth of a variety

of crystalline products of defined and well developed morphology could progress. The problem of slag formation in this system is expected to be self-perpetuating since the slag melt would present a captive surface to which all impacting ash particles would adhere. The evidence is somewhat alarming with respect to the gasification process, in which the principal objective is to avoid ash fusion.

The precise nature of the spinel group remains, as yet, unidentified by XRD analysis. However, the composition, and in particular the crystal morphology, is indicative of a spinel. Spinels are usually found to occur as euhedral (well formed faces) or subhedral grains (imperfectly developed faces), with square or triangular cross-sections.[129] The spinel group is represented by a number of compounds, all conforming to the general formula $A^{2+}B_2^{3+}O_4$. Three series occur, each being defined by the dominant trivalent cation: the spinel series, the magnetite series and the chromite series in which Al^{3+}, Fe^{3+}, and Cr^{3+} are the respective dominant trivalent ions. There exists a continuous replacement series from spinel ($MgAl_2O_4$) to hercynite ($Fe^{2+}Al_2O_4$). The structural variety within the spinel group is further demonstrated by the substitution Zn = Mg, giving an isomorphous series from spinel to gahnite ($ZnAl_2O_4$) and Al = Cr grading into the chromite series. One member of the spinel group was identified, maghemite (γ-Fe_2O_3), which is the end member of the solid solution series represented by γ-Al_2O_3 and γ-Fe_2O_3 within which the replacement of Fe for Ti may occur, such as in ulvospinel (Fe_2TiO_4) where the substitution $2Fe^{3+} = Fe^{2+} + Ti^{4+}$ takes place. Crystalline phases that posses the spinel structure are multifarious and of complex stoichiometry. It is postulated that the unidentified phase(s) of the x-ray diffraction pattern may correspond to that of a spinel within the solid solution series of γ-Al_2O_3 and γ-Fe_2O_3, with considerable substitution of Ti and possibly other cations for Fe and Al. Thames sewage sludge was found to contain a number of trace elements such as Zn and Cr, possibly introduced by industrial effluents, which exhibit solid solubility in the spinel phase, lending credence to the above predictions.

The presence of zoned spinel crystals is indicative that the solidification conditions were non-equilibrium. It is evident from the microstructure that a spinel, on precipitation from the melt, began to react with the surrounding liquid which contained ions (Fe^{3+}, Ti^{4+}, etc) which exhibit solid solubility in the spinel structure. A continuous reaction is expected since spinels readily form solid solutions, although the extent of the reaction is

governed by the maintenance of equilibrium between the precipitate and the adjacent liquid. Cooling rates which are infinitely slow (equilibrium conditions) are conducive to atom diffusion and re-arrangement, allowing the crystals to adjust their compositions to the demands of falling temperature. At faster cooling rates, i.e. non-equilibrium conditions, the crystal will be zoned, that is to say a composition gradient will exist in the crystal from centre to margin. The spinel observed in the microstructure features an Al-rich centre and an Fe-rich surface.

All the polymorphs of phosphorus pentoxide form glasses based upon PO_4 tetrahdra in which one oxygen ion is non-bridging. In this respect P_2O_5 differs from other network formers such as SiO_2 and B_2O_3. However, in the P_2O_5-rich systems of this study, the boiler deposits were not observed to have formed glassy phosphate matrices. The poultry litter and sewage sludge deposits were predominantly a mixture of polycrystalline phosphate phases. The regions of glass formation in several binary phosphate systems are given in Table 6.1.[84]

Table 6.1. Regions of glass formation in binary phosphate systems. [84]

Modifier	Maximum percentage of modifier (mole %)
K_2O	47
Na_2O	60
CaO	56
MgO	60

It is apparent that the co-ordination requirements of the phosphorus ion for glass formation were not satisfied in the poultry litter and sewage sludge ash systems. In all the systems the range of glass formation is continuous from P_2O_5 to the modifier content given, i.e. no regions of stable immiscibility exist.

Investigations of mixed alkali systems have shown that the regions of glass formation are more extensive than in any of the binary systems on quenching from the melt.[84] However at slower cooling rates, the structural changes which occur during the crystallisation/solidification of phosphate melts are more complex in nature, involving the breaking and reforming of P-O bonds to transform the mixture of linear molecular chains of n-PO_4 tetrahedra and of varying length in the melt, to the crystalline forms containing short linear or cyclic molecules. Thus as the modifier content is increased,

the proportion of long chain glass-forming phosphates decreases at the expense of the short chain phosphates which crystallise more readily

6.5 Crystal Morphology

Crystals are formed by the repeated addition of unit cells to the structure in three dimensions. The limiting surfaces, or faces of the crystal depend in part on the shape of the unit. In determining the types of crystal faces that may develop, the internal lattice must be considered. Faces are likely to form on crystals parallel to lattice planes that have a high density of lattice points (nodes). According to the Law of Bravais, the frequency with which a given crystal plane/face is observed is proportional to the number of nodes intersected in the lattice. Furthermore, the angles between pairs of corresponding faces of the same substance, but of *different* morphology, are identical (at the same temperature). What, then, determines the morphology of a crystal?. The development of an individual crystal, or an aggregate of crystals, to produce a particular morphology, depends upon the conditions during formation, such as temperature, pressure, and available volume for free growth. In multicomponent systems, variations in the chemical constitution of the residual melt and relative amounts of each phase present, in addition to the surface area and strain energy constraints associated with the formation of a new phase, will effect both the morphology and the tendency for a new crystal to appear. The microstructure of the deposits, although characterised by the conditions peculiar to each individual process, present information concerning the ambient temperature, oxygen partial pressure, and indeed properties of the melt. For example in one such environment dendritic crystals may form, such as observed by a spinel precipitating from a viscous melt. Conversely, a more fluid melt may enable the precipitating spinel to adopt an euhedral habit.

6.5.1 Strength of deposits

Although the mechanical properties of the deposits were not investigated in this particular study, the microstructure can offer some indication of the strength and fracture resistance of the material, i.e. how difficult the deposit may be to remove from a heat transfer surface. On-load removal of deposits is most successfully achieved by the action of sootblowers which direct a high pressure jet of air, steam or water, through retractable lances, at the deposit surface. A combination of thermal and mechanical

shock is used to initiate cracks within the deposit, which is subsequently dislodged by the scouring action of the jet. Deposits of a more tenacious nature may require boiler shut-down and manual removal. The tenacity of the deposit depends upon the strength of the adhesive bond between the deposit and its substrate, which may be a refractory lined furnace wall or a steel tube with a protective oxide coating. The relationship between the surface and interfacial energies determines to a large extent the wetting behaviour of a liquid on a solid surface. Molten sulphates have much lower surface energies than solid metals and the experience of this study is that K_2SO_4 was found to readily wet and spread on the surface of the superheater tubes of the Eye plant. In the radiant zone of a boiler, the 'keying' characteristics of a slag melt in contact with a refractory substrate will be influenced by the degree of porosity of the refractory. At higher temperatures in this region, and depending on the viscosity and constitution of the slag, a slag-refractory interaction may be encouraged. If the strength of the adhesive bond exceeds that of the cohesive bonding of the deposit, a layer of slag material may remain on the furnace wall following sootblowing, upon which subsequent ash deposition can readily take place.

The deposits from this study show certain analogies to ceramic or glass-ceramic materials, and are thus inherently brittle. That is to say, the arrangement of molecules, with strong covalent and ionic bonding, renders the dislocation and defect populations relatively immobile compared to metals and alloys. Crack propagation in brittle polycrystalline materials is a complex process, involving a number of stochastic microscopic events. However it may be safe to assume that the mechanical strength of the deposits would be largely dependent upon the extent of porosity. The role of a pore as a localised stress-concentrator is clearly recognised. It has been shown that the mechanical strength of a porous slag decreases exponentially with porosity:[66]

$$\sigma = \sigma_o \exp(-nP)$$

where σ is the strength of the porous body, σ_o is the strength of the fully dense material, P is the volume fraction porosity, and n lies in the range 4-7. For a material of high porosity, such as the tube deposit from the Elm Energy car tyre incinerator, the composition and nature of the phases present would have little influence on the mechanical properties . The fouling deposit was found to be extremely friable. In contrast, the dense and highly fused slag from the Warren Springs gasifier, had very few

internal pores and no discernible surface porosity. The material was found to be of great strength.

In a polycrystalline material the grains are crystallographically misorientated with respect to one another. A crack intersecting the boundary between two phases/grains may either traverse the boundary, and thereby continue the propagation through the second phase with relatively minor adjustments to the crack plane, or follow the grain/interphase boundary itself. The former (transgranular fracture) is favoured by small misorientaions and strong grain boundaries. The strength of the grain and interphase boundaries will be dependent on the degree of coherence between the structures of the two phases. It may logically be proposed that the favoured orientation of an incremental extension will be that which minimises the total free energy of the system.

Grain/interphase boundaries constitute planes of relative weakness in the material. This is particularly so in the case of ceramic materials, where violations of the directionality and charge requirements of covalent-ionic bonds can lead to substantial reduction in interfacial cohesion. There is then an increasing tendency for cracks to propagate around instead of through grains as the angular misorientations between crystals increase. The typical intergranular fracture is thereby characterised by a tortuous crack path. While the resistance to fracture may be intrinsically low along the interfaces between phases, the abrupt changes in crack path will lead to substantial reductions in the local mechanical energy release rate: the overall effect may be an increase in the overall fracture energy. This tendency to an increased resistance may be further accentuated at larger grains. Thus it may be hypothesised that the sewage sludge (Warren Springs) and the RDF/chestnut (Power Gasifiers) slags would be inherently resistant to fracture. Both materials were predominantly crystalline, containing an intimate arrangement of phases of variable size, morphology, and orientation. Thus a crack propagating through the microstructure would be forced to circumvent each obstacle in its path. The driving force for the extension of a crack, deviant from a preferred plane, will diminish rapidly with distance from the crack plane, with an attendant increase in the fracture resistance. The random orientation of the crystalline phases of a slag microstructure would give a material with no preferred orientation along which a crack would propagate. The advancing crack front would have to adjust

to accommodate the preferred cleavage plane of each phase in turn. The overall effect would be manifested as an apparent increase in the fracture surface energy and hence fracture resistance.

The microstructures of the poultry litter slags were also characterised by the presence of crystals of variable morphology, however precipitation within a viscous melt resulted in crystals of anhedral habit. The rounded, anhedral crystals of $KCaPO_4$ crystals would present an obstacle to an advancing crack and thereby contribute to the fracture resistance of the deposit. With increasing crystal size, as observed in Eye III, the fracture resistance of the material would be expected to increase, since the crack front would be forced to deviate from a preferred plane through a greater angle. However, it is anticipated that the variable surface and internal porosity of the samples would have more influence on the strength and tenacity of the deposit than other microstructural characteristics.

The crystalline phases of the RDF/chestnut (Power Gasifiers) deposit were found to be embedded within a glassy aluminosilicate matrix. Below Tg, the fracture of a glass is brittle and non-crystallographic, following a random path through the sample. However the interlocking mass of wollastonite laths bonded by the glassy matrix would reinforce the structure, the propagating crack preferring to follow a crystal/glass interface rather than to traverse the crystal.

6.6 RDF/chestnut

The 50kW gasifier operated by Power Gasifiers Int. had been operating on a mixed feed of chestnut chippings and pelletised RDF with the aim of establishing the maximum amount of RDF which could be incorporated before operational difficulties were encountered. The chestnut had originated from a local forest, in which traditional coppicing techniques had been employed since mediaeval times. Consequently the wood was mature, with increased sapwood:bark ratios in relation to the poplar and willow coppice also characterised in this study. The ash content of the chestnut was minimal at <0.5wt%. In contrast the ash contents of the RDF samples averaged 12wt%. In terms of an ash residue, the chestnut ash is expected to have little influence on the bulk ash characteristics of the fuel.

6.6.1 Prediction of slagging propensity

Refuse derived fuel

The composition of the RDFs were found to contain three major components: silica, alumina and lime, which comprised approximately 88wt% of the bulk ash. The inorganic material was largely derived from the fillers, such as quartz, calcite, kaolinite ($Al_2O_3.2SiO_2.2H_2O$) and rutile (TiO_2), used in paper, plastic and rubber products,. With the exception of the latter component, the high temperature ash chemistry may be predicted, as a first approximation, using the phase equilibrium data of the CaO-Al_2O_3-SiO_2 system. The implicit assumption in such an approach is that the minor constituents of the ash have little influence on the fusion characteristics and are thus disregarded. A qualitative allowance for the fluxing properties of certain ash constiuents will be proposed in due course. The normalised Byker RDF ash composition has been plotted on the CaO-Al_2O_3-SiO_2 system shown in Figure 6.15, and is found to lie within the compatability triangle silica-anorthite-mullite. Equilibrium solidification of the melt would commence at ~1540°C (the liquidus) with the precipitation of primary anorthite ($CaO.Al_2O_3.2SiO_2$). The high liquidus temperature would suggest that aluminosilicate and quartz particles would be incompletely fused at gasification temperatures. Crystallisation of anorthite would yield a silica-rich residual liquid. With decreasing temperature, the composition of the residual liquid would increase in silica and consequently become more viscous, thus reducing any tendency towards slagging. The rearrangement of molecules for the continued nucleation and growth of anorthite would be hindered by the increased viscosity of the melt, and thus departure from equilibrium would inevitably favour the formation of a glassy silicate matrix. Assuming equilibrium is achieved at all temperatures, at ~1480°C the binary eutectic reaction (L $\rightarrow$ anorthite + mullite) would progress until the composition of the residual liquid approached that of the ternary eutectic at 1345°C. At the solidus it is predicted that ~20% of a liquid phase, of composition 70wt% SiO_2, 20wt% Al_2O_3, and 10wt% CaO, and a viscosity of $2.5x10^3$ Pa s would solidify by virtue of the following reaction:

$$L \rightarrow CaO.Al_2O_3.2SiO_2 + 3Al_2O_3.2SiO_2(\text{mullite}) + SiO_2\ (\text{tridymite})$$

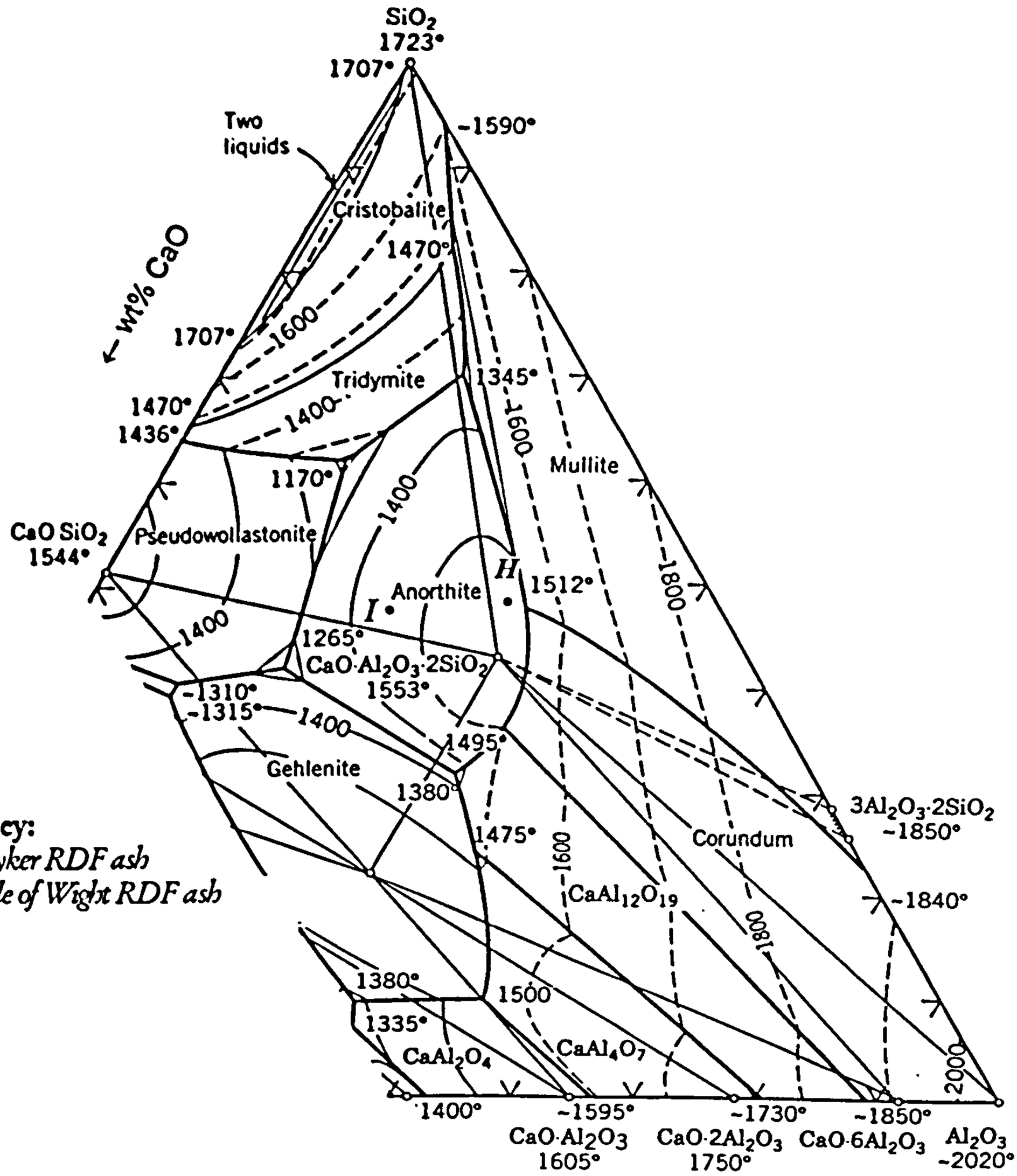

Key:

H *Byker RDF ash*

I *Isle of Wight RDF ash*

Figure 6.15 Normalised Byker and Isle of Wight RDF ash compositions plotted on the CaO-Al_2O_3-SiO_2 system

Isle of Wight RDF

The Byker and Isle of Wight RDF LTA compositions were similar with respect to the main constituents, with the Isle of Wight RDF ash being richer in CaO than the Byker, at the expense of SiO_2 and Al_2O_3. The normalised ash composition is plotted on the CaO-Al_2O_3-SiO_2 ternary system of Figure 6.15. The ash is also found to lie within the primary field of anorthite, although in this example the relevant compatibility triangle is that of silica-anorthite-pseudowollastonite. Anorthite would be the first phase to nucleate at ~1460°C, on cooling from the melt. At ~1305°C the primary solidification

of anorthite would be superseded by the precipitation of the binary eutectic mixture (anorthite + pseudowollastonite). With decreasing temperature, the residual liquid would become enriched in silica accompanied by a marked increase in viscosity, reducing any tendency towards slagging. Solidification would cease at 1170°C via the ternary eutectic reaction:

$$L \rightarrow CaO.Al_2O_3.2SiO_2 + CaO.SiO_2 + SiO_2 \text{ (tridymite)}$$

at which temperature ~8% of the liquid phase, of eutectic composition would solidify. The viscosity of the residual liquid is estimated at ~1.59×10^3 Pa s at 1170°C.

Although both samples of RDF were essentially of similar constitution, this theoretical approach illustrates the consequential reduction in solidus and liquidus temperatures, and in the viscosity of the residual liquid, by an increase of 5wt% CaO. The solidus and liquidus temperatures are expected to be reduced by the fluxing effect of other ash constituents, notably Fe_2O_3 (2.4wt%), MgO (2.2wt%), K_2O (2wt%), Na_2O (2.6wt%) and TiO_2 (3wt%). With reference to silicate binary systems such as Na_2O-SiO_2, K_2O-SiO_2 and Fe_2O_3-SiO_2, an effective lowering of the solidus/liquidus by 150-200°C may be expected. The experimentally observed solidus and liquidus temperatures were approximately 250-400°C lower than the predicted values, lending credence to the above predictions.

Chestnut

With the exception of SO_3, the chestnut fuel ash was found to contain only two major constituents: CaO and K_2O, and thus a simple CaO-K_2O eutectic system would be predicted to describe the fusion behaviour of the ash, for which no equilibrium data is available. Part of the ternary system K_2O-CaO-SiO_2 is published[126], for compositions rich in SiO_2 (>50wt%). Clearly the information is generally not applicable to the chestnut ash system, which contains only 5wt% SiO_2. One can only speculate that in a K_2O-CaO system, CaO, a refractory compound with a melting point 2630°C, may form a relatively low melting eutectic with substantial additions of K_2O, i.e. at the K_2O-rich end of the system.

During the gasification process, the melting point of quartz (1723°C) may plausibly be reduced by the fluxing influence of the oxides CaO and K_2O, and thus able to form a bridge between refractory ash particles. Once an initial bond is established, diffusion

and viscous flow may increase the contact area between the particles, thereby strengthening the bond.

6.6.2 The hearth deposit

Despite the difference in ash content between the chestnut and RDF samples, the increase in CaO, MgO and K_2O concentrations of the hearth deposit relative to the RDF LTA would suggest that the chestnut and RDF inorganics had indeed interacted. The analysis of the hearth deposit revealed a strong correlation between the predictions based upon the $CaO\text{-}Al_2O_3\text{-}SiO_2$ phase equilibrium diagram and microstructural properties of the deposit. The constitution of the hearth deposit was essentially that of an aluminosillicate. X-ray diffraction analysis revealed the presence of three major crystalline phases: gehlenite, wollastonite and anorthite, all consistent with predictions based upon phase equilibria data. Diopside, a pyroxene of general formula $CaO.MgO.2SiO_2$, was also identified and observed as zoned euhedral crystals in the microstructure.

The chestnut ash was also observed to have contributed MgO to the system. The ash system may have been more accurately represented by the four component system $CaO\text{-}MgO\text{-}Al_2O_3\text{-}SiO_2$. The system is of significance in understanding the slag-metal reactions occurring in the iron blast furnace and in Portland cement manufacture. Additions of MgO to the $CaO\text{-}Al_2O_3\text{-}SiO_2$ system result in the formation of a number of primary crystalline phases, for example a spinel phase ($MgO.Al_2O_3$), melilite solid solutions (gehlenite-akermanite, $2CaO.Al_2O_3.SiO_2$ to $2CaO.MgO.2SiO_2$) and pyroxene ($CaO.MgO.2SiO_2$).

Diopside, a pyroxene of general formula $CaO.MgO.2SiO_2$, identified by XRD, was observed as zoned euhedral crystals in the microstructure. This illustrates how the residual liquid is subject to variation in composition being enriched in this instance in MgO as various other constituents are depleted from the melt as the slag cools and crystallises. Compositional zoning is a characteristic feature of the pyroxene group and of the diopside-hedenbergite solid solution series. For example, zoned augites are encountered in rapidly cooled rocks such as the lunar basalts.

6.6.3 Char-rich gasification residues

The reactivity of the charcoal-rich gasification residues was assessed by differential thermal analysis (DTA), in which the temperature of the major exotherm was used as a measure of the char reactivity. The chestnut residue was found to be more reactive than that of the RDF/chestnut mixture. The results suggest that the char produced from RDF under such conditions was significantly less reactive than that from chestnut alone.

At any one temperature, pressure and oxygen partial pressure, the reactivity of a char is influenced by the inherent microstructure, for example the porosity and thus available surface area for reaction, by the structure itself i.e. the number of active sites for oxygen dissociative chemisorption, and by the catalytic influence of certain inorganic impurities. The reaction mechanism involves the diffusion of oxidising species from the bulk gas to the char surface, adsorption of the reactant, chemical reaction and diffusion of gaseous products away from the carbon surface.

The effect of temperature on char reactivity may be illustrated in terms of an Arrhenius plot of log reaction rate versus reciprocal temperature in which there are three distinct zones designated by a change in gradient and hence activation energy, as shown in Figure 6.16.[130]

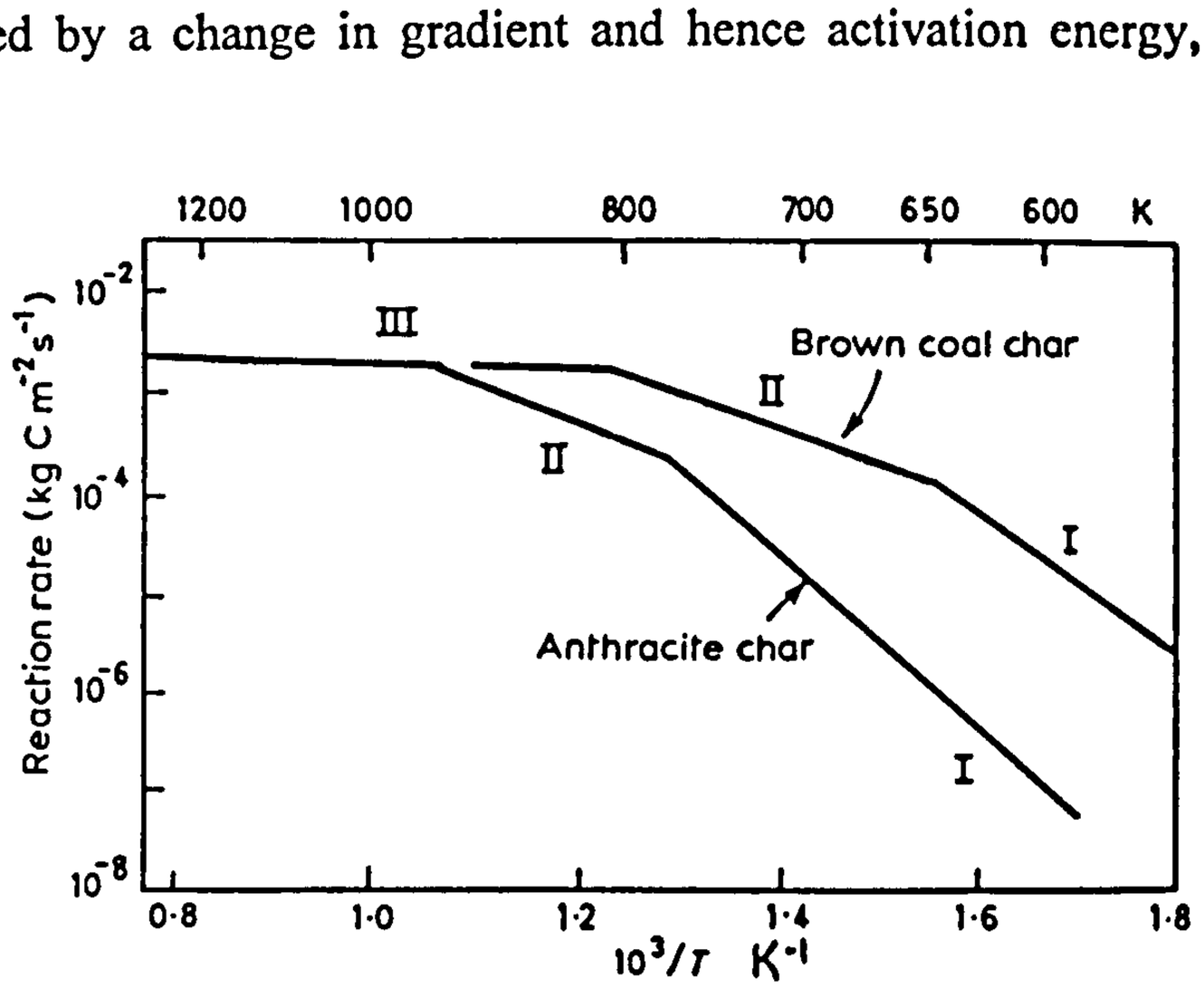

Figure 6.16 Log reaction rate versus temperature for 10mm carbon spheres in air[130]

At low temperatures, the oxidation rate of the char is proportional to the surface area within the pores since the chemical reaction rate (the intrinsic rate) is the rate determining step. The rate of reaction is slow enough for the reactant gas to completely penetrate the porous structure. This temperature region is designated as Zone I. At higher temperatures (Zone II), the reactant is consumed by the oxidising carbon before it

can completely infiltrate the pores and thus the reaction rate becomes dependent on the diffusional resistance of the pore structure *and* on the intrinsic rate and internal surface area. The activation energy in this regime is close to half that of Zone I. At elevated temperatures the rate of reaction is controlled by the diffusion of the oxidising gas from the bulk gas to the particle surface (Zone III).

It has been postulated by McGhee that the polymeric fraction of RDF is rendered less reactive by an ordering of the structure during carbonisation, whereby the carbon structure is gradually ordered, forming a pseudo-crystalline turbostatic structure.[131] A structure containing fewer defects is inherently more stable. Although the temperature of carbonisation and graphitisation depends upon the nature of the precursor, the temperatures are generally much greater than experienced in a a gasifier. However the ability of certain species, notably K^+, to catalyse the rate of oxidation is recognised.[132] Furthermore, in the presence of catalysts, such as $CaCO_3$ and K_2SO_4, the mixture exhibits a synergistic effect. It is suggested that the reduction in reactivity of the char with RDF may be influenced by the corresponding reduction in K_2O, however the explanation is somewhat tentative in the absence of detailed investigations and conclusive results.

6.7 Structure of chars

Carbon chars produced by the pyrolysis of biomass at 900°C or below will be entirely amorphous in nature and much more reactive than crystalline graphite due to the higher free energy of the randomised structure. Carbonaceous materials consist of carbon atoms arranged in hexagonal rings to form polyaromatic lamellar sheets. These macromolecular molecules contain heteroatoms (oxygen, nitrogen, phosphorus, etc.) in addition to chemical and crystallographic defects. There may also be single and multiple atom vacancies in the lamellae, dislocations, grain boundaries, stacking faults, and defects such as point defects, basal and screw dislocations. These imperfect lamellar structures are the building blocks of a carbonaceous material.[133]

The number of defects and the degree of ordering in the lamellar structure is strongly related to the precursor compounds and the pyrolysis temperature. In general, the higher the pyrolysis temperature, the fewer the defects and imperfections the structure will contain, until ultimately the structure approaches that of pure crystalline graphite.

Thus the observed decrease in char reactivity with pyrolysis heat treatment closely follows expected trends. While the aforementioned defect structures can account for changes in chemical reactivity of chars, at temperatures where diffusion may play a rate determining role the microstructure, porosity, and size distribution must also be considered.

6.7.1 Microporosity

In coal combustion, most coal particles pass through a plastic stage during the evolution of the volatile matter, leading to a highly porous char structure; the exception being the inertinite macerals which have a very low volatile matter content and hence their chars show an increased reluctance to oxidise, and fragments of these chars are frequently found in coal ashes.

In contrast, woody and cellulosic materials have a much higher volatile matter content (80% or more), the residual char not having experienced a plastic stage at the temperatures concerned. Thus a char of macro- and micro-porosity is produced as shown in Frames 5.30-5.35 (section 5.6.2, Chapter 5). There is some visual evidence that at high temperatures structural rearrangements have occurred to yield chars with reduced porosity.

6.7.2 Catalytic effect of inorganic species

Inorganic impurities and ash in carbon chars have long been recognised as having catalytic properties for oxidation/gasification reactions. Foremost amongst these catalysts are transition metals (Fe, Ni, Co), alkali metals, and alkaline earths. The extent to which a particular catalyst may accelerate oxidation rates is a function of many variables including the metal concerned, thermal conditions, size and distribution of the catalyst throughout the carbon, and the relative amount of catalyst.

Chars produced from woods and straws will contain residues of the inorganic species present in the precursors. Calcium, a noted carbon catalyst, is present in high proportions in the residual ash. The effect of an acid-treatment prior to char preparation has been studied by McGhee[131] with reference to changes in oxidation rates. Char yields from straw and pinewood produced from HNO_3-treated precursors gave lower char yields and chars with lower ash contents. The proximate, ultimate and ash compositions of raw and acid-treated straw and pine wood are shown in Table 6.2.

Table 6.2 Proximate, Utimate and ash analysis of raw and acid-treated cereal straw and Danish pine

Material	CEREAL STRAW			DANISH PINE		
	Raw	HNO_3 treated*	HCl treated*	Raw	HNO_3 treated*	HCl treated*
Proximate analysis (%, dry basis)						
Volatile matter	84.0	93.6	88.9	77.8	91.9	89.6
Fixed carbon	11.4	3.4	8.3	20.5	7.6	9.8
Ash	4.5	3.0	2.8	1.7	0.5	0.6
Ultimate analysis (%, ash free)						
C	43.4	44.1	47.6	46.2	44.6	49.1
H	6.2	4.9	5.0	6.5	5.6	5.4
N	0.7	0.4	<0.1	1.5	0.8	<0.1
Cl	0.8	<0.1	<0.1	0.13	<0.1	<0.1
O(by diff)	49.0	50.5	47.2	45.7	78.9	45.4
Ash analysis (wt%)						
SiO_2	71.3	90.2	89.7	34.6	42.6	39.4
Al_2O_3	1.0	nd	nd	19.8	nd	nd
Fe_2O_3	0.8	0.8	<0.1	4.3	4.1	2.5
CaO	10.3	0.4	0.5	29.4	8.3	5.7
MgO	1.9	0.1	0.2	2.1	2.0	1.9
TiO_2	0.0	nd	nd	0.6	nd	nd
K_2O	0.4	0.3	0.1	1.4	1.8	1.0
Na_2O	11.4	0.1	.01	3.4	0.3	0.5
P_2O_5	3.0	nd	nd	2.2	nd	nd

nd - *not determined* * *Strathclyde data*

The chars produced showed significantly lower reactivity towards oxygen as shown by the oxidation rates at 653°K which in the case of the HNO_3 treated materials were an order of magnitude lower than from the untreated precursors. In the present study, the reactivity of the chars has been compared using DTA and observing changes in the temperatures of peak exothermic reactions, as a function of precursor treatment and pyrolysis temperature. A trend of decreasing reactivity towards oxygen with increasing pyrolysis temperature was observed. Similar features were observed with chars prepared from RDF. The peak temperatures for each exotherm from the Byker char

samples were lower than those from pine wood chars. Thus RDF pyrolysis char was found to be slightly more reactive than the corresponding chars from pinewood. A greater decrease in reactivity was observed between chars prepared at 500 and 700°C, than between those prepared at 700 and 900°C. This could be accounted for by the reduction in microporosity and the role played by oxygen diffusion at the higher temperatures. The effect of the acid treatment procedure was to produce chars of a less reactive nature, with peak temperatures reduced by up to 45°C. This would indicate that alkali cations present in the untreated sample have provided significant catalytic activity for oxidation.

6.8 Concluding remarks

In this study a wide range of biomass materials with calorific values typically half those of fossilised fuels have been studied with a view to using these materials as an energy source. Many of these materials currently pose serious disposal problems, for example dumping of sewage sludge in the North Sea. In any combustion/gasification system, which is the primary means of recovering the chemical energy in the form of heat for steam raising, the properties of the incombustible fraction of the fuel have always raised major technical and process engineering challenges. Thus in the change from stoker to pf (pulverised fuel) firing of coal at power stations, the higher combustion temperatures led to major slagging and fouling problems from the mineral matter inherent in all coals. Boiler design and operation (load capacity), have been optimised to minimise these problems, although changes in fuel quality and supply still lead to expensive, unscheduled outages.

Residues from combustion of biomass have compositions which contain higher quantities of alkali metals and P_2O_5. In terms of ash fusion properties and volatilisation, these would pose serious problems in any combustion system, as has been experienced by many local authorities with waste incineration. Thus fuel technologists have actively considered gasification of biomass fuels as a more desirable alternative, since the lower gasification temperatures would reduce the vapour pressures of the volatile species and possibly avoid the fusion of ash residues. In this study, the high temperature properties of biomass residues, and the slags and deposits from a wide variety of experimental and pilot plant gasification processes have been studied.. In each case, almost without

exception, these processes have produced troublesome slags and deposits which for a full scale plant would pose serious operational problems. While overall gasification temperatures of 1000°C or so would be envisaged, local temperature adjacent to burning fuel particles would suggest that temperatures have been several hundred degrees higher, thus vaporisation of alkali metal constituents have produced fouling deposits on heat exchangers, while partial fusion of ash residues have produced dense slags. The one exception to these somewhat general remarks has been the study of the residues from the TPS wood gasification process where no deposits or agglomeration of ash particles were encountered. Thus two major demonstration plants, currently under design and construction as part of the Thermie Arbre programme, will be followed with much interest and scrutiny by the energy industry.

For the remaining biomass materials, gasification and combustion of each individual fuel remains a technical challenge. Another option as a means of disposing of these wastes, with the added advantage of recovering the inherent chemical energy, is to co-fire with coal in conventional systems. Again, such processes are under active study, with considerable financial support from the EU. The results to date would suggest that with the right mix of fuels many of the problems associated with biomass alone can be successfully avoided.

Conclusions

1. The characterisation of a range of biomass and waste materials, including short rotation coppice, poultry litter, sewage sludge, straw and RDF, revealed these substances to be grossly inhomogeneous in nature. The deposits and ash residues from combustion and gasification processes reflect the heterogeneity of the presursor materials.

2. In a boiler system chemical equilibrium is seldom attained due to the heterogeneous nature of the fuel and, though residence times vary from one process to another, to the transient exposure to high temperature. However, phase equilibria studies have proved a valuable technique in predicting the nature of boiler residues and deposits.

3. Short rotation coppice

A characterisation of the major woody tissues of poplar and willow coppice showed a distinct segregation of inorganic material throughout the plant anatomy. Calcium oxalate crystals were found to be concentrated in the phloem (inner bark) of both species; microstructural examinations revealed columns of multifaceted *and* rhomboidal calcium oxalate crystals, each secured by an organic membrane within individual parenchyma cells. X-ray diffraction revealed calcium oxalate to be present in the leaves, catkins and twigs, but absent in the sapwood and heartwood. The latter xylem tissues of poplar comprised two major crystalline phases; calcite ($CaCO_3$) and syngenite [$K_2Ca(SO_4)_2.H_2O$].

The ash content of the bark was four to five times greater than that of the wood. The twigs and topmost fractions of the main stem possessed greater ash contents than those at the base, and thus a trend of decreasing ash content from top to bottom of the main stem was observed. The bulk ash content of the willow coppice from Long Ashton was found to decrease with maturity. These observations reflect the variation in bark-to-sapwood ratios of the fractionated stem.

The xylem tissues (sapwood and heartwood) were found to contain increased concentrations of K_2O, and consequently displayed lower ash fusion properties than the CaO-enriched bark. Solidus and liquidus temperatures of the sapwood ash were 100-200°C lower than those of the bark. Calculated Urbain viscosities differed by an order of magnitude, the bark ash melt being more viscous than the sapwood counterpart. The bark residue is beneficial to the high temperature ash fusion characteristics of the fuel, raising the temperature at which liquids form and increasing the melt viscosity, thereby reducing the driving force for viscous flow sintering between ash particles.

Significant differences were observed in the ash chemistry of poplar and willow species cultivated at different sites. The willow grown at Silsoe was found to contain twice the concentration of CaO than the corresponding willow from Long Ashton, which was notably richer in K_2O and P_2O_5. Consequently, the ash fusion behaviour was distinctly different, with the Silsoe willow ash exhibiting solidus and liquidus temperatures some 200-350°C higher than the Long Ashton counterpart, thus reducing the propensity to form deposits. The results suggest that the variation in ash composition was attributable to the different soil conditions and would present a major variable in fuel quality for potential energy recovery processes.

The characterisation of cyclone dust samples from the gasification of willow coppice at (TPS, Sweden) revealed a predominantly refractory ash, attributable to the major components CaO and MgO, with no evidence of agglomeration or interaction of ash particles. Since MgO was not found to be a major constituent of the willow ash it would appear that dolomite from the tar cracker contributed to the raised ash fusion temperatures.

4. Tyre waste

The tube deposit from the Elm Energy waste car tyre incinerator was composed of a highly porous assembly of predominantly fused aluminosilicate ash particles bonded together by condensed peripheral layers of ZnO. Distinct necks had formed between particles, thus supporting the mechanism of liquid phase sintering. Further infilling of the porosity had occurred with the formation of $CaSO_4$ and $ZnSO_4$ in the remaining voids.

5. Poultry Litter

The poultry litter was found to possess high moisture contents (50-60%), with ash contents of ~14wt% (dab). The fuel was characterised by an ash composition rich in CaO, K_2O, P_2O_5 and SO_3. The inherent inorganic matter contained hydroxyapatite [$Ca_5(PO_4)_3(OH)$] and arcanite (K_2SO_4). The ash fusion properties were represented by low solidus and liquidus temperatures, typically 800°C and 1100°C, reflecting the appreciable quantities of K_2O, Na_2O, CaO and MgO in the fuel ash, all of which exhibit strong fluxing characteristics. Consequently molten or partially molten ash particles would be produced during combustion, increasing the probability of adherence on collision. Furthermore, the relatively high vapour pressures of potassium salts and P_2O_5 would infer that the formation of alkali and phosphate bonded deposits are inevitable in such a system.

The nature of the superheater deposit was consistent with the predictions based on thermodynamic data. K_2SO_4 was found to have initiated fouling by condensation of the salt on superheater tubes and on the surface of ash particles. The microstructure was characterised by fused calcium-potassium phosphate particles, bonded by a dense matrix of K_2SO_4. Due to the volatile character of K^+ species and P_2O_5, the temperature is a critical variable to preclude excessive fouling of the convective passes.

Phase equilibria studies based on the CaO-P_2O_5 and K_2O-CaO-P_2O_5 systems have predicted the crystallisation products of a poultry litter ash melt with considerable accuracy. The microstructure of the Eye Power Station boiler slags revealed evidence of the crystallisation of molten or partially molten ash, with the growth of a variety of calcium and potassium phosphate crystals from a viscous silicate liquid phase.

6. Sewage sludge

The ash content of the sewage sludges were found to be relatively high, at ~30wt% (dab), compared to the majority of biomass and fossil fuels. The ash was essentially an aluminosilicate containing appreciable amounts of CaO and P_2O_5. Quartz and calcite were crystalline phases common to both Paisley and Thames Water samples, with the latter sludge also containing kaolin ($Al_2O_3.2SiO_2.2H_2O$) and $Ca_3(PO_4)_2$. The solidus temperature of the Paisley sewage sludge ash was 950°C, considerably higher than that

of the Thames Water sample at 880°C, reflecting the increased SiO_2 content of the Paisley ash. Liquidus temperatures were subject to less variation, averaging 1290°C.

Predictions of ash fusion behaviour based upon phase equilibria in the $CaO-Al_2O_3-SiO_2$ and $CaO-Al_2O_3-SiO_2-P_2O_5$ systems were largely inaccurate due to the unexpected enrichment of Fe_2O_3 (22wt%) in a pilot plant gasifier slag. Iron was found to be present in the ferrous and ferric valency states, as troilte (FeS) and maghemite (γFe_2O_3), indicative of the varying oxygen potential within the gasifier and of non-equilibrium conditions during deposit formation. The microstructure of the Warren Springs gasifier deposit was characterised by the presence of a variety of predominantly crystalline phases, including calcium phosphate, a spinel, FeS and a pyroxene [$(Fe,Ca)SiO_3$], the crystal morphologies of which would strongly suggest that the deposit had been molten at an early stage of formation. Ash fusion characteristics were similar in nature to those of the fuel ash.

8. RDF/Chestnut

The chestnut fuel was characterised by a low ash content of <0.5wt% (dab) and an ash composition very different to the coppiced willow and poplar. The major constituents of the ash were SO_3, CaO and K_2O, with appreciable concentrations of SiO_2, MgO and MnO. The ash comprised two major crystalline phases, those of calcium oxalate and quartz.

The Byker and Isle of Wight RDF samples were found to be of a similar constitution, and contained on average 12wt% ash (dab). The bulk chemical composition was largely that of an aluminosilicate, with substantial concentrations of CaO. Quartz, kaolin, calcite and rutile (TiO_2) were identified in both samples, and thought to have been derived from the inorganic fillers used extensively in paper and plastic products.

Despite the marked difference in ash content between the chestnut and RDF samples, an analysis of the hearth deposit suggested that the inorganic matter had interacted. The deposit contained three major crystalline phases, gehlenite, wollastonite and anorthite, all consistent with the predictions based upon thermodynamic data. The nature of the deposit was accurately predicted from the $CaO-Al_2O_3-SiO_2$ phase equilibrium diagram,

the deposit characterised by a heterogeneous assembly of phases, predominantly crystalline products from a molten aluminosilicate.

The ash content of a charcoal-rich residue that had been formed while co-firing chestnut with 30% RDF was considerably higher than that from chestnut alone. During the gasification process, the chestnut residue had become enriched in SiO_2, Al_2O_3, Fe_2O_3, CaO and surprisingly Na_2O. The addition of 30% RDF to the chestnut fuel resulted in a pronounced increase in SiO_2 and Al_2O_3 in the gasification residue. DTA revealed that the char from the mixed fuel containing RDF was distinctly less reactive than that from chestnut alone.

9. Collaboration with Strathclyde university

The reactivity of chars prepared by pyrolysis at varying temperature (500°C, 700°C and 900°C) revealed a progressive trend of decreasing reactivity towards oxygen with increasing pyrolysis temperature. The Byker RDF char was found to be the most reactive of all the precursor materials, with the Isle of Wight RDF and straw slightly less reactive, and Danish pinewood the least reactive at all temperatures.

The wood char morphology revealed that the cellular structure of the raw material had been retained with a slight increase in char density as the pyrolysis temperature was increased. The morphologies of the straw chars were also cellular in nature, with little variation in topography with pyrolysis temperature. The RDF chars were essentially fibrous materials containing inorganic residues from fillers and glass.

The consequence of the HNO_3-treatment of the chars was to decrease both the ash content and reactivity towards O_2. The observations are in support of previous studies which have shown that alkali ions act as catalysts for the oxidation of carbonaceous materials, and that their removal reduces the carbon reactivity.

The inorganic crystalline phases present in the RDF chars was dependent upon the pyrolysis temperature. Quartz was the major phase at all temperatures, while calcite was present at 500°C, but absent at 700°C and above, the CaO formed having reacted with SO_2 to produce anhydrite ($CaSO_4$). The HTA from the RDF contained quartz, gehlenite and nepheline $(Na,K)AlSiO_4$. The presence of the latter phases, not present in

the LTA, clearly reflect the reactions which had occurred at high temperatures during preparation of the HTA.

10. It may be concluded that large scale combustion and gasification processes which use biomass and wastes as energy sources will require meticulous and precautionary design considerations to reduce potential problems from the ash residues.

Suggestions for further work

The results of this study suggest that the bulk ash chemistry of biomass and wastes are subject to variation depending on their origin. The observations are further compounded by the heterogeneous nature of these materials. Further work is required to establish the range of ash compositions likely to be encountered. The study of deposit formation in a laboratory rig would supplement the information obtained regarding the nature and fate of the inorganic species.

Phase equilibria studies have been used to predict the high temperature behaviour of the biomass and waste ash systems. Whereas the crystallisation products have been predicted with considerable accuracy, experimental high temperature microscopy observations have yielded solidus and liquidus temperatures several hundred degrees lower than predicted values, reflecting the more complex fusion properties of a multicomponent system. A qualitative allowance has, in many instances, been proposed for the fluxing characteristics of the alkalis present in the ash, with particular reference to documented silicate systems. Further work is required to establish the quantitative effect of K_2O, Na_2O, CaO, MgO, MnO and TiO_2 in reducing the temperature of initial liquid formation and in lowering the viscosity of the residual melt.

With the exception of straw, the biomass ashes characterised in this study contained appreciable concentrations of P_2O_5 (10-30wt%), and minor quantities of SiO_2. Thermodynamic data for multicomponent phosphate systems is extremely limited, and the extension of ternary and quaternary phase equilibrium data may constitute a potentially valuable area of study, with the aim of developing a slagging index for these potential fuels based upon chemical composition.

References

1. *Clean Coal Technology, Options for the future*, ETSU OECD/IEA, 1993

2. **Matlàry, J. H.,** *Energy Policy in the European Union*, Ed. Nugent, N., Paterson, W. E., and Wright, V., MacMillan Press Ltd., 1997.

3. **Grassi, G.,** *The Biomass Research and Development Programme of the Commission of the European Communities*, an EC Publication, 1997.

4. *DTI Digest of UK Energy Statistics,* HMSO, August 1997.

5. **O`Neill, P.,** *Environmental Chemistry*, Second Edition, Chapman & Hall, London, 1993.

6. *An Assessment of Renewable Energy for the UK*, ISBN 0115153489, ETSU, HMSO, London, 1994.

7. **Greenwood, N. N., and Earnshaw, A.,** *Chemistry of the Main Group Elements*, Pergamon Press, Oxford, 1992.

8. DTI Energy Paper No. 62, *New and Renewable Energy: Future Prospects in the UK*, March 1994.

9. **Kendall, A., McDonald, A., and Williams, A.,** *The Power of Biomass*, Chemistry & Industry 9, 342-345, 1997.

10. **Patterson, W.,** *Power from Plants. The Global Implications of New Technologies for Electricity from Biomass*, Royal Institute of International Affairs, Earthscan Publications Ltd., London, 1994.

11. **Macpherson, G.,** *Home-Grown Energy from Short Rotation Coppice*, Farming Press Books, UK, 1995.

12. **Abrutat, P. H., Edwards, R. P., and Wilkins, C.,** *Growing Energy Crops on Land Contaminated by Heavy Metals,* International Land Reclamation and Mine Drainage Conference and the Third International Conference on the Abatement of Acidic Drainage, p305-312, April1994.

13. *Renewable Energy: A Commercial Opportunity-A Guide for Lenders, Investors and Advisers*, DTI-ETSU brochure, 1994.

14. **Nellist, M. E., Bartlett, D. I. and Moreea, S. B. M.,** *Storage Trials with Arable Coppice*, report from Silsoe Research Institute, 1994.

15. **Riddel-Black, D.,** *Sewage Sludge as a Fertilliser for Short Rotation Coppice*, paper given at IEA BA Task VIII Activity 9 Meeting: Willow Vegetation Filters for Municipal Wastewaters and Sludges-a Biological Purification System, Swedish University of Agricultural Sciences, Uppsala, 5-10 June, 1994.

16. **Bever, B. M.** (Ed.), Encyclopedia of Materials Science, *Soil Additives: Phosphate, Potash and Sulphur*, , volume 6, 4476, Pergamon Press, Oxford, 1986.

17. **Riddell-Black, D.,** *Heavy Metal Uptake by Fast Growing Willow Species*, Water Research Centre, summary presented at the 8th European Conference on Biomass for Energy, Environment, Agriculture and Industry, October 1994.

18. **Hewitt, E. J. and Smith, T. A.,** *Plant Mineral Nutrition*, The English Universities Press Ltd., 1975.

19. **Sutcliffe, J. F.,** *The Role of Manganese and Potassium in Plant Nutrition and the Mechanism of their Absorption by cells*, Technical Bulletin No. 14 *Soil Potassium and Magnesium*, HMSO, London, 1967.

20. **Trewavas, A. J.** (Ed.), *Molecular and Cellular Aspects of Calcium in Plant Development*, Plenum Press, London, 1986.

21. **Loewus, F.A. and Runeckles, V. C.,** *The Structure, Biosynthesis and degradation of wood, Recent Advances in Phytochemistry Vol 11*, Plenum Press, 1977.

22. **Carlquist, S.,** *Comparative Wood Anatomy*, Springer-Verlag, 1988.

23. **Butterfield, B. G. and Meylan, B. A.,** *Three Dimensional Structure of Wood, An Ultrastructural Approach*, Chapman & Hall, 1980.

24. **Sutcliffe, J. F. and Baker, D. A.,** *Plants and Mineral Salts*, Edward Arnold Ltd., 1974.

25. *Downdraft Gasifiers under 200kWe*, ETSU B/M3/00388/04/REP, 1993

26. **Dagnall, S.**, *UK Strategy for Energy from Agricultural Animal Wastes*, poster presented at the 8th European Conference on Biomass for Energy, Environment, Agriculture and Industry, October 1994.

27. Fibropower Ltd., Eye Power Station, Suffolk, technical brochure.

28. Fibropower Ltd., Eye Power Station, Fibrophos information pamphlet.

29. **Cambel, I.**, *Biomass, Catalysts and Liquid Fuels*, Holt, Rinehart & Winston, London, 1983.

30. **Braunstein, H.**, et al., *Biomass Energy Systems and the Environment*, Pergamon Press, 1981.

31. **Etegni, L. and Cambell, A. G.**, *Physical and Chemical Characteristics of Wood Ash,* Bioresourse Technology **37**, 173-178, 1991.

32. **Grohmann, K., Wyman, C. E. and Himmel, M. E.**, *Potential Fuels from Biomass and Wastes*, American Chemical Society, 1992.

33. **Livingston, W. R.**, *Straw Ash Characteristics*, Contractor Report, Babcock Energy Ltd., Renfrew, 1991.

34. **Ghaly, A. E.** et al., *Physical and Thermochemical Properties of Cereal Straw*, Energy Sources, **12**, 131-145, 1990

35. **Raask, E.**, *Mineral Impurities in Coal Combustion*, Hemisphere Publishing Corporation, 1985.

36. Department of Environment, *Digest of Environmental Protection and Water Statistics*, Ed. Martin, J., HMSO, London, 1994

37. *Encyclopedia of Materials Science: Resource Recovery*, Ed. Bever, B. M., volume 6, 4231-4238, Pergamon Press, Oxford, 1986.

38. **Agrawal, R. K.**, *A Rapid Technique for Characterisation and Proximate Analysis of Refuse-derived Fuel and its Implications for Thermal Conversion*, Waste Management and Research **6**, 271, 1988.

39. **Barboza, M. J.,** *Air Pollution Engineering Manual: Municipal Solid Waste Landfill Gas Emissions*, Ed. Buonicore, A. and Davis, W., Van Nostrand Reinhold, 1992.

40. Daily Telegraph, 1st December, 1994.

41. **Wheatley, R. J. and Hedgecock, J. J.,** International Conference on Renewable Energy Clean Power 2001, Conference Publication No. 385, IEE, London, 1993.

42. **Livingston, W. R., Gibson, J. R. and Birch, M. C.,** *The Combustion of Pelletised Refuse Derived Fuel*, J. Inst Energy **63**, 151, 1990.

43. *Slagging and Fouling in Combustion Plants*, EDSU Report 92012, 1992.

44. **Rampling, T. W. A.,** *Pot Furnace Research on RDF Combustion*, Warren Springs Laboratory Report No. LR 683(MR), 1988.

45. **Gunn, D. C. and Johnston, J,** *The use of Refuse Derived Fuel pellets in Boilers,* Energy World, 22, July/August, 1990.

46. **Kubachewski, O., Alcock, C. B., Spencer, P. S.,** *Materials Thermochemistry*, 6th Edition, Pergamon Press, Oxford, 1993.

47. *The Waste Manager*, Ed. Rose, J., p.5, October 1995.

48. **Dyke, P.,** *Emissions and their Control for Small Scale Waste Combustion*, Institute of Energy 1st International Conference on Combustion and Emissions Control, September, 1993.

49. **Bosshard, A. W., Schlumpf, H. P., and Plüss-Stanfer, A. G.,** *Fillers and Reinforcements*, Chapter 9 in *Plastics Additives Handbook*, Ed. Gächter, R. and Müller, H., 2nd Edition, Hanser Publishers (Carl Hanser Verlag München Wein), 1987.

50. **Morton-Jones, D. H.,** *Polymer Processing*, Chapman & Hall, London, 1989.

51. **Deer, W. A., Howie, R. A., and Zussman, J.,** *Rock-forming Minerals Vol 3 Sheet Silicates*, Longmans, Green & Co. Ltd., London, 1966.

52. *Encyclopaedia of Materials Science: Paper and Paperboard Substrates-Composition,* Ed. Bever, B. M., volume 5, 3410-3416, Pergamon Press, Oxford, 1986.

53. **Williams, P. T. and Besler, S.,** *Pyrolysis-Thermogravimetric Analysis of Tyres and Tyre Components*, Fuel **74**, 1277-1283, 1995.

54. **Barlow, F. W.,** *Rubber Compounding Materials: Principles, Materials and Technologies*, Marcel Dekker Inc., 1988.

55. **Billmeyer Jr., F. W.,** *Textbook of Polymer Science*, 3rd Edition, John Wiley & Sons Inc., 1984.

56. *Elastomers and Rubber Compounding Materials*, Ed. Franta, I., Elsevier, 1989.

57. **Cowie, J. M. G.,** *Polymers: Chemistry and Physics of Modern Materials*, Blackie, London, 1991.

58. **Rampling, T. W. A. and Gill, P. J.,** *Pot Furnace Research on the Combustion of Tyres,* Warren Springs Laboratory Report No. LR 863(MR), 1988.

59. The Financial Times, September, 1993.

60. **Livingston, W. R.,** *Sewage Sludge Disposal- A Review of the Combustion Options*, Babcock Energy Ltd., Renfrew, 1992.

61. *Secondary Materials in Domestic Refuse as Energy Sources*, Europool, Communication Consulting Research in Europe, Graham & Trotman Ltd., 1977.

62. **Burton, F. L. and Tchobanoglous, G.,** *Wastewater Engineering, Treatment, Disposal and Reuse*, McGraw-Hill Publishing Company, London, 1991.

63. **Marsh, M. K.,** Ph.D. Thesis, *The Effect of Mineral Salts on Deposit Formation During Fluidised Bed Combustion of Coal*, University of London, 1989.

64. **Couch, G.,** *Understanding Slagging and Fouling During pf Combustion*, Report No. IEA CR 172, IEA Coal Research, London, 1994.

65. **Wain, S. E.,** Ph.D. Thesis, *Thermal and Mechanical Properties of Pulverised Fuel Boiler Slags*, University of London, 1991.

66. **Bridgewater, A. V.,** *The Technical and Economical Feasibility of Biomass Gasification for Power Generation*, Fuel **74**, 631, 1995.

67. *Gas from Coal*, a National Coal Board report

68. **Hall, M. D., and Overend, R.P.,** Biomass, Regenerable Energy, John Wiley & Sons, London, 1987.

69. **Smith, E. L.,** *Reactors, Some Design Perspectives (Keyhole Paper)* in *Thermochemical Processing of Biomass*, Ed. Bridgewater, A.V., Butterworths, London, 1984.

70. **Lacey, J. A.,** *Gasification: A key to the Clean Use of Coal*, Robens Science Lecture Part 1, Energy World, Inst of Energy, 3, February 1988.

71. *Downdraft Gasifiers under 200kW$_e$*, ETSU B/M3/00388/04/REP, 1993.

72. **Hedley, A.,** *Gasification: Its Role in the Future Technological and Economic Development of the UK*, Elsevier Applied Science Publishers, London, 1989.

73. **Williams, R. H. and Larson, E. D.,** *Advanced Gasification-based Biomass Power Generation*, p729 *Renewable Energy Sources for Fuels and Electricity*, Ed. Johansson, T. B., Kelly, H., Reddy, R. H. W., and Burnham, L., Earthscan Publications Ltd., London, 1993.

74. **Dainton, D.,** *Clean Coal Technology for Power Generation: An Overview*, Clean Coal Conference, London, 1988.

75. **Kaupp, A. and Goss, J. R.,** *Small Scale Gas Producer-Engine Systems*, Vieweg & Sohn, Braunschweig, Germany, 1984.

76. **Merrick, D.,** *Coal Combustion and Conversion Technology*, Coal Research Establishment, MacMillan, 1984.

77. **Yates, J. G.,** *Fundamentals of Fluidized-bed Chemical Processes*, Butterworths, London, 1983.

78. *Coal Comes Clean*, A British Coal Environmental Review, British Coal

79. *Fluidised Bed Combustion of Coal*, a National Coal Board Report, Ed. Harrison, J., Willis, D. and Woodhouse, N., 2nd Edition, 1985

80. **West, S. S.**, Ph.D. Thesis, *Coal Mineral Interactions During Fluidised Bed Gasification Processes*, University of London, 1993

81. **Bemtgen, J. M., Hein, K. R. G. and Minchener, A. J.**, *APAS Clean Coal Technology Programme Vol 1: Co-utilisation of Coal, Biomass and Waste*, 1992-1994.

82. **Baxter, L., Miles, J. R., Bryers, R. W., Jenkins, B. M. and Oden, L. L.**, *Alkali Deposits found in Biomass Power Plants: A Preliminary Investigation of their Extent and Nature*, Executive Summary from National Renewable Energy Laboratory for Engineering Foundation Meeting, *Applications of Advanced Technology to Ash-Related Problems in Boilers*, Waterville Valley, NH, 1995.

83. **Kingery, W. D., Bowen, H. K. and Uhlmann, D. R.**, *Introduction to Ceramics*, 2nd Edition, John Wiley & Sons, 1976.

84. **Rawson, H.**, *Inorganic Glass Forming Systems*, Academic Press Inc., Ltd, London, 1967.

85. **Holloway, D. G.**, *The Physical Properties of Glass*, Wykeham Publications Ltd., London, 1973.

86. **Strnad, Z.**, *Glass Ceramic Materials*, Glass Science and Technology 8, Elsevier, Amsterdam, 1986.

87. **Pye, L. D., LaCourse, W. C., and Stevens, H. J.** (Ed.), *The Physics of Crystalline Solids*, Taylor& Francis, London, 1992.

88. **Porter, D. A. and Easterling, K. E.**, *Phase Transformations in Metals and Alloys*, Chapman & Hall, London, 1981.

89. **Turkdogan, E. T.**, *Physicochemical Properties of Molten Slags and Glasses*, The Metals Society, London, 1983.

90. *Phase Diagrams for Ceramists*, Ed. Levin, E., Robbins, C. R. and McMurdie, H. F American Ceramic Society, 1964.

91. **West, D. R. F.**, Ternary Equilibrium Diagrams, Second Edition, Chapman & Hall, London, 1982.

92. **Sanyal, A. and Williamson, J.,** *Slagging in Boiler Furnaces: An Assessment Technique Based on Thermal Behaviour of Coal Minerals*, J. Inst. Energy, **158**, 158, 1981.

93. **Kalmanovich, D. P.,** Ph.D. Thesis, *Reactions in Coal Ash Melts*, University of London, 1983.

94. *Phase Diagrams for Ceramists*, Fig. 630 CaO-Al_2O_3-SiO_2, p219, Ed. Levin, E., Robbins, C. R. and McMurdie, H. F, American Ceramic Society, 1964.

95. British Standards Institution, *Fusibility of Coal Ash and Coke Ash*, BS 1016, Part 15, 1970.

96. **Huffman, G. P., Huggins, F. E. and Dumyre, G. R.,** *Investigation of the High Temperature Behaviour of Coal Ash in Reducing and Oxidising Atmospheres*, Fuel **60**, 585, 1981.

97. **Huggins, F. E., Kosmak, D. A. and Huffman, G. P.,** *Correlation Between Ash Fusion Temperatures and Ternary Equilibrium Phase Diagrams*, Fuel **60**, 577, 1981.

98. **Todor. D. N.,** *Thermal Analysis of Minerals*, Abacus Press, Tunbridge Wells, 1976.

99. **Grim, R. E.,** *Applied Clay Mineralogy*, McGraw-Hill Book Co. Inc, 1962.

100. **Deer. W. A., Howie, R. A., and Zussman, J.,** *Rock-Forming Minerals Volume 3 Sheet Silicates*, Longmans, Green & Co. Ltd., London, 1965.

101. **Rawson, H.,** *Properties and Applications of Glass*, Glass Science and Technology 3, Elsevier, Oxford, 1980.

102. **Yet-Ming Chiang, Birnie, D. P., and Kingery, W. D.,** *Physical Ceramics*, John Wiley & Sons, Inc., Chichester, 1997.

103. **Williamson, J., West, S. S., and Laughlin, M. K.,** *Behaviour of Bed Material during Fluidised Bed Gasification: The Effects of Mineral Matter Distributions*, Fuel, **72**, 697, 1993.

104. **Greaves, G. N.,** *EXAFS and the Structure of Glass*, Non-Cryst. Solids **71**, 203, 1985.

105. **Richard, A., Catlow, A. and Vessal, B.,** *Atomistic Models for Silicate Glasses,* Advances in Amorphous State Chemistry, Society of Glass Technology, 1993.

106. **Corbridge, D. E. C.,** *Phosphorus: An Outline of its Chemistry, Biochemistry and Technology*, 4th Edition, Elsevier Science Publishers B. V., Oxford, 1990.

107. **Nowok, J. W., Benson, S. A., Steadman, E. N. and Brekke, D. W.,** *The Effect of Surface Tension/Viscosity Ratio of Melts on the Sintering Propensity of Amorphous Coal Ash Slags*, Fuel **72**, 1055-1061, 1993.

108. **Uhlmann, D. R. and Kreidl, N. J.,** *Glass Science and Technology Volume 3, Viscosity and Relaxation,* Academic Press Inc, London, 1986.

109. **Doremus, R. H.,** *Glass Science*, Second Edition, John Wiley & Sons Inc., 1994

110. **Hofmaier, G. and Urbain, G.,** *Science of Ceramics*, British Ceramic Society, **4**, 25, 1968

111. **Watt, J. D. and Fereday, F.,** J. Inst. Fuel, **99**, 338, 1969.

112. **Urbain, G.,** *Viscosity of Silicate Melts,* J. Br. Ceram Soc **80**, 139, 1981.

113. **Urbain, G., Cambier, F., Deletter, M, Anseau, M. R.,** Trans. Brit. Ceram. Soc., 139, 80, 1981.

114. **Mills, K. C.,** *Viscosities of Molten Slags, Chapter 9, Slag Atlas*, Ed. Verein Deutscher Eisenhüttenleute (VDEH), Second Edition, Verlag Stahleisen GmbH, D-Düsseldorf, 1995.

115. **Kalmanovich, D. P. and Frank, M.,** *An Effective Model of Viscosity for Ash Deposition Phenomena*, p89 in *Mineral Matter and Ash Depostion from Coal*, Ed. Bryers, R. W. and Vorres, K. S., Engineering Foundation Conferences, United Engineering Trustees Inc., 1990.

116. **Machin, J. S., Yee, T. B. and Hanna, J.,** Amer. Ceram. Soc. **35**, 322-325, 1952.

117. **Atkins, P. W.,** *Physical Chemistry*, Fourth Edition, Oxford University Press, 1990.

118. **Ray, P. M.,** *The Living Plant*, Second Edition, Rinehart & Winston, Inc, 1972.

119. **Iler, R. K.,** *The Chemistry of Silica, Chapter 7 Silica in Biology*, John Wiley & Sons, Inc, 1979.

120. **Skoog, D. A., and Leary, J. J.,** *Principles of Instrumental Analysis*, 4th Edition, Saunders College Publishing, London, 1992.

121. **Morrison, R. T. and Boyd, R. N.,** *Organic Chemistry*, 5th Edition, Allyn & Bacon Inc, London, 1987.

122. **Kaye, G. W. and Laby, T. H.,** *Tables of Physical and Chemical Constants and some Mathematical Functions*, Longman Group Ltd., London, 1986.

123. **Street, H. E. and Opik, H.,** *The Physiology of Flowering Plants: Growth and Development*, Edward Arnold Publishers Ltd., London, 1970.

124. *Phase Diagrams for Ceramists*, Fig. 246, system $CaO-P_2O_5$, p107, Ed. Levin, E., Robbins, C. R. and McMurdie, H. F, American Ceramic Society, 1964.

125. *Phase Diagrams for Ceramists*, Fig. ?, system K_2O-SiO_2, p78 1969 Supplement, Ed. Levin, E., Robbins, C. R. and McMurdie, H. F, American Ceramic Society, 1969.

126. *Phase Diagrams for Ceramists*, Fig. 391, system $K_2O-CaO-SiO_2$, p149, Ed. Levin, E., Robbins, C. R. and McMurdie, H. F, American Ceramic Society, 1964.

127. *Phase Diagrams for Ceramists*, Fig. 958, system $Ca_3(PO_4)_2-Al_2O_3-SiO_2$, p310, Ed. Levin, E., Robbins, C. R. and McMurdie, H. F, American Ceramic Society, 1964.

128. *Phase Diagrams for Ceramists*, Fig. 1902, system FeS-FeO, p522, Ed. Levin, E., Robbins, C. R. and McMurdie, H. F, American Ceramic Society, 1964.

129. *Rutley's Elements of Mineralogy*, Ed. Gribble, C. D., 27th Edition, Unwin Hyman, London, 1988.

130. **Barnard, J. A. and Bradley, J. N.,** *Flame and Combustion*, Chapman & Hall, 1985.

131. **McGhee, B.,** Ph.D. Thesis, University of Strathclyde, 1997.

132. **Zaror, C. A., Hutchings, I. S., Pyle, D. L., Stiles, H. N., and Kandiyoti, R.,** *Secondary char formation in the Catalytic Pyrolysis of Biomass*, Fuel, 64, 990-994, 1985.